



FEDERAL UNIVERSITY OF SANTA CATARINA
DEPARTMENT OF CHEMICAL ENGINEERING AND FOOD ENGINEERING
GRADUATE PROGRAM IN CHEMICAL ENGINEERING

Rodrigo Battisti

**FALLING FILM DISTILLATION ASSISTED BY A TWO-PHASE CLOSED
THERMOSYPHON: contributions to modeling, control, optimization, and techno-
economic assessment of the pilot-scale unit**

Florianópolis

2021

Rodrigo Battisti

**FALLING FILM DISTILLATION ASSISTED BY A TWO-PHASE CLOSED
THERMOSYPHON: contributions to modeling, control, optimization, and techno-
economic assessment of the pilot-scale unit**

Thesis submitted to the Graduate Program in
Chemical Engineering at the Federal University of
Santa Catarina to obtain the degree of Doctor in
Chemical Engineering.

Advisor: Prof.^a Dr.^a Cintia Marangoni
Co-advisor: Prof. Dr. Ricardo A. F. Machado
Co-advisor: Prof. Dr. Flavio Manenti

Florianópolis

2021

Identification sheet of the work

Battisti, Rodrigo

Falling film distillation assisted by a two-phase closed thermosyphon: contributions to modeling, control, optimization, and techno-economic assessment of the pilot scale unit / Rodrigo Battisti; orientadora, Cintia Marangoni, coorientador, Ricardo Antonio Francisco Machado, coorientador, Flavio Manenti, 2021.

216 p.

Tese (doutorado) - Universidade Federal de Santa Catarina, Centro Tecnológico, Programa de Pós-Graduação em Engenharia Química, Florianópolis, 2021.

Inclui referências.

1. Engenharia Química. 2. Intensificação de processos. 3. Destilação. 4. Filme líquido descendente. 5. Tubos de calor.

I. Marangoni, Cintia. II. Machado, Ricardo Antonio Francisco. III. Manenti, Flavio IV. Universidade Federal de Santa Catarina. Programa de Pós-Graduação em Engenharia Química. V. Título.

Rodrigo Battisti

**FALLING FILM DISTILLATION ASSISTED BY A TWO-PHASE CLOSED
THERMOSYPHON: contributions to modeling, control, optimization, and techno-
economic assessment of the pilot-scale unit**

The present work at doctoral level was evaluated and approved by an examining board composed of the following members:

Prof.^a Dr.^a Ana Paula Meneguelo
Federal University of Espírito Santo

Prof. Dr. Bruno Francisco Oechsler
Federal University of Santa Catarina

We certify that this is the **original and final version** of the conclusion work that was deemed appropriate to obtain the degree of doctor in Chemical Engineering.

Prof.^a Dr.^a Débora de Oliveira
Coordination of the Graduate Program

Prof.^a Dr.^a Cintia Marangoni
Advisor

Florianópolis, 2021.

This work is dedicated to my dear parents.

ACKNOWLEDGMENTS

First of all, I would like to thank my family, especially my parents Mércio and Lara, and my sister Graciela, for their support, encouragement at all times, and for always being by my side when I needed them most.

To Prof.^a Cintia Marangoni, my advisor, I am so grateful for the trust placed in me, for the dedication, patience, and for all the knowledge shared with me along this journey that made this work possible. You are an inspiration in my professional career.

To Prof. Ricardo Machado, my co-advisor, thanks for all the valuable contributions given throughout this process and for the opportunity to join an excellent research group, allowing me remarkable professional growth.

To Prof. Flavio Manenti, from Politecnico di Milano, who received me (although remote) with availability, and the members of his research team SuPER (Sustainable Process Engineering Research), I thank for the excellent contributions given to my work.

To Dr. Carlos Alberto Claumann, for the valuable and insightful collaborations, besides the deep discussions leading to moments of great learning.

To the members of the examining board, for the willingness and dedication to contribute to the improvement of this thesis work.

To all the professors of the Graduate Program in Chemical Engineering (PósENQ) of the Federal University of Santa Catarina (UFSC), who have demonstrated their commitment to the quality and excellence with education and scientific research.

To the Laboratory of Control and Polymerization Processes (LCP), and to the Department of Chemical Engineering and Food Engineering (EQA), for providing the entire necessary infrastructure to carry out this work.

To the Coordination for the Improvement of Higher Education Personnel (CAPES), to the Federal Institute of Santa Catarina (IFSC), and to the Foundation for Research and Innovation of the State of Santa Catarina (FAPESC), for the financial support for this work.

To my colleagues and friends at the LCP, for their collaboration and fun moments that made living together enjoyable, and to my colleagues of the graduate course who provided wonderful moments of study and friendship.

Finally, I would like to thank everyone who somehow contributed and supported me during this incredible journey of academic and human formation.

[...] reconhece que a única realidade para si [homem de ciência] é ele próprio, e o único mundo real o mundo como a sua sensação lho dá. Por isso, em lugar de seguir o falso caminho de procurar ajustar as suas sensações às dos outros, ciência objetiva, procura, antes, conhecer perfeitamente o seu mundo, e a sua personalidade. Nada mais objetivo do que os seus sonhos. Nada mais seu do que a sua consciência de si. Sobre essas duas realidades requinta ele a sua ciência.

Fernando Pessoa, Livro do Desassossego.

RESUMO EXPANDIDO

Introdução: Preocupações globais com as crescentes demandas energéticas resultaram na emergência de processos químicos intensificados e mais sustentáveis. Na vanguarda deste compromisso está a destilação, uma vez que esta operação é reconhecidamente intensiva no consumo de energia, podendo ser responsável por mais de 40% do gasto total de uma planta industrial (MELLO *et al.*, 2020). É consenso que a intensificação de processos compreende modificações com intuito de reduzir o tamanho dos equipamentos, aumentar o seu desempenho, diminuir o uso de utilidades e matérias-primas, e aumentar a eficiência dos processos (PONCE-ORTEGA; AL-THUBAITI; EL-HALWAGI, 2012). Comprometido com essas diretrizes, nosso grupo de pesquisa vem desenvolvendo uma unidade de destilação por filme líquido descendente, assistida energeticamente por um termossifão, denominada tecnologia Destubcal. Este aparato incorpora a destilação por filme líquido descendente, tecnologia já consolidada e estudada há décadas, com o fornecimento de calor por meio de um termossifão bifásico. Enquanto uma configuração de destilação convencional fornece calor apenas no refeedor e retira o calor no condensador de topo, a abordagem Destubcal possui uma distribuição uniforme de energia ao longo de todo o comprimento do tubo de destilação, sendo assim um equipamento mais compacto, seguro e eficiente termicamente (BATTISTI; MACHADO; MARANGONI, 2020). Estudos experimentais consolidados apontam que essa tecnologia é eficaz na separação e purificação de diversas misturas, com menor consumo de energia em relação à destilação convencional, tais como etanol-água (MARANGONI *et al.*, 2019b, 2019a), mistura aromática de tolueno, para-xileno, meta-xileno, orto-xileno e etilbenzeno (SILVA FILHO *et al.*, 2018), monoetilenoglicol-água (PIRES *et al.*, 2020), e nafta petroquímica sintética (QUERINO; MACHADO; MARANGONI, 2019). Estes trabalhos apontam que a unidade Destubcal é uma opção tecnológica promissora, o que motiva a continuidade e aprofundamento dos estudos em direção a consolidar esta tecnologia como um processo de destilação avançada viável economicamente. Para isso, há uma demanda crucial em entender o comportamento dinâmico desse aparato a fim de avançar nas estratégias de controle, visando minimizar custos e maximizar a produtividade. A compreensão do comportamento da influência e interação das variáveis operacionais e, conseqüentemente, a otimização desses parâmetros também se mostra necessária para viabilizar futuras aplicações. Além disso, o conhecimento dos custos de capital e operação tornam-se imprescindíveis para análise da viabilidade econômica do processo e sua consolidação estratégica.

Objetivo: O escopo norteador deste trabalho é oferecer contribuições científicas no campo da modelagem, do controle, da otimização e da avaliação técnico-econômica de uma unidade de destilação por filme líquido descendente em escala piloto assistida por um termossifão bifásico fechado, visando consolidar e difundir esta tecnologia como um processo viável de destilação intensificada energeticamente.

Metodologia: Este estudo está dividido em capítulos, sendo que cada capítulo representa uma das contribuições propostas nos tópicos abordados. Em cada um dos capítulos utiliza-se uma metodologia particular, a fim de atingir os objetivos previamente delineados. A parte comum a todos os capítulos é execução experimental na unidade em escala piloto, que foi utilizada para realização dos ensaios experimentais, coleta de dados e validação dos modelos matemáticos desenvolvidos. O capítulo de revisão da literatura traz uma perspectiva histórica dos fundamentos conceituais, dos tipos de processos e das diferentes formas de operação já utilizadas, além dos avanços tecnológicos produzidos ao longo dos anos a respeito dos

múltiplos e complexos fatores que influenciam a eficiência da destilação por filme líquido descendente. Para isso foi realizado um amplo levantamento nas bases bibliográficas Scopus e Google Scholar de trabalhos publicados e patentes depositadas relacionadas aos tópicos "colunas de filme líquido descendente" e/ou "colunas de parede molhada" desde meados do início do século XX, mais especificadamente no ano de 1942, até os dias atuais, no ano de 2020. Em seguida, para elucidar o comportamento dinâmico do aparato, uma modelagem transiente baseada em rede térmica com extensa validação experimental foi proposta. Após o modelo estar validado experimentalmente, o projeto de um controlador PID foi executado, e o modelo simulado em ambiente Simulink® a fim de avaliar o sistema de controle *feedback* da temperatura do termossifão atuando na potência das resistências elétricas. Posteriormente, com o intuito de avaliar o desempenho da unidade, um modelo preditivo de aprendizado de máquina baseado em redes neurais foi implementado para separação da mistura etanol-água. A temperatura de alimentação, a temperatura do evaporador e a vazão de alimentação foram as três variáveis de entrada do modelo, enquanto a fração mássica de etanol no destilado, a vazão mássica de destilado, o fator de recuperação e o fator de separação foram os quatro indicadores de desempenho avaliados. Uma vez que a topologia ideal do modelo de redes neurais foi estabelecida, uma otimização baseada em algoritmo genético foi realizada utilizando-se a modelagem de aprendizado de máquina, a fim de otimizar as variáveis operacionais do processo. Por fim, uma avaliação técnico-econômica e energética da unidade Destubcal em escala piloto foi realizada, aplicada à recuperação de etanol em grau desinfetante de 70 vol% em álcool. Essa análise foi motivada pelo aumento dramático da demanda por sanitizantes à base de etanol devido à emergência da pandemia de COVID-19, que chegou a levar à escassez em muitas cidades do Brasil. A performance da unidade foi avaliada experimentalmente com base em 64 corridas na unidade piloto, e a avaliação de custos de capital e custos operacionais foi realizada a fim de verificar a viabilidade técnica e econômica da planta como uma alternativa frente à destilação convencional de etanol.

Resultados e discussão: A revisão da literatura demonstrou que as colunas de filme líquido descendente representam cerca de 10,9% do total de trabalhos publicados nos últimos 80 anos. Estas colunas têm sido predominantemente usadas para pesquisas fundamentais de transferência de calor e massa. Apesar desta configuração não estar entre as maiores demandas de aplicação, ao longo dos anos vários dispositivos de película líquida descendente foram projetados, aprimorados e patenteados, tais como colunas monotubulares, colunas multitubulares, colunas verticais de placas planas, e colunas integradas energeticamente. No entanto, no que diz respeito à aplicação industrial, os conceitos de destilação de filme descendente ainda são relativamente pouco utilizados. Estudos em estado estacionário de eficiência de separação já estão bem consolidados, sendo que a maioria dos trabalhos publicados confirma a minimização do consumo de energia quando comparados às colunas de destilação convencionais. Ficou evidenciado que há lacunas de conhecimento no que tange o comportamento dinâmico destes processos de destilação. Desta forma, os desafios daqui a diante devem ser focalizados em esclarecer a dinâmica do processo, para que se avance no sentido de melhorar as estratégias de controle e otimização. Isso permitirá avançar nas melhorias operacionais da coluna para elevar essa tecnologia a um nível mais alto de viabilidade econômica. Considerando a complexidade do processo e a quantidade de variáveis que podem sofrer distúrbios ao longo do tempo, além da sensibilidade do filme descendente, o modelo transiente proposto baseado em rede térmica foi capaz de descrever o comportamento dinâmico da temperatura do termossifão com boa precisão. Os coeficientes de transferência de calor experimental e predito mostraram concordância satisfatória dentro da faixa de desvio de $\pm 25\%$, considerada admissível segundo a literatura. O controlador PID com parâmetros de

sintonia ajustados pelo método Ziegler-Nichols mostrou-se mais eficiente em atingir o *setpoint* de temperatura desejado mais rapidamente, com menor *overshoot* e menor oscilação na variável manipulada, conseqüentemente, reduzindo o consumo de energia elétrica da unidade em 3,1%. O modelo de aprendizado de máquina baseado em redes neurais foi capaz de prever com precisão os quatro principais parâmetros de desempenho da unidade, com um coeficiente de correlação geral satisfatório de 0,95 para todos os dados. A topologia ideal do modelo de redes neurais *feed-forward* foi alcançada com um arranjo de 10 neurônios dentro de uma camada oculta (3:10:4). De acordo com os gráficos de generalização, as variáveis operacionais influenciaram de forma individual e sinérgica as respostas analisadas. Há uma relação de compromisso com a pureza do produto de topo, representada pela fração mássica do etanol no destilado, e a produtividade, representada pela vazão mássica do destilado. Geralmente, alta pureza é alcançada com vazões de destilado mais baixas, e alta produtividade leva à redução da pureza. Buscando extrair o máximo desempenho da unidade frente a todas as respostas simultaneamente, a otimização baseada em algoritmo genético levou a uma fração mássica de 50,6% de etanol no destilado, 4,91 kg/h de destilado, com um fator de recuperação de 84,9%, e um fator de separação de 57,4. Com relação à avaliação técnico-econômica, a análise de desempenho mostrou que sob uma vazão de alimentação de 14 L/h, uma temperatura de alimentação de 80 °C e uma temperatura de evaporador de 93 °C a unidade atinge o consumo específico mínimo de energia de 571,12 W·h/kg, com uma recuperação máxima de etanol de 40,66%. O impacto dos elementos na parcela do custo de capital mostrou que a instrumentação e controle (27,8%) e tubulação e equipamentos auxiliares (27,6%) são os custos predominantes, enquanto que o custo dos principais equipamentos de processo representa apenas 6,2%, revelando-se uma tecnologia de baixo custo e de fácil implementação. O maior gerador de custos operacionais foi a mão de obra (51,3%), visto que a unidade em escala piloto tem capacidade inferior às plantas industriais. No entanto, a unidade Destubcal gasta com utilidades cerca de 31,6 \$/m³_{alimentado}, o que representa uma economia total de 43,8% em comparação com as destilarias convencionais. Além disso, a unidade Destubcal economiza cerca de 1,78 MJ/kg (46,4%), aliada a uma redução de 59,2% na altura da coluna em comparação a uma coluna convencional, sendo considerada economicamente viável para a recuperação de etanol em grau sanitizante.

Considerações finais: A integração das técnicas de destilação por filme descendente com fornecimento de calor por meio de um termossifão bifásico, que resultou na tecnologia Destubcal, representa melhorias notáveis para o campo das separações térmicas, uma vez que a combinação dessas duas tecnologias bem estabelecidas deu origem a um novo aparato de destilação, mais compacto, mais seguro e mais econômico. Como consequência dos desafios e perspectivas identificados foi possível planejar estratégias para preencher as lacunas encontradas na tecnologia Destubcal, e avançar na consolidação deste processo de destilação intensificada. O modelo baseado em rede térmica conseguiu descrever com boa precisão a dinâmica do fornecimento de calor e pode ser aplicado para o projeto de equipamentos futuros com maior capacidade de processamento e diferentes fins de separação. A modelagem de aprendizado de máquina baseada em redes neurais foi aplicada com sucesso mostrando boa capacidade preditiva, e a técnica de otimização via algoritmo genético conseguiu extrair um desempenho satisfatório da unidade em escala piloto. Por fim, a análise técnico-econômica indicou que a unidade Destubcal em escala piloto tem potencial para ser uma alternativa viável na recuperação de etanol em grau desinfetante, 70 vol% em álcool, e pode ajudar a evitar escassez deste produto causada pela pandemia atual e futuros eventos.

Palavras-chave: Destilação por filme descendente. Termossifão. Intensificação de processos.

ABSTRACT

Worldwide efforts in process intensification led to innovative designs for distillation, notably known as an energy-intensive process. Our research team has been developing a novel thermosyphon-assisted falling film distillation technology, called Destubcal. This apparatus combines the falling film distillation, a well-consolidated technology, with the innovative heat supply through a two-phase closed thermosyphon. Previous experimental studies pointed out that the Destubcal unit is a promising technology in separating different mixtures with energy gains, motivating the continuity towards consolidating this technology as an economically-feasible distillation process. A broad and deep survey in bibliographical bases of published works and deposited patents from the beginning of the 20th Century until nowadays was realized and pointed out knowledge gaps that still limit the popularization of this technology, which must be elucidated. Based on this, the guiding goal of this work is to offer scientific contributions on modeling, control, optimization, and techno-economic evaluation of the pilot-scale thermosyphon-assisted falling film distillation unit to move forward in operational and design improvements, aiming to raise this technology to a higher level of feasibility for industrial separations. The thermal network-based dynamic modeling proposed and validated by dedicated experimental campaigns with the pilot-scale unit accurately predicted the transient behavior and steady-state temperature of the two-phase closed thermosyphon. The experimental and predicted heat transfer coefficients showed reasonable agreement within the $\pm 25\%$ deviation band. A feedback control of the thermosyphon's evaporator temperature was performed in Simulink[®] to manage the steam chamber temperature. PID technique was adopted to achieve faster and smoother the control target, with the secondary effect to reduce mechanical stresses, increasing life cycle, and reducing energy consumption by 3.1%. From a dataset of 64 experimental runs carried out in the pilot-scale unit, a machine learning predictive model based on artificial neural networks was developed. Despite the high non-linearity, the machine learning approach was capable of modeling the process accurately. The optimal topology was achieved with a network arrangement of 10 neurons within one hidden layer (3:10:4), with a correlation coefficient higher than 0.95 for all data. The optimal operating conditions achieved by the genetic algorithm technique were a feed temperature of 90.6 °C, an evaporator temperature of 109.6 °C, and a feed flow rate of 26.3 L/h. The cost impact of the components associated with the construction and installation of the Destubcal unit revealed that instrumentation and control, and piping and auxiliary equipment are the predominant cost elements (more than 55%) of the capital cost, while major process equipment represent a small portion (6.2%), indicating a low capital investment cost when compared to other unconventional distillation devices. The major operating cost-driver is the labor (51.3%) since the pilot-scale unit has a lower capacity than industrial plants. However, the Destubcal unit spends on utility costs about 31.6 $\$/\text{m}^3_{\text{feed}}$, which represents a total saving of 43.8% compared to conventional distilleries. Furthermore, the Destubcal unit saves about 1.78 MJ/kg (46.4%), with 59.2% less column height than a conventional column, being considered techno-economically feasible for sanitizer-grade ethanol (70 vol%) recovery.

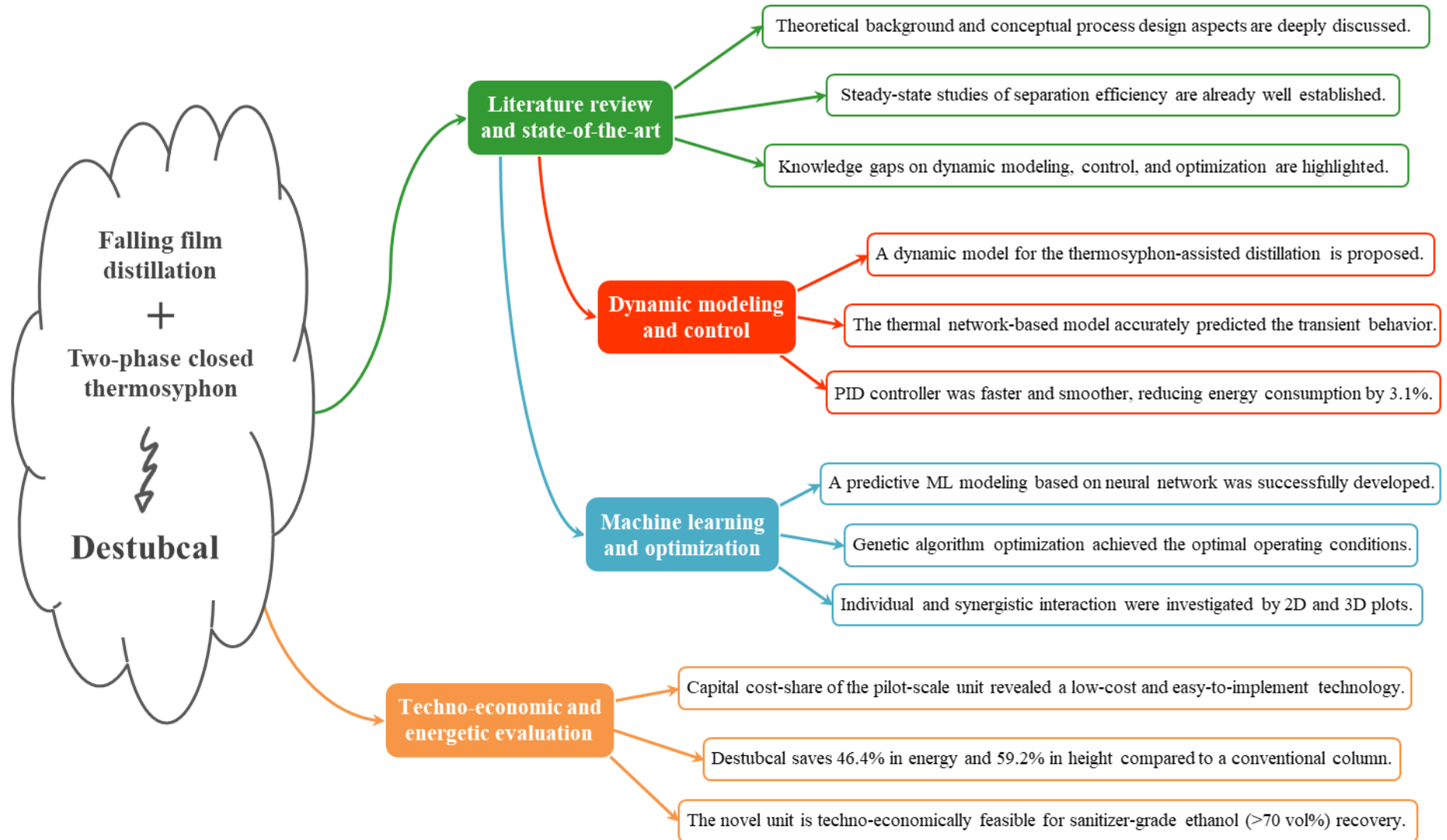
Keywords: Falling film distillation. Two-phase closed thermosyphon. Process intensification.

RESUMO

Esforços mundiais em intensificação de processos têm gerado projetos inovadores de destilação, notadamente conhecida como um processo intensivo energeticamente. Nosso grupo de pesquisa vem desenvolvendo uma tecnologia de destilação por filme descendente assistida por termossifão, denominada Destubcal. Esse aparelho combina a destilação por filme descendente, uma tecnologia já consolidada, com o fornecimento de calor por meio de um termossifão. Estudos experimentais prévios apontaram que a unidade Destubcal é promissora para separação de diferentes misturas, motivando a continuidade dos estudos a fim de consolidar essa tecnologia intensificada. Um amplo levantamento nas bases bibliográficas de trabalhos publicados e patentes depositadas desde o início do século 20 até os dias atuais foi realizado, apontando lacunas de conhecimento que ainda limitam a popularização dessa tecnologia, as quais devem ser elucidadas. O objetivo deste trabalho é oferecer contribuições científicas para modelagem, controle, otimização e avaliação técnico-econômica da unidade de destilação por filme descendente assistida por termossifão em escala piloto, visando elevar essa tecnologia a um nível viável para separações industriais. A modelagem dinâmica baseada em rede térmica validada experimentalmente previu com precisão o comportamento transiente e a temperatura no estado estacionário. Os coeficientes de transferência de calor experimentais e preditos mostraram concordância razoável dentro da faixa de desvio de $\pm 25\%$. A estratégia de controle para a temperatura do evaporador foi realizada em Simulink[®] para rastrear o *setpoint* da temperatura da câmara de vapor. A técnica PID foi adotada para atingir de forma mais rápida e suave a meta de controle, reduzindo tensões mecânicas, aumentando o ciclo de vida e reduzindo o consumo de energia em 3,1%. A partir de 64 experimentos, um modelo preditivo de aprendizado de máquina baseado em redes neurais foi desenvolvido. Apesar da alta não linearidade, a abordagem de aprendizado de máquina foi capaz de modelar o processo com precisão. A topologia ideal foi alcançada com 10 neurônios dentro da camada oculta (3:10:4), com um coeficiente de correlação superior a 0,95. As condições operacionais ótimas obtidas pela técnica de algoritmo genético foram: temperatura de alimentação de 90,6 °C, temperatura do evaporador de 109,6 °C e vazão de alimentação de 26,3 L/h. O impacto do custo dos componentes associados à construção e a instalação da unidade Destubcal revelou que a instrumentação e controle, e a tubulação e equipamentos auxiliares são os elementos de custo predominantes (mais de 55%) no custo de capital, enquanto os equipamentos principais representam uma pequena parcela (6,2%), indicando um baixo custo de investimento de capital quando comparado a outros dispositivos de destilação não convencionais. O maior gerador de custos operacionais foi a mão de obra (51,3%), visto que a unidade em escala piloto tem uma capacidade inferior às plantas industriais. No entanto, a unidade Destubcal gasta com utilidades cerca de 31,6 \$/m³ alimentado, o que representa uma economia de 43,8% em comparação às destilarias convencionais. Além disso, a unidade Destubcal economiza 1,78 MJ/kg (46,4%), com 59,2% menos em altura da coluna quando comparada à uma coluna convencional, sendo considerada técnica-economicamente viável para recuperação de etanol grau sanitizante (70 vol%).

Palavras-chave: Destilação por filme descendente. Termossifão. Intensificação de processos.

CONCEPTUAL MAP OF THE THESIS



LIST OF FIGURES

Figure 1 – Timeline of main historical landmarks for falling film distillation.....	37
Figure 2 – Proportion of publications for each type of process in falling film columns.....	43
Figure 3 – Publication evolution on falling film distillation in wetted-wall columns.....	44
Figure 4 – Temperature, concentration and velocity profiles for falling film distillation in a wetted-wall column: (a) binary; (b) binary with sidewall heating; (c) multicomponent.....	53
Figure 5 – Working principle for molecular distillation.	58
Figure 6 – Monotube falling film distillation designs: (a) Total reflux; (b) Partial reflux; And (c) no reflux. Schematic diagram of an experimental falling film distillation unit (d). Illustration of a monotube longitudinal cross-section column (e). Images of constructed monotube falling film distillation columns: (f) with stainless steel; (g) with borosilicate glass.	61
Figure 7 – Constructive design of multitube wetted-wall distillation columns: (a) Schematic diagrams of cross-section and top view of a 20-equal space-distributed tubes column; (b) Outer shell and inner tube hole images of a multitube steel column; (c) Elevation view diagram of a typical multitube feed distribution system.	62
Figure 8 – Scheme of a two-phase closed thermosyphon.	66
Figure 9 – Glass prototype representation of the thermosyphon-assisted falling film Destubcal technology (a); Thermosyphon closed-cycle operational diagram (b).....	67
Figure 10 – Types of liquid distributors: (a) Perforated ceramic ring; (b) Grooved cone-shaped distributor; (c) Distributor with inclined needles.	71
Figure 11 – Key factors affecting separation efficiency in falling film distillation units.	72
Figure 12 – Behavior of a falling liquid film on the surface of a distillation wetted-wall tube at different feed flow rates.	75
Figure 13 – Schematic diagram of the experimental pilot-scale Destubcal unit.	93
Figure 14 – Photograph of the Destubcal pilot-scale experimental unit (a); Feed cone distributor detail (b); Column cross-sectional detail (c).....	94
Figure 15 – Schematic diagram of the thermosyphon-assisted unit (a) and the thermal network-based model (b).....	97
Figure 16 – Representation of the heat transfer in electrical resistances.....	100
Figure 17 – Representation of the heat transfer in the steam chamber and distillation tube..	101

Figure 18 – Representation of the heat transfer in the evaporator.	102
Figure 19 – Comparison of evaporator temperature predicted by the model and by experimental runs under different power inputs and falling film flow rates: (a) 14 L/h; (b) 17 L/h; (c) 23 L/h; and (d) 32 L/h.	108
Figure 20 – Experimental and predicted overall thermal resistances over input heat powers in the evaporator of the thermosyphon: (a) 14 L/h; (b) 17 L/h; (c) 23 L/h; and (d) 32 L/h.	110
Figure 21 – Comparison between predicted and experimental overall thermal resistance. ...	111
Figure 22 – Comparison between experimentally measured and predicted heat transfer coefficients in the evaporator section (a) and in the condenser section (b).	112
Figure 23 – Control components of model integration in the Simulink® environment.....	115
Figure 24 – Control performance for T_e (a1) and Q_{in} (a2) with Robust Response Time; T_e (b1) and Q_{in} (b2) with Ziegler-Nichols; and T_e (c1) and Q_{in} (c2) with Chien, Hrones and Reswick methods.....	116
Figure 25 – Structure of an artificial neuron.	123
Figure 26 – Effect of the number of neurons on the ML training performance.	129
Figure 27 – Optimal topology of the ML model.	130
Figure 28 – <i>MSE</i> for training, validation, and test data subsets.	131
Figure 29 – Comparison between predicted values by ML model and experimental data. ...	134
Figure 30 – Neural network generalization plots of predicted responses in 3D output surface showing the behavior of ethanol x_D (a ₁), \dot{m}_D (b ₁), RF (c ₁), and SF (d ₁); and 2D contour-line maps of ethanol x_D (a ₂), \dot{m}_D (b ₂), RF (c ₂), and SF (d ₂). All plots are in function of T_F and T_e varying for a fixed $Q_F=23$ L/h.	138
Figure 31 – Neural network generalization plots of predicted responses in 3D output surface showing the behavior of ethanol x_D (a ₁), \dot{m}_D (b ₁), RF (c ₁), and SF (d ₁); and 2D contour-line maps of ethanol x_D (a ₂), \dot{m}_D (b ₂), RF (c ₂), and SF (d ₂). All plots are in function of Q_F and T_F varying for a fixed $T_e = 101.5$ °C.	139
Figure 32 – Neural network generalization plots of predicted responses in 3D output surface showing the behavior of ethanol x_D (a ₁), \dot{m}_D (b ₁), RF (c ₁), and SF (d ₁); and 2D contour-line maps of ethanol x_D (a ₂), \dot{m}_D (b ₂), RF (c ₂), and SF (d ₂). All plots are in function of Q_F and T_e varying for a fixed $T_F = 83$ °C.	140
Figure 33 – Detailed process flowchart of the pilot-scale Destubcal unit.....	145

Figure 34 – Ethanol concentrations achieved in the distillate product under different operating conditions for the feed flow rates of 14 L/h (a), 17 L/h (b), 23 L/h (c), and 32 L/h (d).	155
Figure 35 – Energy and ethanol recovery performance under different operating conditions.	156
Figure 36 – Energy efficiency over the different feed flow rates performed.	157
Figure 37 – Fractional contribution of various cost elements in the CAPEX and OPEX for sanitizer-grade ethanol recovery by the thermosyphon-assisted falling film distillation unit.....	161
Figure 38 – Payback time of the Destubcal unit for different selling prices of commercialized sanitizer-grade ethanol.	165
Figure 39 – Comparison between Destubcal and conventional distillation units for energy load (a) and column height (b).	166

LIST OF TABLES

Table 1 – Scientific contributions of this thesis.	33
Table 2 – Experimental falling liquid film distillation systems in wetted-wall columns.....	46
Table 3 – Deposited patents on falling film distillation in wetted-wall columns.....	50
Table 4 – Modeling and simulation works on falling film distillation in wetted-wall columns.	81
Table 5 – Initial operating process conditions.....	95
Table 6 – Thermal resistance network equations and descriptions.	99
Table 7 – Tuned PID controller parameters.	114
Table 8 – Performance of PID controller tuning methods.....	118
Table 9 – Process operating conditions of input variables.	128
Table 10 – Optimal values of weights and biases for the ML model.....	132
Table 11 – Optimal conditions determined by the ML-GA method.	141
Table 12 – Experimental operating conditions adopted in the pilot-scale unit.	146
Table 13 – Appraised cost of components associated with the construction of the Destubcal pilot-scale thermosyphon-assisted falling film distillation unit.	159

LIST OF ABBREVIATIONS AND ACRONYMS

2D	Two-dimensional
3D	Three-dimensional
ANN	Artificial neural network
CAPEX	Capital expenditure
CFD	Computational fluid dynamics
DWC	Dividing-wall column
GA	Genetic algorithm
HETP	Height equivalent to the theoretical plate
HIDiC	Heat-integrated distillation column
HOG	Height of an overall gas transfer unit
HTU	Height of a transfer unit
ML	Machine learning
OPEX	Operational expenditure
TPCT	Two-phase closed thermosyphon
VOF	Volume of fluid
WHO	World health organization

LIST OF SYMBOLS

Symbol	Description	Unit (SI)
A	Area or net input argument	$\text{m}^2, -$
b	Bias term for a neuron	-
\mathbf{b}	Bias vector for a layer	-
C	Thermal capacity	J/K
CC	Capital cost of distillation unit	\$
C_{fer}	Fermentation operating cost	\$/yr
C_{elec}	Annual electrical cost	\$/yr
c_p	Specific heat at constant pressure	J/kg·K
CPL	Cost of distilled ethanol per liter	\$/m ³
D_{12}	Mass diffusivity	m ² /s
d	Diameter	m
E	Error function	-
$e(t)$	Error signal	-
f	Plant availability factor	%
F	Feed flow rate	m ³ /s
g	Gravity acceleration	m/s ²
grad	Gradient of performance function	-
h	Convective heat transfer coefficient	W/m ² ·K
H	Enthalpy	J/kg
i	Interest rate	%
IW	Input weight matrix	-
k	Thermal conductivity	W/m·K
k_G	Gas-phase mass transfer coefficient	kg/m ² ·s
k_L	Liquid-phase mass transfer coefficient	kg/m ² ·s
k_v	Vapor-phase mass transfer coefficient	kg/m ² ·s
K_d	Derivative time of PID controller	-
K_i	Integral time of PID controller	1/s
K_p	Proportional gain of PID controller	s
$logsig$	Log-sigmoid transfer function (Matlab syntax)	-

L	Length or total number of weights and biases	m, -
LW	Layer weight matrix	-
m	Mass or number of artificial neurons	kg, -
\dot{m}	Mass flow rate	kg/s
MSE	Mean-squared-error (performance function)	-
M_{yearly}	Annual distillate production	m ³
n	Number of input variables or plant lifetime	-, yr
N	Number of elements or number of experimental runs	-
N_t	Number of transfer units	-
<i>purelin</i>	Linear transfer function (Matlab syntax)	-
P	Pressure	Pa
P_c	Critical pressure	Pa
P_{evap}	Power supplied to the evaporator	W
q	Heat transfer flux	W/m ²
Q	Energy flux or volumetric flow rate	W, m ³ /h
r	Radius	m
R	Thermal Resistance or correlation coefficient	m ² ·K/W, -
RF	Recovery factor	%
RR	Recovery ratio	%
SF	Separation factor	-
SP	Selling price of sanitizer-grade ethanol	\$/L
$STEC$	Specific thermal energy consumption	W·h/kg
T	Temperature	K
T_c	Critical temperature	K
t	Time	s
<i>tansig</i>	Hyperbolic tangent sigmoid transfer function (Matlab syntax)	-
u	Velocity	m ² /s
$u(t)$	Control signal	-
V	Volume	m ³
w	Weight (neural network connection)	-
W	Vector of current weights and biases	-
x	Liquid-phase mass fraction	-

\mathbf{x}	Vector of normalized input variables	-
x_i	Normalized level of input variable	-
x_1, x_2, x_3	Normalized levels of input variables	-
y	Vapor-phase mass fraction or normalized output variable	-
Y	Performance index (experimental value/target)	-
\hat{Y}	Performance index (predicted value/network output)	-
$\hat{\mathbf{Y}}$	Vector of network output predicted values	-
z_i	Actual level of input variable	-
z_1, z_2, z_3, z_4	Actual levels of input variables	-

Greek alphabet

α	Thermal diffusivity	m^2/s
Γ	Wetting rate	$\text{kg}/\text{m}\cdot\text{s}$
δ	Film thickness	m
η	Learning rate	-
η_p	Finance payback time	yr
Δ	Variation difference	-
ΔL	Small amount for network extrapolation capability	-
ΔU	Small amount for network extrapolation capability	-
λ	Net input argument	-
μ	Dynamic viscosity	Pa/s
π	Pi number	-
ρ	Specific mass	kg/m^3
σ	Superficial tension	N/m^2
τ	Time constant	s
ν	Kinematic viscosity	m^2/s
Ψ	Vector of transfer function	-

Dimensionless numbers

Ka	Kapitza number
Ga	Galilei number
Gr	Grashof number
Nu	Nusselt number

Pr	Prandtl number
Ra	Rayleigh number
Re	Reynolds number
Sc	Schmidt number
Sh	Sherwood number

Subscripts and superscripts

<i>amb</i>	Ambient
<i>atm</i>	Atmospheric
<i>av</i>	Average
<i>b</i>	bulk
<i>B</i>	Bottom stream
<i>cond</i>	Condensation
<i>conv</i>	Convection
<i>D</i>	Distillate stream
<i>e</i>	Evaporator, external
<i>exp</i>	Experimental value
<i>etOH</i>	Ethanol component
<i>f</i>	film
<i>F</i>	Feed stream
<i>G</i>	Gas
<i>H₂O</i>	Water component
<i>i</i>	Component, interface, iteration index
<i>in</i>	Input
<i>iso</i>	Insulation
<i>j</i>	Component, interface, iteration index
<i>k</i>	Integer number showing the layer of ML
<i>L, l, ℓ</i>	Liquid
<i>lv</i>	Phase change
<i>m</i>	Integer variable (subscript)
<i>max</i>	Maximal level
<i>min</i>	Minimal level
<i>n</i>	N th integer number (iteration index)

<i>norm</i>	Normalized value
<i>out</i>	Outlet
<i>pred</i>	Predicted value
<i>q</i>	Positive integer number (iteration index)
<i>s</i>	Stainless steel
<i>sat</i>	Saturation
<i>r</i>	Electrical resistance
<i>t</i>	Total
<i>trans</i>	Transferred
<i>V, v</i>	Vapor
<i>z</i>	Z direction
<i>w</i>	Wall

TABLE OF CONTENTS

1	INTRODUCTION	28
1.1	MOTIVATION.....	29
1.2	OBJECTIVES.....	30
1.2.1	General objective	30
1.2.2	Specific objectives	30
1.3	STRUCTURE OF THE THESIS	31
2	A BACKGROUND REVIEW ON FALLING FILM DISTILLATION IN WETTED-WALL COLUMNS: FROM FUNDAMENTALS TOWARDS INTENSIFIED TECHNOLOGIES.....	34
2.1	INTRODUCTION	34
2.2	BACKGROUNDS AND CHRONOLOGY	36
2.3	STATE-OF-THE-ART OF FALLING FILM DISTILLATION.....	42
2.4	BASIC CONCEPTS AND WORKING PRINCIPLES.....	51
2.4.1	Binary falling film distillation.....	54
2.4.2	Multicomponent falling film distillation.....	55
2.4.3	Molecular distillation.....	57
2.5	PROCESS DESIGN AND COLUMN CONFIGURATIONS	59
2.5.1	Monotube columns	60
2.5.2	Multitube columns	61
2.5.3	Flat-plate columns	63
2.5.4	Internally heat-integrated columns.....	64
2.5.5	Thermosyphon-assisted columns.....	65
2.5.6	Feed liquid distributors	70
2.6	SEPARATION EFFICIENCY ASPECTS	72
2.6.1	Feed temperature.....	73
2.6.2	Feed flow rate.....	74

2.6.3	Operational pressure	76
2.6.4	Film thickness	77
2.6.5	Interfacial area	78
2.7	MODELING AND SIMULATION APPROACHES	80
2.7.1	Analogy between distillation and absorption	86
2.8	INDUSTRIAL APPLICATIONS	87
2.9	SUMMARY AND CONCLUDING REMARKS	88
3	DYNAMIC MODELING WITH EXPERIMENTAL VALIDATION AND CONTROL OF A TWO-PHASE CLOSED THERMOSYPHON AS HEAT SUPPLIER OF A NOVEL PILOT-SCALE FALLING FILM DISTILLATION UNIT	90
3.1	INTRODUCTION	90
3.2	EXPERIMENTAL METHODOLOGY	93
3.2.1	Description of the pilot-scale unit	93
3.2.2	Operating conditions and experimental assessment	95
3.3	DYNAMIC MODELING	96
3.3.1	Thermal network model	96
3.3.1.1	<i>Thermal balance in the electrical resistances</i>	100
3.3.1.2	<i>Thermal balance in the steam chamber and distillation tube</i>	101
3.3.1.3	<i>Total balance for the evaporator</i>	102
3.3.1.4	<i>Correlations for the heat transfer coefficients</i>	103
3.3.1.5	<i>Falling film distillation material balance</i>	106
3.3.2	Numerical simulation procedure	106
3.4	MODEL VALIDATION	107
3.4.1	Numerical and experimental behavior	107
3.4.2	Heat transfer analysis	109
3.5	CONTROL STRATEGY PROPOSAL	112
3.5.1	Control design	112

3.5.1.1	<i>PID controller</i>	113
3.5.1.2	<i>Tuning methods</i>	113
3.5.1.3	<i>Controller performance</i>	114
3.5.2	Control analysis results	115
3.6	SUMMARY AND CONCLUDING REMARKS	118
4	MACHINE LEARNING MODELING AND GENETIC ALGORITHM-BASED OPTIMIZATION OF A NOVEL PILOT-SCALE THERMOSYPHON-ASSISTED FALLING FILM DISTILLATION UNIT	120
4.1	INTRODUCTION	120
4.2	THEORETICAL BACKGROUND ON ML MODELING AND GA OPTIMIZATION.....	122
4.2.1	ML modeling	122
4.2.2	GA optimization	124
4.3	METHODOLOGY	126
4.3.1	Experimental procedure	126
4.3.2	Data normalization	127
4.3.3	Model development and optimization procedure	127
4.4	RESULTS AND DISCUSSIONS	129
4.4.1	ML modeling	129
4.4.2	GA optimization	141
4.5	SUMMARY AND CONCLUDING REMARKS	142
5	TECHNO-ECONOMIC AND ENERGETIC ASSESSMENT OF AN INNOVATIVE PILOT-SCALE THERMOSYPHON-ASSISTED FALLING FILM DISTILLATION UNIT FOR SANITIZER-GRADE ETHANOL RECOVERY	143
5.1	INTRODUCTION	143
5.2	EXPERIMENTAL SETUP AND METHODS	145
5.2.1	Pilot-scale plant description	145

5.2.2	Thermosyphon-assisted distillation performance.....	146
5.2.2.1	<i>Recovery ratio.....</i>	146
5.2.2.2	<i>Specific thermal energy consumption.....</i>	147
5.2.3	Energy efficiency.....	147
5.3	TECHNO-ECONOMIC ASSESSMENT.....	148
5.3.1	Capital expenditure	148
5.3.1.1	<i>Major thermosyphon-assisted process equipment.....</i>	148
5.3.1.2	<i>Piping and auxiliary equipment.....</i>	148
5.3.1.3	<i>Instrumentation and control system.....</i>	149
5.3.1.4	<i>Construction and installation</i>	150
5.3.1.5	<i>Fermentation capital cost.....</i>	150
5.3.1.6	<i>Annualized capital cost.....</i>	150
5.3.2	Operating expenditure	151
5.3.2.1	<i>Electricity.....</i>	151
5.3.2.2	<i>Cooling water</i>	151
5.3.2.3	<i>Fermentation operating cost.....</i>	152
5.3.2.4	<i>Labor</i>	152
5.3.2.5	<i>Other operating costs</i>	152
5.3.3	Financial analysis.....	153
5.3.4	Comparative assessment with a conventional column	153
5.4	RESULTS AND DISCUSSIONS	154
5.4.1	Thermosyphon-assisted distillation performance.....	154
5.4.2	Energy efficiency.....	157
5.4.3	Techno-economic assessment.....	158
5.4.4	Comparative evaluation	165
5.5	SUMMARY AND CONCLUDING REMARKS	167
6	CONCLUSIONS.....	168

6.1	TECHNOLOGY PERSPECTIVES AND FUTURE DEVELOPMENTS.....	169
	REFERENCES	170
	APPENDIX A – Constructive design data of the apparatus	211
	APPENDIX B – Thermophysical properties of materials	212
	APPENDIX C – Material balance data of the falling film distillation.....	214
	APPENDIX D – Experimental dataset for the ML modeling	215

1 INTRODUCTION

Undoubtedly, distillation remains as the most important thermal separation method in the chemical process industry. However, despite its many known benefits and its widespread use, the main disadvantage of the conventional distillation is the high energy requirement. It is estimated more than 40,000 distillation columns consuming about 40% of the total energy used in petrochemical and chemical process industries in North America, for example (JANA, 2017; RODRÍGUEZ; LI; DÍAZ, 2017). Besides, distillation columns can account for over 50% of the operating cost of an industrial chemical process facility (BATTISTI *et al.*, 2019; WEI *et al.*, 2012). Towards reducing energy expenditure in distillation processes, our research team is developing a novel distillation apparatus, called Destubcal technology. It operates by falling film technique, which is a widely known and well-established approach (WEN *et al.*, 2020), and is assisted by a two-phase closed thermosyphon, a special type of heat pipe, which is responsible for supplying energy to the distillation process (BATTISTI *et al.*, 2020b).

Basically, the Destubcal technology consists of a vertical tube surrounded by a steam chamber in which the liquid flows down by gravity, creating a thin film through the walls of the distillation tube. The energy provided by the two-phase closed thermosyphon supports the thermal separation of the chemical components of the film within the distillation tube, promoting mass and heat transfer from the liquid phase (film) to the vapor phase flowing countercurrent to the liquid (BATTISTI; MACHADO; MARANGONI, 2020). The two-phase closed thermosyphon is a gravity-assisted wickless heat pipe where heat is delivered in the bottom by the evaporator and removed in the condenser region, being considered a more reliable and low-maintenance device (MANTELLI; ÂNGELO; BORGES, 2010). It resulted in a compact, safer, and less energy-consumer apparatus when compared to conventional distillation columns (ALVES *et al.*, 2020).

The pilot-scale Destubcal unit already has demonstrated feasibility in separating several feedstocks such as ethanol-water binary mixture (MARANGONI *et al.*, 2019b, 2019a), aromatic mixture (containing toluene, para-xylene, meta-xylene, ortho-xylene, and ethylbenzene) (SILVA FILHO *et al.*, 2018), monoethylene glycol-water mixture (PIRES *et al.*, 2020), and synthetic petrochemical naphtha (QUERINO; MACHADO; MARANGONI, 2019; QUERINO; MARANGONI; MACHADO, 2018). The main distinguishing feature over conventional falling film distillers is that Destubcal unit operates under atmospheric pressure

inside the distillation tube, thus avoiding high vacuum operating costs, as occurs with the molecular or short-path distillation (BATTISTI *et al.*, 2020a).

The promising results previously obtained in the pilot-scale unit encouraged the research group to move forward towards consolidating the Destubcal technology as an advanced distillation process ready to be scaled-up to industrial chemical plants. Modern process plants have reached a high degree of complexity, which require systematic design methodologies and model-based approaches to ensure correct and competitive performance. In this sense, simulation has therefore become a decisive tool in solving engineering problems. Through its use it is possible to predict the behavior of processes, seeking to optimize operability, thus maximizing profits and productivity. Therefore, the present study presents technological and scientific advances in understanding the dynamic behavior of the novel Destubcal process, the interrelation and dependence between operational variables, and the techno-economic viability of the pilot-scale unit. Hence, this work seeks to expand and consolidate the knowledge about Destubcal technology, in order to open up future paths for optimized strategies aimed at minimizing costs and maximizing productivity of the unit.

1.1 MOTIVATION

Since the pilot-scale unit was constructed, the thermosyphon-assisted falling film distillation process has been extensively explored experimentally under different process and operating conditions. However, in order to consolidate this process with possible industrial-scale viability, a broad dynamic and techno-economic knowledge of the unit is necessary. Direct manipulation of process variables is not always possible and feasible, as it could drive major drawbacks regarding the continuity of the process, with the consequence of large productivity losses. A quick and less expensive way to obtain information about the dynamic behavior of a process is from the development of mathematical models and process simulation. Simulation is an extremely important tool for engineers, as it allows the analysis of the stability and the behavior of the process, in order to effectively control the process. Although there are a large number of studies in the literature dedicated to the study of mathematical models for dynamic two-phase closed thermosyphons operation, there is no model developed with the purpose of supplying heat to a falling film distillation process. This is one innovative differential that motivated the development of this thesis.

Besides, the second point that motivated the development of this work was the need to find optimal process parameters and operating conditions for the pilot-scale unit. For this end, using the ethanol-water representative mixture, a machine learning modeling based on artificial neural networks was established, highlighting that this model-based is unprecedented for the thermosyphon-assisted falling film distillation process. This non-parametric type of modeling facilitates the application as objective functions in optimization algorithms, since this model uses fewer process parameters, and consequently, runs faster when compared to complex phenomenological models. As a third relevant aspect in terms of motivations, the increasing demand for ethanol-based sanitizers and disinfectants due to the COVID-19 pandemic has driven the emergence of innovative strategies to avoid the risk of shortage of this product, and reducing production costs. Therefore, a techno-economic and energetic assessment of the novel pilot-scale thermosyphon-assisted falling film distillation unit was performed for recovering ethanol at 70 vol%, considered a suitable sanitizing degree according to recommendations established by WHO and the Brazilian health regulatory agency.

1.2 OBJECTIVES

1.2.1 General objective

The general objective of this study is to offer scientific contributions on modeling, control, optimization, and techno-economic assessment of the pilot-scale falling film distillation unit assisted by a two-phase closed thermosyphon, aiming to move forward towards consolidating this technology as an advanced distillation process.

1.2.2 Specific objectives

To accomplish the main purpose described above, the following specific objectives are proposed:

- a) To address theoretical backgrounds and fundamental concepts of the falling film distillation in wetted-wall columns produced over the years since the mid-last century, in order to assist for future innovation perspectives on this technology;

- b) To develop and experimentally validate a thermal network-based dynamic modeling with control system tuning (using PID techniques) for the two-phase closed thermosyphon as a heat supplier to the pilot-scale falling film distillation plant;
- c) To implement a machine learning predictive model based on artificial neural networks for the separation of the ethanol-water binary mixture, aiming to optimize the process operating conditions via genetic algorithm technique;
- d) To evaluate techno-economically and energetically the pilot-scale thermosyphon-assisted falling film distillation unit applied to recover sanitizer-grade ethanol in the suitable concentration of 70 vol% in alcohol.

1.3 STRUCTURE OF THE THESIS

To facilitate the comprehension, this work is divided into six chapters. Apart from this introduction, the content of the following chapters is based on the four manuscripts published in international journals, as listed by the scientific contributions in Table 1. It is important to highlight that chapters 2, 3, 4, and 5 consist of four articles already published in different international journals with outstanding scientific reputation and high impact factor. In each of the chapters, the experimental apparatus and procedures are described as well as the pertinent literature review and concluding remarks. The summary content of the chapters is described below:

- Chapter 2: **A background review on falling film distillation in wetted-wall columns: From fundamentals towards intensified technologies** ⇒ In this chapter, a historical perspective of theoretical and experimental works as well as deposited patents on falling film distillation and wetted-wall columns from the beginning of 20th Century to present are reviewed through a broad and deep survey in bibliographical bases. Theoretical background and conceptual aspects related to efficiency improvement and process intensification were deeply discussed, aiming to guideline future perspectives for this technology at separation processes.

- Chapter 3: **Dynamic modeling with experimental validation and control of a two-phase closed thermosyphon as heat supplier of a novel pilot-scale falling film distillation unit** ⇒ This chapter is dedicated to the thermal network-based dynamic modeling and control design for the two-phase closed thermosyphon coupled to the falling film distillation unit. The model is validated by dedicated experimental campaigns with the pilot-scale unit, and thus the proposed model was implemented in the Simulink® environment in order to design and tune the thermosyphon temperature feedback control system acting on the electrical resistances power.
- Chapter 4: **Machine learning modeling and genetic algorithm-based optimization of a novel pilot-scale thermosyphon-assisted falling film distillation unit** ⇒ In this chapter, a machine learning predictive model based on artificial neural networks is implemented for the ethanol–water binary mixture separation in order to evaluate the performance of this energy-intensified distillation process. The predictive abilities of the model were harnessed to investigate individual and synergistic interaction effects of the operating variables by plotting generalization graphs, and the optimal operating conditions were evaluated simultaneously by the genetic algorithm technique.
- Chapter 5: **Techno-economic and energetic assessment of an innovative pilot-scale thermosyphon-assisted falling film distillation unit for sanitizer-grade ethanol recovery** ⇒ Motivated by the emergency of the COVID-19 pandemic, the chapter 5 aims to provide further knowledge about the techno-economic feasibility of the pilot-scale thermosyphon-assisted falling film distillation unit applied to recover sanitizer-grade ethanol with the minimum 70 vol% in alcohol, considered a suitable concentration for sanitization purposes according to WHO and Brazilian health agency guidelines. In addition, energetic and structural analyses were performed to compare the Destubcal technology to a conventional tray distillation column for the same ethanol-enriched recovering degree.
- Chapter 6: **Conclusions** ⇒ Although at the end of each chapter partial concluding remarks are listed, in the last chapter of the thesis the general conclusions are presented and some suggestions for future works are also provided.

Table 1 – Scientific contributions of this thesis.

Chapter	Published journal	Article
2		BATTISTI, R.; MACHADO, R. A. F.; MARANGONI, C. A background review on falling film distillation in wetted-wall columns: From fundamentals towards intensified technologies. Chemical Engineering and Processing - Process Intensification , v. 150, p. 107873, 2020.
3		BATTISTI, R.; CLAUMANN, C. A.; MANENTI, F.; MACHADO, R. A. F.; MARANGONI, C. Dynamic modeling with experimental validation and control of a two-phase closed thermosyphon as heat supplier of a novel pilot-scale falling film distillation unit. Computers & Chemical Engineering , v. 143, p. 107078, 2020.
4		BATTISTI, R.; CLAUMANN, C. A.; MANENTI, F.; MACHADO, R. A. F.; MARANGONI, C. Machine learning modeling and genetic algorithm-based optimization of a novel pilot-scale thermosyphon-assisted falling film distillation unit. Separation and Purification Technology , v. 259, p. 118122, 2021.
5		BATTISTI, R.; GALEAZZI, A.; PRIFTI, K.; MANENTI, F.; MACHADO, R. A. F.; MARANGONI, C. Techno-economic and energetic assessment of an innovative pilot-scale thermosyphon-assisted falling film distillation unit for sanitizer-grade ethanol recovery. Applied Energy , v. 297, p. 117185, 2021.

Source: The author (2021).

2 A BACKGROUND REVIEW ON FALLING FILM DISTILLATION IN WETTED-WALL COLUMNS: FROM FUNDAMENTALS TOWARDS INTENSIFIED TECHNOLOGIES

The content of this chapter is based on the following published article:

BATTISTI, Rodrigo; MACHADO, Ricardo Antonio Francisco; MARANGONI, Cintia. A background review on falling film distillation in wetted-wall columns: From fundamentals towards intensified technologies. **Chemical Engineering and Processing - Process Intensification**, v. 150, p. 107873, 2020. DOI: 10.1016/j.cep.2020.107873.

2.1 INTRODUCTION

Distillation is one of the most important thermal separation methods in chemical process industry. However, despite its numerous known benefits and widespread use, the main drawback of conventional distillation is the significant energy requirement, since distillation columns may be responsible for more than 50% of the operational cost of an industrial chemical facility (ANEESH *et al.*, 2016; ARPORNWICHANOP; KOOMSUP; ASSABUMRUNGRAT, 2008; BATTISTI *et al.*, 2019; WEI *et al.*, 2012). With the increasing need for improved energy efficiency processes, coupled with the search for higher yields and purity on separations, the distillation column is considered a priority unit to be optimized. Thus, significant efforts have been made to develop intensified configurations, with smaller size and higher energy efficiency (KISS; LANDAETA; FERREIRA, 2012; OLUJIC *et al.*, 2009; YILDIRIM; KISS; KENIG, 2011; ZAKHAROV; MARTYNOVA; PRUSACHENKOVA, 2018). The concept of process intensification is quite interesting from the industrial point of view, since small volumes are used; so the safety is significantly improved and the size of the separation processes also tends to be reduced (MONNIER; KANE; FALK, 2012; PORTHA; FALK; COMMENGE, 2014). These characteristics are achieved by falling film technology, which is already well known and studied for decades (ÅKESJÖ *et al.*, 2017; KANE *et al.*, 2011; RIBATSKI; JACOBI, 2005).

In falling film technology, a thin liquid film flows over a vertical or inclined surface in the presence of an adjacent gas or vapor layer (KALLIADASIS *et al.*, 2012). This technique has inherent advantages as short contact time between the process fluid and the

heated surface, high heat transfer coefficients, minimal pressure drop, minimal static head, and small process fluid holdup (ALHUSSEINI; TUZLA; CHEN, 1998). Short contact time is desirable when processing heat-sensitive fluids because it minimizes thermal degradation effects; High heat transfer coefficients are mainly due to the large specific surface area; Minimization of pressure drop is a key advantage when handling viscous liquids as is often the case of chemical specialties and polymer industries; Absence of static head minimizes boiling point elevation which is especially important in processes conducted under vacuum conditions; And the small process fluid holdup is important when handling environmentally hazardous fluids (ÅKESJÖ *et al.*, 2018; ALHUSSEINI; TUZLA; CHEN, 1998; ZUÑIGA LIÑAN *et al.*, 2012). Not surprisingly, this class of flow has attracted the attention of researchers around the world since the beginning of last century. Consequently, falling films columns have a wide range of technological applications, in particular concerning the processes involving simultaneous heat and mass transfer (HUANG; HU; DENG, 2018; LU *et al.*, 2017; WANG *et al.*, 2010). Typical industrial examples include evaporators (ZHOU; YU; GAO, 2019), coolers (ARMBRUSTER; MITROVIC, 1998), reactors and microstructured reactors (RUSSO *et al.*, 2019; YEONG *et al.*, 2004; ZANFIR *et al.*, 2005), vapor condensation (FORD; MISSEN, 1968), gas rectification (RAICHLE; BILLET, 1965), absorption (NOSOKO; MIYARA; NAGATA, 2002), desorption (DETERMAN; GARIMELLA, 2011), distillation (BLAKE; WILLOCKS, 1981), and seawater desalination industrial plants (MACIVER *et al.*, 2005).

Although falling film columns, also called in literature of wetted-wall columns, have been widely used for heat and mass transfer research in the last century, relatively few papers address the mass transfer characteristics under distillation conditions. Sparse studies were conducted over the years to evaluate the contribution of the liquid-side resistance in the overall mass transfer resistance, i.e., the relative liquid phase resistance in distillation setup (REJL *et al.*, 2016). Nevertheless, the works that have been proposed to study the falling film technology in distillation condition pointed out prominent advantages in this operation, such as a process with low residence time and simple constructive structure when compared to conventional tray distillation, besides the high heat and mass transfer rates due to the small thickness flowing in the longitudinal direction of the inner wall of the distillation surface (BATISTELLA; MACIEL, 1996; HAIDL *et al.*, 2016). All these features lead to the desirable process intensification yearnings combined with expected productivity that a separation process like distillation needs to provide, as lower production costs, inherently

safer process designs, improved energy efficiency, and a sustainable use of resources. Highlighting these unique favorable characteristics as potentialities that falling film distillation in wetted-wall columns can provide is one of the main motivations that led to the elaboration of this work.

Despite all these advantages, the concepts of falling film distillation in wetted-wall columns are still relatively little used in large-scale applications. The scale-up of chemical processes is not such a trivial process and requires a certain understanding of the involved steps (PICCINNO *et al.*, 2016). For the scale-up of a distillation column from the laboratory scale to the industrial scale it is necessary the knowledge of many constructive and operational parameters. If the process to be developed is a modification of an existing large-scale process, enough knowledge may be available to allow the design of the new equipment in a way that ensures the specifications of the products (SCHOENMAKERS; SPIEGEL, 2014). At this point, it is important to highlight the considerable importance of this literature review, which methodologically gathers the theoretical backgrounds and fundamental concepts of falling liquid film distillation in wetted-wall columns produced over the years, to assist for future innovation perspectives on this technology, and motivating the dissemination of these devices, which are still relatively restricted to laboratories, for large-scale applications. The novelty of this literature review is the historical and conceptual approach of the technological progress of falling film distillation in wetted-wall columns through published works and patents since the mid-last century. In addition, a deep discussion of the key factors in separation efficiency for these columns are made, as well as the main modeling and simulation approaches already used in the solution of momentum, heat and mass transfer phenomena for this process.

2.2 BACKGROUNDS AND CHRONOLOGY

Due to its several advantages as the ability to handle a wide range of feed flow rates, the ability to separate feeds with a wide range of concentrations, and the ability to produce high product purity, virtually no other separation technique can compete with distillation in terms of large-scale capacity (SMITH; JOBSON, 2000). Even so, this process carries as the main disadvantage a high energy requirement and a low thermodynamic efficiency, which in general, for a conventional distillation column, ranges from 5% to 18% (ARAÚJO; BRITO; VASCONCELOS, 2007; HASELDEN, 1958; KISS, 2013). This issue was ignored until the

first and second energy crises in the mid-1970s and early 1980s, respectively, when process industries were confronted to the explosion of oil and energy prices (KISS; OLUJIC, 2014). Figure 1 shows a representative timeline of the main historical landmarks for falling film distillation in wetted-wall columns, from the first study reported in the literature until to the year of 2020.

Figure 1 – Timeline of main historical landmarks for falling film distillation.



Source: Battisti, Machado and Marangoni (2020).

In terms of visibility of the contributions by the academic community, the year 1946 was considered a favorable landmark for distillation. Many advances were made until 1945, but were not published due to wartime restrictions. In 1946, the publication of data on wartime projects was already widespread, and this led to a significant increase in knowledge about distillation (WALSH, 1947). Published articles about distillation can be conveniently

grouped according to the direction in which they have extended the boundaries of past information. Concerning falling film processes, at that particular time, some researchers had already investigated the mass transfer in wetted-wall columns. In several studies, the evaporation of pure liquids into air streams had already been published. These experiments, as opposed to distillation in a wetted-wall column, are suitable for measuring gas-phase resistance, since there is no liquid side resistance to mass transfer (CRAUSE; NIEUWOUDT, 1999). Gilliland and Sherwood (1934) were the pioneers in the use of wetted-wall columns for studies of gas-phase mass transfer. They published extensive data about vaporization of nine different pure liquids. The authors further proposed an empirical mass transfer correlation that satisfactorily represented the experimental conditions, and later, with proper compliance, to express the total resistance as the sum of the liquid film and vapor core resistances. At the same time, Chilton and Colburn (1934) obtained, albeit limited, important data on the vaporization of water into air in a pilot-scale falling film tower. A year later, the same authors introduced the concept of height of a transfer unit (H_i), and number of transfer units (N_i), as a measure of the difficulty of a separation (CHILTON; COLBURN, 1935).

Less than ten years later, the results of falling film distillation on two different types of equipment were simultaneously published. Johnstone and Pigford (1942) were able to verify the separation factor in four wetted-wall distillation systems, and concluded that the liquid film resistance could be considered negligible. Surowiec and Furnas (1942) investigated the distillation of ethanol-water system, and based their conclusions on the applicability of the correlation of Gilliland and Sherwood (1934). Liquid film resistances were reported to be 30% to 40% of the total resistance, indicating acceptable liquid film resistance present; however, this was considered to be within the experimental error, showing that there was still much uncertainty in the extracted experimental data.

At that moment, investigations of mass transfer on wetted-wall columns were showing results that were not fully converging for all studied cases. Because of this, Jackson and Ceaglske (1950) were dedicated to perform a work to offer a refinement in the technique, with the expectation that these differences could be reconciled, particularly for the falling film distillation process. The primary objective was the direct comparison of vaporization (transfer of a component in one direction) with distillation (equimolar, counter-diffusion) in the same equipment. Also, the available data for partial reflux distillation were scarce, which led them to study this parameter in the separation experiments. In packed columns, earlier published results showed that undesirable liquid channeling occurred frequently, and the surface area

available for mass transfer varied, couldn't being accurately estimated. This observation led Lindsey, Kiefer and Huffines (1952) to predict that a series of small wetted-wall pipes could be an excellent rectifying device. Thus, from this insight, the authors proposed the first multitubular falling film distillation column, composed of seven equal distributed tubes, only modifying a single batch distillation apparatus already existing in the laboratory.

Contributions in distillation processes until the early 1960s were summarized in a review article from Dodge (1963), where, according to the author, for the discussion at the time, the term "evaporation" was considered synonym of "distillation". Although evaporation is the most common term in general chemical engineering practice, in the case of seawater desalination, distillation seemed to be the most appropriate term to use. Also, three main characteristics of the distillation processes must be distinguished: (I) they separate the water directly, using a liquid-vapor interface; (II) can use heat or work (mechanical and, indirectly, electrical), and; (III) the energy requirement is not directly related to the latent heat of vaporization. In other words, heat to vaporize water must be largely recovered if the energy requirement is maintained within practical limits.

Historically, distillation has been studied as a purely mass transfer process, where diffusion occurs through the liquid-vapor interface. From the 1960s, aspects of heat transfer began to be considered. However, the effect of heat transfer was only considered secondary an independent source for mass transfer. Kayihan, Sandall and Mellichamp (1975) presented an important theoretical approach to examine the simultaneous process of heat and mass transfer from binary distillation in falling film columns. This new approach made it possible to obtain the individual mass transfer coefficients in the liquid film from the distillation experiments by measuring the temperatures and compositions of the liquid phase as column height functions. The same authors, using this new theoretical approach in a following work (KAYIHAN; SANDALL; MELLICHAMP, 1977), were able to experimentally determine the individual mass transfer coefficients, proving that the mechanism that controls the distillation in falling film is the vapor-phase diffusion.

The state of the liquid phase is critical since it determines whether or not all of the resistance to the mass transfer is in the vapor phase. For the wetted-wall distillation column of the methanol-water binary system, Kayihan, Sandall and Mellichamp (1977) found that the liquid phase was saturated, i.e., the measured liquid phase bulk temperature and bulk composition were found to be on the bubble point curve. This indicated that for their system, the mass transfer resistance resides completely in the vapor phase. Also, according to Bravo

and Fair (1982), the individual mass transfer coefficients show a type of dependence on two key variables, such as diffusivity and velocity, the latter being quantified by the Reynolds number. Therefore, although the diffusivity of the chemical species in the liquid phase being lower than in the vapor phase, the Reynolds number of the falling liquid film must be higher than the Reynolds number of the rising vapor. So, in this case, the Reynolds number of the vapor phase should control the mass transfer coefficient.

The 1980s are marked by great advances in mathematical modeling and simulation of miscible liquid separation systems. Until then, computational tools for design and simulation of multistage separation processes, such as distillation and absorption, were based on the equilibrium stage-based approach models that were already well-established at that time (HENLEY; SEADER, 1981; HOLLAND, 1975; KING, 1980). Concerning falling film distillation, a relatively successful non-equilibrium stage-based model was proposed by Krishnamurthy and Taylor (1985a). This model was applied to predict the temperature profile and composition of a wetted-wall distillation processes and a tray column distillation, and then, extended for a packed distillation column and an absorption tower (KRISHNAMURTHY; TAYLOR, 1985b, 1985c). Since then, several authors have started to use this non-equilibrium approach in modeling of falling liquid film processes.

At that time, great efforts were also being focused on improving energy efficiency of chemical processes, especially distillation. The concept of heat integration was introduced almost 70 years ago (JANA, 2010). The basic idea of heat integration is that hot process flows are exchanged with cold ones. In this way, thermal resources are used more economically. The first practical effort to improve the thermal efficiency of industrial distillation columns were implemented for heat pump assisted distillation (JANA, 2014; NULL, 1976), which effectively reduces exergy losses by minimizing the temperature difference between the inlet and output heat. The internally heat-integrated distillation columns (HIDiC) were an advance in this respect and used principles of heat pump assisted distillation (CABRERA-RUIZ; JIMÉNEZ-GUTIÉRREZ; SEGOVIA-HERNÁNDEZ, 2011; NAKAIWA *et al.*, 1997, 2003). This technology began to be studied by Takamatsu and Nakaiama in Japan in 1985 (IWAKABE *et al.*, 2006). In this configuration, all, or some part of the rectifying section is connected to the stripping section, in order to exchange heat and consequently increase the energy efficiency. On the improvement of energy efficiency in falling film distillation columns, a pioneer experimental work was carried out by Lueprasitsakul *et al.* (1990). The results suggested that the HIDiC system could be feasible even using wetted-wall columns.

In recent years, several academic groups have been actively researching topics in high energy efficiency distillation columns, such as engineering design (HUANG *et al.*, 2007; MUSTAFA *et al.*, 2014; WANG *et al.*, 2019), energy analysis (IWAKABE *et al.*, 2004; RIVERA-ORTEGA *et al.*, 1999), and process control strategies (EGGER; FIEG, 2019; LIU; QIAN, 2000; PORRU; BARATTI; ALVAREZ, 2015). Since 1990, many distillation structures with heat integration have also been patented (FANG *et al.*, 2018). However, little progress was observed concerning the multiplicity of steady states, the design of optimized processes, the identification of systems, the design and implementation of nonlinear controllers and the experimental testing of these energy-efficient configurations. A relevant work was proposed by Saifutdinov *et al.* (1999), patenting a compact separation unit that uses a thermal fluid to conduct heat transfer to the distillation tube, where the falling liquid film internally flows to be distilled. As a way of increasing mass and heat transfer efficiency, the distillation tubes in the portion of the rectifying section and/or in the part of the evaporator have means for supplying irregular (variable) amounts of heat between the inside and the outside of the tube along its height. According to the authors, this could reduce the dimensions of the separation unit by 3 to 10 times compared to a conventional distillation unit. This technology, called Linas technology, contemplates considerable modifications in the design, construction, and operation of a distillation column. It is a distillation system that does not exhibit equilibrium steps. Its design involves the distillation by an internal liquid film flowing in vertical tubes thermally insulated by heat transporting fluids. This new device of falling film distillation offers some attractive, like simple construction, low resistance for flow rate, and good separation capacity (SAIFUTDINOV *et al.*, 2002a). Since then, Linas technology has been addressed in many industrial applications, with approximately 33 industrial projects in oil refining, 19 rectification units installed in Russia, and a great deal of planning work (SAIFUTDINOV *et al.*, 2002b).

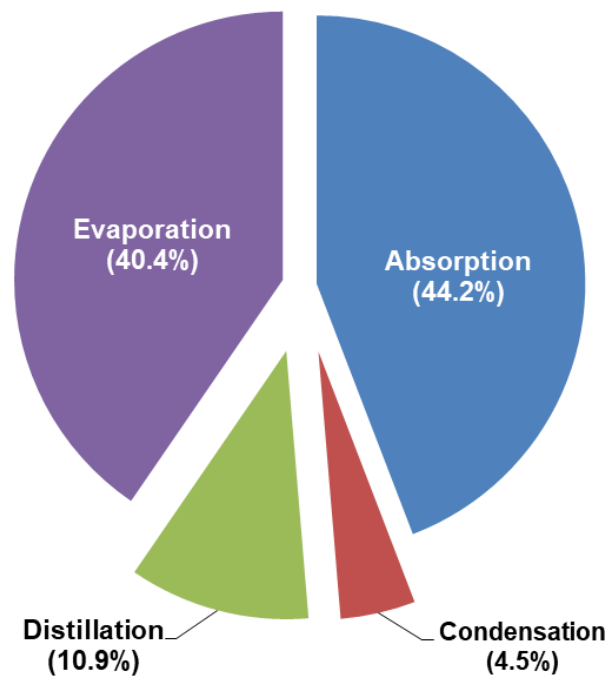
Even knowing that Linas technology had some limitations that could hinder the design of units with high productive capacity, its innovative character encouraged the development of the Destubcal technology, which resulted in a deposited patent (MEDINA *et al.*, 2014). Three experimental apparatuses were constructed: (i) a glass prototype; (ii) a single-tube carbon steel unit; and (iii) a multitubular carbon steel unit (with nine uniformly distributed tubes). The main innovative feature of Destubcal technology lies in the fact that the distillation tubes are surrounded by a steam chamber, which is part of a two-phase closed thermosyphon that is responsible for energy supply to the falling film distillation process.

Another advantage is that this technology operates at atmospheric pressure, which in addition to lowering the operational cost of the process, allows the recovery of only one oil cut. As well as many other works published over time, all the published works involving the Destubcal technology pointed out to the energy minimization when compared with conventional technologies. Steady-state studies of separation efficiency have already been carried out with some binary ethanol-water (MARANGONI *et al.*, 2019b, 2019a), monoethylene glycol-water (PIRES *et al.*, 2020), triethylene glycol-water (PERUZZO, 2013), and multicomponent synthetic naphtha (QUERINO; MACHADO; MARANGONI, 2019; QUERINO; MARANGONI; MACHADO, 2018), and aromatic toluene-xylenes mixture (SILVA FILHO *et al.*, 2018). Now it is understood that there is a knowledge gap regarding the process dynamics. Currently, the main research focus of the works is being directed to further investigation of empirical and phenomenological dynamic models of these experimental devices, aiming to contribute with future proposals for optimization and process control strategies for falling film distillation in wetted-wall columns.

2.3 STATE-OF-THE-ART OF FALLING FILM DISTILLATION

To quantify the relevance and importance of the falling film distillation process, a detailed survey of published works available in Scopus and Google Scholar database literature, delimited since the mid-last century, more specifically in the year 1942, until recent years, more specifically in the year 2020, was done to verify the number of reports as published articles, deposited patents and master's or doctoral theses related to the topics "falling liquid film columns" and/or "wetted-wall columns". Initially, the search stratification was done by the type of process applied to falling film columns or wetted-wall columns, namely as the following keywords: distillation, absorption, evaporation, and condensation. Figure 2 shows the proportion of publications found for falling film columns, or wetted-wall columns, operating on each type of process.

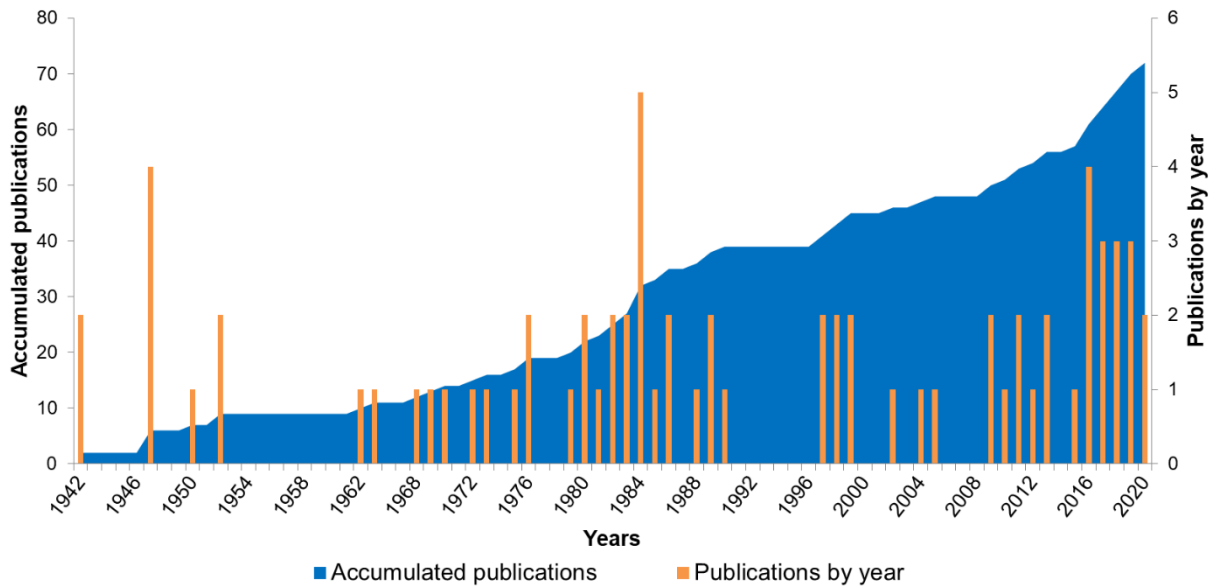
Figure 2 – Proportion of publications for each type of process in falling film columns.



Source: Battisti, Machado and Marangoni (2020).

It can be observed that falling film columns are mostly related to the use in absorption (44.2%) and evaporation processes (40.4%), whose applications are already well consolidated even at industrial scale (SRIKHIRIN; APHORN RATANA; CHUNGPAIBULPATANA, 2001; THOME, 1999). The use of this type of column for distillation condition process represents about 10.9%, and for condensation process only 4.5% of the total works found in literature. Although it is not among the predominant application demands, the use of wetted-wall columns for distillation purposes is quite significant, since it has kept researchers motivated to this theme for almost one century. The evolution in the publications related to falling film distillation in wetted-wall columns over the last 80 years, as well as the number of publications accumulated until the recent year are shown in Figure 3. The first recorded publication of falling film columns for distillation process was in 1942. Since then, there has been an increase in publications, with periods of higher or lesser degree of interest in the subject. The 1980s can be considered as the most promising period of publications on this subject, most probably due to the emergence of computational technologies for simulation of heat and mass transfer phenomena in falling liquid films.

Figure 3 – Publication evolution on falling film distillation in wetted-wall columns.



Source: Battisti, Machado and Marangoni (2020).

Table 2 presents a list of experimental works related to falling film distillation in wetted-wall columns, with details of the constructive and operational conditions used in the apparatus. Regarding the different types of volatile substances already distilled in wetted-wall columns, mixtures containing alcohols (methanol, ethanol and propanol) were the most used experimentally, followed by mixtures of aromatic compounds (benzene, toluene and xylene) and hydrocarbons (hexane and cyclohexane). These mixtures are usually easily distilled in systems operating at atmospheric or just below atmospheric pressure. Despite this, there are also some applications of wetted-wall columns for esters distillation, such as the works by Watanabe and Munakata (1976) and Matsuda *et al.* (1980). The singular difference of these works was the significant reduction in the operating pressure inside the distillation tube, given that the volatility of these components (esters) is much less than alcohols or hydrocarbons. The sizes (diameter and length) of the wetted-wall columns for falling film distillation also vary depending on the feed flow rate. In general, the columns found in the literature have diameters of 1.0 cm until 9.0 cm and lengths of 20.0 cm until 5.0 m. These sizes are well applicable for laboratory-scale or pilot-scale equipment. The only industrial-scale application reported was the work of Saifutdinov *et al.* (2002b) who reported a falling film distillation of crude oil at a refinery in Russia.

The materials of construction for distillation columns are important mainly for strength and resistance to corrosion (TORSNER, 2010). Materials such as stainless steel or

titanium, are preferred, although certain combinations of coated metals are also operable, i.e., glass coated, ceramic coated, and Teflon coated steels are acceptable in many embodiments. Stainless steel, e.g., 304 or 316, is preferred for its combination of ready availability, reasonable cost, and excellent corrosion resistance (GRAND; ODIO, 1987). As the first decision factor, the material has to be compatible with the process fluid. In addition, the temperature inside the column is a determinant factor regarding the corrosion resistance of the material (PROVERBIO; BONACCORSI, 2002). The wetted-wall columns applied on laboratory-scale, that is, smaller size, were generally constructed in glass. As the flow rate is increased, the column size is also increased and consequently the preferred construction material in this case is stainless steel. The vast majority of wetted-wall columns applied to falling film distillation was built in a tubular format with a single tube, although the multitubular type was applied since 1952, when Lindsey, Kiefer and Huffines (1952) first documented it. Another important point to be highlighted among the configurations of wetted-wall columns is regarding to reflux type. The literature shows that there are three possibilities of operating the reflux in a wetted-wall column, as total reflux, partial reflux or no reflux. It is worth noting that the columns that operate at total reflux are those applied only to extract thermophysical data for heat, mass and momentum transfer coefficients, while the columns that operate at partial and no reflux are also used to collect distilled product on the top, i.e., it has the advantage of could being scaled-up to increase productivity.

Table 2 – Experimental falling liquid film distillation systems in wetted-wall columns.

System	Diameter (cm)	Length (cm)	Feed flow condition ⁽¹⁾	Pressure (kPa)	Reflux	Construction material	Type of column	Reference
Ethanol-water	n.a.	n.a.	n.a.	n.a.	Partial	n.a.	Monotube	(SUROWIEC; FURNAS, 1942)
Benzene-toluene, ethanol-water, and acetone-chloroform	2.97	183	Laminar	n.a.	Total and partial	n.a.	Monotube	(JOHNSTONE; PIGFORD, 1942)
Ethanol-water	7.5	463.3	15 – 400 L/h	101.3	Partial	Copper	Monotube	(KIMMEL, 1947)
Carbon tetrachloride-toluene	5.08	137.2	7.02 – 18.41×10 ⁻⁶ mol/s and $Re_L = 26.4–66.1$	101.3	Partial	Pyrex glass	Monotube	(GILBERT, 1947)
Methylcyclohexane-2,2,4-trimethylpentane	7.44	58.4	0.6 – 4.7 L/h	101.3	Total	Metal	Rotary concentric-monotube	(WILLINGHAM <i>et al.</i> , 1947)
Carbon tetrachloride-benzene	3.6	162.6	1.75 – 33.5 kg/h (vapor)	101.3	Total and partial	Pyrex glass	Monotube	(WHITESELL, 1947)
2-Propanol-water	3.82	182.9	0.33 – 2.93 lbmol/h	101.3	Total and partial	Copper	Monotube	(JACKSON; CEAGLSKE, 1950)
Methanol-water and toluene-trichloroethylene	10.16	298.7	2.0 – 8.2 g/s	101.3	Partial	Copper	Multitube (7 tubes)	(LINDSEY; KIEFER; HUFFINES, 1952)
Trichloroethylene-tetrachloroethylene	1.905; 1.27 and 2.54	63.5	0.01 – 0.2 g/min	98.2 – 101.3	Partial	Metal	Multitube-plate	(MARTIN, 1952)
Chlorobenzene-ethylbenzene	1.90	125.1	3.36 – 139.4 g/min and $Re_G = 520 – 18.60$	98.1; 40.0; 13.3 e 2.7	Total	Glass	Monotube	(STERN, 1962)

Benzene-n-butanol	2.54	122.0	90 – 140 g/min	101.3	Total	Glass	Monotube	(BRADY, 1969)
Methylcyclohexane-toluene	2.54 – 5.08	182.9	$Re_G < 2600$	101.3	Total	Glass and copper	Concentric monotube	(GABBAY, 1970)
n-Butanol-benzene and n-propanol-benzene	2.3	127.0	1.03 – 1.28 cm ³ /min	101.3	Total	Stainless steel	Monotube	(CHATLYNNE, 1972)
Ethyl oxalate-methyl salicylate and di-n-butyl phthalate-di-n-butyl sebacate	7.5 O-D, 3.5 I-D	100 or 30	3.09×10^{-2} – 3.73×10^{-2} g/cm ³ s	0.03 – 0.04	Partial	Swathed glass, ground glass, stainless steel	Annular monotube	(WATANABE; MUNAKATA, 1976)
Methanol-water	2.21	100	50 – 100 g/min	101.3	Total	Stainless steel	Monotube	(KAYIHAN; SANDALL; MELLICHAMP, 1977)
Benzene-toluene-ethylbenzene	2.21	100	n.a.	101.3	Total	Stainless steel	Monotube	(DRIBIKA; SANDALL, 1979)
Methanol-water and ethanol-water	1.80 (wide)	19.6	$Re_G = 4,500 – 31,000$	101.3	Total	Brass	Vertical flat-plate	(ITO; ASANO, 1980)
Ethyl oxalate-methyl salicylate, cyclohexane-toluene, and n-heptane-toluene	0.485; 0.9; 1.6 and 2.0	36.0; 50.0; 60.0; 80.3 and 90.5	$Re_G = 500$ – flooding	0.533 – 101.3	n.a.	n.a.	Monotube	(MATSUDA <i>et al.</i> , 1980)
Methanol-water	1.80 (wide)	19.6	$Re_G = 17,000$	101.3	Total	Brass	Plate-fin device	(ITO; ASANO, 1982)
Methanol-ethanol-water	2.2	100	$Re_G = 1990$ and $U_v = 30 – 102$ m/s	101.3	Total	Brass	Monotube	(KOSUGE; ASANO, 1982)
n-Hexane-toluene	15.2 (wide) 0.95 (thick)	232	1.8×10^{-5} to 9.0×10^{-5} kmol/s	103.2 – 125.6	Total	Aluminum	Plate-fin	(DAVIS; TUNG; MAH, 1984)

Acetone-methanol-ethanol	2.2	Variable (until 100)	$Re_G = 1990$ and $U_v = 0.2 - 0.8$ m/s	101.3	Total	Pyrex glass	Monotube	(KOSUGE; ASANO, 1984a)
Acetone-methanol-ethanol	2.2	59.0	$Re_G = 900$ to 3.600	101.3	Total	Pyrex glass	Monotube	(KOSUGE; JOHKOH; ASANO, 1985)
Isopropanol-water and isopropanol-water-methanol	2.0	58.0	5.0 – 80 mol/h	n.a.	No reflux	Metal	Monotube	(FULLARTON; SCHLÜNDER, 1986)
Ethanol-water	3.9/4.3 7.6/8.6 (in/out)	104.0	273.6 – 389.5 mol/h	103.0 – 206	Partial	n.a.	Concentric double-tube	(LUEPRASITSAKUL <i>et al.</i> , 1990)
Nitrogen-oxygen and argon-oxygen	2.51	55.0	2.5×10^{-3} kg/s	107 – 182	Total	Stainless steel 304	Monotube	(EGOSHI; KUSUNO; KAWAKAMI, 1997)
Nitrogen-Argon-Oxygen	2.51	55.0	2.5×10^{-3} kg/s	107 – 182	Total	Stainless steel	Monotube	(EGOSHI; KAWAKAMI; ASANO, 1999)
Oil (crude oil)	50	150.0	1.14 ton/h	110	No reflux	Steel	Monotube	(SAIFUTDINOV <i>et al.</i> , 2002b)
Isopropyl alcohol-water	4.0	55.7	0.065 – 0.213 kg/(m·s)	101.3	No reflux	n.a.	Monotube	(DZIAK; KUBALA, 2010)
Ethanol-n-propanol	9.0 (wide)	18.0	1.0 – 8.0 g/min	101.3	No reflux	Brass	Vertical plates	(KANE <i>et al.</i> , 2011)
Ethanol-water	2.6	100	17.0 L/h	101.3	No reflux	Glass	Monotube	(MARANGONI <i>et al.</i> , 2011)
Ethanol-water	1.7	75.0	2.58×10^{-3} m ³ /h	98.5	Total	Stainless steel	Monotube	(SINGH; PRASAD, 2011)
Ethanol-water	2.6	100	4.0 – 22.0 L/h	101.3	No reflux	Glass	Monotube	(PARISOTTO, 2013)
Triethylene glycol-water	2.6	100	13.0 – 17.0 L/h	101.3	No reflux	Glass	Monotube	(PERUZZO, 2013)

Monoethylene glycol-water	2.6	100	11.0 – 40.0 L/h	101.3	No reflux	Stainless steel	Monotube	(PIRES, 2016)
Methanol-n-propanol and ethanol-n-propanol	2.5	210	1.0 – 3.0 g/s	101.3	Total	Glass	Monotube	(REJL <i>et al.</i> , 2016)
Ethanol-water	3.2 (wide)	25.6	$Re_G = 1.7 \times 10^3$ $\sim 1.08 \times 10^4$	101.3	Total	Copper	Vertical flat plate	(PARK <i>et al.</i> , 2017)
p-Xylene, m-xylene, o-xylene and ethylbenzene	2.64	100	15 – 24 kg/h and 211 – 218 kg/h	101.3	No reflux	Stainless steel	Monotube and Multitube (9 tubes)	(SILVA FILHO <i>et al.</i> , 2018)
Synthetic naphtha (n-hexane, cyclohexane, toluene and xylene)	2.64	100	13.0 – 22.0 kg/h	101.3	No reflux	Stainless steel	Monotube	(QUERINO; MARANGONI; MACHADO, 2018)
Ethanol-water	2.64	100	17.0 and 27.0 kg/h	101.3	No reflux	Stainless steel	Monotube (temperature-profile operation)	(MARANGONI <i>et al.</i> , 2019a)
Ethanol-water	2.64	100	17.0 and 27.0 kg/h	101.3	No reflux	Stainless steel	Monotube (isothermic operation)	(MARANGONI <i>et al.</i> , 2019b)
Synthetic petrochemical naphtha	2.64	100	13.0 to 23.0 kg/h	101.3	No reflux	Stainless steel	Monotube	(QUERINO; MACHADO; MARANGONI, 2019)
Monoethylene glycol-water mixture	2.64	100	23.0 and 43.0 kg/h	101.3	No reflux	Stainless steel	Monotube	(PIRES <i>et al.</i> , 2020)

⁽¹⁾ Units may vary by application and are therefore presented individually.

n.a.: Not available or not applicable.

Source: Battisti, Machado and Marangoni (2020).

Table 3 summarizes the patents that have been deposited over the last century until nowadays about falling film distillation in wetted-wall columns. It is noted that the interest in patenting apparatuses for separation of numerous mixtures by means of falling film technology is not recent. The first patent deposited for this purpose dates back to the year 1950, shortly after the first published article on wetted-wall distillation that pointed to its separation efficiency. Coincidentally, the first patents also appeared only after the end of World War II. Since then, over the years several structures using the falling film technique have been emerging and being patented, such as single tubular columns (monotube), multitubular columns (multitube), vertical plates, inclined plates, and even rotary plates. The application areas of these columns are generally aimed to the separation of hydrocarbons mixtures from petroleum or organic fractions, which is a major application of distillation in general, but some of them are more specific, such as desalination of seawater, for example.

Table 3 – Deposited patents on falling film distillation in wetted-wall columns.

Identification	Type of column	Operating condition	Application	Reference
US2514944	Flat-plate film	Reduced pressure (high vacuum)	Various organic mixtures	(FERRIS; LAMSON; SMITH, 1950)
US2580646	Multitubular (20 concentric tubes)	Not specified	Volatile material present in some liquid mixture	(BELDEN; BERWYN, 1952)
US2608387	Multiple vertical plates	Not specified	Various fractional mixtures	(RANDALL, 1952)
US3211633	Inclined plates side-by-side	Pressurized feed (sprayer)	Saline water or impure water	(HAMMER; SOMERS, 1965)
US3214351	Vertical plates on film	Atmospheric conditions	Brackish water	(LICHTENSTEIN; BUCAIO, 1965)
US3226306	Multiple rotating disks	Sub atmospheric Pressure	Solvent of an impure composition (mainly saline water)	(HAUSNER, 1965)
US3249516	Inclined aluminum plates	Low pressure drop and temperature	Heavy water distillation	(MUELLER, 1966)
US3291704	Vertical corrugated plates	Not specified	Distillation of saline water	(DIEDRICH; LOTZ, 1966)
US3558438	Multitubular in open tubes	Dependent on the volatility of the compound with the lowest boiling point	Fractions with low boiling point	(SCHOENBECK, 1971)

US4402793	Vertical parallel plates	Atmospheric pressure	Liquids with multiple components of different volatilities	(PETREK; CANTRELL, 1983)
US5423952	Multi-effect column (four vertical tubes)	Atmospheric pressure	Distillation of seawater and chemicals in general, such as alcohols	(STOUT, 1995)
US6376732	Tubular centrifugal wetted-wall	Pressure of about 70-80 psig	Hydrocarbons (heavy olefins)	(NGAN <i>et al.</i> , 2002)
US7476298	Vertical flat baffles	Not specified	General multi-component distilleries	(STOUT, 2009)
US7588666	Annular multitubular	Pressurized (> atm.)	Mixing of multiple components	(SAIFUTDINOV <i>et al.</i> , 2009)
BR10201402976	Unitubular assisted by thermosyphon	Atmospheric pressure	Oil fractions	(MEDINA <i>et al.</i> , 2014)

Source: Battisti, Machado and Marangoni (2020).

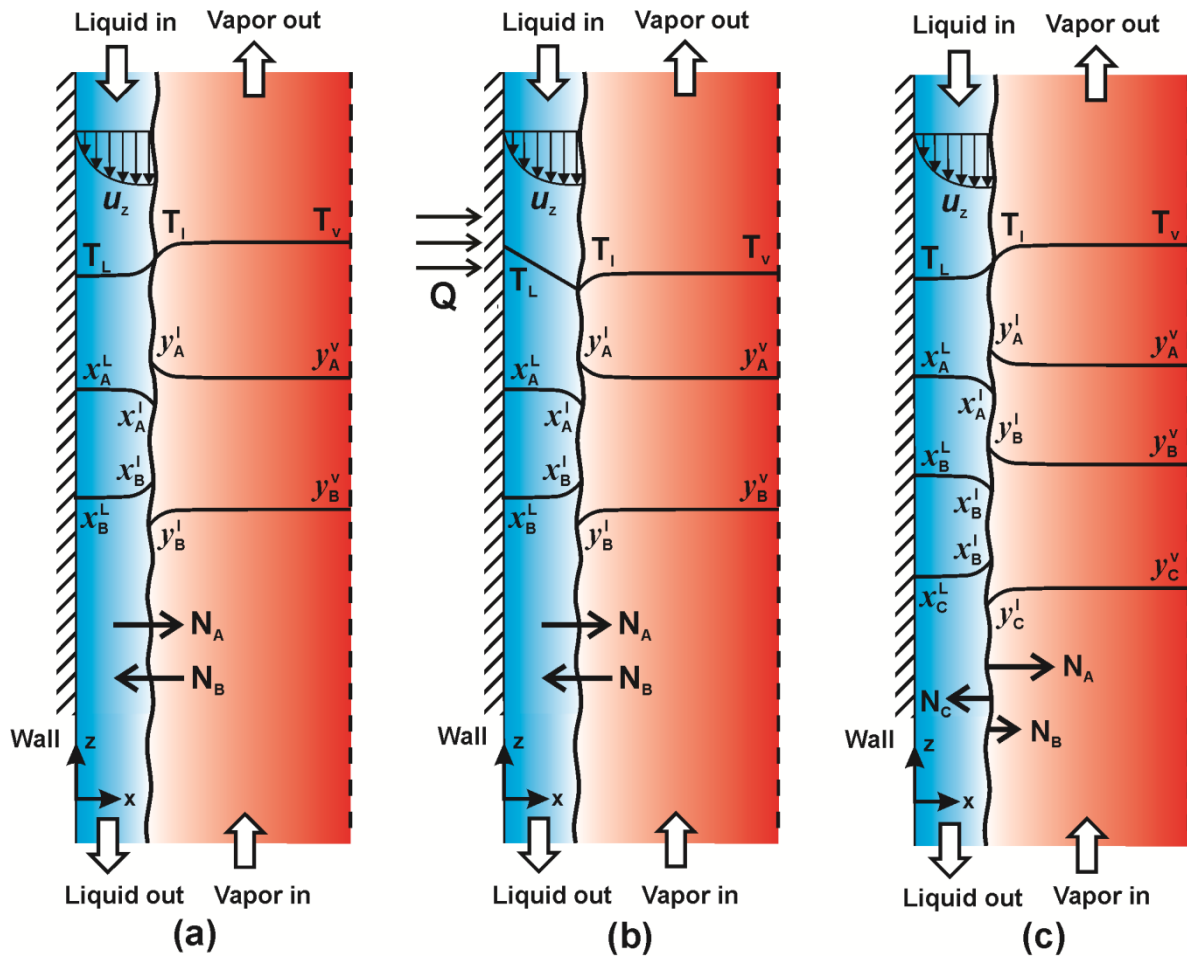
2.4 BASIC CONCEPTS AND WORKING PRINCIPLES

Generally, falling liquid films are 0.5 – 1.0 mm thick and flow along a vertical or inclined surface. This type of gravitational flow is part of the general class of flows with a free frontier, and they have a strategic position in both pure and applied sciences (ALBERT; MARSCHALL; BOTHE, 2014; DIETZE; AL-SIBAI; KNEER, 2009; DIETZE; KNEER, 2011; KALLIADASIS *et al.*, 2012). Not surprisingly, the inherent characteristics of falling liquid films has attracted attention of researchers for several decades. The large interfacial area found in this class of flow through the film makes this a favorable device for various processes of gas-liquid and vapor-liquid contact. Common process equipment using falling liquid film flow includes cooling towers (IBRAHIM; NABHAN; ANABTAWI, 1995; YINGJIAN *et al.*, 2011), nuclear reactors (ARIAS, 2010), condensers (RUAN *et al.*, 2018; YAMAMURA *et al.*, 2009), absorption refrigeration machines (NARVÁEZ-ROMO *et al.*, 2017), falling film evaporators (KLYKOV; ALUSHKINA, 2018; OLBRICHT; LUKE, 2018; QIU *et al.*, 2018; SALVAGNINI; TAQUEDA, 2004), columns with structured packing (SUN *et al.*, 2013), photo-reactors (AZIZ *et al.*, 2018; GHEZZAR *et al.*, 2013), wetted-wall distillation columns (WANG *et al.*, 2017), among others. In addition, liquid films are also used for coating metallic or polymeric surfaces (ZHOU *et al.*, 2014).

In distillation, the more volatile component is transferred from the liquid phase to the vapor phase, and the less volatile is transferred from the vapor phase to the liquid phase (BANDINI; GOSTOLI; SARTI, 1992; KIENLE; GROEBEL; GILLES, 1995; LIANG *et al.*, 2017). As these components undergo to a phase change, evaporation and condensation are occurring continuously at the interface. At this fictitious boundary, it is assumed that there is no transfer resistance, so the phases are in thermodynamic equilibrium. These may or may not be in saturated conditions (bubble point) (KAYIHAN; SANDALL; MELLICHAMP, 1975). Since Danckwerts, Sawistowski and Smith (1960) introduced the concept of thermal distillation, this operation in continuous contact equipment began to be explained as a simultaneous heat and mass transfer process. The authors suggested that the efficiency of a distillation column can be influenced by the thermal effect of the temperature difference between the vapor and liquid phases, and the change in surface tension due to a liquid composition profile. As is generally done, the liquid and vapor streams are grouped into two phases, separated by a fictitious interface through which heat and mass transfer occurs. The transfer fluxes are defined in terms of the individual phase driving forces and transfer coefficients, plus the convective flow terms (PARK *et al.*, 2017). Figure 4 shows the temperature, concentration, and velocity profiles for falling film distillation in a wetted-wall column, in contact with adjacent vapor phase, under three main differentiated conditions: (a) binary system without sidewall heating; (b) binary system with sidewall heating; and (c) multicomponent system without sidewall heating.

To describe a falling film distillation process in a wetted-wall column, one can take as base case the model proposed by Westhaver (1942), the pioneer work in the use of wetted-wall columns for distillation purposes. It was considered a long, vertical, heat-compensated tube with a bottom reboiler and a top condenser as a continuation of the tube; assumed that a small constant pressure gradient produces an upward vapor flow; the falling reflux film was considered ideal, i.e., having negligible surface transfer resistance and uniform composition along its radial thickness, and evenly wetting the entire surface of the tube. Negligence in the transfer resistance in the liquid phase can be justified by considerations of the kinetic theory (LINDSAY; BROMLEY, 1950), which shows that the vapor which pumps the surface of the liquid is of the order of grams per $\text{cm}^2\cdot\text{s}$, most of which is condensed and replaced by another material evaporating at the same speed. This rapid process ensures the balance between the surface of the liquid and the portion of the vapor moving near it.

Figure 4 – Temperature, concentration and velocity profiles for falling film distillation in a wetted-wall column: (a) binary; (b) binary with sidewall heating; (c) multicomponent.



Source: Battisti, Machado and Marangoni (2020).

In the liquid-vapor interface, it is commonly assumed that the two phases are in thermodynamic equilibrium (DE KOEIJER; KJELSTRUP, 2004). Except for an azeotropic composition, the molar fraction of the more volatile component will be higher on the vapor side than on the liquid side. Regarding the liquid composition at the interface, the more volatile component will be transferred from the liquid phase to the vapor phase at a rate higher than the less volatile component. This relative transfer rate causes a local decrease in the concentration of the most volatile component, and an accumulation of the concentration gradient, which is accompanied by mass diffusion. This description will be valid regardless of the direction of the mass transfer (ZUIDERWEG; HARMENS, 1958). However, the existence of heat input through the wall will superimpose an evaporation of the liquid in the mass transfer process aforementioned, thereby increasing the mass transfer flux through the

interface (DAVIS; TUNG; MAH, 1984). The vapor stream is delimited by the liquid film boundary on the inside wall of the column. Thus, the surface condition of the liquid can be expected to influence the vapor flow in the same way that the roughness of the wall influences the flow in the pipes. In the turbulent stream flow region, a decrease in operating pressure (the constant vapor phase Reynolds number) causes an increase in column efficiency (LIU; JOBSON, 1999).

2.4.1 Binary falling film distillation

Figure 4 (a) illustrates the heat and mass transfer phenomena of a conventional binary falling film distillation under a condition in which the reflux is flowing along in continuous contact with adjacent vapor. The diffusion rate and the conduction heat transfer rate of the vapor phase component "A" in the "x" direction of the interface are defined based on the concentration and temperature gradients between the vapor stream and the vapor-liquid interface. In the bulk vapor phase, both temperature and composition (in molar fraction) will be constant in the transverse direction. When a heat flux (Q) is imposed through the wall (Figure 4 b) most of the heat transfer occurs in the transverse direction. Heat is transferred through the falling film and the liquid-vapor interface to the bulk phase. Only a small fraction of the heat transferred through the wall is charged by the falling liquid film and contributes to the continuous increase in liquid temperature as it moves down the column.

In gas-liquid continuous contact devices for binary distillation, most studies published after Murphree (1925) until the 1950s were carried out from the point of view in which mass transfer depended solely on its diffusivity. Johnstone and Pigford (1942) performed experiments on a wetted-wall column with diameter of 2.97 cm and length of 1.83 m. Benzene-toluene, ethanol-water, and acetone-chloroform were the binary systems distilled in the apparatus. The compositions at the top and the bottom of the wetted-wall column and the average flow rates were presented for various experimental conditions involving the three binary systems mentioned above. Van Es and Heertjes (1956) studied the benzene-toluene binary mixture as a function of the amount of condensed vapor and the mass transfer coefficient in the vapor phase. Comparing the liquid phase resistance with the condensation vapor resistance, the authors concluded that the highest resistance for heat transfer was indeed in the liquid film. Therefore, the overall heat transfer coefficient slowly decreased from the top to the bottom of the distillation tube. In addition, the authors

concluded that the mass transfer coefficient in the vapor phase for Reynolds number above 2000, i.e., turbulent flow (ARGYROPOULOS; MARKATOS, 2015), was shown to be a linear function of Re , without major interference.

Kayihan, Sandall and Mellichamp (1977) used a wetted-wall column operated at total reflux to measure the local mass transfer coefficients of methanol-water binary system at atmospheric pressure. They concluded that the vapor phase is the control resistance for mass transfer in the distillation and so there is no additional evaporation within the liquid phase caused by the heat transferred from the vapor phase, as had been proposed by some previously researchers. In order to investigate the thermal effects of partial condensation of the vapor mixture on the binary distillation of methanol-water system, Ito and Asano (1982) conducted theoretical and experimental approaches for measurements of heat and mass fluxes in a wetted-wall column. The authors proposed a new method for the prediction HOG (total number of transfer units in the vapor phase) for non-adiabatic binary distillation with a good agreement between theoretical and experimental values. Egoshi, Kusuno and Kawakami (1997) developed an experimental approach for heat and mass transfer in the cryogenic binary distillation of nitrogen-oxygen and argon-oxygen systems in a wetted-wall column under total reflux condition for a wide range of turbulent vapor flows. The authors observed that the diffusion fluxes for each component in binary distillation were proportional to their concentration driving forces, while the observed mass fluxes were not. They concluded that the convective mass flow has a significant effect on the total mass flow for cryogenic binary distillation. The authors also proposed a new correlation for vapor phase diffusion fluxes that was applied with good agreement for the nitrogen-oxygen and argon-oxygen binary systems. Although binary distillation is a process of simultaneous heat and mass transfer in which a mixed vapor encounters its condensate, much of the works have considered this as a simple process of mass transfer. Therefore, there are still many unresolved or partially solved problems that need further discussion, including the effect of partial condensation on mass transfer rates and the effect of liquid concentrations on separation efficiencies.

2.4.2 Multicomponent falling film distillation

Figure 4 (c) shows the heat and mass transfer phenomena in multicomponent falling film distillation, where a reflux liquid is flowing down along a vertical wall continuously in contact with an adjacent countercurrent vapor flow. It is widely known that the mass and heat

transfer processes in the distillation (including multicomponent) are controlled by the vapor phase (DRIBIKA; SANDALL, 1979; KAYIHAN; SANDALL; MELLICHAMP, 1977; KOSUGE; ASANO, 1984b). Moreover, the effect of the interactions between the diffusion fluxes of the components is insignificant; therefore, the diffusion flux of each component is proportional to its concentration driving force. Complex multicomponent systems are commonly found in the process and separation industry (AGRAWAL, 1996; DEJANOVIĆ *et al.*, 2011; RONG; KRASLAWSKI; NYSTRÖM, 2001). However, unlike binary systems for which the calculation methods are well developed and experimentally verified, the amount of experimental data that can validate the computational methods proposed in literature for multicomponent systems is still relatively small and somewhat limited (KRUPICZKA; ROTKEGEL, 1997).

Mass transfer in multicomponent mixtures is more complicated than in binary systems because of the possible coupling between the individual concentration gradients (AGRAWAL, 1999; KRISHNA; STANDART, 1979; KUMAR; MAZUMDER, 2007). Phenomena such as reverse or osmotic diffusion are possible in multicomponent systems, which is not seen in binary systems (TOOR, 1957). By the late 1970s, the knowledge about heat and mass transfer in ternary and/or multicomponent distillation was undeveloped. Although some experimental approaches had already been taken to evaluate the performance of separation in ternary distillation, no reliable method for its prediction was well known. Hutchison and Lulis (1968) carried out experiments on a wetted-wall column with two ternary systems (acetone-benzene-chlorobenzene and benzene-toluene-m-xylene); and with four binary systems (benzene-toluene, cyclohexane-toluene, methylethylketone-toluene, and isopropanol-toluene). The results indicated that the predominant mass transfer mechanism was diffusion, with thermal distillation practically insignificant. The authors suggested it might be possible to predict the performance of the equipment by separating the ternary systems using correlations for the resistance of individual films obtained from experiments with binary systems. Another ternary distillation system of benzene-toluene-ethylbenzene mixture was studied by Dribika and Sandall (1979) in a wetted-wall column of 1.0 m length and internal diameter of 2.2 cm. The authors pointed to a reasonable agreement between their experimental measurements and a theoretical model that included the use of the Krishna and Standart (1976) method (based on Stefan-Maxwell's equations describing diffusion in multicomponent systems) to calculate the mass transfer rates, with mean deviations of 15.8% for benzene, 23.1% for toluene and 23.3% for ethylbenzene.

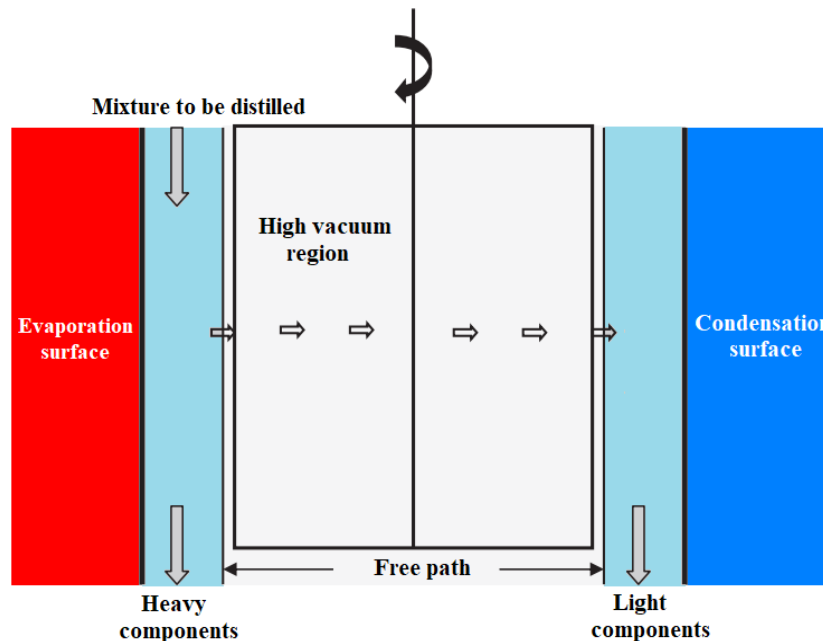
An experimental study of the mass and sensible heat fluxes for a ternary distillation of methanol-ethanol-water system was done by Kosuge and Asano (1982) on a wetted-wall column under total reflux condition. Measurements of the vapor temperature profiles and mass fluxes of each component were made, and the fluxes of diffusion, sensible heat and interfacial velocities were compared with the theoretical values. Thus, the authors proposed a new method to calculate the diffusion fluxes from the mass flows, but showing a weak correlation to the vapor phase. Shortly thereafter, Kosuge, Johkoh and Asano (1985) conducted experimental studies of a ternary distillation of acetone-methanol-ethanol system for wide ranges of liquid concentrations. The intermediate component (methanol) showed unusual behavior of a finite mass flow near the region of the zero-driving force. This behavior was explained because of the interfacial velocity caused by mass flows of the other components. The diffusion fluxes were shown to be proportional to the concentration driving forces, whereas the mass fluxes were not. These facts may indicate the assumption that mass flows are proportional to their concentration gradient forces, which is the basis for the use of transfer units for mass transfer data correlation, is not valid for the case in ternary distillation, as already pointed out by Ito and Asano (1982) for binary distillation. The multicomponent cryogenic distillation in a wetted-wall column was also studied by Egoshi, Kawakami and Asano (1999). Experiments were done for the nitrogen-argon-oxygen system under total reflux conditions and wide flow rate ranges (especially in the turbulent flow region). The heights of the transfer units for the intermediate component, argon, show the discontinuity near the zero-driving force region. The observed diffusion fluxes of each component are proportional to their driving forces, while the mass fluxes observed are not. This result is similar to that obtained in binary cryogenic distillation and probably is due to the convective mass flows caused by the mass flows of the other components. The diffusion fluxes observed in ternary distillation show good agreement with the binary correlation previously developed using effective diffusion coefficients of Wilke and Chang (1955).

2.4.3 Molecular distillation

By definition, molecular distillation (or short-path-distillation) is characterized by the use of a high vacuum (10 to 5 Pa), a relatively low evaporator temperature, a short residence time of the liquid, and a small physical distance between evaporator and condenser (TOVAR *et al.*, 2011). The vacuum is the driving force of this type of diffusional mass transfer

operation. Without this, it would be impossible to work with this equipment through this phenomenon, since with higher pressures this operation would be in vapor/liquid equilibrium. With the presence of a high vacuum, the kinetic theory of gases shows that an evaporable molecule migrates to the condensation zone virtually unobstructed. Thus, the mass transfer between the evaporation zone and the condensation zone only walks in one direction because of the absence of collisions during its course with other molecules due to the vacuum. For this, it is necessary that the molecules find a "free path" between the evaporator and the condenser, which is facilitated by the low pressure in the system. As a consequence, the condenser must be separated from the evaporator by a distance less than the mean free path of the molecules being evaporated (BATISTELLA; MACIEL, 1996; KAWALA; DAKINIEWICZ, 2002; LUTIŠAN; CVENGROŠ, 1995; ZHANG; XU; ZHOU, 2005), as shown in Figure 5.

Figure 5 – Working principle for molecular distillation.



Source: Sørensen, Lam and Sudhoff (2014).

This special falling film thermal separation technique is widely used in recovery, purification and concentration of thermally sensitive substances such as tocopherols (MARTINS *et al.*, 2006), carotenoids (BATISTELLA *et al.*, 2002) and essential oils (TOVAR *et al.*, 2010), as well as compounds with high boiling point, high viscosity, and low relative volatility, as glycerides (FREGOLENTE *et al.*, 2010), chlorinated residues (BILLS;

SLOAN, 1967), biomass pyrolysis oil (GUO *et al.*, 2010), and petroleum residues (ZUÑIGA LIÑAN *et al.*, 2012). According to Batistella (1999), there are several types of equipment for this technology, among them, falling film distillers, sliding scraper distillers, multicompartment distillers, and centrifugal distillers, which are the most commonly (due to simple construction and high distillation rate). Due to its high purification capacity, sustained interest in molecular distillation is targeted for industrial applications. In contrast, studies concerning the basic theory of molecular distillation are still limited. Most of the works are focused on hydrodynamics and heat and mass transfer on the liquid film. Hence, there is still insufficient information about the behavior of the vapor phase under high vacuum conditions to support the development of molecular distillation on a larger scale (LI; XU, 2014).

2.5 PROCESS DESIGN AND COLUMN CONFIGURATIONS

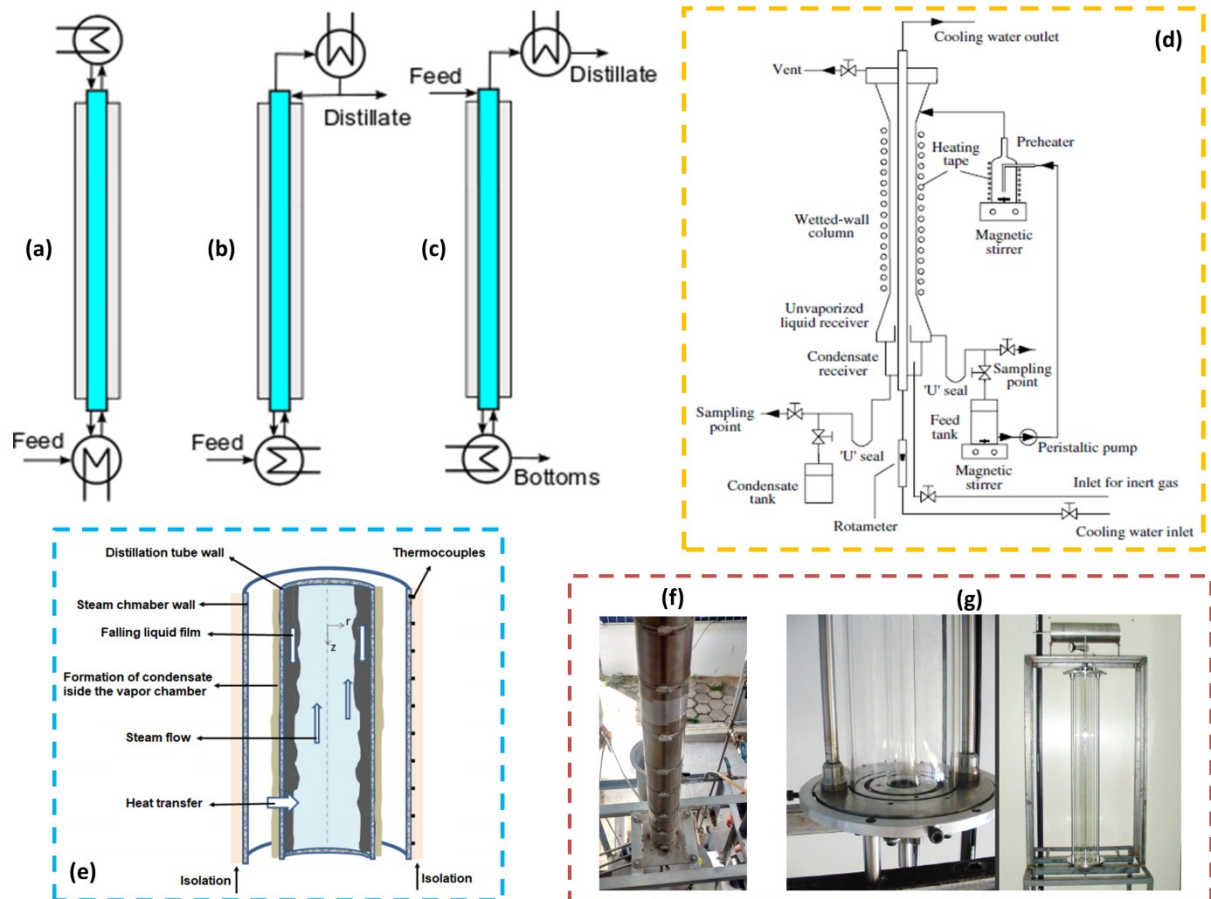
Throughout the history, several types of distillation columns have been designed to promote the enrichment of the less volatile fraction in the condensate and the more volatile fraction in the vaporized liquid, aiming improvements in liquid-vapor contact. Some common examples are sieve trays, bubble cap trays, valve trays, random and structured packings, and falling film flows, usually treated in publications as wetted-wall columns (MUELLER, 1966; OLUJIĆ, 2014). Among these experimental gas-liquid contactors, wetted-wall columns have been found to be one of the most studied in the literature (LIANG *et al.*, 2015). This is because: (i) their surface area can be directly measured (BISHNOI; ROCHELLE, 2002); and (ii) the physical coefficients, especially the diffusivity, can be accurately determined (SAHA; BANDYOPADHYAY; BISWAS, 1995). In addition, wetted-wall columns can operate in countercurrent mode that is close to real systems (SEMA *et al.*, 2012). In the conventional wetted-wall distillation column type, the liquid charge is introduced in order to form a thin film along the wall of the tube or surface. This type of tower can provide a preferable temperature gradient in performing certain fractional operation. Besides, the operation may be preferable, or necessary, to distill and remove a component from a material that is viscous or where a conventional distillation procedure can cause large amounts of bubbles and foam, which, in turn, would prevent a clean cut separation (FERNANDEZ-SEARA; PARDINAS, 2014). Basically, the conventional configurations for falling film distillation columns widespread since the middle of the last century are monotube, multitube and vertical flat-plate columns. These configurations were widely used until the 1990s, both experimentally and in

numerical studies. Since then, the concepts of energy intensification established for conventional distillation columns began to be incorporated into falling film technology, such as internally heat-integrated columns and thermosyphon-assisted columns.

2.5.1 Monotube columns

Wetted-wall columns have been mainly used for experimental work and generally with only one single tube for the fractionation surface, designated as “monotube” wetted-wall columns. Although the efficiency of these columns depends on several factors, it can be widely argued that the fractionation efficiency is an inverse function of the pipe diameter. Tiny pipes are required to achieve high fractionation efficiencies but can hardly be installed in a commercially-sized industrial plant. This arrangement is also uneconomical in that a small percentage of the total cross-sectional area of a column structure would employ a large number of small tubes (RANDALL, 1952). According to Whitesell (1947), a monotube wetted-wall column has advantages, which is much less likely to be flooded than a column composed of several wetted-wall tubes (multitube), where the inner tube area is the liquid flow passage area. Figure 6 shows the main design and construction arrangements involving monotube falling film or wetted-wall distillation columns. Regarding the feed conditions and internal liquid reflux operating modes, the three main types used on wetted-wall columns are: total reflux, as shown in Figure 6 (a); partial reflux, as shown in Figure 6 (b); or no reflux, as shown in Figure 6 (c). Figure 6 (d) represents a schematic diagram of an experimental unit operated under total reflux mode, i.e., all distilled vapor is condensed and returned as liquid back from the top of the column, and no top distilled product is collected. This type of column is mainly used for collecting data on mass and heat transfer and hydrodynamic falling film flow, but has no purpose for separation efficiency assessment and distillate productivity. Figure 6 (e) shows the illustration of a monotube longitudinal cross-section of a column. Images of constructed monotube falling film distillation columns can be seen in Figure 6 (f) of stainless steel, and Figure 6 (g) of borosilicate glass.

Figure 6 – Monotube falling film distillation designs: (a) Total reflux; (b) Partial reflux; And (c) no reflux. Schematic diagram of an experimental falling film distillation unit (d). Illustration of a monotube longitudinal cross-section column (e). Images of constructed monotube falling film distillation columns: (f) with stainless steel; (g) with borosilicate glass.



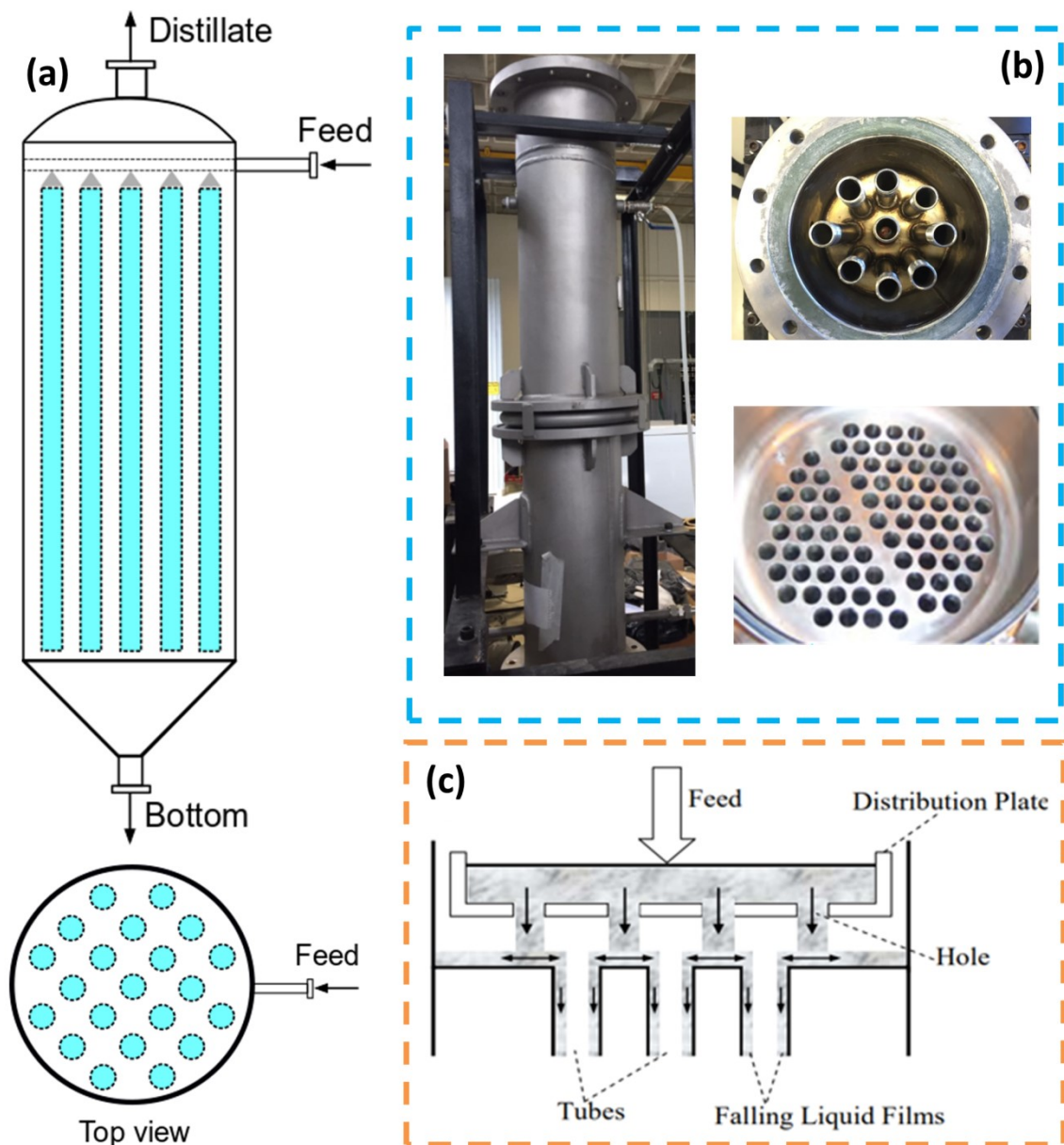
Source: Battisti, Machado and Marangoni (2020).

2.5.2 Multitube columns

From the results obtained in monotube columns, several researchers stated that a column consisted on many of these tubes in parallel should have a necessary height of a transfer unit (*HTU*) comparable, if not better, than a packed column of the same diameter, providing the same distillate flow rate (WILLINGHAM *et al.*, 1947). According to Whitesell (1947), in the practical design of a multitubular wetted-wall column it would be advisable to have the column comprising by a series of independent piping units. This would be a precautionary measure in case of some tubes are not thoroughly wetted, allowing one to have

control over the possibility of repair at the film breaking, and thus maintain the overall efficiency of the column. Figure 7 shows particular details of the constructive design of multitube wetted-wall distillation columns with images and cross-sections of feed liquid distribution inside the tubes.

Figure 7 – Constructive design of multitube wetted-wall distillation columns: (a) Schematic diagrams of cross-section and top view of a 20-equal space-distributed tubes column; (b) Outer shell and inner tube hole images of a multitube steel column; (c) Elevation view diagram of a typical multitube feed distribution system.



Source: Battisti, Machado and Marangoni (2020).

For Lindsey, Kiefer and Huffines (1952), it seemed reasonable that a commercially acceptable multitube wetted-wall column may be similarly constructed to a tube bundle heat exchanger. The upper end of each tube may be cooled to serve as a partial condenser providing its reflux. With equal area and refrigerant flow, there should be uniform reflux in all tubes. Such column may combine a high transfer rate with a relatively low pressure drop, which would make it industrially interesting, particularly for vacuum distillations. Pressure has a major impact on phase equilibrium in terms of relative volatilities, column temperatures and the existence of azeotropes, which affect energy requirements, utility costs and process configurations. Since many separations are favored by low temperatures, pressures in most columns are established by the desire to use inexpensive cooling water as the heat sink in the condenser (LUYBEN, 2016). An interesting multitube wetted-wall distillation column was patented by Belden and Berwyn (1952). This invention is related to an apparatus for distilling a volatile material from any simple or complex liquid mixture. More specifically, the innovation improvement made by the authors at that time was directed to redistribution of the liquid flow in the walls, and thereby providing a multistage evaporation and condensation, i.e., distillation operation. Schoenbeck (1971) presented an invention which comprised a multitube wetted-wall column equipped with recompression of the vaporized reflux to combine heating and cooling operation in the separation of compounds with different boiling points. This patent was created with the objective of separating low boiling point fraction from a mixture of compounds with close boiling points. It gave to this apparatus an innovative differential, as is well known, in most cases, the separation of close boiling point mixtures cannot be economically realized by the conventional methods (GAIKAR; MAHAPATRA; SHARMA, 1989; LEI; LI; CHEN, 2003; MUJTABA, 1999).

2.5.3 Flat-plate columns

Although flat-plate falling film columns are typically used to evaluate separation efficiency in distillation processes, wetted-wall vertical flat-plate design has been also used extensively by decades for experimental measurements of heat and mass transfer fluxes, as can be seen in studies done by Ito and Asano (1980, 1982), and Davis, Tung and Mah (1984). This design column configuration also has inspired several inventors in their quest for improved yields of miscible mixtures separations, primarily petroleum derivatives. Numerous patents have been deposited over the years. Randall (1952), for example, patented an

invention related to an apparatus for fractional falling film distillation in which the innovative design was conceived by a wetted-wall column with multiple flat vertical plates. The objective of this invention was to provide an improved apparatus for distillation of multicomponent mixtures and a simple form of fractionation equipment for commercial distillation plants. It should be noted that vertical flat-plate columns do not appear as main falling film distillation equipment. Its application is much more concentrated in heat, mass and momentum transfer determination (DEFRAEYE; BLOCKEN; CARMELIET, 2012; HALICI; TAYMAZ; GÜNDÜZ, 2001).

2.5.4 Internally heat-integrated columns

An internally heat-integrated distillation column (HIDiC) is characterized by a better energy saving potential than its conventional counterparts (KATAOKA *et al.*, 2014; NAKAIWA *et al.*, 2003; NODA *et al.*, 2000). An experimental research of high relevance was carried out by Lueprasitsakul *et al.* (1990) using a wetted-wall column. The authors showed that heat integration system could be feasible even in falling film distillation columns. However, a HIDiC system for industrial use requires much higher internal heat transfer and also better distillation efficiency in each section. Industrial-scale researches on this setting are few so far. Nakanishi *et al.* (2008) successfully operated a HIDiC pilot-scale plant, which consisted of seven concentric double-tube unit. The double-tube unit is a fractional and heat transfer apparatus in which the inner tube works as a rectifying section, the outer tube works as a stripping section, and in the inner tube wall is where heat transfer occurs. The energy consumption of this pilot-scale HIDiC was reduced by at least 40% compared to a conventional distillation column with the same scale capacity, pointing out the technical feasibility of this column design.

A laboratory-scale structured annular column with internal heat integration was constructed by Xu *et al.* (2014) to investigate the heat transfer and separation performances. The authors demonstrated that heat transferred in this setting increased with the pressure ratio, and about 50% of the heat from the inner column was transferred to the outer column when the pressure ratio was 1.6. In this case, the heat transfer rate was 1.5 times higher than a similar wetted-wall column distillation to the same separation system. Their experimental results further demonstrated that although heat transferred with the internal thermal heat-integration has increased with the pressure ratio, the total heat transfer coefficient and the

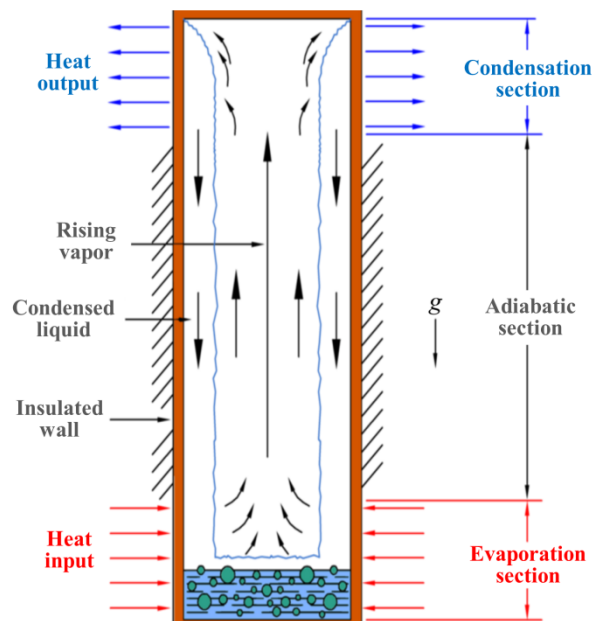
separation efficiency of the outer column have decreased. This indicates that heat transfer capacity cannot be increased by increasing the pressure ratio, and a suitable pressure ratio must be selected to obtain good heat transfer as well as separation efficiency for the HIDiC system on wetted-wall distillation columns.

2.5.5 Thermosyphon-assisted columns

Thermosyphons are closely related to heat pipes, and the investigation and their applications into thermal engineering are known for years (HUMINIC *et al.*, 2011). The use of heat pipes within traditional systems provides a full utilization of the superconducting property, leading to high heat transfer rates. This equipment has attracted attention to a large number of applications, such as solar collectors (RASSAMAKIN *et al.*, 2013), refrigeration of electronic components (CHANG *et al.*, 2008; ZHU *et al.*, 2019), heating of asphalt tanks (MILANEZ; MANTELLI, 2010), reactor cooling in nuclear plants (GE; LI; SHAN, 2019), cooling of miniature compressors (POSSAMAI; SETTER; VASILIEV, 2009), among many others. Regarding the special type of thermosyphon-assisted technologies, these are also already well-established (DA SILVA; MANTELLI, 2004; MANTELLI; ÂNGELO; BORGES, 2010; MILANEZ; MANTELLI, 2010), and aimed at optimizing the heat exchange required for the process, leading to energy minimization, and with it being possible to operate the process with a more compact equipment. In this sense, a novel proposal related to falling film distillation was presented by Saifutdinov *et al.* (2009), where distillation occurs through a falling liquid film formed inside vertical tubes thermally insulated by an energy transporting fluid. According to the authors, this process requires less amount of energy for the same separation, as well as the dimensions of the apparatus are reduced. Thus, it is an equipment more compact, versatile and economical, since separations by conventional distillation demand higher amounts of energy and occupied process area. However, the use of vacuum inside the distillation tubes is an unfavorable feature in this proposal, which imposes some restrictions for the equipment operation. To overcome this limitation and towards reducing energy expenditure in falling film distillation processes, our research group recently solicited a patent of a new distillation apparatus that operates through falling liquid film, called Destubcal technology. This device has coupled a two-phase closed thermosyphon (TPCT) that is responsible for the energy supply to the process. A two-phase closed thermosyphon (Figure 8) is a particular type of heat pipe, in which the condensate returns to the evaporator, driven

by gravitational forces (FRANCO; FILIPPESCHI, 2012). This equipment operates in a two-stage cycle where evaporation and condensation enthalpies are used for heat transfer (FERRANDI *et al.*, 2012; HE; MEI; LONGTIN, 2017; JAFARI *et al.*, 2017). The main advantage of the TPCT is that no mechanical pumping is required as its operation is completely passive. There are no moving parts and the device is permanently sealed at the time of manufacture. As a consequence, these devices are cheaper and more reliable (MANTELLI, 2013).

Figure 8 – Scheme of a two-phase closed thermosyphon.

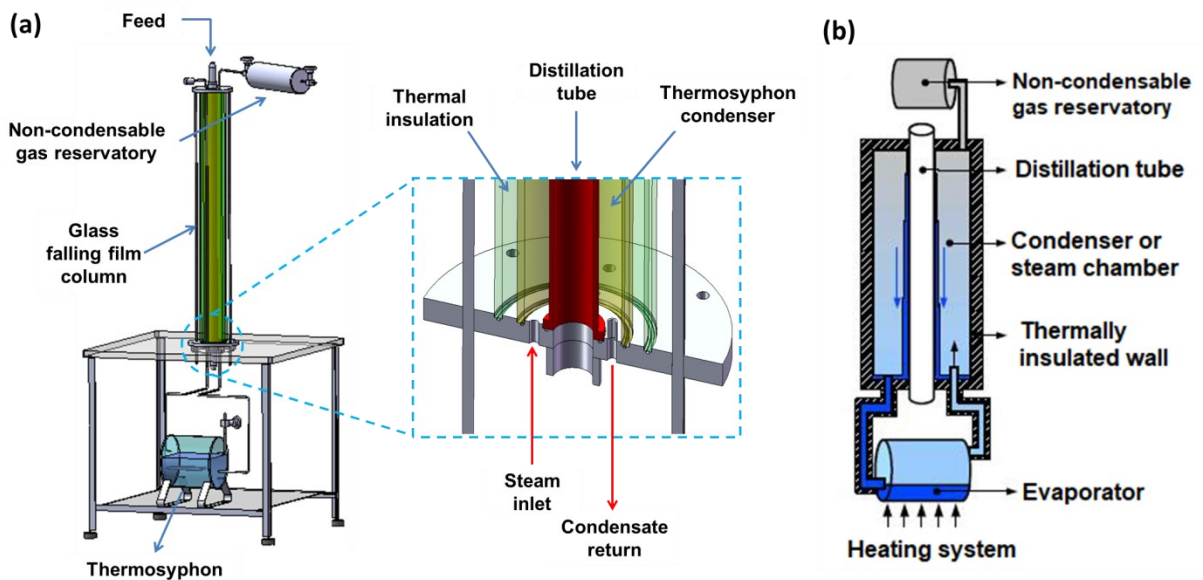


Source: Kannan and Natarajan (2010).

Thermosyphon-assisted Destubcal technology consists of a vertical falling film unit, in which the liquid flows by the gravity force, creating a thin liquid film on the wall of an inner distillation tube. The energy supplied by the electric resistances in the thermosyphon is responsible for the separation of the volatile components present in the falling liquid film into the distillation tube, promoting heat and mass transfer from the liquid phase (film) to the vapor phase (bulk). Throughout the column, the direct contact of the falling liquid film with the rising vapor allows continuous evaporation and condensation at the interface, which characterizes the distillation process. Figure 9 illustrates the experimental prototype of the Destubcal technology, built in borosilicate glass. In the detail, the first concentric tube, called distillation tube, is where liquid film formation occurs and distillation takes place. In the

second concentric tube, or also called the steam chamber, is where the transporting energy fluid flows, which is responsible for heat transfer. The third and last concentric tube has the thermal insulation function of the column, vacuumed inside to avoid heat loss to the environment. The distilled vapor exits at the top of the column; it is condensed and collected as the light product, while the bottom liquid exits at the bottom of the column and goes to a storage tank as the heavy product. It is important to note that this unit can operate with two different modes of heating (isothermal and temperature-profile) through the steam chamber, which differentiates it from other technologies. With this form of energy supply, heat is transferred along the entire height of the distillation column by the thermosyphon's steam chamber located externally to the distillation tube. In addition to the distribution of heat from a single point to the whole unit, there is a more efficient energy source, which is the use of a closed-cycle thermosyphon. Further, Destubcal unit has the great differential of operating inside the distillation tube at atmospheric pressure, without the need of vacuum.

Figure 9 – Glass prototype representation of the thermosyphon-assisted falling film Destubcal technology (a); Thermosyphon closed-cycle operational diagram (b).



Source: Battisti, Machado and Marangoni (2020).

Marangoni *et al.* (2011) worked with the experimental prototype, conducting tests with a binary ethanol-water mixture under different flow rates and temperature conditions. Although the new proposal showed a relatively lower degree of purification than the conventional ones, the results indicated that the process had viability, since the new model of

heat supply allowed the purification of the ethanol to a satisfactory grade. The authors reported that the main advantage of this new unit is the reduction of physical dimensions; therefore, this is a promising result for the petroleum industry, since it allows distillation in environments with reduced space such as offshore platforms. Parisotto (2013) performed an experimental work in this unit, testing the heat supply in two ways: with the steam chamber operating in isothermal condition, and with the steam chamber operating in temperature-profile condition. For the first case, smaller ethanol mass fractions were obtained, but when the operational condition was set as temperature-profile, the process presented results that were compared with a conventional distillation column corresponding to the seventh tray (in a 13-stage column with the recovery of 92% ethanol by volume). Peruzzo (2013) evaluated the dehydration of triethyleneglycol using this new thermosyphon heat-assisted falling film distillation column. The results showed a significant reduction of 38.4% to energy consumption when compared to a conventional sieve tray distillation column. More recently, two new thermosyphon-assisted stainless steel falling film distillation units were built with the same Destubcal technology: a monotube unit (with only one distillation tube), and a multitube unit (with nine equal space-distributed distillation tubes), both have the same length (1.0 m) and diameter (2.64 cm) dimensions of the glass prototype distillation tube.

Silva Filho *et al.* (2018) carried out several experiments in both pilot-scale Destubcal units to evaluate the separation of an aromatic mixture, running isothermal and temperature-profile conditions. The longitudinal temperature of the steam chamber in the isothermal condition is reached without the presence of non-condensable gases, by imposing a vacuum in this region of the apparatus, thus the temperature along the distillation tube remains constant. When in the presence of non-condensable gases, a dead zone is created and the temperature drops abruptly (HE *et al.*, 2017). Thus, the heat transfer in the non-condensable gas region is significantly smaller than the section of the condenser where the phase change is taking place, decreasing the effective heat exchange length (SAUCIUC; AKBARZADEH; JOHNSON, 1996; STEVANOVIC; STOSIC; STOLL, 2006; ZHOU; COLLINS, 1995). Therefore, the imposition of a temperature-profile condition in the steam chamber is obtained with a certain volume of non-condensable gases, which is realized in practice by the operation with pressure in the steam chamber of 0.34 bar, in this case, and a temperature gradient is imposed along the distillation tube. In this way, it is possible to operate the distillation unit in isothermal condition (axially constant temperatures) or with a temperature-profile condition (different temperatures) along the unit height. According to the authors, the best separation result was

found using the monotube unit, with about 25.2 wt% enrichment of toluene mass fraction in the distillate stream. The authors also proved with simulations in Aspen Hysys[®] that Destubcal technology is an alternative for the distillation of aromatic compounds, requiring less energy consumption than conventional sieve tray columns. Using the same experimental apparatus, Pires *et al.* (2020) evaluated the feasibility of recovering monoethyleneglycol in the monotube unit of the Destubcal technology. For experiments in isothermal mode, conditions with lower values of feed flow rate required higher power in the evaporator (P_{mass}). In this condition of lower flow rate in the distillation column, the fluid flow with higher viscosity approaches the laminar region, thus reducing the heat transfer coefficient between the steam chamber and the distillation tube, which requires more power in the evaporator to achieve the same degree of separation. Under temperature-profile condition an increase in feed flow rate caused a reduction in the difference between the bottom and top temperatures in all conditions. Thus, less power is required for the same recovery, indicating that temperature-profile operation could be more thermally efficient. Nevertheless, higher amounts of power were required to get higher mass fractions of monoethyleneglycol in the bottom stream, reaching 88.61% of recovery in the best condition. Increasing the feed flow rate increased the bottom flow rate, but reduced the monoethylene glycol fraction, consequently reducing the product recovery. This behavior was attributed to the fact that an increase in the feed flow rate led to an increase in the thickness and velocity of the liquid film, which made monoethylene glycol separation difficult. The authors also demonstrated that the monotube column presented a lower energy requirement when compared to a conventional sieve tray tower (reduction of 22.6%), emphasizing that is necessary only two passes in series through the falling film column to obtain the same recovery that an industrial conventional system provides.

Querino, Marangoni and Machado (2018) used the stainless steel monotube thermosyphon-assisted unit to evaluate the separation of a multicomponent mixture of synthetic naphtha in indirect series of falling film columns, i.e., the bottom product leaving the first distillation enters as a feed for the second distillation, and so on. For the first, second, and third series of distillation, the enriched hexane mass fractions obtained in the upper stream were 0.58, 0.72 and 0.82 wt%, respectively. Energy analysis of the overall process also showed a 12% reduction in energy consumption of the falling liquid film column compared to the conventional distillation under the same process conditions. In two recent complementary works, the viability of separation of the water-ethanol binary mixture was tested in the same

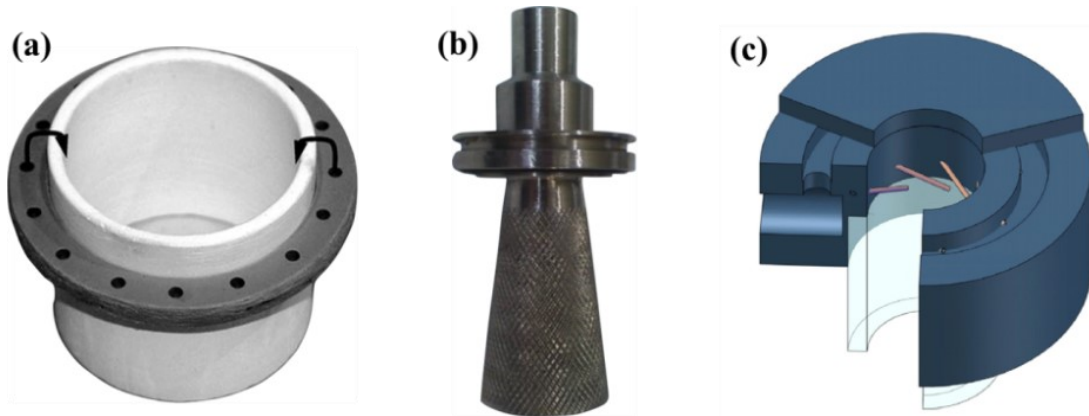
monotube column in order to compare the two possible operational conditions of the steam chamber (isothermal and temperature-profile). Marangoni *et al.* (2019a) carried out experiments in isothermal condition (Part I), and Marangoni *et al.* (2019b) operated the steam chamber in temperature-profile condition (Part II). The effect of different process conditions was studied, such as feed flow rate, steam chamber temperature, and feed mixture temperature. In both works, the authors demonstrated the feasibility of using this new separation technology for the water-ethanol azeotropic system, which motivates the continuation of the works and encourages new proposals on optimization, energy consumption evaluation, and dynamic modeling of this novel process.

2.5.6 Feed liquid distributors

To ensure the efficiency of these design applications systems, the heat and mass transfer surface must be completely and uniformly wetted with the thin liquid film. This requires the liquid to be evenly distributed at the top of the wall, and to establish a thin liquid film over the entire surface of the column. This wetting process is directly influenced by the properties of the liquid film and the surface itself, the apparatus geometry, and the operational parameters (LU *et al.*, 2017; MANOUCHEHRI; BANISTER; COLLINS, 2015; MORISON; BROOME, 2014). The initial formation of the liquid film significantly influences the wetting behavior of the tubes. For perfect wetting behavior, falling film units are generally implemented with a liquid distributor for the feed flow. Important rules for the design of liquid distribution in falling shell-tube evaporators have been published by Goedecke (2006). Morison, Worth and O’dea (2006) studied the wetting behavior on a falling film column with a vertical stainless steel tube of 1.0 m long and 48.0 mm of internal diameter. Water and other aqueous solutions of glycerol, alcohol and calcium chloride were used as feed liquid mixture. The authors used a widespread distributor type, which is a perforated plate arranged horizontally above the tube sheet. The distributor chosen was an unglazed ceramic ring having the same internal diameter as the evaporator tube, as shown in Figure 10 (a). The solution flowed from an outer connection through a perforated ring and over the dispenser to form a coherent film in the ceramic, before flowing into the tube. Another differentiated distributor for a feed system of a wetted-wall column was studied by Pehlivan and Özdemir (2012). The distributor device forms a ditch with a triangular slit in combination with a single groove around the inner circumference of the tube. The authors concluded that this feed

distribution device provided a homogeneous distribution and has a significant effect on overall performance, being directly responsible for the film thickness in the inner tube system.

Figure 10 – Types of liquid distributors: (a) Perforated ceramic ring; (b) Grooved cone-shaped distributor; (c) Distributor with inclined needles.



Source: Haidl et al. (2016); Morison, Worth and O’dea (2006); Teleken et al. (2012).

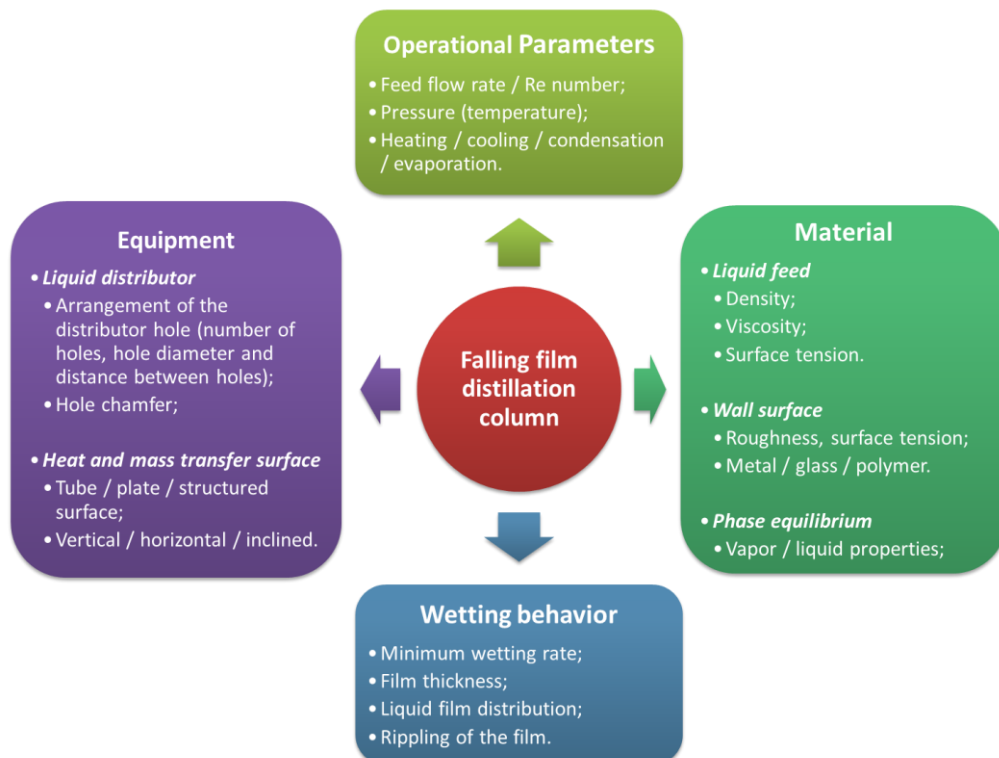
In recent years, a considerable interest is emerging for using computational fluid dynamics (CFD) to model multiphase discharges within many chemical engineering equipments (NORILER *et al.*, 2008). Teleken et al. (2012) presented a CFD computational study to assist the design of a feed distribution system for a falling film distillation process. By simulations, two different systems were evaluated, one static and other with rotational movement. The distribution system consisted of a grooved cone-shaped distributor, as shown in Figure 10 (b), which led to the formation of the liquid film near the wall of the distillation tube. Based on this study, the cone system was built and installed in the pilot-scale units. Another interesting system of liquid distribution was presented in two sequential works done by Rejl *et al.* (2016) and Haidl *et al.* (2016). The liquid is fed into the inner wall of the column using 8 needles which are inserted into the distributor, as shown in Figure 10 (c). Needles with an inner diameter of 0.8 mm and length of 25 mm are aligned tangentially by the perimeter and inclined at 30° to the axis of the column. Thereby, the liquid flow entering the column has a tangential velocity component which ensures the fusion of the individual fillets into the uniform liquid film along the entire perimeter at the top of the column. This liquid dispenser was able to provide a stable corrugated film at flow rates over 110 mL/min for pure water, and 80 mL/min for NaOH solution and organic solvents. Recently, Liu et al. (2017) studied the optimal design through numerical simulation of a liquid feed distribution

system in a falling film column. The authors concluded that design of the upper surface of the distributors can improve the liquid distribution and the use of perforated baffles can avoid non-uniform flow fields, bringing substantial economic benefits for the process.

2.6 SEPARATION EFFICIENCY ASPECTS

The distillation process efficiency can be considerably improved by intensified designs (BALDEA, 2015; KIM, 2016; REAY; RAMSHAW; HARVEY, 2013). In this approach, one must consider the minimum use of capital and energy resources over the useful and safe life of the process (KEIL, 2018). The intelligent design of a distillation column involves the following approach levels: (1) The materials used for construction and the available resources; (2) The process design and configurations; (3) The internal optimization of the project (ANEESH *et al.*, 2016; NEVES; SILVA; OLIVEIRA, 2005). The efficiency intensification in falling film units may be influenced by several variables, such as liquid film properties, surface characteristics, design apparatus, and operational parameters (ÅKESJÖ *et al.*, 2017; LU *et al.*, 2017), as shown in the schematic diagram of Figure 11.

Figure 11 – Key factors affecting separation efficiency in falling film distillation units.



Source: Battisti, Machado and Marangoni (2020).

2.6.1 Feed temperature

According to Brauner, Maron and Harel (1985), the minimum wetting rate for a dry or wet solid surface, and the minimum flow required to maintain a continuous flow of the liquid film are functions of the feed temperature and feed concentration of the mixture. The net properties, such as density, surface tension, and viscosity affect to a great extent the required wetting and breaking rates of continuous films. In falling film distillation, the transfer efficiency generally increases with increasing evaporation temperature. The vapor pressure is an exponential function of temperature (WILSON, 1964). Therefore, the concentration difference between the evaporation and condensation sides, and so the transferred molar flux, strongly increases with increasing temperature. Thus, at high evaporation temperatures, high transfer efficiencies are obtained even with low selectivities based on the diffusion separation effect; and at low temperatures, high selectivities are obtained with low transfer efficiencies (FULLARTON; SCHLÜNDER, 1986). Marangoni *et al.* (2019a) experimentally analyzed the effect of feed temperature on a falling film distillation process with ethanol-water binary mixture in a wetted-wall column. That column is characterized by the lateral-side heating system which is supplied by a steam chamber along the entire distillation tube. The authors found that ethanol recovery is favored when feed temperatures are higher than the saturation temperature (bubble point) of the feed mixture and associated with higher temperatures of the steam chamber, provided by the thermosyphon. In these cases, heat flux is favored and higher distillate product flows were observed.

Lateral heating of the column walls causes a temperature gradient within the film. Thus, the fluid temperature consequently also changes due to lateral-side heating causing this gradient (ÅKESJÖ *et al.*, 2018). According to Schnabel and Schluender (1980), for turbulent films, most of the heat transport resistance is found in the boundary layer close to the wall. For laminar flow, the temperature profiles within the film are different. For the case of evaporation, the temperature profile is linear, while for heating it has an exponential decline, indicating a resistance to heat transfer throughout almost the entire film. The highest heat transfer is usually achieved in the laminar regime for very low flow rates due to the thin liquid film or for very high flow rates in the turbulent regime, due to the increase in the fluid mixture. However, industrial scale units are often operated in the transition regime, as low feed flow rates can lead to dry surface problems (film breakage), and high feed flow rates lead to increased heat loss and operating costs (JOHANSSON; VAMLING; OLAUSSON, 2009).

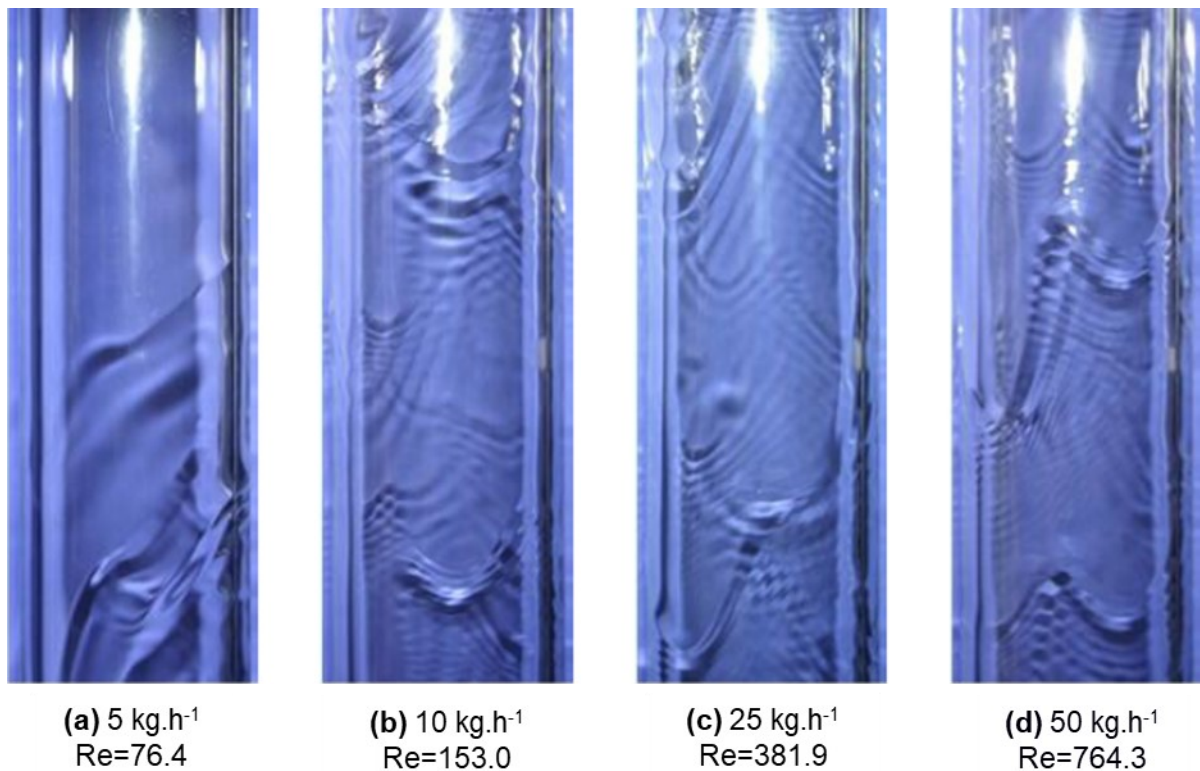
2.6.2 Feed flow rate

The flow hydrodynamics of falling liquid films has been extensively studied in the literature. Regardless of the field of application, it can be assumed that hydrodynamics governs other physical phenomena (heat and mass transfer, for example), as well as the overall performance of the equipment (ÅKESJÖ *et al.*, 2017). Density, viscosity, surface tension and flow rate were identified as determinant factors for the hydrodynamics of the falling liquid films (ZHANG *et al.*, 2009). Most of the preliminary investigations (GILBERT, 1947; SELKER; BURK; LANKELMA, 1940; STERN, 1962) on the performance of wetted-wall distillation columns were intended to empirically compare the relative efficiencies of conventional and packed columns, rather than do any fundamental study of the apparatus itself. The columns used were mostly of small diameter, generally less than 1.0 cm, and the liquid flow rate was such that the laminar vapor flow always prevailed. In general, experimental data show that the separation efficiency decreases with increasing liquid flow rate of the film. According to Gilbert (1947), at high reflux rates (i.e., falling liquid flow rates) in a wetted-wall column, lower *HTU* values result from what would be expected due to the flow in pseudo-streamline, causing ripples in the liquid film in Reynolds numbers of the film greater than 25. The flow rate in pseudo-streamline is characterized by wavy movement that produces turbulence in the liquid film, based on the Reynolds number as being greater than 25 and smaller than 1500. Contrary to the usual findings for separations with falling liquid films (where low feed flow rates are recommended), Marangoni *et al.* (2019a) observed that higher values for the feed flow rate improved the separation of ethanol-water system. This fact may be characteristic of the low viscosity of the mixture and due to the atmospheric pressure operation of the apparatus (falling film distillation columns are usually low pressure or vacuum operated). With a higher flow rate, a thicker film is formed, and due to the combination of the thermal conditions of the feed and the steam chamber there may be increased and high-quality evaporation of ethanol.

Li *et al.* (2018) studied the flow characteristics of a liquid film flowing over a smooth surface and structured surface under a Reynolds number range from 10 to 1121. The authors pointed out that feed flow rates have high effects on wettability, film velocity and film thickness. Liquid films with low flow rates have poor wettability and small thickness, which decreases heat transfer resistance but also increases the possibility of dry spots. In addition, the authors also showed in a CFD study that the ripple surface structure hinders the liquid film

movement, reflected in a lower velocity and a larger film thickness compared to the smooth surface. Teleken (2013) carried out a study of the falling liquid film behavior with a gradual increase of the feed flow rate, as a function of Re , as can be visualized in Figure 12. From the images of the liquid film flow on the inner distillation tube, the influence of feed flow rate on maintenance and flow characteristics was qualitatively related. Increasing the feed flow rate, the flow regime goes from laminar, $Re=76.4$, with the feed flow rate of $5 \text{ kg}\cdot\text{h}^{-1}$, for transition, $Re=153.0$ and $Re=381.9$, with feed flow rates between 10 and $25 \text{ kg}\cdot\text{h}^{-1}$ respectively; and later turbulent, $Re=764.3$, with feed flow rate of $50 \text{ kg}\cdot\text{h}^{-1}$. In the experiments with feed flow rates of 10 , 25 and $50 \text{ kg}\cdot\text{h}^{-1}$, 100% coverage of the evaporating surface was obtained by the falling liquid film. The results obtained are within the range of values obtained by Batistella (1999), with a maximum feed flow rate of $50 \text{ kg}\cdot\text{h}^{-1}$ and a minimum feed flow rate of $5 \text{ kg}\cdot\text{h}^{-1}$. It is important to observe this behavior, because at high feed flow rates the velocity of the falling liquid film becomes very high, raising the number of waves on the surface of the film and also resulting in a shorter residence time on the evaporating surface of the distillation tube, which may hinder the distillation process, as well as separation and energy efficiency.

Figure 12 – Behavior of a falling liquid film on the surface of a distillation wetted-wall tube at different feed flow rates.



Source: Teleken (2013).

2.6.3 Operational pressure

When a binary or a multicomponent thin liquid film flows onto a heated surface under vacuum, evaporation at the free surface leads to the depletion of the more volatile component (or components) of the liquid phase (BHANDARKAR; FERRON, 1988; HO; UDELL, 1992). The transfer rate of the volatile species to the vapor phase is affected by heat and mass transfer rates through the liquid flow, and the heat and mass transfer rates are in turn coupled through the interfacial conditions, i.e., the operational pressure at the film interface (DAVIS; HUNG; DUNN, 1973). According to Lindsey, Kiefer and Huffines (1952), in the evaluation of a rectifying equipment there are two primordial considerations, i.e., the size of the apparatus required to effect a certain separation, and the pressure drop suffered by the vapor when passing through the apparatus. The pressure drop consideration is particularly important in vacuum distillation process because the increasing in the column pressure can cause an undesirable rise in the liquid boiling point (HICKMAN, 1944).

In the literature, however, there is a dearth of data for liquid films at low pressures. Shahzad *et al.* (2013) showed that heat transfer coefficient is found to increase with decreasing evaporator saturation temperatures, i.e., decreasing operational pressure, and this is due to bubble agitation effect because of high vapor specific volume. With low pressures micro bubbles are generated near to the tube wall surfaces and they enhanced the heat transfer by two to three folds. Stern (1962) conducted an investigation about the effect of reduced pressure on the performance of a wetted-wall distillation column operating under total reflux condition. The wetted-wall column was chosen instead of a packed column in the expectation that the elimination of the column packaging as a variable, i.e., elimination of the liquid-vapor contact area as a variable would allow a more fundamental examination of the reduced pressure effect in the distillation process. The most important conclusion drawn from the results of this research is that in all regions of vapor flow (laminar, transition and turbulent), a decrease in operational pressure causes an increase in column separation efficiency. Munakata and Matsuda (1973) and Munakata, Matsuda and Watanabe (1974) showed that falling film columns are applicable to vacuum distillation because of the low pressure drop, and therefore its high admissible vapor load, but the operational limits were still uncertain due to insufficient experimental and theoretical research done up to that time. Based on this, the authors conducted experimental and numerical studies to predict how these limits would vary over a pressure range from atmospheric to strong vacuum in a wetted-wall column. It was

pointed out that both the upper sonic speed limit and the upper pressure limit should be considered as upper vapor flow limits in a falling film column under vacuum distillation condition.

2.6.4 Film thickness

The more accurately the film thickness can be evaluated, the more precise can be analyzed the heat and mass transfer characteristics of the liquid film (AOUNE; RAMSHAW, 1999). In addition, with a better understanding of the film flow characteristics, the dynamic interfacial contact area can be more accurately evaluated, i.e., the effect of corrugations on the liquid film in the interfacial area can be taken into account to provide better design information, even in the case where the liquid film plays a relatively small role in the overall process, and that the vapor film is what controls the transfer resistance (BOUTEBILA, 2009; KLETT, 1965). The minimum specific net flow required to establish or maintain total surface coverage is known as the minimum wetting rate (Γ_{min}). From the transport point of view, it is more desirable to operate with the thinnest uniform film possible, that is, $\Gamma_{dry} < \Gamma < \Gamma_{flooded}$. The average thickness of liquid films was and continues to be extensively measured and mapped for different equipment configurations and operating conditions (LUKACH; RADCHENKO; TANANAYIKO, 1972). Jackson (1955) tested six liquids with different viscosities from 0.5 to 20 cP, during falling flow in the inner wall of a vertical tube. A trace of radioactive material dissolved in a liquid was used which allows the thickness of a moving film to be determined by the measurement of the radiation emitted. The method was fast and accurate, and a mean thickness was obtained directly, although the surface of the film may be irregular. Karimi and Kawaji (1998) performed simultaneous measurements of the local film thickness and the instantaneous velocity profile within a liquid film using the high-speed photography technique and the laser induced photochromic dye technique. In addition, as measurement techniques became increasingly sophisticated, it became possible to study the structure of the flow below the liquid interface and measure velocity components with such techniques as the laser doppler velocimetry (LDV) (DIETZE; AL-SIBAI; KNEER, 2009), particle image velocimetry (PIV) (HAMBLETON; HUTCHINS; MARUSIC, 2006), particle tracking velocimetry (PTV) (ZADRAZIL; MATAR; MARKIDES, 2014), and thermographic particle velocimetry (TPV) (CHAROGIANNIS; ZADRAZIL; MARKIDES, 2016).

Particularly for laminar falling films, the heat transfer increases as the film thickness decreases (LIU *et al.*, 2020), hence it is desirable to keep the films as thin as possible. Zhong, He and Longtin (2020) recently proposed a new pulsed flow technique to maintain a continuous falling film inside a vertical tube 750 mm long and 22.2 mm of diameter to reduce fluid power, fluid flow rate and film thickness. It was found that the minimum flow rate situation of 0.38 L/min flow rate with 20% duty cycle was able to maintain a continuous film approximately three times thinner than the minimum obtainable film for continuous flow, and a volume flow rate reduction of up to 80%. In addition to a thinner average film thickness, the authors demonstrated that the pulsed falling film provides for potentially reduced power consumption by the pump. Also, by actively controlling the mass flow rate, dryout can be avoided (actively managed) by detecting situations where the film becomes too thin and increasing the liquid mass flow rate.

2.6.5 Interfacial area

Falling liquid films exhibit a complex free surface topology due to the occurrence of surface waves, developed as a result of the inherent instability caused by disturbances of the gas-liquid or vapor-liquid interface (DIETZE; KNEER, 2011). Kapitza and Kapitza (1965) were the pioneers in this field, and used the liquid shadow photograph technique to study the development of flowing waves. Since then, several authors have observed that the presence of wavy motion on the surface of a falling liquid film significantly increases the heat and mass transfer rates between the liquid film and the adjacent gas/vapor phase (BANERJEE; SCOTT; RHODES, 1968; PORTALSKI; CLEGG, 1971; STIRBA; HURT, 1955). In some cases, these changes are quite substantial, reaching a twenty-fold increase in the rate of carbon dioxide absorption, for example, as presented by Davies (1964). These increased rates are most likely due to the combination of three effects: vigorous mixing due to ripples, increased turbulence in the gas/vapor stream, and some increase in the interfacial area caused by wave motion (PORTALSKI, 1964). Although there have been some attempts to investigate the effect of interfacial area quantitatively, there are many discrepancies in the literature regarding the extent to which the interfacial area increases due to undulations. Brauer (1956), for example, observed an increase of 0.5% to 3%, whereas Tailby and Portalski (1960) found an increase of up to 50% for water films ($Re_L \in 200-2000$). Estimations to describe wave formation and incorporate the effect on mass transport rate were conducted by Barrdahl (1988), Wasden and

Dukler (1990), and Yoshimura, Nosoko and Nagata (1996). According to Nielsen *et al.* (1998), high gas/vapor flow rates may be the main factor influencing the formation of undulations in falling liquid film, as demonstrated by experimental work.

At a higher level (top of the falling film column), the liquid phase flow may be both turbulent and laminar. Thus, even laminar liquid films can present complex wave dynamics. Instability in the liquid film grows as it moves downward and evolves to various flow regimes, depending on the operating conditions. The onset of instability is only a small part of the evolution of the waves in a falling film. As predicted by theory, falling liquid films generally exhibit a symmetry-breaking cascade that leads from flat film flow to two-dimensional periodic waves (chain and height dimension), which eventually evolves into three-dimensional waves (dimensions and height in axial and transverse directions) (ALEKSEENKO *et al.*, 2005). In general, as Fulford (1964) pointed out, smooth laminar flow occurs only in small Reynolds numbers on the order of 10. Gravity ripples begin to appear in moderate Reynolds numbers. The capillary waves are present mainly in larger flows. Scrolling waves often occur above a Reynolds number of the order of a few hundred. The wave structure gradually changes from stationary to non-stationary as the flow increases, and finally changes to a stochastic nature when the turbulent flow begins. With Reynolds number of approximately 1100–2000, the falling liquid film then becomes totally turbulent.

Several researchers have already shown that the occurrence of wave fluctuations on free falling films cause dramatic increases in mass transfer, especially in laminar flow conditions (WASDEN; DUKLER, 1990). To generate the wavy or turbulent liquid film, an effective heat and mass transfer enhancement techniques are usually used. Coated division tubes (WANG *et al.*, 2010) and micro-structures (DONG; QUAN; CHENG, 2014) were the technologies most widely adopted to increase film fluctuation and enhance heat and mass transfer. Recently, many researchers have devoted efforts to prevent or hinder the appearance of dry spots in falling films by adding nano-fluid, hydrophilic modification and porous coating (JEONG; CHANG; CHANG, 2008). Zheng *et al.* (2020) proposed a superhydrophilic treatment processed with a micro/nano structure in copper tubes. The liquid film spreading width for the superhydrophilic tube is two times higher than that of plain surface and little relevance to spray density. That further offered a higher mass transfer performance for the falling film on the superhydrophilic surface at a low spray density.

2.7 MODELING AND SIMULATION APPROACHES

Computational tools for multistage separation processes design and simulation, such as distillation and absorption, are generally based on equilibrium stage-based model approach, which is already well established in textbooks (HENLEY; SEADER, 1981; HOLLAND, 1975; KING, 1980). It assumes that liquid and vapor streams that leave any stage are in thermodynamic equilibrium. In this case, it is necessary that the contact time between phases would be enough to establish the vapor-liquid equilibrium between the output streams of each stage. Until mid-1985 all mathematical models of falling film or wetted-wall column separation were based on equilibrium stage approach modeling. Since then, with the boosted expansion of computational tools, more sophisticated models based on non-equilibrium stage-based approaches, as well as CFD designs, have spurred the development of several numerical techniques for predicting hydrodynamic behavior, heat and mass transfer, and separation efficiency in falling liquid films in distillation conditions. Table 4 summarizes the modeling and simulation approaches for falling film distillation in wetted-wall columns over the years, pointing out the main differentials brought and their system applications already made.

The simultaneous heat and mass transfer process in falling film distillation was modeled and simulated for the first time by Davis, Hung and Dunn (1973). The authors were able to rigorously analyze the convective diffusion phenomena associated with a thin film vacuum distillation to predict separation efficiencies as functions of the length of the heated wall surface over which the thin liquid flowed. Two years later, Kayihan, Sandall and Mellichamp (1975) modeled as a simultaneous heat and mass transfer process the binary distillation of methanol-water in a wetted-wall column. Combining the mass and energy balances with equilibrium ratios for the liquid and vapor phases, the set of equations provided information on the phase's temperature and compositions, and completely defined the physical state of each phase. Noting that conventional methods before were directed to provide only the compositions, so this new approach made it possible to predict the individual mass transfer coefficients of the film by measuring the temperatures and compositions of the liquid phase, such as column height functions. Krishna (1977) modeled the non-equimolar interphase mass transfer process for falling film distillation of a multicomponent mixture through the 2-pentene-ethanol-water system. It is observed that when the chemical species composing the mixture are very different in terms of molecule size and nature, both the diffusional interaction effects and the non-equimolar mass transfer effects become important.

Table 4 – Modeling and simulation works on falling film distillation in wetted-wall columns.

Simulated mixture	Model equations	Condition process	Phase approach	Algorithm	Software	Predicted output information	Reference
Benzene-n-butanol	Liquid and vapor phases, energy and mass balance	Steady-state	Equilibrium	Analytical	n.a.	Number of transfer units	(BRADY, 1969)
Methyl-cyclohexane-toluene	Empirical and theoretical material balance	Steady-state	Equilibrium	Regression	Fortran [®]	Efficiency and correlation for number of transfer units	(GABBAY, 1970)
n-Butanol-benzene and n-propanol-benzene	Overall mass and energy balance and physical properties	Steady-state	Equilibrium	Analytical	n.a.	Height of a wetted-wall distillation column	(CHATLYNNE, 1972)
Fatty acids (C ₆ – C ₂₀) from tall oil	Laminar film flow in inclined surface; energy balance and convective diffusion equation	Steady-state	Equilibrium	Newton-Raphson	n.a.	Concentration profiles for various axial positions and separation efficiencies	(DAVIS; HUNG; DUNN, 1973)
Methanol-water	Energy and material balances around the liquid and vapor phases	Steady-state	Equilibrium	n.a.	n.a.	Liquid and vapor phases temperature and compositions	(KAYIHAN; SANDALL; MELLICHAMP, 1975)
Pentane-2-ethanol-water	Thin film model and interphase relations	Steady-state	Equilibrium	Analytical	n.a.	Multicomponent mass transfer coefficients and transfer rates	(KRISHNA, 1977)
Benzene-toluene-ethylbenzene	Overall mass, energy and component balances around three envelopes	Steady-state	Equilibrium	n.a.	n.a.	Individual mass transfer rates as function of column height	(DRIBIKA; SANDALL, 1979)
Methanol-water	Energy balance at the vapor-liquid interface	Steady-state	Equilibrium	Quasi-linearization	n.a.	Overall vapor phase height of a transfer unit	(ITO; ASANO, 1982)

Methanol-ethanol-water	Energy and mass balance for the liquid film	Steady-state	Equilibrium	n.a.	n.a.	Interfacial velocity as a function of heat and diffusion fluxes	(KOSUGE; ASANO, 1982)
n-Hexane-toluene	Mass and energy balance; Film theory and zero mass transfer resistance in the vapor phase and linear temperature profile in the liquid phase	Steady-state	Equilibrium	Adams' or Euler's method	n.a.	Phase temperature and composition profiles along the axial height	(DAVIS; TUNG; MAH, 1984)
Acetone-methanol-ethanol	Energy and material balance and auxiliary relations	Steady-state	Equilibrium	Euler's method	n.a.	Axial distributions of liquid concentrations, reflux flow rates and temperatures	(KOSUGE; ASANO, 1984b)
Benzene-toluene, ethanol-water, acetone-chloroform; Benzene-toluene-ethylbenzene, acetone-methanol-water, methanol-isopropanol-water, acetone-methanol-ethanol, benzene-toluene-m-xylene	Material and energy balance equations for each phase together with mass and energy transfer rate equations around the interface	Steady-state	Non-equilibrium	Newton's method	n.a.	Composition and temperature profiles for each phase	(KRISHNAMURTHY; TAYLOR, 1985a, 1985b)

H ₂ O-HTO isotope	Continuity equation for multicomponent fluid and auxiliary relations	Steady-state	Equilibrium	Newton's iterative method	n.a.	Mole-fraction profiles along the axis of the tube	(SUGIYAMA <i>et al.</i> , 1998)
Water and oil	Navier-Stokes equations and phase field model	Steady-state	n.a.	Finite element method	COMSOL [®]	Flow profile along the distillation tube with different inlet velocities	(GONÇALVES <i>et al.</i> , 2014)
Ethanol-water	Momentum, heat and mass transfer equations based on the laminar boundary layer theory	Steady-state	Equilibrium	Quasi-linearization method	n.a.	Heat and mass transfer rates in the vapor phase	(PARK <i>et al.</i> , 2017)
Benzene-toluene and p-xylene-o-xylene	A vertical multitube-type heat exchanger package of equations implemented in a predefined object in order to simulate a multitube-type HIDiC	Steady-state	Equilibrium	n.a.	Aspen Plus [®] and Fortran [®]	Operational parameters as compression ratio, temperature profile and energy saving, as well as economic evaluation of total annual cost	(CONG <i>et al.</i> , 2017)
Ethanol-water	Mass and energy conservation equations connected by mass and energy balances at the interface	Steady-state	Non-equilibrium	Newton's method	Matlab [®]	Ethanol mass fraction at the top, distillate flow rate, top temperature and power in the resistance	(CLAUMANN <i>et al.</i> , 2020)

n.a.: Not available or not applicable.

Source: Battisti, Machado and Marangoni (2020).

Dribika and Sandall (1979) used the theoretical model of Kayihan, Sandall and Mellichamp (1975), extending it to the benzene-toluene-ethylbenzene ternary system. They validated the data experimentally in a wetted-wall column of 2.2 cm diameter and 100 cm height, equipped with unique probes designed for simultaneous sampling of liquids and temperature measurements. The authors indicated that there is no resistance to mass transfer in the liquid film, in agreement with the results of Kayihan, Sandall and Mellichamp (1977), who performed a binary distillation for methanol-water system in a wetted-wall column, and Honorat and Sandall (1978), with a packed column distilling toluene-trichloroethylene binary system. The authors concluded that the mass transfer process for wetted-wall distillation column can only be described in terms of the mass transfer coefficients of the vapor phase. However, it is known that in a real operation in distillation columns, the consideration of equilibrium stages rarely or never occurs, since there is a finite flow (not tending to zero) in the mass transfer between phases. The usual way of treating such deviation from equilibrium in modeling is with the incorporation of separation efficiency parameters (HAUSEN, 1953; HOLLAND; MCMAHON, 1970; LEWIS, 1922; MURPHREE, 1925). However, there is no consensus as to which definition of efficiency is the best. Also, this approach may lead to possible inconsistencies in terms of the number of stages, optimal feeding location, lateral withdrawals, and control points (KOOIJMAN; TAYLOR, 1995), mainly for separation of multicomponent mixtures.

The way to circumvent these inaccuracies of the equilibrium stage-based model, even when corrected by separation efficiency parameters, has been resorting to non-equilibrium stage-based modeling. In the case of distillation, the thermodynamic equilibrium is assumed to exist only at the liquid-vapor interface (KATARIYA *et al.*, 2008; TAYLOR; KRISHNA; KOOIJMAN, 2003), in which the use of separation efficiencies are totally avoided. Krishnamurthy and Taylor (1985a) developed the pioneer theoretical non-equilibrium stage-based model used to predict the temperature and composition profile of a falling film distillation process in a wetted-wall column. Then the same authors extended the application of this model to packed distillation columns and absorption towers (KRISHNAMURTHY; TAYLOR, 1985b). Since then, several authors have started to use this approach in their modeling. In another sequential study, Krishnamurthy and Taylor (1985c) assessed the effects of diffusional interaction on the non-equilibrium model. The authors found that neglecting the effects of diffusional interaction may lead to a sub-projected column; there is between 9% and 15% difference in the stage requirement predicted by the

non-equilibrium model with a rigorous mass transfer model and a non-equilibrium model that ignores these interaction effects. More recently, Claumann *et al.* (2020) develop a novel non-equilibrium stage-based model to predict ethanol composition, temperature profiles, distillate flow rate, and required power for a falling film distillation column assisted by a two-phase closed thermosyphon, which is responsible for supplying the thermal energy to the distillation process. The model showed good predictability, with deviations in the top temperature below 2.60%, 6.59% in the distilled ethanol mass fraction, 12.32% in the resistance power, and only one case above 10% for distillate flow rate.

Kosuge and Asano (1984b) carried out simulations for falling film distillation of acetone-methanol-ethanol ternary system in a wetted-wall column in total reflux condition. The authors considered that heat and mass transfer processes are controlled by vapor phase and the diffusive flux of each component is proportional only to its driving force. The distribution of liquid film concentrations in the wetted-wall column, vapor flow, and temperatures predicted by the new method showed good agreement with the values observed experimentally in previous work (KOSUGE; ASANO, 1982). Falling film distillation had already numerical application implemented even in the nuclear field. A mathematical model was proposed by Sugiyama *et al.* (1998) for simulation of H₂O-HTO isotope separation in a wetted-wall column. The equation system describing the diffusional processes of the vapor and liquid phases were solved simultaneously, and the fractional mole profiles were obtained numerically, suggesting the validity of the presented model.

More recently, within the computational fluid dynamics (CFD), Gonçalves *et al.* (2014) performed a numerical simulation study using the finite element method and a phase field model implemented in COMSOL Multiphysics[®] software. The authors tested liquids with different viscosities and specific densities, obtaining good results in the formation of a thin and long liquid film, uniform and stable, corroborating with experimental evidence found in the literature. Through the use of a commercial simulator, Cong *et al.* (2017) proposed an interesting design to evaluate the performance and optimization of multi-tube type HIDiC in Aspen Plus[®]. A vertical multi-tube type heat exchanger predefined object was used to simulate the multi-tube type HIDiC as the heat transfer configuration. The tube and shell pass are designed as the rectifying and stripping section respectively to ensure that the heat from the rectifying section is delivered into the stripping section without interacting with the surrounding environment. Besides the traditional evaluating parameters such as compression ratio, temperature profile and energy saving, a systematic economic evaluation was applied to

assist the structural optimization process. Compared to the conventional distillation columns, the multi-tube HiDiC could take an advantage in total annual cost (TAC). Savings for the p-xylene and o-xylene splitter can reach to 33.3%, while it is just 5.4% with benzene and toluene.

2.7.1 Analogy between distillation and absorption

It is well known that distillation is the most commonly used process for separating mixtures of miscible fluids based on volatility differences of components. However, a fundamental difference between distillation and absorption processes is based on the fact that a temperature gradient is required throughout the device or apparatus, if more than one separation stage is required (LAM; SORENSEN; GAVRIILIDIS, 2013). Despite this, absorption and distillation have the same phenomenological and physicochemical background, based on interfacial mass transfer between the gas/vapor phase and the liquid phase, which is characterized by a mass transfer coefficient on the gas/vapor side (k_G or k_V) and a mass transfer coefficient on the liquid side (k_L), as reported by Linek *et al.* (2005). Therefore, distillation and absorption can be treated as analogous processes of mass transfer. The assumed analogy implies that the phenomena that occur in both processes can be described with the same setting of models that deal with phase hydrodynamics, phase equilibria, and heat and mass transfer phenomena (SHILKIN; KENIG; OLUJIC, 2006).

Individual mass transfer coefficients are measured under conditions where the involved overall resistance to the process is due mainly to one of the phases. Absorption experiments, unlike distillation, are suitable for this task as they can directly address each characteristic by selecting a suitable absorption system (LINEK; MOUCHA; REJL, 2001). The difficulty in reaching such conditions in distillation and the analogy of this unit operation with absorption suggest the use of individual coefficient correlations obtained in absorption experiments to design distillation columns (OVEJERO *et al.*, 1992). According to Rejl, Valenz and Linek (2010), it could be possible to use the mass transfer characteristics of packed columns measured by standardized experiments under the absorption conditions to predict the mass transfer efficiency under the distillation conditions. Despite all the efforts already given to this topic, the successful estimation of mass transfer parameters from the absorption to the distillation conditions has never been fully mastered. Many authors suggest that such situation is well explained by the fact that the process conditions are significantly

different. Absorption experiments are generally based on cold air/water system, while distillation is mainly performed with hot organic systems. Brady (1969) pointed out that the difference between the gas absorption predictions and the experimental results with distillation in wetted-wall columns were shown to be due to the thermal effects which exist in distillation, but do not exist in gas absorption operations. Linek, Sinkule and Brekke (1995) have shown that there are still large errors in estimating the equivalent height of a theoretical distillation plate (*HETP*), and it can reach up to 100% when using correlations based on absorption mass transfer coefficients.

Recently, Rejl *et al.* (2016) published a detailed work with great enlightening advances on the analogy between distillation and absorption in wetted-wall columns. The authors disclose mass transfer data (*HETP*, k_L and k_V) obtained under distillation conditions in a falling film distillation column for the methanol-*n*-propanol binary system under atmospheric pressure and total reflux. The same type of column was used in a previous study done by Haidl *et al.* (2016), for measurements of the mass transfer coefficients under absorption conditions with Reynolds and Schmidt numbers of the phases adjusted to cover the entire range reached during the distillation experiments. The results of the absorption experiments were correlated in the form of dependencies of $Sh=f(Re,Sc)$, and presented an uncertainty regarding predicted *HETP* values of approximately 10% to 20%, considered very satisfactory facing the wide margin of errors found in the literature.

2.8 INDUSTRIAL APPLICATIONS

Distillation, as the main chemical separation process, is a key technology in industry. Distillation undertakes the vast majority of tasks for the separation and purification in industry, e.g., in crude distillation separation, catalytic cracking, delayed coking, elemental light hydrocarbons separation, and other sections of the petroleum refining industry. The development tendency of large-scale distillation units is remarkable in the world (LI *et al.*, 2016a). Compared to conventional trays and packings columns, or distillation assisted by an external force field like extractive distillation, dividing-wall columns and internally heat-integrated distillation, the falling film distillation columns are still limited in industrial applications. As far as is known, to date, the only industrially applied falling film distillation column is Linas technology, patented by the Linas Group (SAIFUTDINOV *et al.*, 2009). The first industrial application of Linas technology was accomplished in 1999 for distillation of

fluorine-organic compounds at the Angarsk chemical plant (SAIFUTDINOV *et al.*, 2002b). The height of the column is only 1.4 m. After three years of continuous operation the rectification column did not demonstrate any distillation problem. Therefore, in 2002 Linas Group designed and manufactured the first industrial oil refinery based on Linas distillation technology. The oil refinery has capacity of 10,000 Mt/year of crude oil and is in operation in the city of Miass, Russia. Since then, Linas Group is operating projects in the area of mini refinery and carried out more 33 industrial projects. Till middle of 2014, Linas Group operated only in Russia. At September 2014 Linas Group began the first project outside of Russia, in Republic of Kazakhstan. At moment the main commercial product of Linas Group is a rectification unit for atmospheric distillation of crude oil for producing three or four oil products: straight run gasoline, kerosene, diesel fuel, and black fuel.

2.9 SUMMARY AND CONCLUDING REMARKS

This literature review highlighted one of the most important separation techniques of homogeneous liquid mixtures, the falling film distillation in wetted-wall columns. A broad and deep survey in bibliographical bases of published works and deposited patents from the beginning of the 20th Century until nowadays was realized. As the main contribution this study carries is the historical perspective in background of the conceptual foundations, constructive geometries, and different forms of operation already applied, beyond the knowledge produced over the years about the multiple and complex factors that influence the efficiency in falling film distillation in wetted-wall columns. This investigation showed that falling film columns have been predominantly used for fundamental heat and mass transfer research over the years. The distinct advantages that falling liquid film technology provides, such as large specific surface area, high heat and mass transfer rates, and low pressure drop, have maintaining researchers dedicated to this topic for the last decades. However, concerning industrial application, the concepts of falling film distillation are still relatively little used. The applications of these columns are generally aimed for separation of binary and multicomponent mixtures of water-alcohols-hydrocarbons, organic fractions of petroleum, but some are more specific such as esters of carboxylic acids and desalination of seawater. These varieties of applications show the versatility of the apparatus.

Wetted-wall columns for distillation purposes represent about 10.9% of the total works published in the last 80 years. Despite not being among the highest demands of the

application, over the years several devices using the falling liquid film technique have been designed, improved and patented, such as monotube columns, multitube columns, and vertical flat-plates wetted-wall columns. It is important to note that process intensification concepts began to be incorporated into falling film technology more recently, giving rise to intensified settings as internally heat-integrated falling film columns and thermosyphon-assisted falling film columns. Compared to other unconventional column configurations that have emerged in recent years, falling film design can be considered a more specific technology that still has some scale-up limitations, particularly in relation to high throughputs flows, and that usually still cannot compete with the known distillation techniques in the industry. Nevertheless, it does not detract from the meaningful relevance that this technology represents from the point of view of contributions to separations science.

Steady-state studies of separation efficiency are already well established, and the great majority of the published works involving falling film distillation units demonstrate energy consumption minimization when compared with conventional distillation columns. From now, it is clear that there is a knowledge gap about the dynamic behavior of the falling film distillation process in wetted-wall columns. There is no record of research that has studied the dynamic modeling and control strategies design for falling film distillation in wetted-wall columns. In this way, the challenge hereafter must be focused on clarifying the process dynamics, so that progress can be made in order to improve control and optimization strategies. This will make it possible to move forward in operational column improvements to raise this technology to a higher level of economic feasibility for chemical process separations.

Practical industrial applications researches with falling film distillation in wetted-wall columns are still scarce. The in-depth analysis of the studies presented in this review, as well as the conceptual insights raised will certainly provide substantial theoretical basis for the future popularization and development of falling film distillation. Breakthroughs should be made in design, control, and operation of falling film distillation columns in the future. In addition, advanced simulation software such as CFD technology should assist to simulate the two-phase flow field inside the towers. Studying the vapor-liquid mass transfer mechanism and optimizing height, diameter, improved surfaces, and liquid distributors are important development directions for falling film distillation columns design.

3 DYNAMIC MODELING WITH EXPERIMENTAL VALIDATION AND CONTROL OF A TWO-PHASE CLOSED THERMOSYPHON AS HEAT SUPPLIER OF A NOVEL PILOT-SCALE FALLING FILM DISTILLATION UNIT

The content of this chapter is based on the following published article:

BATTISTI, Rodrigo; CLAUMANN, Carlos Alberto; MANENTI, Flavio; MACHADO, Ricardo Antonio Francisco; MARANGONI, Cintia. Dynamic modeling with experimental validation and control of a two-phase closed thermosyphon as heat supplier of a novel pilot-scale falling film distillation unit. **Computers & Chemical Engineering**, v. 143, p. 107078, 2020. DOI: 10.1016/j.compchemeng.2020.107078.

3.1 INTRODUCTION

The possible use of heat pipes for heat transfer applications has led to a growing demand for numerical predictive tools that would allow engineers to perform design and operational analysis. Over the past thirty years, heat pipe analytical and numerical modeling has been extensively studied to develop reliable design tools (JAFARI *et al.*, 2016, 2017). Initially, almost all analytical studies focused only on vapor flow dynamics, with liquid flow and coupling between phases being neglected due to their complexity. Cao and Faghri (1991) developed a model for two-dimensional transient analysis with compressible vapor flow in high-temperature pulsed heat input. The dynamics of one-dimensional compressible vapor flow in heat pipes were modeled by Jang *et al.* (1991), where the transient behavior of the thermosyphon under subsonic, sonic and supersonic velocities was successfully predicted. Vincent and Kok (1992) investigated the performance of a thermosyphon in transient operation, considering countercurrent liquid and vapor flows. A control volume approach was applied to describe the motion of system phases, also used by Dobran (1985), simplifying modeling in one-dimensional equations. It was found that the vapor-liquid density ratio, the dimensionless friction coefficient, and the length of the water column determine, respectively, the general dynamic behavior characteristics such as response time, damping, and oscillation frequency. Harley and Faghri (1994) presented a two-dimensional transient model, combining the heat transfer through the wall and the falling condensed film. The transient two-dimensional conservation equations were solved for vapor flow and tube wall, and the liquid

film was modeled using a quasi-stationary Nusselt-type solution. The model was validated by comparison with existing experimental data for a low-temperature thermosyphon.

In general, until the early 1990s, theoretical dynamic models consisted of a set of nonlinear partial differential equations whose solution required significant programming and computational time efforts. Then Zuo and Faghri (1998) proposed a simple and practical engineering model for heat pipe dynamic analysis, which was considered a thermal network of connected components. Ziapour and Shaker (2010) developed a simplified thermal network model for a TPCT based on the model of Zuo and Faghri. This transient model neglects the influence of fluid dynamics within the heat pipe, the effect of gravity, and the dependence of evaporation-condensation phase change on vapor saturation temperature. Transient behavior was described by ordinary differential equations and provided a reasonably simple and accurate way dynamic analysis. The model has been validated in transient and steady-state regimes, tested with different refrigerants such as water, ammonia, R-11, R-22, and R-134, providing a relatively simple way to calculate temperatures and heat fluxes in the thermosyphon. Farsi *et al.* (2003) developed a transient mathematical model to obtain an analytical expression of the response time of a TPCT. Experimental and theoretical research on the behavior of the two-phase thermosyphon revealed that the response time dependence, according to the various parameters, is linked to the equipment geometry and heat transfer. Molz *et al.* (2004) presented a transient TPCT model for applications such as heat exchangers. To describe and explain the dynamic behavior (and, at the limit, also at steady-state) a semi-clustered capacitor model was introduced, which makes use of Nusselt condensation analysis as a quasi-stationary approximation.

More recently, models based on the lumped capacitance have been successfully developed and refined. Ferrandi *et al.* (2012) developed a lumped capacitance numerical model able to simulate both the transients and steady-state of a mini heat-pipe with different dimensions (8, 5 and 3 mm outside diameter, 1 mm, sintered copper-wick and water as filler). Matallah *et al.* (2016) presented a transient model based on the grouped capacitance method of a TPCT to analyze an industrial-scale sub-atmospheric preheating system. The numerical model was validated by comparison with experimental results in a pilot-scale unit. Jafari *et al.* (2017) addressed experimental analysis and numerical simulation of a TPCT with different filling rates, including wall-to-wall heat transfer, vapor core, liquid pool, and downward condensation film. The two-dimensional conservation equations for mass, momentum, and energy are solved using a finite volume technique. Numerical predictions showed the best

performance for the filling ratio below 35%. However, at this filling rate, a high risk of drying insurgency or undesirable excessive boiling can be encountered. Alammar *et al.* (2016) applied computational fluid dynamics modeling (CFD), and demonstrated that this is a relevant tool and can be used to investigate the complex physical phenomena of evaporation and condensation phase change processes within thermosyphons.

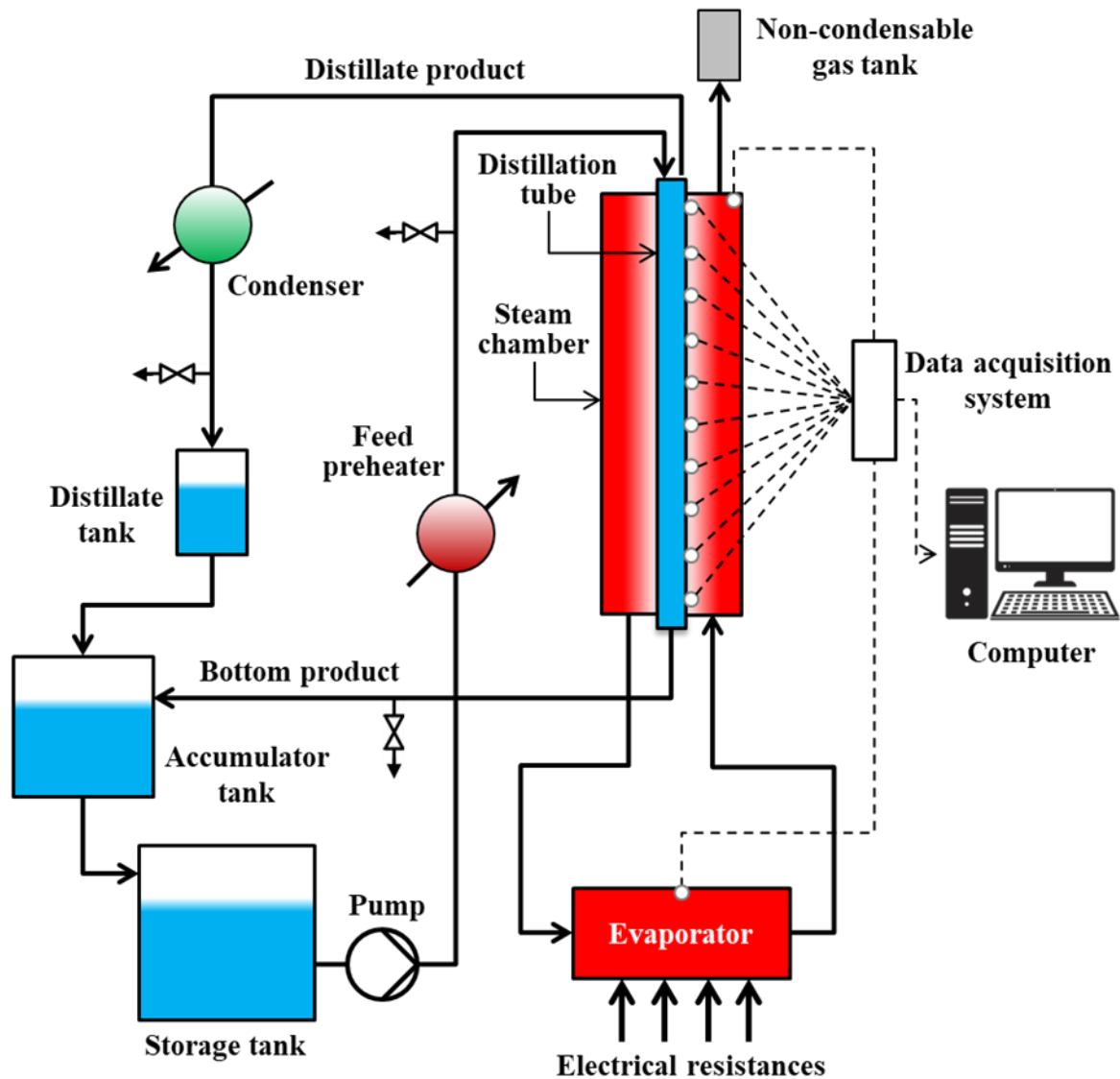
As mentioned above, the operation of a thermosyphon is quite complex and it makes hard the comparison of different approaches. More fundamental works, and more accurate dynamic simulations, as well, are needed to understand the physical phenomena and behavior of TPCTs, and they must be supported by accurate experimental analysis for design and operational purposes. Although there are a large number of studies in the literature dedicated to propose mathematical models for dynamic thermosyphons operation, there is no record of a modeling work developed for a thermosyphon operation in order to provide heat to a falling film distillation process. The objective of a falling film distillation process is to recover the largest amount of the most volatile component present in the feed stream with the least amount of energy possible. For this reason, the distributed form of energy supply through the two-phase closed thermosyphon expresses the main point of innovation proposed by the Destubcal technology. In the acquaintance of the authors, it is the first dynamic modeling proposed in the literature that describes the thermal behavior of a TPCT as the heat source for a falling film distillation process. In addition, several works published by our research team proved the feasibility of the unit for separation of several liquid mixtures, with the main benefits of energy and occupied space reduction when compared to conventional configurations. The promising outcomes obtained previously encourage the team for improving the unit, so that it can move from the pilot-scale stage to the industrial stage, thus consolidating this device as an advanced distillation process. Therefore, there is a crucial demand to better understand the dynamic behavior of this new process to move forward in control strategies aimed at minimizing costs and maximizing productivity. Concerning this background, the objective of this work is to develop and experimentally validate a new closed-loop (using PID techniques) dynamic modeling for a two-phase closed thermosyphon applied as a heat supplier to a pilot-scale falling film distillation plant.

3.2 EXPERIMENTAL METHODOLOGY

3.2.1 Description of the pilot-scale unit

Experiments were performed in the pilot-scale thermosyphon-assisted falling film distillation unit (Figure 13 and Figure 14). The apparatus is built with stainless steel and consists of: (i) an inner tube, called distillation tube, where the falling liquid film flows to be distilled; (ii) an outer tube, called the steam chamber of the thermosyphon, which supplies heat to the distillation tube. The steam chamber operates with water/steam as a thermal conducting fluid between the hot source (evaporator) and the cold source (distillation tube).

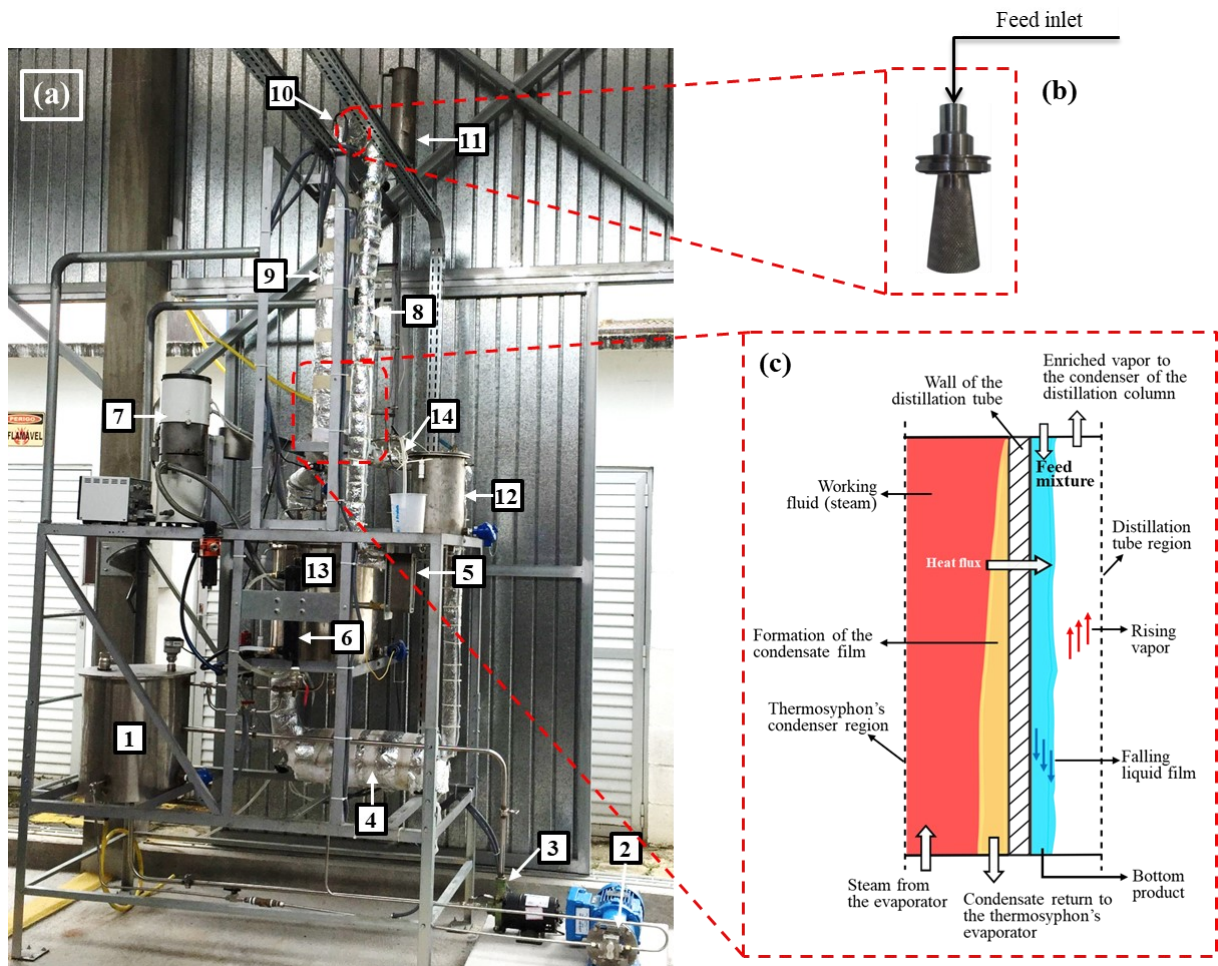
Figure 13 – Schematic diagram of the experimental pilot-scale Destubcal unit.



Source: Battisti *et al.* (2021a).

The thermal fluid flows throughout the steam chamber in saturated state, as the liquid phase is boiled by the hot source (the evaporator with electrical resistances). The vapor phase is condensed by the cold source, the distillation tube, which acts as a thermosyphon's condenser by removing latent heat from the thermal fluid. The distillation process takes place over the inner surface of the vertical pipe with 26.0 mm of diameter, 3.0 mm of wall thickness, and 1.0 m of height. The liquid film flows in countercurrent with the vapor generated at a given pressure and temperature, while the tube wall is kept at a constant temperature by the steam chamber of the heat pipe that surrounds the entire distillation pipe.

Figure 14 – Photograph of the Destubcal pilot-scale experimental unit (a); Feed cone distributor detail (b); Column cross-sectional detail (c).



Legend: (1) Storage tank; (2) Feed pump; (3) Recirculation pump; (4) Evaporator; (5) Feed plate-type heat exchanger; (6) Bottom's sample cooler; (7) Heating bath; (8) Feed inlet pipe; (9) Steam chamber and distillation tube; (10) Feed cone distributor; (11) Non-condensable gas reservoir; (12) Distillate tank; (13) Accumulator tank; (14) Distillate flow sample collector.

Source: Battisti *et al.* (2020a).

The unit is fed in the upper part through a distribution cone (Figure 14 b), allowing a uniform distribution of the fluid through the inner wall of the distillation tube. A cross-sectional detail of the column (Figure 14 c) shows that the system is composed of two distinct regions: (1) distillation tube; (2) steam chamber section (thermosyphon's condenser). The entire unit is thermally insulated with glass wool. The steam chamber was designed with three entry points, aiming to generate a better distribution of the steam inlet. The distillation process operates continuously in a closed system by mixing the top (ethanol-rich stream), and the bottom (water-rich stream) in a storage tank of suitable dimensions (60 L) to eliminate disturbances in feed composition. The pilot-scale unit is instrumented with level, pressure, and temperature sensors. The feed flow rate is controlled by the feed pump rotation and ethanol composition was measured with an alcoholmeter.

3.2.2 Operating conditions and experimental assessment

In order to investigate the thermal performance of the two-phase closed thermosyphon and validating the proposed thermal network-based model, a set of experimental runs and numerical simulations were performed under several operating conditions. Four different feed flow rates (14 L/h, 17 L/h, 23 L/h, and 32 L/h), and three input heat flux steps (400 W, 900 W, and 1500 W) were performed in order to cover the entire operational range of the experimental pilot-scale unit. Based on preliminary studies carried out on the prototype glass column, these parameters showed having the highest influence on the operation of the unit. The same initial process conditions adopted for both numerical simulations and experimental runs were defined as shown in Table 5.

Table 5 – Initial operating process conditions.

Input variable	Values
Feed flow rate	14.0; 17.0; 23.0; and 32.0 L/h
Feed flow temperature	80.0 °C
Feed composition	10.0 wt% (ethanol)
Input heat flux	400 W; 900 W; and 1500 W

Source: Battisti *et al.* (2020a).

The experimental procedure consisted initially in preparing the storage tank with the ethanol-water mixture under the desired composition, reaching the approximate value of 10.50 ± 0.7 wt% (ethanol). Subsequently, the feed flow rate was adjusted by controlling the rotation of the feed pump, reaching the desired values. The feed temperature of the mixture was adjusted by the thermostatic bath, waiting until stabilization at the desired temperature, which reached about 80.3 ± 0.01 °C. Before each run to start, all the system was kept at the falling film temperature until stabilization. Then, input heat flux was set to the starting value with a step heating, and the dynamic behavior was observed up to a steady-state regime. Three positive power steps were applied: 400 W; 900 W; and 1500 W. All the temperatures of the input, output, and outside thermosyphon walls along the axial length were measured over time. In the experimental data analysis, the average heat transfer rate into the evaporator and into the condenser section was estimated. From the data measured experimentally of the wall temperature and the vapor temperature (equivalent to the wall temperature of the adiabatic section), the heat transfer coefficient in the evaporator (h_e) and in condenser section (h_c) can be evaluated, as described by Jafari *et al.* (2017), using the following equations:

$$h_e = \frac{Q_{av}}{\pi d_i L_e (T_{e,av} - T_v)} \quad (1)$$

$$h_c = \frac{Q_{av}}{\pi d_i L_c (T_v - T_{c,av})} \quad (2)$$

The experimental effective overall thermal resistance of the thermosyphon was calculated by applying the electrical analogy in the form:

$$R_{overall} = \frac{T_{e,av} - T_{c,av}}{Q_{av}} \quad (3)$$

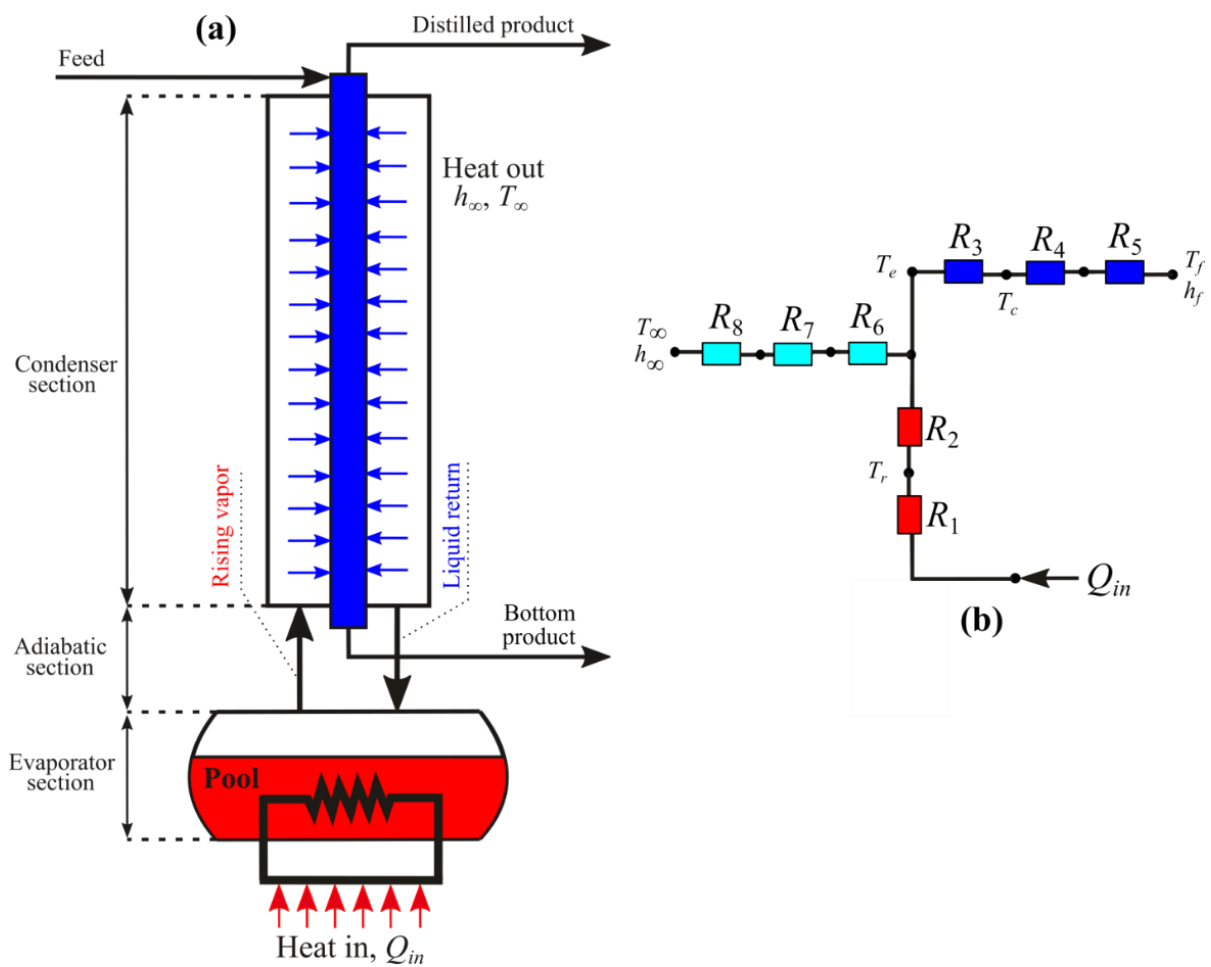
3.3 DYNAMIC MODELING

3.3.1 Thermal network model

As illustrated in Figure 15 (a), the thermosyphon is a closed vessel filled with a certain amount of working fluid, water in this case, which generates steam to work as a

thermal conducting fluid. In the process, heat is added in the evaporator section through electrical resistances, which evaporates the liquid water in the pool. The generated steam rises to the thermosyphon's condenser section, which acts as an energy sink, removing latent heat. The heat transported is then absorbed by the distillation tube by a condensation process. The condensate forms a liquid film that flows back down by gravity, returning to the evaporator and generating a continuous closed-loop system. The thermosyphon dynamic model was proposed based on the thermal network approach, where the thermosyphon is seen as a system of thermal resistances for conduction and convection of heat (ZUO; FAGHRI, 1998). This model provides a simplified way to predict temperatures and heat fluxes in the thermosyphon's section. There is an analogy between heat transfer and electric charge, described by Darcy's law. As an electrical resistance is associated with electricity conduction, a thermal resistance may be associated with heat conduction or convection.

Figure 15 – Schematic diagram of the thermosyphon-assisted unit (a) and the thermal network-based model (b).



Source: Battisti *et al.* (2020a).

The equipment was divided into several components, each one with a specific thermal resistance, except for vapor and liquid flows, which has negligible effects on heat transfer and were disregarded in the balances. According to Ziapour and Shaker (2010), the thermal resistance of vapor flow is considerably lower than other processes. Therefore, vapor flow can be neglected from the thermal grid without causing any significant discrepancy. Figure 15 (b) illustrates the thermal network-based model applied to the TPCT process, which consists of heat conduction processes (R_1 , R_4 , R_6 , and R_7), and heat convection processes (R_2 , R_3 , R_5 , and R_8). Although the return of the liquid to the process is necessary for working fluid circulation, it has little effect on heat transfer and was therefore not considered in this work. Convection heat transfer is represented by the following parts:

- (i) nucleate boiling in the evaporator;
- (ii) condensation of the water film in the steam chamber;
- (iii) convection of the distillation film.

Conduction heat transfer is present on the walls of the electrical resistances, and on the walls of the distillation tube and steam chamber. Heat transfer on the walls of fluid transport pipes may be neglected as they are insulated (adiabatic section). Working fluid and evaporated fluid are presumed to have the same temperature. Input energy (Q_{in}) is assumed to be the energy provided by the power of the electrical resistances. The feed inlet temperature of the liquid film in the distillation tube (T_F) is a known variable, assumed as the inlet temperature of the mixture to be distilled, which in this case will be the ethanol-water feed (10.0 wt% of ethanol). The equations obtained from the verified analogy and the respective descriptions of the thermal resistances are listed in Table 6.

Table 6 – Thermal resistance network equations and descriptions.

Description	Formula	Equation
Conduction resistance on the wall of electrical resistances	$R_1 = \frac{\ln(r_2/r_1)}{2\pi k_s L_r}$	(4)
Evaporator nucleated boiling convection resistance	$R_2 = \frac{1}{h_e A_e}$	(5)
Condensation resistance of the steam chamber film	$R_3 = \frac{1}{h_c A_c}$	(6)
Conduction resistance on the distillation tube wall	$R_4 = \frac{\ln(r_4/r_3)}{2\pi k_s L_c}$	(7)
Convection resistance of the distillation falling film	$R_5 = \frac{1}{h_f A_f}$	(8)
Evaporator wall conduction resistance	$R_6 = \frac{\ln(r_6/r_5)}{2\pi k_s L_e}$	(9)
Conduction resistance by evaporator insulation	$R_7 = \frac{\ln(r_7/r_8)}{2\pi k_{iso} L_e}$	(10)
Evaporator convection heat loss resistance	$R_8 = \frac{1}{h_\infty L_e}$	(11)

Source: Battisti *et al.* (2020a).

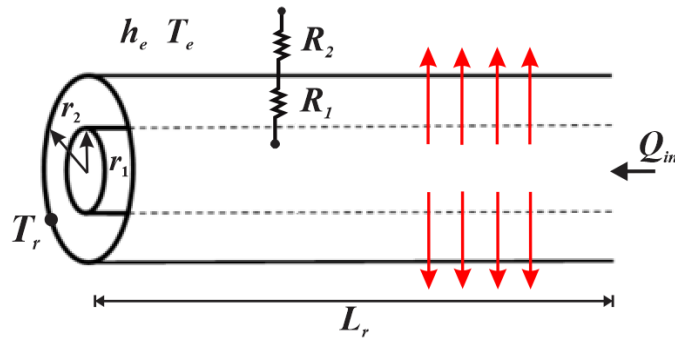
To obtain the dynamic model of the thermosyphon heat transfer, the analysis was based on energy conservation. Therefore, the general transient heat transport equation that governs each “node” or “loop” within each control volume is described by Eq. (12). Each node is described by a differential equation, so that the global transient problem can be reduced to a system of linear differential equations easily implemented in a programming code and numerically solved.

$$C_i \frac{dT_i}{dt} = \pm \sum \frac{|T_i - T_j|}{R_{ij}} \quad (12)$$

3.3.1.1 Thermal balance in the electrical resistances

The evaporator consists of a 304 stainless steel cylindrical tube with 101.6 mm outside diameter, 3.0 mm wall thickness, and 400.0 mm in length. In the lower base of the evaporator and along its longitudinal length were inserted two stainless steel tubes, with an internal diameter of 12.7 mm, where the electrical resistances were allocated. This construction aspect makes it easy to replace if necessary. For the heat supply in the evaporator, two cartridge-type resistances were inserted with a power of 4,800 W each one. Figure 16 shows the schematic representation of the heat transfer in electrical resistances in the evaporator of the two-phase closed thermosyphon.

Figure 16 – Representation of the heat transfer in electrical resistances.



Source: The author (2021).

The energy balance in this control volume in cylindrical coordinates gives the following differential equation:

$$\left[2\rho\pi L r_{avg} (r_2 - r_1) c_p \right]_r \frac{dT_r}{dt} = Q_{in} - \frac{(T_r - T_e)}{\left(\frac{\ln(r_2/r_1)}{2\pi k_s L_r} \right) + \left(\frac{1}{h_e A_r} \right)} \quad (13)$$

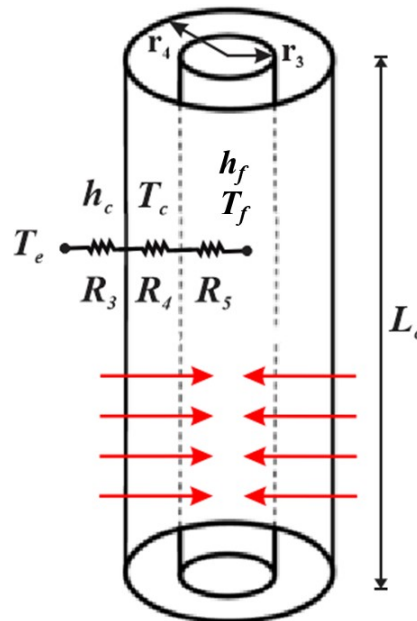
When $\alpha = \left[2\rho\pi L r_{avg} (r_2 - r_1) c_p \right]_r$, the ordinary differential equation describing the temperature on the electrical resistances inside the evaporator (T_r) is:

$$\frac{dT_r}{dt} = \frac{Q_{in}}{\alpha} - \frac{(T_r - T_e)}{\alpha(R_1 + R_2)} \quad (14)$$

3.3.1.2 Thermal balance in the steam chamber and distillation tube

The steam chamber, which analogously corresponds to the condenser of a conventional-circuit thermosyphon, consists of two 1.0 m long concentric cylindrical tubes. The distillation tube is where the falling liquid film flows over the inner vertical surface in order to promote the distillation process. The steam chamber is filled with the rising steam coming from the evaporator and is constructed with an internal diameter of 32.0 mm. Figure 17 shows the heat transfer in the steam chamber and distillation tube.

Figure 17 – Representation of the heat transfer in the steam chamber and distillation tube.



Source: The author (2021).

The energy balance in this control volume in cylindrical coordinates gives the following differential equation:

$$\left[2\rho\pi Lr_{avg}(r_4 - r_3)c_p\right]_c \frac{dT_c}{dt} = \frac{T_e - T_c}{\left(\frac{1}{h_c A_c}\right) + \left(\frac{\ln(r_4/r_3)}{2\pi k_s L_c}\right)} - \frac{T_c - T_f}{\left(\frac{\ln(r_4/r_3)}{2\pi k_s L_c}\right) + \left(\frac{1}{h_f A_f}\right)} \quad (15)$$

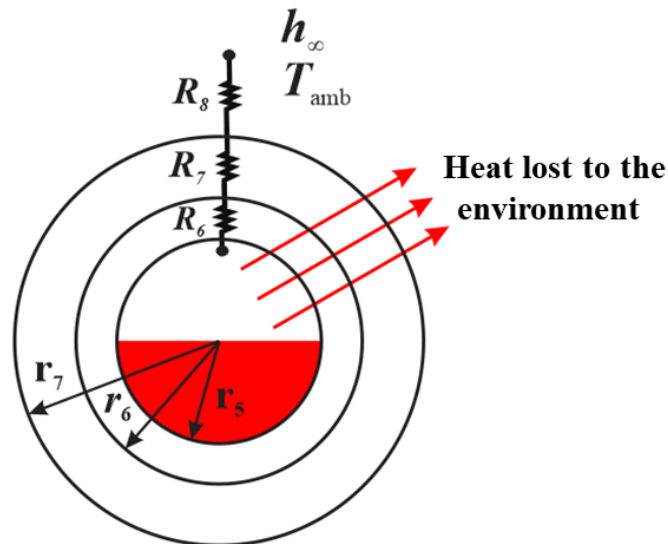
When $\beta = \left[2\rho\pi Lr_{avg}(r_4 - r_3)c_p\right]_c$, the ordinary differential equation describing the condensation temperature inside the steam chamber (T_c) is:

$$\frac{dT_c}{dt} = \frac{(T_e - T_c)}{\beta(R_3 + R_4)} - \frac{(T_c - T_f)}{\beta(R_4 + R_5)} \quad (16)$$

3.3.1.3 Total balance for the evaporator

Since the ultimate goal of the dynamic model for the thermosyphon is to obtain the evaporator temperature (T_e), it is necessary to perform a total energy balance in the evaporator. Figure 18 shows the heat transfer resistances in the thermosyphon evaporator.

Figure 18 – Representation of the heat transfer in the evaporator.



Source: The author (2021).

Considering that all the energy that is added by the electric resistances is dissipated by the distillation tube and by losses through thermal insulation, the differential equation obtained is:

$$C_e \frac{dT_e}{dt} = \frac{T_r - T_e}{\left(\frac{\ln(r_2/r_1)}{2\pi k_s L_r} \right) + \left(\frac{1}{h_e A_r} \right)} - \frac{T_e - T_f}{\left(\frac{1}{h_c A_c} \right) + \left(\frac{\ln(r_4/r_3)}{2\pi k_s L_c} \right) + \left(\frac{1}{h_f A_f} \right)} -$$

$$\frac{T_e - T_{amb}}{\left(\frac{\ln(r_6/r_5)}{2\pi k_s L_w}\right) + \left(\frac{\ln(r_7/r_6)}{2\pi k_{iso} L_w}\right) + \left(\frac{1}{h_\infty A_{iso}}\right)} \quad (17)$$

When $\gamma = C_e$, or $\gamma = (\rho V c_p)_e$, the ordinary differential equation describing the evaporator temperature (T_e) is:

$$\frac{dT_e}{dt} = \frac{(T_r - T_e)}{\gamma(R_1 + R_2)} - \frac{(T_e - T_f)}{\gamma(R_3 + R_4 + R_5)} - \frac{(T_e - T_{amb})}{\gamma(R_6 + R_7 + R_8)} \quad (18)$$

3.3.1.4 Correlations for the heat transfer coefficients

The heat transfer coefficients at different levels of the two-phase closed thermosyphon were based on empirical correlations extracted from the best-established literature. There are a complex flow and heat transfer behaviors inside the evaporator, such as convection, evaporation, and nucleated boiling, which result from the circulation of the working fluid inside the thermosyphon (LATAOUI; JEMNI, 2017). However, Park, Kang and Kim (2002) found that nucleated boiling in the liquid pool is the predominant mechanism in the evaporator when the filling rate is above 30%. Nucleated pool boiling occurs when a heater is submerged in an initially stagnant liquid pool. When the heater surface temperature exceeds the saturation temperature of the liquid in sufficient quantity, vapor bubbles are nucleated on the heater surface (TONG; TANG, 1997). In the literature, there are several empirical correlations for heat transfer coefficients inside evaporators, all with some agreement with the experimental values (JOUHARA; ROBINSON, 2010). In this work, Imura *et al.* (1979) correlation was defined to calculate the heat transfer coefficient in the evaporator section (h_e) because it was specifically developed for pool nucleate boiling, as shown in Eq. (19).

$$h_e = 0.32 \left(\frac{\rho_l^{0.65} k_l^{0.3} c_{p,l}^{0.7} g^{0.2} q^{0.4}}{\rho_v^{0.25} h_{lv}^{0.4} \mu_l^{0.1}} \right) \left(\frac{P_{sat}}{P_{atm}} \right)^{0.3} \quad (19)$$

The steam chamber acts as biphasic thermosyphon's condenser. Inside the steam chamber, saturated steam will condense, releasing heat to the distillation tube surface. According to Reay *et al.* (2013), condensation in heat pipes can occur basically in two ways, either by condensing steam forming a continuous liquid surface or forming a large number of droplets. Several aspects of condensation heat transfer have been studied experimentally and theoretically. In the condenser of a closed biphasic thermosyphon, condensation can be described by the theory proposed by Nusselt, for infinite flat laminar flow (PARK; KANG; KIM, 2002). The Eq. (20) represents the theoretical correlation derived from this theory to the condensation heat transfer coefficient (h_c) adopted in this work.

$$h_c = 0.943 \left\{ \frac{\rho_l g k_l^3 (\rho_l - \rho_v) h'_{lv}}{\mu_l L_c (T_v - \bar{T}_c)} \right\}^{1/4} \quad (20)$$

Where the modified latent heat of vaporization (h'_{lv}) is calculated as:

$$h'_{lv} = h_{lv} + 0.68 c_{p,l} (T_v - \bar{T}_c) \quad (21)$$

The falling liquid film that flows into the distillation tube absorbs heat from the evaporator. The liquid consists of the mixture to be distilled, fed at the top of the column. There are many correlations to predict heat transfer from heated vertical or horizontal tubes in forced and natural convection situations. Hilpert (1933) was one of the first researchers in the area of forced convection from heated pipe surfaces. The author developed the following correlation, which was used to calculate the convective heat transfer coefficient of the liquid film inside the distillation tube (h_f):

$$\overline{Nu} = \left(\frac{\bar{h}D}{k} \right) = C Re^m Pr^{1/3} \quad (22)$$

Where the dimensionless numbers of Reynolds (Re) and Prandtl (Pr) can be calculated as:

$$Re = \frac{4\dot{m}_f}{\pi\mu_f D} \quad (23)$$

$$\text{Pr} = \frac{c_{p,f} \mu_f}{k_f} \quad (24)$$

The values of “C” and “m” are adjustable coefficients that allow describing different flow regimes, such as:

$$\left\{ \begin{array}{lll} C = 0.981 & m = 0.330 & 0.4 \leq \text{Re} \leq 4 \\ C = 0.911 & m = 0.385 & 4 \leq \text{Re} \leq 40 \\ C = 0.683 & m = 0.466 & 40 \leq \text{Re} \leq 4,000 \\ C = 0.193 & m = 0.618 & 4,000 \leq \text{Re} \leq 400,000 \\ C = 0.027 & m = 0.805 & 400,000 \leq \text{Re} \leq 40,000,000 \end{array} \right.$$

For the recommended column flow rate, which ranges from 14 L/h (minimum) to 60 L/h (maximum), the calculated Reynolds number is in the range of $40 \leq \text{Re} \leq 4,000$. Thus, the constants to be used in the calculation of the convective transfer coefficient of the film are $C = 0.683$ and $m = 0.466$. Once the bubble temperature of the mixture is reached, the evaporation process begins. The correlation developed by Hsu and Westwater (1958) was used to model this phenomenon, which deals with boiling in liquid films inside vertical tubes:

$$\overline{Nu} = 0.943 (Ra_D^*)^{1/2} \left\{ \frac{H_{fg} [1 + 0.34 c_{p,v} (T_w - T_{sat}) / H_{fg}]^{1/2}}{c_{p,v} (T_w - T_{sat})} \right\}^{1/2} \quad (25)$$

With Ra_D^* defined as:

$$Ra_D^* = (\text{Gr}_D)(\text{Pr}_D) = \left[\frac{D^3 \rho_v (\rho_l - \rho_v) / g}{\mu_v^2} \right] \left(\frac{c_{p,v} \mu_v}{k_v} \right) \quad (26)$$

With considerable environmental heat losses around the evaporator, it will be necessary to estimate the convective heat transfer coefficient for heat loss (h_∞). Churchill and Bernstein (1977) proposed a widely used equation to estimate the average Nusselt number for a cross-flow cylinder at various air speeds. This equation covers the full range of Re_D for

which data is available, as well as a wide range of Pr. The equation recommended for all $Re_D Pr \geq 0.2$ has the following form:

$$\overline{Nu}_D = 0.3 + \frac{0.62 Re_D^{1/2} Pr^{1/3}}{\left[1 + (0.4 / Pr)^{2/3}\right]^{1/4}} \left[1 + \left(\frac{Re_D}{282,000}\right)^{5/8}\right]^{4/5} \quad (27)$$

Thus, the system of equations of the thermal network model applied to the heat transfer process in the two-phase closed thermosyphon coupled to the falling film distillation column is complete. For the solution of the model, it will also be necessary to inform the constructive data of the equipment (Appendix A), and the thermophysical properties of the materials (Appendix B), extracted from consolidated thermodynamic correlations which fit within the operating ranges in terms of temperature and pressure performed.

3.3.1.5 Falling film distillation material balance

The phenomenological predictive characteristic of the proposed thermal network-based model is concentrated in the region of heat supply of the thermosyphon-assisted falling film distillation unit. To allow an accurate prediction of the heating dynamics of the two-phase closed thermosyphon, the mass balance data from the falling film distillation tube region are based on experimental regression of outputs streams from the pilot-scale unit, which can be consulted in the Appendix C. Therefore, the proposed model can be considered a "hybrid model", since the part related to the energy dynamics is predicted by the thermal network-based model, while the mass balance of the distillation tube is based on data from experimental runs carried out with the ethanol-water mixture. The separation conditions predicted by the empirical regression, as well as the thermophysical properties of the liquid-vapor mixture, are dynamically updated by the algorithm at each time step performed.

3.3.2 Numerical simulation procedure

The system of linear and first-order ordinary differential equations (ODE) governing the transient operation of the TPCT coupled to the falling film distillation column can be described as in Eq. (28). This ODE system was implemented in Matlab[®] software version 8.5 (R2015a) and solved using the standard solver of ordinary differential equations, represented

by the “ode45” function available in the Matlab toolbox. This function uses the Runge-Kutta 4th order method with a variable time step, aiming at efficiency to the numerical procedure. The transfer coefficients (h_e , h_c , h_f , and h_∞) and all other physical and thermodynamic properties of the ethanol-water mixture and the building materials of the equipment, which are inherently temperature-dependent, are therefore updated at each time step of the algorithm.

$$\begin{cases} \frac{dT_r}{dt} = f(t, T_r, T_e, h_e) \\ \frac{dT_c}{dt} = f(t, T_c, T_e, T_f, h_c, h_f) \\ \frac{dT_e}{dt} = f(t, T_e, T_r, T_f, h_e, h_c, h_f, h_\infty) \end{cases} \quad (28)$$

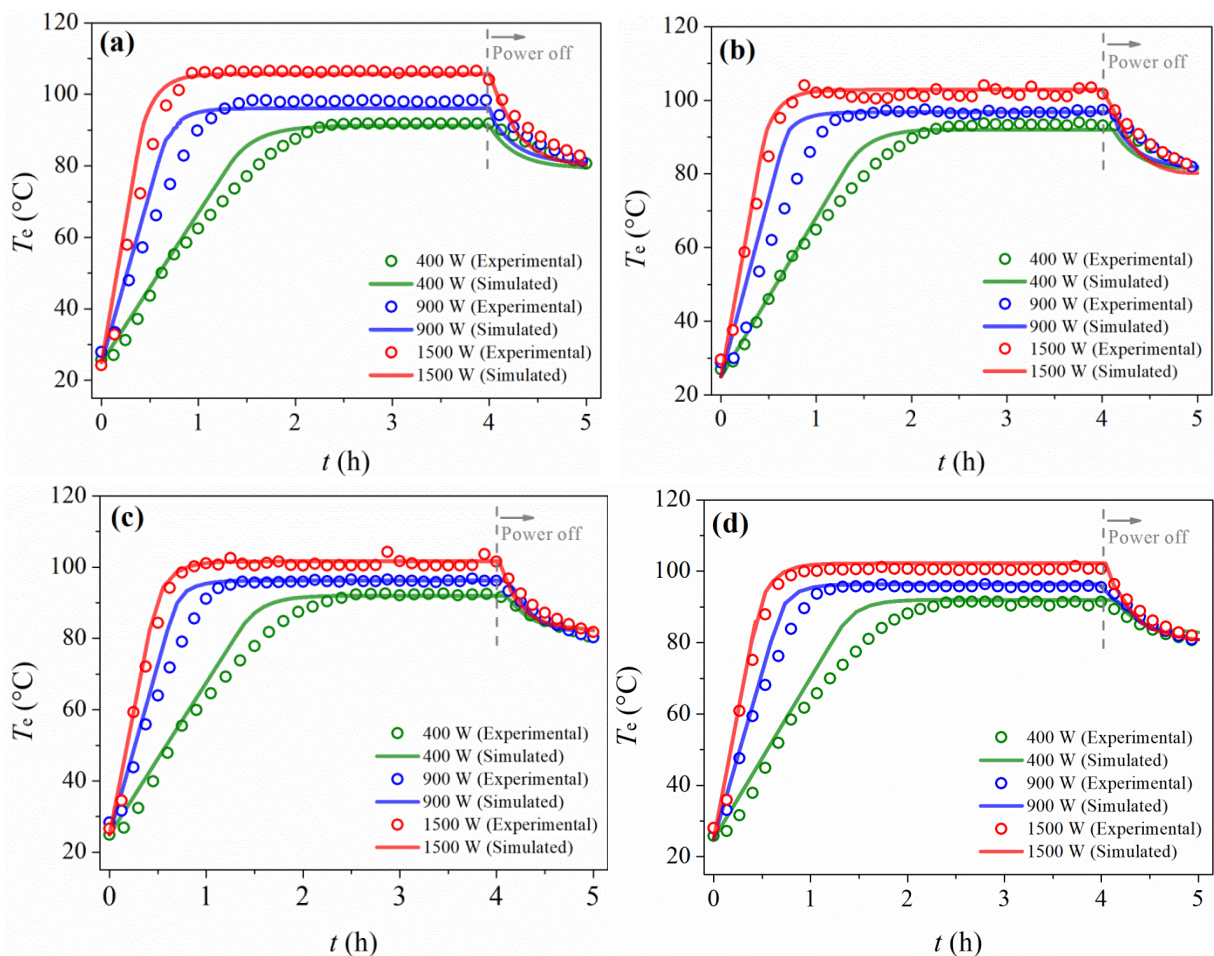
3.4 MODEL VALIDATION

3.4.1 Numerical and experimental behavior

Uniform heat flow and convective cooling conditions were applied to the thermosyphon-assisted falling film distillation unit. Initially, the steam chamber of the thermosyphon was kept in equilibrium with the feed falling film temperature (80 °C). Then a uniform heat flux was applied in the evaporator. After the steady-state was completely reached (about 4 h of operation), the power supply of the electrical resistances was turned off to evaluate the cooling behavior of the dynamic model in comparison with the experimental data. The curves shown in Figure 19 compare the simulated and the experimental transient temperature behaviors generated in the evaporator (T_e), which is consequently the same temperature that reaches the steam chamber to provide latent heat of condensation to the falling film distillation tube. As can be seen, the higher the power applied in the evaporator, the higher the temperature in the steam chamber and the faster the steady-state is reached. Another important characteristic to be observed is that the higher the column feed flow rate, the lower the temperature that the evaporator reaches with the same applied power. It is because with higher flow rates of liquid fed into the distillation tube, more heat is absorbed by the liquid film that flows on the inner wall of the distillation tube.

The thermal network-based model accurately predicted the general trends of the thermosyphon's evaporator temperature, in both heating and cooling stages, as all simulated runs were very close to the experimental ones. However, slight overpredictions of the vapor temperature were observed, especially in the early stage of the transient, which might be due to the underestimated heat losses to the environment (ZUO; FAGHRI, 1998). Additionally, since the model does not include heat resistance of thermal radiation of insulation layers, the predicted thermosyphon transients were slightly faster than those measured experimentally. However, the steady-state temperatures, which are the most important variable to observe in this case, were very close, with deviation from predictions to experimental measurements for all cases less than 5%.

Figure 19 – Comparison of evaporator temperature predicted by the model and by experimental runs under different power inputs and falling film flow rates: (a) 14 L/h; (b) 17 L/h; (c) 23 L/h; and (d) 32 L/h.



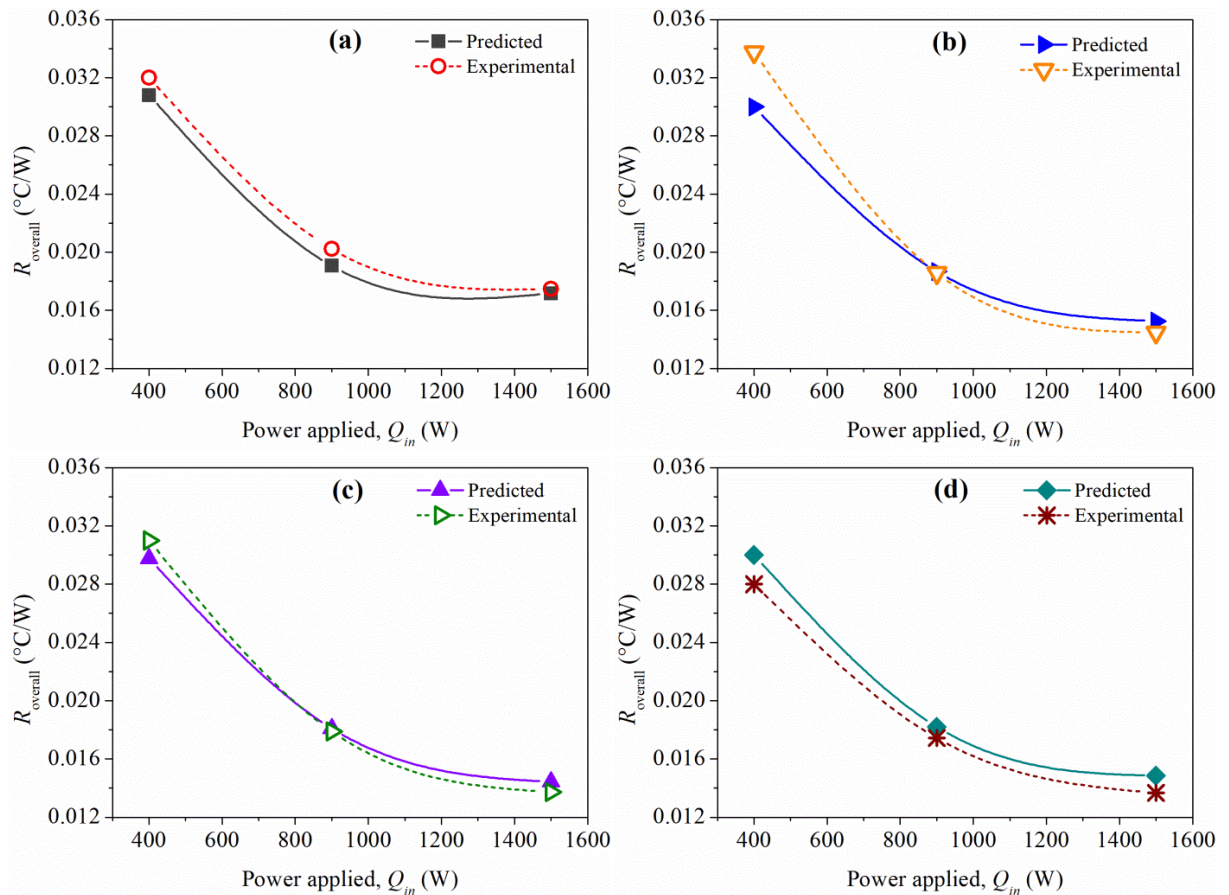
Source: Battisti *et al.* (2020a).

3.4.2 Heat transfer analysis

The overall thermal resistance and heat transfer coefficients in the evaporator and the condenser of the thermosyphon were also evaluated in order to comprehensively realize the viability of the dynamic model proposed. It should be highlighted that to analyze the heat transfer parameters it would not be necessary to develop a dynamic modeling of the process, given that there are well established steady-state models in the literature for evaluating these parameters. However, a simple steady-state modeling analysis would not capture the slow dynamics of this specific thermosyphon (in order of magnitude of hours to reach steady-state temperature). Thus, the dynamic modeling serves not only to validate the heat transfer parameters but also for control strategy purposes, as performed in the Simulink® application further on. The heat transfer behavior of the thermosyphon is well described by the thermal resistance analysis. Figure 20 shows the comparison between experimental and simulated results of the overall thermal resistance versus the power input in the evaporator for the different flow rates of the falling film performed. It is clear that all cases showed a similar qualitative trend; thermal resistance decrease as the input power increases, as reported by several authors (ALAMMAR; AL-DADAH; MAHMOUD, 2016; CATALDO; THOME, 2017; JAFARI *et al.*, 2017; JOUHARA; ROBINSON, 2010).

Experimental and predicted overall thermal resistances are in very good agreement. Notably, thermal resistance depends strongly on the imposed power in the evaporator, varying between $R = 0.03 \text{ }^\circ\text{C/W}$ at $Q_{in} = 400 \text{ W}$ to $R = 0.015 \text{ }^\circ\text{C/W}$ at $Q_{in} = 1500 \text{ W}$. In other words, the thermal resistance is practically reduced by half with an 1100 W increase, thus increasing the heating dynamics of the unit. This behavior is a result of the contribution of the evaporator and the condenser thermal resistances. The steep increase in the net thermal resistance as heat flux decreases is a compound influence of both individual increase in evaporator (R_e) and condenser (R_c) resistances. Manova *et al.* (2020) stated that a decrease in thermal resistance is due to an increase in the number of nucleation sites. Jouhara and Robinson (2010) reported that, for the evaporator section, this is due to the less rigorous nucleated boiling, while in the condenser section, this is probably due to the entrainment of liquids that deteriorates heat transfer.

Figure 20 – Experimental and predicted overall thermal resistances over input heat powers in the evaporator of the thermosyphon: (a) 14 L/h; (b) 17 L/h; (c) 23 L/h; and (d) 32 L/h.

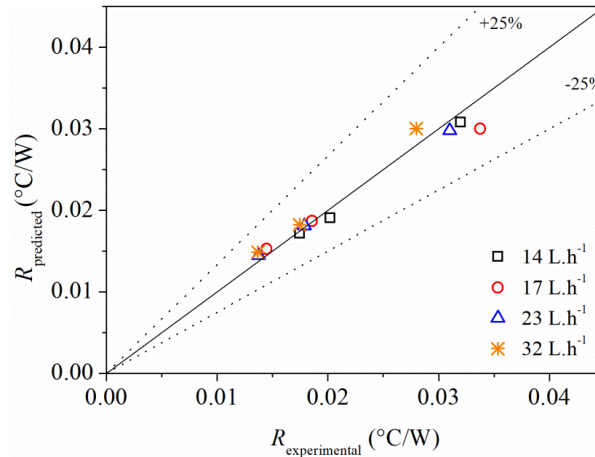


Source: Battisti *et al.* (2020a).

Figure 21 shows the comparison between the predicted and experimental measured overall thermal resistances. All runs show reasonable agreement within the $\pm 25\%$ deviation band. Agreement worsens as the thermal resistance increases, i.e., lower heat flux levels. The overall thermal resistance tends to be under-predicted at lower heat fluxes and lower flow rates, although the agreement is still reasonable and consistent over the entire range tested. The comparison between the calculated and experimental heat transfer coefficients in the evaporator and the condenser sections are shown in Figure 22 (a) and (b), respectively. According to Sauciuc *et al.* (1995), for the evaporator section there is no correlation or set of correlations that is completely enough to predict the nucleate pool boiling heat transfer coefficient in all thermosyphons types. In general, it is a practice to choose one or more boiling correlations to compare with the experimental data. The most suitable correlation is then thought to best represent the specific thermal and hydrodynamic conditions for the experimental conditions investigated (PARK; KIM; HONG, 2004). The correlation proposed

by Imura *et al.* (1979), used in this work, was developed specifically for nucleate pool boiling in two-phase closed-type thermosyphons.

Figure 21 – Comparison between predicted and experimental overall thermal resistance.

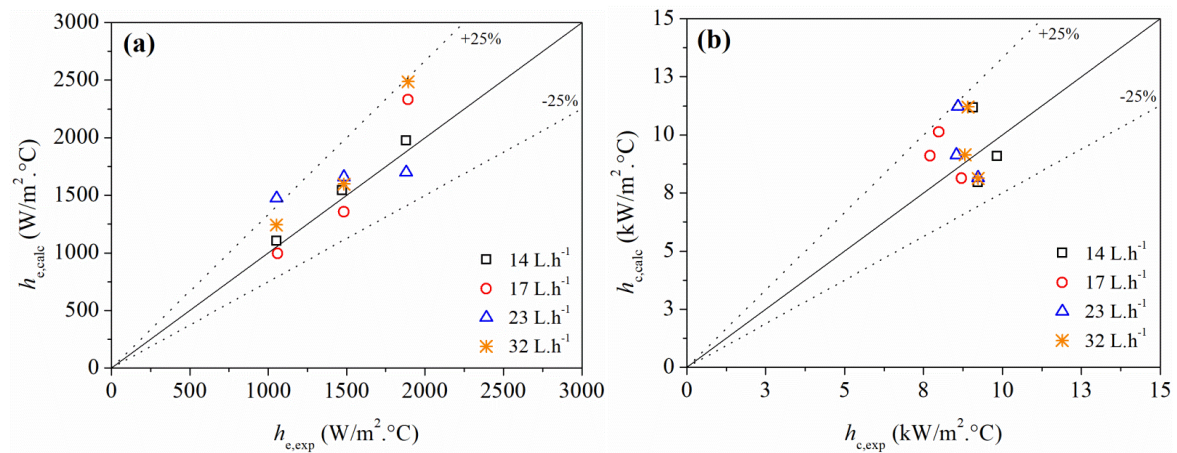


Source: Battisti *et al.* (2020a).

Figure 22 (a) shows that Imura correlation was able to accurately predict the pool boiling heat transfer coefficients in the evaporator of the thermosyphon-assisted unit, as expected from findings of the literature. As the falling liquid flow rate increases, there is a slight decrease in the agreement between predicted and experimental results, but still with majority points well-agreed, with only one overpredict point out of $\pm 25\%$ band. It is unclear why this overprediction occurs though it may be due to the working fluid, heater surface morphology, confinement, or other thermal-hydraulic effects (JOUHARA; ROBINSON, 2010). However, as pointed out by Park, Kim and Hong (2004), and Noie (2005), for pipe diameters much larger than bubble departure diameter, the use of the Imura correlation seems rational. It generally shows relatively good agreement with the experimental measurements. Concerning the heat transfer coefficients of the thermosyphon's condenser section, as shown in Figure 22 (b), within the laminar regime, it is very common to use the averaged version of Nusselt's theory for filmwise condensation on a horizontal flat plate (GROSS, 1992). It was the correlation used in the condenser section and showed good agreement with the experimental measurements for all runs of the studied range within the $\pm 25\%$ band. These thermal performance results confirm and corroborate the validation of the dynamic thermal network-based model proposed for the thermosyphon-assisted falling film unit. Also, all

transfer coefficients data simulated by the model were very accurate in comparison with the experimental data from the pilot-scale unit.

Figure 22 – Comparison between experimentally measured and predicted heat transfer coefficients in the evaporator section (a) and in the condenser section (b).



Source: Battisti *et al.* (2020a).

3.5 CONTROL STRATEGY PROPOSAL

3.5.1 Control design

To evaluate the transient performance of the thermosyphon-assisted falling film distillation column, the thermal network-based model developed was implemented in the dynamic simulation environment of the Simulink[®] software. The dynamic model, composed by the differential equations and the thermophysical property equations were inserted in the Matlab[®] Function Block tool, interconnecting this block with all necessary control system components. The block diagram scheme for the dynamic model as a closed-loop system with a PID controller is shown further up in Figure 23. The controlled variable is the evaporator temperature (T_e), which is regulated by acting on the evaporator power (Q_{in}) for both the regulatory and servo mechanism problems. It is important to highlight that the PID control strategy adopted is widely known. However, the application of the PID scheme in this specific distillation technology has not been reported yet. As previously stated, the core of the innovation of this work is focused on the dynamic modeling of the new process with experimental validation. Therefore, the objective of the control application, in this case, is to

demonstrate that the proposed dynamic modeling can be used satisfactorily to control the temperature of the thermosyphon's pilot-scale unit with a conventional PID controller.

3.5.1.1 PID controller

A PID controller is designed to stabilize the system and provide good setpoint tracking and good disturbance rejection with robust parameter uncertainty. In addition, PID controllers are still the most widely used in industrial facilities, mainly due to the robustness and easy parameter adjustment (FERNÁNDEZ *et al.*, 2020). The general function of the PID controller is to keep the controlled variable at the desired value, and the control action of a PID is defined as:

$$u(t) = K_p e(t) + \tau_i \int_0^t e(t) dt + \tau_d \frac{de(t)}{dt} \quad (29)$$

Where K_p is the proportional gain, τ_i is the integral gain and τ_d is the derivative gain. The three gains are the tuning parameters for the controller. The control signal is the sum of the three error functions from a specified setpoint. Proportional control has the effect of increasing loop gain to make the system less sensitive to load disturbances, error integral is used to eliminate steady-state error, and the derivative term helps improve closed-loop stability (OLUMAYEGUN; WANG, 2019).

3.5.1.2 Tuning methods

Over the past decades, several methods for determining the best parameters of PID controllers have been developed and tested. In order to achieve a practical strategy for tuning the PID controller parameters, the robust response time tuning method provided by the Control System Toolbox™ application of Matlab® was initially employed. This method allows designing a single-input and single-output (SISO) controller for feedback systems. In order to determine the transfer function of the system, 15 disturbances were applied in the heat input power of the electric resistances (Q_{in}), under different feed flow rate conditions, observing the evaporator temperature (T_e) as a response in open loop. Considering that the process is satisfactorily described by a first-order model, the obtained K (system gain) and τ

(time constant) parameters were within the following ranges: $0.122 \leq K \leq 0.164$; and $1,128.7 \leq \tau \leq 3,551.3$. The design of the PID controller was performed with the average values. However, its performance was evaluated in the nonlinear model, implemented in Simulink® environment, as described before. In addition to the robust response time method, two other tuning methods, Ziegler and Nichols (1942) and Chien, Hrones and Reswick (1972), were used to obtain the design parameters of the PID controller. Table 3 shows the tuning parameters obtained for each tested method.

Table 7 – Tuned PID controller parameters.

Tuning method		K_p	τ_i	τ_d
Robust Response Time	PI	7.56	0.11	-
	PID	9.70	0.094	-729
Ziegler-Nichols	PI	37.85	0.33	-
	PID	50.47	0.20	0.05
Chien, Hrones and Reswick	PI	14.72	0.67	-
	PID	25.24	0.58	0.05

Source: Battisti *et al.* (2020a).

3.5.1.3 Controller performance

A set of performance indicators can be used as a tool to evaluate the best results of the tuning methods. These performance indicators, Integral Absolute Error (IAE) and Integral Time-weighted Absolute Error (ITAE), were evaluated using Eqs. (30) and (31), respectively. In addition, as a parameter for evaluating the control action performance, the total electricity consumption in the evaporator over time was assessed.

Integral Absolute Error (IAE)

$$IAE = \int_0^t |e(t)| dt \quad (30)$$

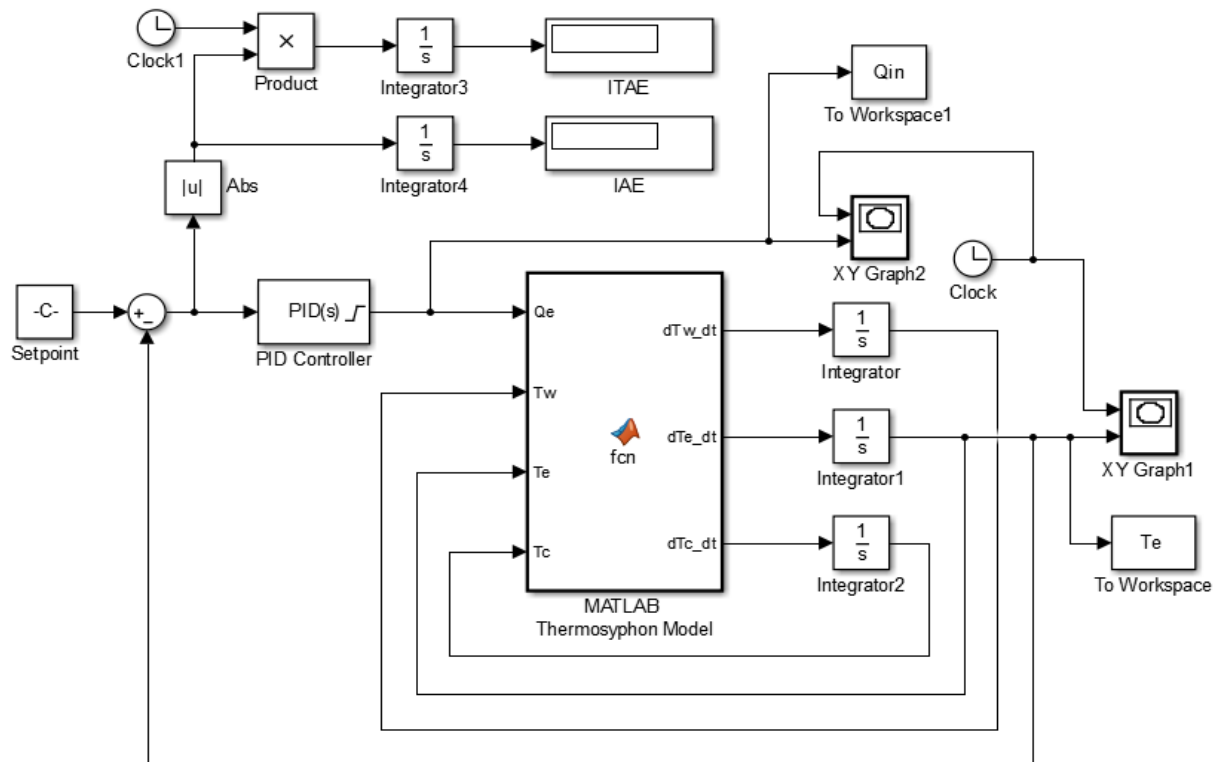
Integral Time-weighted Absolute Error (ITAE)

$$ITAE = \int_0^t t |e(t)| dt \quad (31)$$

3.5.2 Control analysis results

Precise temperature control of heat pipes has been of particular interest to achieve accurate temperature operating of these devices (JOUNG; LEE, 2019). The steam temperature from the evaporator, which is considered the operating temperature of the thermosyphon, and directly affects the temperature of the heat-generating components, is known to be affected by the temperature of the thermohydraulically linked compensation chamber (steam chamber). This linkage enables the temperature control by thermal action on the compensation chamber in several forms, as already studied using heaters (BIENERT; KROTIUK; NIKITKIN, 1999), thermoelectric modules (MELNICK *et al.*, 2012), pressure regulating valves (TORRES *et al.*, 2012), among others. PID is the most commonly controller used in industrial processes due to the easy implementation, simple structure, and robustness (OLUMAYEGUN; WANG, 2019). The dynamic thermal network-based model proposed for the thermosyphon-assisted falling film distillation unit was implemented in the Simulink[®] environment (Figure 23). It is composed of the system of differential equations, heat transfer correlations, and design parameters, in addition to the overall PID feedback control structure.

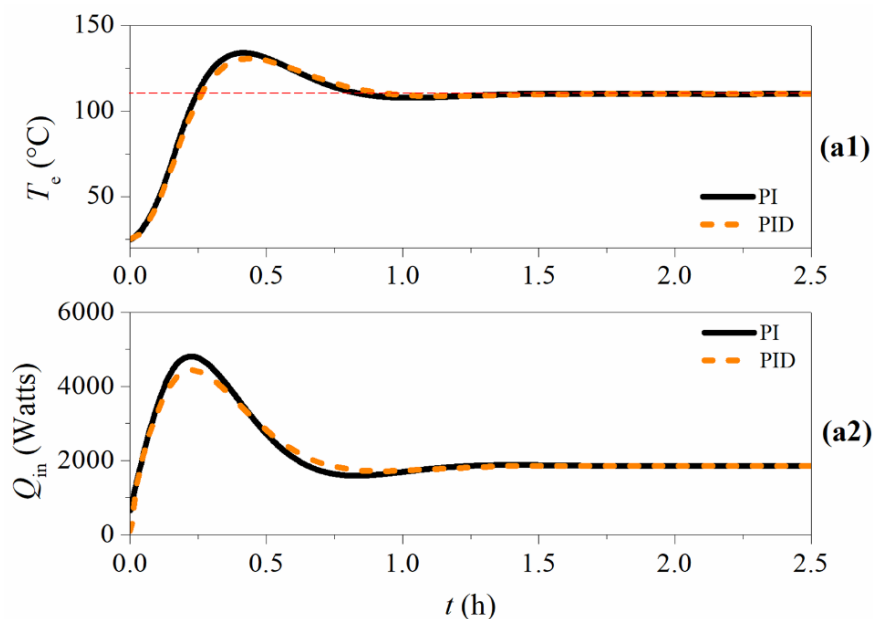
Figure 23 – Control components of model integration in the Simulink[®] environment.

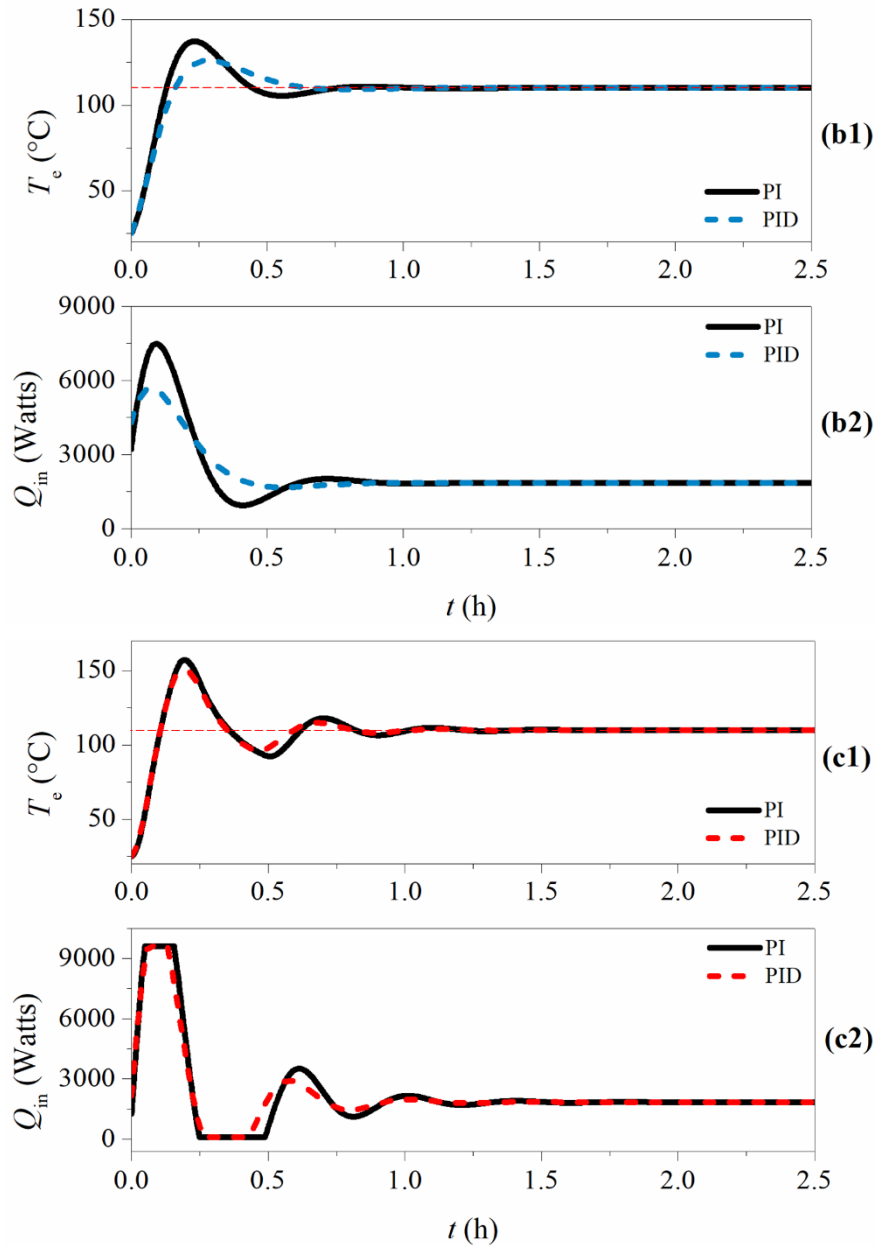


Source: Battisti *et al.* (2020a).

The feedback control of the thermosyphon's evaporator temperature (T_e) aims to keep the steam chamber's temperature at the setpoint value. This is achieved by manipulating the input power in the electrical resistances (Q_{in}). This PID temperature controller has the function of maintaining the purity of the distillate product of the falling film unit at or above one specified value. The setpoint of the temperature controller must be high enough to ensure that the purity of the distillate is equal to or above the value specified in the worst distillation condition, i.e., at the bubble temperature of the feed. Currently, the tuning rules for PID controllers have been one of the main researches focuses in the area of process control. From the original works of Ziegler and Nichols (1942) and Cohen and Coon (1953), a large number of methods with different approaches have been proposed. Tuning the controller means to find the parameters that reach the steady-state of operation of some device more quickly, to better reach quality requirements, process safety, satisfy eventual environmental restrictions and increased profitability (ENGELL, 2007). Three tuning methods for the PID controller were used in this work: (i) Robust Response Time; (ii) Ziegler-Nichols; and (iii) Chien, Hrones and Reswick. Figure 24 presents the results of the controller implemented for the thermosyphon's evaporator temperature (T_e), by manipulating the input power of the electric resistances (Q_{in}) for the three different tuning methods studied.

Figure 24 – Control performance for T_e (a1) and Q_{in} (a2) with Robust Response Time; T_e (b1) and Q_{in} (b2) with Ziegler-Nichols; and T_e (c1) and Q_{in} (c2) with Chien, Hrones and Reswick methods.





Source: Battisti *et al.* (2020a).

In general, as is already known for temperature control, the PID controller reaches the setpoint slightly faster, and demonstrates a smoother response when compared to the PI controller, with lower overshoot values. Even knowing that this is the expected behavior, however, as it is a new proposal, the PI controller was tested to verify if this behavior would be confirmed. The comparison of tuning methods was made to show the closed-loop performance of the thermosyphon-assisted unit using two different criteria: the integral absolute error (IAE) and the integral-time absolute error (ITAE). Table 8 shows the values of the performance criteria obtained for the controllers. Ziegler-Nichols method presented the

lowest performance error indicators, since its parameters led to the steady-state faster and with less overshoot, an important factor because it causes less mechanical stress and consequently less wear on electrical resistances. When analyzing the demand for electrical resistances, another important factor to be considered is safety. It is observed that in the case of the Chien, Hrones and Reswick tuning method (Figure 24 c), the electrical resistances are activated quickly at the beginning of the heating process, which raises the power to its maximum limit (9.6 kW). In the real system, it may cause a risk of evaporator overheating, generating an unwanted and dangerous increase in internal evaporator pressure. In addition, it is worth highlighting that for all cases, the PID controllers caused less overshoot of the manipulated variable, in this case, the variation of power added in the resistances (Q_{in}), generating lower energy consumption, which is positive from the point of view of saving electricity in the process. The PID controller adjusted by the Ziegler-Nichols method showed a reduction of 3.1% in energy during the total time of the performed run (2.5 h), and was 13.7% faster to reach the steady-state setpoint compared to the PI controller, being considered the most suitable controller for this specific process.

Table 8 – Performance of PID controller tuning methods.

Tuning method		IAE	ITAE	Total Q_{in} (kW)
Robust Response Time	PI	7.902×10^4	7.309×10^7	1.986×10^4
	PID	7.886×10^4	7.148×10^7	1.973×10^4
Ziegler-Nichols	PI	4.591×10^4	2.904×10^7	1.983×10^4
	PID	4.193×10^4	2.499×10^7	1.946×10^4
Chien, Hrones and Reswick	PI	6.086×10^4	5.501×10^7	2.008×10^4
	PID	5.289×10^4	3.995×10^7	1.997×10^4

Source: Battisti *et al.* (2020a).

3.6 SUMMARY AND CONCLUDING REMARKS

A thermal network-based dynamic modeling and control design for the innovative Destubcal technology was proposed and experimentally validated. The most relevant aspects rely on the development of the dynamic model, the first one in the acquaintance of the

authors, and its experimental validation for this novel application of heat supply to a falling film distillation unit. The thermal network-based approach assumes each process system as thermal resistances. Considering the complexity of the process and the number of variables that can suffer disturbances over time, in addition to the sensitivity of the falling film, the thermal network model was able to describe the dynamic behavior of the temperature of the thermosyphon with great accuracy. The experimentally validated dynamic model was implemented in the Simulink[®] environment in order to design and tune the thermosyphon temperature feedback control system, acting on the power supplied by electrical resistances. Notably, the PID controller with tuning parameters adjusted by the Ziegler-Nichols method proved to be more efficient in reaching the desired temperature setpoint faster, with less overshoot, and less oscillation in the manipulated variable, consequently reducing the plant's electricity consumption by 3.1%.

4 MACHINE LEARNING MODELING AND GENETIC ALGORITHM-BASED OPTIMIZATION OF A NOVEL PILOT-SCALE THERMOSYPHON-ASSISTED FALLING FILM DISTILLATION UNIT

The content of this chapter is based on the following published article:

BATTISTI, Rodrigo; CLAUMANN, Carlos Alberto; MANENTI, Flavio; MACHADO, Ricardo Antonio Francisco; MARANGONI, Cintia. Machine learning modeling and genetic algorithm-based optimization of a novel pilot-scale thermosyphon-assisted falling film distillation unit. **Separation and Purification Technology**, v. 259, p. 118122, 2021. DOI: 10.1016/j.seppur.2020.118122.

4.1 INTRODUCTION

Mathematical models play a meaningful role in the simulation and optimization of distillation systems, leading to efficient and economical designs of separation processes (AL-HOTMANI *et al.*, 2020; OCHOA-ESTOPIER; JOBSON; SMITH, 2014; SKIBOROWSKI; WESSEL; MARQUARDT, 2014). Mathematical modeling of any process is based on two basic approaches: (i) theoretical (or parametric) models based on fundamental knowledge of the process, also known as the knowledge-based approach; and (ii) empirical (or non-parametric) models, which do not involve the knowledge of fundamental principles governing the process (MAZUR, 2006; SHAHSAVAND; CHENAR, 2007). As known, distillation columns are fairly complex devices and exhibit nonlinear behavior due to their non-ideal vapor-liquid equilibrium relationships, complex processing configurations, and high product purities (ABDULLAH; AZIZ; AHMAD, 2007). It somewhat limits the applicability of the theoretical-based models. Besides, an advantage of empirical modeling tools over theoretical models consists of the possibility to develop the objective function useful for process optimization easily (KHAYET; COJOCARU; ESSALHI, 2011). Machine Learning (ML) is a modeling technique dealing with non-parametric models also known as the “black-box” models (ELSHEIKH *et al.*, 2019). Imitating the way of dealing with data by humans, ML adopts biological frameworks that can make decisions based on the previous experience to handle incomplete information and multiple input-output situations. Due to the advantages of high precise prediction, no requirement of exact relationship between input and output data,

and almost no simplifying assumptions, ML became a powerful tool to model non-linear systems by means of the application of artificial neural networks (ABIODUN *et al.*, 2018; LI *et al.*, 2016b).

Distillation on wetted-wall columns (or falling film distillation) has been successfully modeled by ML approaches for multiple purposes. The best-known falling film column operation is the molecular distillation. It is characterized by the use of a high vacuum and by a distance between the evaporation and condensation surfaces in the order of magnitude of the mean free path of the molecules so that equipment operates in a non-equilibrium condition (MAZIERO *et al.*, 2019). Dantas *et al.* (2020) modeled the molecular distillation of patchouli oil through artificial neural networks to obtain a desired quality of the patchoulol-rich fractions. The authors selected three factors as input variables (evaporator temperature, condenser temperature, and agitation speed), and two output answers were analyzed (percentage of residue and patchoulol concentration in the residue). ML demonstrated a good predictive capability, thus being a suitable tool to model this process.

Tehlah, Kaewpradit and Mujtaba (2016) develop two different ML models to predict the content of beta-carotene, tocopherol, and free fatty acid from falling film molecular distillation of refined palm oil. The first ML model was based on three inputs (feed flow rate, column temperature, and pressure), and the second model on two inputs (column temperature and pressure). The proposed ML models proved to be an appropriate tool to model the process accurately, also being able to predict the outputs very close to those predicted by a commercial knowledge-based simulator. Another successful approach in modeling falling film distillers was done by Borgarello *et al.* (2015), who considered the effects of evaporation temperature and feed flow rate on thymol concentration in the residue fractions from molecular distillation of oregano essential oil. The authors also highlighted the viability of this ML modeling tool to be used to ensure a defined product quality, as a first step towards the design of an automatic process control in real time.

It is worth highlighting that falling film distillation columns are usually operated under low-pressure conditions, such as molecular distillation. However, the use of vacuum inside the distillation tube imposes some restrictions on the equipment and increases operational costs. Destubcal falling film distillation unit has the related-key differential of operating inside the distillation tube at atmospheric pressure, besides the heat being supplied by a two-phase closed thermosyphon, with energy distributed throughout the distillation tube length. Within this context, this chapter is dedicated to the ML modeling of four operating

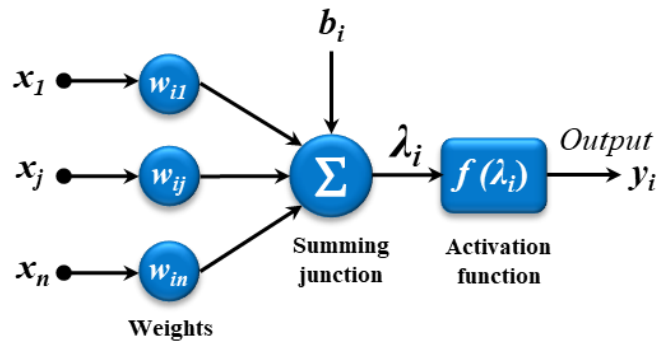
variables of ethanol recovery by the thermosyphon-assisted falling film distillation, namely the ethanol mass fraction in the distillate (x_{eOH}^D), the distillate mass flow rate (\dot{m}_D), the recovery factor (RF), and the separation factor (SF), considering as input factors the feed temperature (T_F), the evaporator temperature (T_e), and the feed flow rate (Q_F). With the ML model constructed and validated, an optimization approach is performed by the Genetic Algorithm (GA) technique in order to find the optimal conditions of these parameters simultaneously. As far as the authors are aware, this is the first study of ML modeling and GA optimization of a thermosyphon-assisted falling film distillation. Furthermore, this work offers important tools to consolidate Destubcal technology as an intensified-advanced distillation process for the chemical process industry, once it can be used to optimally separate and purify several mixtures in a pilot-scale unit.

4.2 THEORETICAL BACKGROUND ON ML MODELING AND GA OPTIMIZATION

4.2.1 ML modeling

ML is a data-driven technique for accomplishing the identification of unit operations, reactors, or processes. Among the several ML algorithms available, neural networks play an important role due to their wide applicability, as their main advantage (WUEST *et al.*, 2016). Besides, neural networks are usually more able to easily provide incremental learning, tending to perform much better than other methods when dealing with high-dimensional data and continuous variables, offering high accuracy in most cases (KOTSIANTIS; ZAHARAKIS; PINTELAS, 2006). Assuming a numerical structure based on artificial neural networks, it is a mathematical model composed of simple interconnected components that perform tasks and process information in response to external inputs, trying to imitate the behavior of biological neural networks (GIL *et al.*, 2018). Each artificial neuron (Figure 25) is a unitary computational processor with a summing junction operator and a transfer function. The connections between inputs, neurons, and outputs consist of weights and biases, which are considered design parameters of the neural network (KHAYET; COJOCARU, 2013).

Figure 25 – Structure of an artificial neuron.



Source: Battisti *et al.* (2021a).

Considering the model of a single neuron, any scalar input x_j is transmitted via a connection that multiplies its strength by the scalar weight w_{ij} to form the product $w_{ij} \times x_j$. The bias b_i is responsible for lowering or increasing the summation's output, and it is simply added to the product $w_{ij} \times x_j$ by a summing junction. The summing junction operator of a single neuron summarizes the weights and bias into a net input λ_i known as argument to be processed:

$$\lambda_i = \sum_{j=1}^n (x_j \cdot w_{ij}) + b_i \quad (32)$$

Where x_j is the input variable, w_{ij} are the connection weights, i and j are the integer indexes ($i = 1, m; j = 1, n$), m is the number of artificial neurons, n is the number of input variables, and b_i is called the bias of a single artificial neuron (i). The argument λ_i is converted into a scalar value employing a transfer function. The most used transfer functions to solve linear and non-linear regression problems are linear transfer function (*purelin*), log-sigmoid transfer function (*logsig*), and hyperbolic tangent sigmoid transfer function (*tansig*) (KHAYET; COJOCARU, 2012):

$$\text{purelin}(\lambda_i) = \lambda_i \quad (33)$$

$$\text{logsig}(\lambda_i) = \frac{1}{1 + \exp(-\lambda_i)} \quad (34)$$

$$\text{tansig}(\lambda_i) = \frac{1 - \exp(-\lambda_i)}{1 + \exp(-\lambda_i)} \quad (35)$$

The arrangement in which neurons are grouped and connected is known as the topology or architecture of the neural network. In general, neurons are grouped in different layers, such as hidden and output layers. The most frequently used neural network topology is the multi-layer feed-forward (CLAUMANN *et al.*, 2018; YANG *et al.*, 2020). Once the architecture of the network is defined, the weights and biases are adjusted utilizing a training algorithm. One of the most used training algorithms for the feed-forward neural network is the back-propagation (BP) algorithm, based on the gradient descent method (YI *et al.*, 2007). The network training by BP algorithm includes an iterative optimization process where the weights and biases are updated while minimizing a performance criteria function, commonly employed the mean-squared-error (*MSE*), as defined as follows:

$$MSE = \frac{1}{N} \sum_{j=1}^N \left(Y_{j,exp} - \hat{Y}_{j,pred} \right)^2 \quad (36)$$

Where $Y_{j,exp}$ is the experimental response (target), $\hat{Y}_{j,pred}$ is the predicted response (network output), N is the number of data points, and j is the integer index. Generally, a single iteration of the BP algorithm using the gradient descent method can be written as:

$$\mathbf{W}^{(k+1)} = \mathbf{W}^{(k)} - \eta^{(k)} \cdot \mathbf{grad}^{(k)}(MSE) \quad (37)$$

where $\mathbf{W}^{(k)}$ is a vector containing current weights and biases, $\mathbf{grad}^{(k)}(MSE)$ is the current gradient of performance function and $\eta^{(k)}$ is the learning rate (KHAYET; COJOCARU; ESSALHI, 2011). Once the ML is trained, the optimal weights and biases are saved, and the neural network model can be used for simulation and optimization procedures.

4.2.2 GA optimization

Genetic algorithms (GA) are adaptive heuristic search algorithms designed to solve optimization problems by imitating principles of biological evolution in the natural genetic system (CHEN; WANG, 2009). These algorithms maintain and manipulate a population of

solutions and implement their search for better solutions based on the 'survival of the fittest' strategy (SHEN; WANG; LI, 2007). Due to its global searching ability, GA has become a popular tool in the engineering optimization field. Since GA can produce a complete set of simultaneous solutions in a single run, it has been widely used for a great deal of multi-objective optimization problems (KUNDU *et al.*, 2018), mainly dealing with design purposes thanks to its robustness. It is worth mentioning that GA optimization is performed after the neural network is trained, validated, and tested in order to find the set of operating variables that optimize the performance parameters of the thermosyphon-assisted falling film distillation unit.

As a pattern procedure, GA performs random searches through a given set for finding the best criteria of goodness. These criteria are expressed as an objective or fitness function. Fitness function is defined as to be either maximized or minimized (MADAENI *et al.*, 2010). The objective of the optimization problem here is to find the optimal values of the input variables ($z_1, z_2, z_3,$ and z_4) in order to ensure the maximum value of the performance indices (\hat{Y}), simultaneously. Therefore, the formulation of the optimization step can be written, in this case, as follows:

$$\begin{aligned} & \max \{ \hat{Y}(z_1, z_2, z_3, z_4) \} \\ & \text{subjected to: } z_i \in [z_i^{\min}, z_i^{\max}], i = \overline{1, 4} \end{aligned} \quad (38)$$

GA working involves random initialization of population (i.e., members are randomly generated to cover the entire search space uniformly) to start the process. Then, evaluation of the objective function, selection of parents, and applying genetic operations, recombination operator for creation of offsprings, and mutation operation for perturbing the individuals to produce a new population are conducted. The steps are repeated until a termination condition is satisfied (JANGA REDDY; NAGESH KUMAR, 2020).

4.3 METHODOLOGY

4.3.1 Experimental procedure

The falling film distillation experiments were carried out in the pilot-scale thermosyphon-assisted unit, shown schematically in Figure 13, whose operation is described in the item 3.2.1. ML modeling was developed using a total of 64 experimental runs, covering a wide operating range of the input variables. Aiming to evaluate the efficiency of the thermosyphon-assisted falling film distillation unit from the degree of separation, the recovery factor (RF) of the most volatile component (ethanol) was calculated according to Eq. (39):

$$RF(\%) = \frac{\dot{m}_D \cdot x_{etOH}^D}{\dot{m}_F \cdot x_{etOH}^F} \times 100 \quad (39)$$

Where \dot{m}_D is the distillate mass flow rate, x_{etOH}^D is the ethanol mass fraction in the distillate stream, \dot{m}_F is the feed mass flow rate, and x_{etOH}^F is the ethanol mass fraction in the feed stream. Another parameter used to analyze the falling film distillation process is the separation factor (SF), achieved by Eq. (40). SF corresponds to the ratio of the mass fraction of the most volatile component at the top of the distillation tube (ethanol) to the mass fraction of the less volatile component in the bottom of the distillation tube (water); hence SF is a measure that indicates the effectiveness of separation of a mixture concerning the output streams (SKOGESTAD, 1997).

$$SF = \frac{\left(x_{etOH}/x_{H_2O}\right)_D}{\left(x_{etOH}/x_{H_2O}\right)_B} \quad (40)$$

Where x_{etOH} is the ethanol mass percentage (light component), x_{H_2O} is the water mass percentage (heavy component), and D and B denotes the top and the bottom section of the falling film distillation column, respectively.

4.3.2 Data normalization

For a more effective development of the ML model, data normalization should be considered for both the network inputs (operating variables) and the targets (experimental response). In this work, the network inputs and targets have been normalized before training in order to facilitate the generalization of the network and to avoid over-fitting that may appear due to very large or very small weights. The experimental variables and targets have been normalized in the range between 0 (minimum level) and 1 (maximum level) since the activation function employed (*logsig*) also ranges from 0 to 1. For normalization of the input variables, the following equation was used (KHAYET; COJOCARU, 2012):

$$x_i = \frac{z_i - z_i^{\min}}{z_i^{\max} - z_i^{\min}} \quad (41)$$

Where x_i represents the normalized operational variable, while z_i , z_i^{\min} , and z_i^{\max} are the actual, minimum, and maximum values of operating variables, respectively. The target data was normalized in the range 0.1–0.9 through the following expression (GIL *et al.*, 2018):

$$y_{\text{norm}} = \left(1 - \Delta^U - \Delta^L\right) \frac{(y - y^{\min})}{(y^{\max} - y^{\min})} + \Delta^L \quad (42)$$

where y_{norm} is the normalized target, y is the actual value, y^{\max} and y^{\min} are the maximum and minimum values of the target to be normalized, and Δ^U and Δ^L are the upper and lower bounds considered to define the output network range ($\Delta^U = \Delta^L = 0.1$).

4.3.3 Model development and optimization procedure

As inputs of the neural network, three operating variables were considered: the feed inlet temperature (T_F), the evaporator temperature (T_e), and feed flow rate (Q_F). The process operating conditions of each input variable is shown in Table 9. For the evaluation of the falling film distillation unit performance, four responses were considered, used as outputs for

the neural network: the ethanol mass fraction in the distillate (x_{etOH}^D), the distillate mass flow rate (\dot{m}_D), the recovery factor (RF), and the separation factor (SF).

Table 9 – Process operating conditions of input variables.

Variable	Operating conditions
Feed inlet temperature, T_F (°C)	60; 80; 90; 95
Evaporator temperature, T_e (°C)	93; 100; 104; 110
Feed flow rate, Q_F (L/h)	14; 17; 23; 32

Source: Battisti *et al.* (2021a).

Most of the literature suggests that a feed-forward neural network with only a single hidden layer with a sufficient number of neurons provides a good approximation for a continuous function (ZHANG; MORRIS, 1998). The number of neurons in one hidden layer was varied while the mean-squared-error (MSE) and the regression coefficient (R) were evaluated as selection criteria in order to find the best ML model architecture. The transfer function adopted in the hidden layers was the *logsig*, whereas the one employed in the output layer was the *purelin* (GIL *et al.*, 2018). The Levenberg–Marquardt back-propagation algorithm (LM-BP) was employed for training as this algorithm is fast and consumes less computational memory (SANGWAN; SAXENA; KANT, 2015).

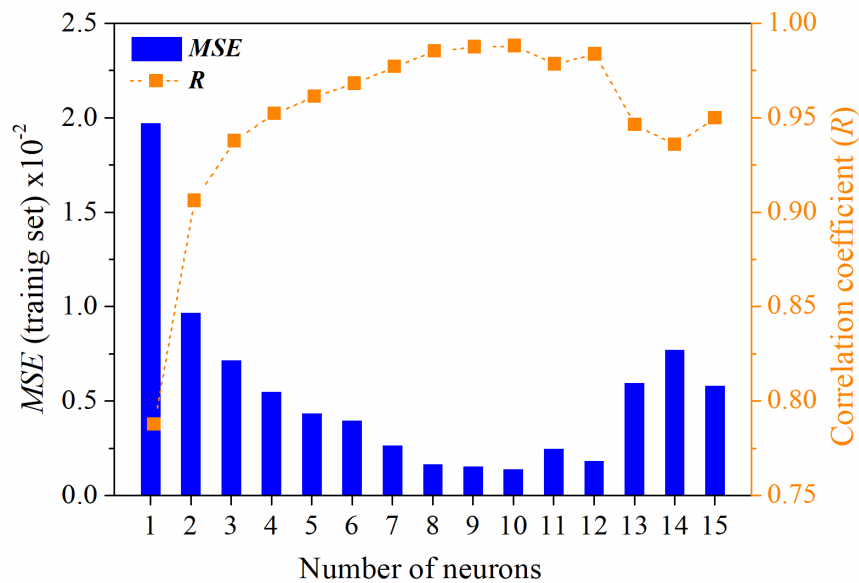
Once the ML model is established, GA optimization was performed using the developed ML modeling function to optimize the process operational variables. The input values of GA optimization are the three operating variable values established within the minimum and maximum range of Table 9. To perform the optimization, GA chooses randomly the input values to be used within the established range, and the saved ML function is accessed at each run to predict the four output performance parameters. In the present study, the fitness function is based on the maximization of the four output responses of the predicted ML model simultaneously, i.e., mathematically described by the maximum summation of the ethanol mass fraction in the distillate, distillate mass flow rate, recovery factor, and separation factor. As GA was designed to generate maximum values, the default minimization problem was converted into a maximization problem by changing the fitness function into inverse (KALATHINGAL; BASAK; MITRA, 2020). ML modeling was accomplished in Neural Network Toolbox and optimization was performed in the Genetic Algorithm Toolbox, both from Matlab[®] software version 8.5 (R2015a).

4.4 RESULTS AND DISCUSSIONS

4.4.1 ML modeling

The experimental dataset used to construct the ML model are summarized in Appendix D. About 65% of the experimental trials available were used for training, 15% for validation, and 20% for testing. As all data is labeled, the supervised ML algorithm learns to predict the output from the input data (WUEST *et al.*, 2016). As output responses (targets) for the ML model, the ethanol mass fraction in the distillate (x_{etOH}^D) varied from 21.64 – 68.34 wt%, the distillate mass flow rate (\dot{m}_D) varied from 0.48 – 14.3 kg/h, the recovery factor (RF) varied from 12.03 – 93.25%, and the separation factor (SF) varied from 3.75 – 90.97. These values are the minimum and maximum experimental values achieved of each performance response analyzed and represent the most extensive range that the unit has reached for the ethanol-water mixture. The effect of increasing the number of neurons on the model's performance was evaluated in order to optimize the neural network architecture. The optimum number of neurons was determined based on the minimum value of MSE and the maximum value of R from the training set. Further simulations were carried out by varying the number of neurons from 1 to 15 to find the best ML model, as shown in Figure 26.

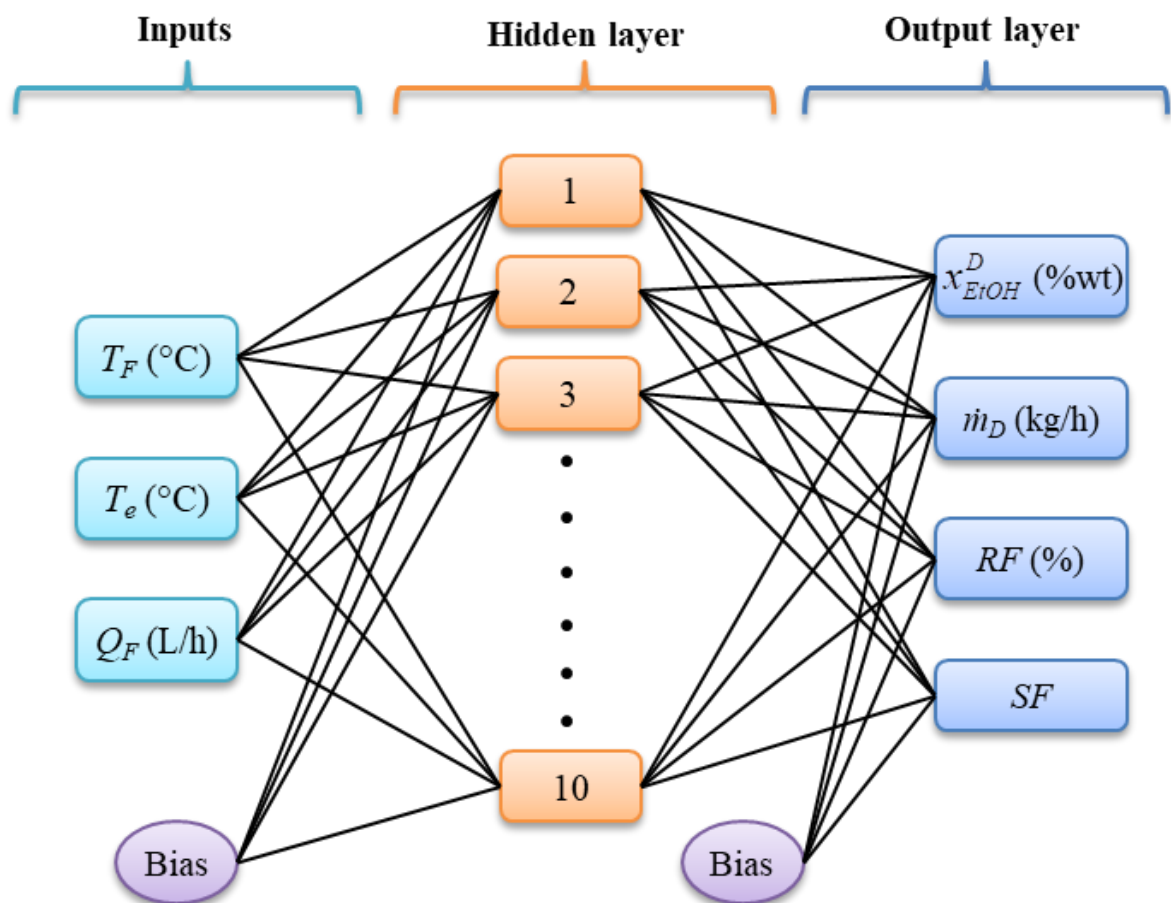
Figure 26 – Effect of the number of neurons on the ML training performance.



Source: Battisti *et al.* (2021a).

Increasing the number of neurons significantly reduces the error and improves the R , up to a certain point, when these indicators start to worsen again. The higher MSE value of 1.974×10^{-2} and lower R value of 0.79 were observed when one neuron was used. When the number of neurons was increased to 10, the MSE decreased to 1.395×10^{-3} and the best R value of 0.99 was achieved. From 10 neurons, it was observed a slight increase in the MSE but still with R values of approximately 0.95. This worsening of the performance criteria of the neural network is certainly explained by overfitting, and indicates that the optimal number of neurons has been reached (NANDAGOPAL; ABRAHAM; SELVARAJU, 2017). Therefore, in this case, the optimal topology of the ML model includes three inputs, one hidden layer with 10 neurons, and one output layer with four outputs. Thus, the notation of the developed feed-forward neural network may be written as (3:10:4), referring to the number of inputs and the number of neurons in the hidden and output layer, respectively. The optimal topology of the ML model is shown in Figure 27.

Figure 27 – Optimal topology of the ML model.

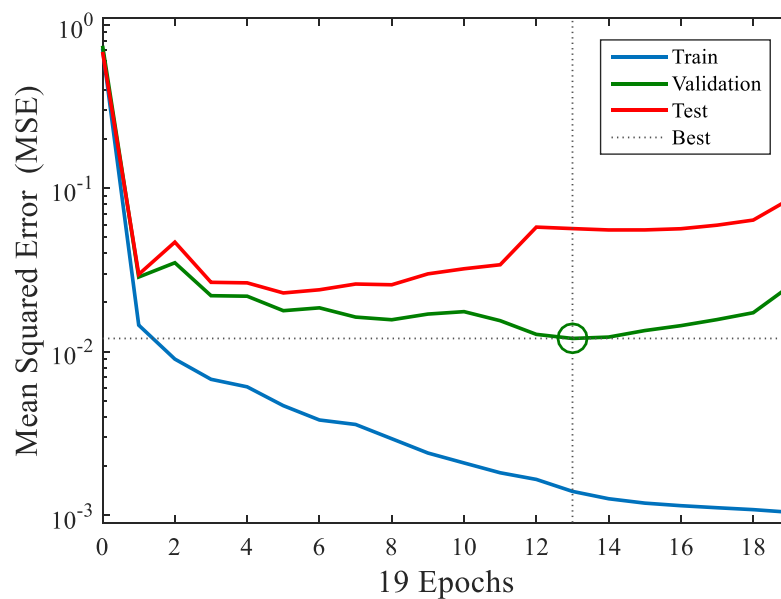


Source: Battisti *et al.* (2021a).

As can be seen, the connections consist of weights and biases between inputs and neurons as well as between neurons from different layers. The input weight matrix $\mathbf{IW}^{(1,1)}$ has a size (3×10) and the layer weight vector is $\mathbf{LW}^{(2,1)}$, where the superscripts indicate the source and destination connections, respectively. All neurons from the network have the bias vector $\mathbf{b}^{(l)}$ where the superscript indicates the layer index. According to Khayet and Cojocaru (2013), the biases connected to all artificial neurons from the hidden and output layer play a similar role to the offset terms in multiple regression models.

The ML model has been trained using the back-propagation method (BP) based on Levenberg–Marquardt algorithm (LMA) to assess the optimal values of weights and biases, as for a small and moderate total number of the net weights, LMA is the most efficient calculation procedure adapted for learning (WILAMOWSKI; YU, 2010). Figure 28 shows the resulted performance of the ML model for training, validation, and testing at increasing epochs. It can be seen from Figure 28 that from 13 to 19 epochs (iterations) *MSE* training remains to decrease. However, validation and test error begin to have a slight increase. Yang *et al.* (2020) also observed the same behavior by modeling a vacuum membrane distillation process using artificial neural networks, where validation and the test errors started increasing after 11 epochs, while training error continued to decrease. This is another factor that indicates the occurrence of network overfitting (JAWAD; HAWARI; ZAIDI, 2020). Therefore, to achieve the best validation performance, the training set quit after 13 epochs.

Figure 28 – *MSE* for training, validation, and test data subsets.



Source: Battisti *et al.* (2021a).

After the training process being considered successfully terminated, the obtained optimal values of weights and biases were saved for the developed ML model could be used for simulation and optimization of the thermosyphon-assisted falling film distillation process. The optimal values of weights and biases in vector-matrix format are summarized in Table 10.

Table 10 – Optimal values of weights and biases for the ML model.

Input weight matrix, IW {Destination: hidden layer Source: inputs}	IW{1,1} =			
	0.5631	-2.1290	1.5968	
	0.7239	2.6732	-1.9262	
	-2.9439	0.0126	-0.1765	
	2.1004	-0.2651	1.5314	
	0.5670	2.9243	-0.2667	
	-2.0601	-1.4100	0.8647	
	-2.0559	-0.0925	2.3629	
	0.6002	2.3020	-1.3975	
	2.7555	1.8434	-0.1739	
1.9443	2.0520	-1.6953		
Bias vector, b {Destination: hidden layer}	b{1} =			
	-3.2725			
	-2.3560			
	3.0279			
	-1.5389			
	-1.4282			
	-0.8651			
	-1.1422			
	0.9785			
2.2216				
2.9518				
Layer weight vector, LW {Destination: output layer Source: hidden layer}	LW{2,1}^T =			
	-0.1862	-0.7705	-0.3872	-0.5332
	-0.0074	-0.1877	0.5160	0.6632
	0.9430	-0.2519	0.0463	0.7704
	0.2254	-0.0162	0.2549	0.4140
	-0.1085	0.2845	-0.1508	-0.1315
	-0.0421	0.6592	0.5272	0.2536
	-0.6638	0.1729	0.1519	-0.3417
	-0.2987	0.3530	0.8728	0.2112
	-0.2366	0.6734	0.4770	0.1040
0.4070	-0.2841	-0.2052	-0.2058	

Bias vector, \mathbf{b}	$\mathbf{b}\{2\} =$
{Destination: output layer}	-1.0755
	-1.1316
	-0.0811
	-1.0546

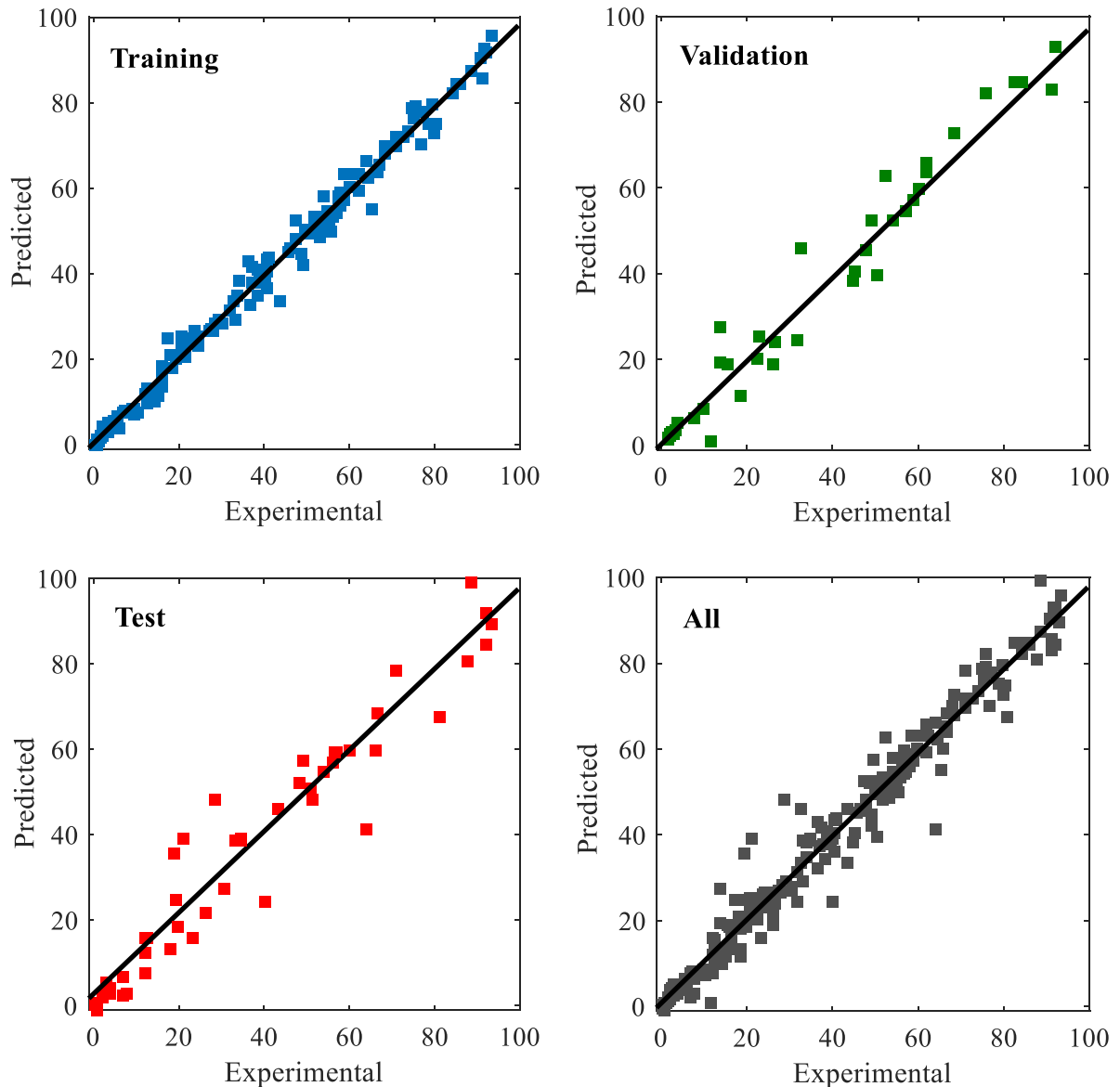
Source: Battisti *et al.* (2021a).

It is important to note that these optimal values of connections (weights and biases) are related to coded inputs (factors) and normalized targets (responses). Hence, the ML model developed for the prediction of the four performance parameters of the novel Destubcal unit can be presented mathematically as an input-output composite mapping, as shown in Eq. (43):

$$\hat{\mathbf{Y}}_n(\mathbf{x}) = \boldsymbol{\psi}^{(2)} \left[\mathbf{LW}^{(2,1)} \boldsymbol{\psi}^{(1)} \left(\mathbf{IW}^{(1,1)} \mathbf{x} + \mathbf{b}^{(1)} \right) + \mathbf{b}^{(2)} \right] \quad (43)$$

Where $\hat{\mathbf{Y}}_n$ is the vector of normalized responses (predicted outputs), \mathbf{x} is the vector of input variables, $\boldsymbol{\psi}^{(1)}$ is the vector of the transfer function (*logsig*) corresponding to the hidden layer, $\boldsymbol{\psi}^{(2)}$ is the vector of the transfer function (*purelin*) corresponding to the output layer, $\mathbf{IW}^{(1,1)}$ is the input weight matrix, $\mathbf{LW}^{(2,1)}$ is the layer weight vector, $\mathbf{b}^{(1)}$ and $\mathbf{b}^{(2)}$ are the bias vectors. Figure 29 shows the regression analysis between the target (experimental observations) and the network output (predictions) from the ML model for each phase: training, validation, and test sets. The linear correlation coefficients obtained were: 0.996 for the training data subset, 0.968 for the validation data subset, and 0.943 for the test data subset. The training set showed the best correlation coefficient data as it was also used to train the neural network. The validation and test subsets are used as supplemental data to assist the training process for checking the model generalization capability (KHAYET; COJOCARU, 2012). The linear correlation coefficient for all data set (training, validation, and test together) was 0.980. When looking at the literature of distillation modeling by neural networks, the overall linear correlation coefficients between the experimental and predicted outputs of the networks are in the range of 0.80 (KHAYET; COJOCARU, 2013), 0.840 (BORGARELLO *et al.*, 2015), 0.980 (DANTAS *et al.*, 2020), 0.988 (GIL *et al.*, 2018), 0.992 (KHAYET; COJOCARU, 2012), up to 0.998 (TEHLAH; KAEWPRADIT; MUJTABA, 2016). Therefore, these correlation values reveal that the ML model proposed for the falling film distillation has a satisfactory fit between the experimental data employed and the predicted results, being able to predict the pilot-scale unit's performance with remarkable accuracy.

Figure 29 – Comparison between predicted values by ML model and experimental data.



Source: Battisti *et al.* (2021a).

The trained neural network was applied to plot 3D surface graphs and 2D contour-line maps, showing the simultaneous effects of two variables at a time on each response, in order to evaluate the influence of the three operating variables of the Destubcal unit on the studied responses. This is an important finding as it is the first time that the operating variables of the thermosyphon-assisted falling film distillation have been analyzed in such a wide range for ethanol-water mixture separation, making it possible to elucidate the individual and synergistic effects on the unit's performance. Figure 30 shows the generalization plots of predicted responses in 3D output surface and 2D contour-lines maps as a function of feed

temperature (T_F) and evaporator temperature (T_e) varying, for a fixed feed flow rate (Q_F) of 23 L/h. In Figure 31 the variables analyzed are Q_F and T_F for a fixed $T_e = 101.5$ °C, and in Figure 32, Q_F , and T_e are the variables investigated for a fixed $T_F = 83$ °C. It is important to highlight that the fixed variables used are always an average value between the minimum and maximum range used in the construction of the ML model.

It can be seen that the ethanol mass fraction in the distillate (x_{eOH}^D) reaches higher values with milder evaporator temperatures and median feed temperatures, around 85 °C (Figure 30 a₁ and a₂). This is because lower evaporator temperatures favor the depletion of ethanol, enriching the distillate stream in the most volatile component. In contrast, when the evaporator temperature is increased to values above 100 °C, water is evaporated in a higher quantity, which ends up reducing the ethanol mass fraction in the distillate. Considering that the bubble temperature of the mixture fed into the column (10 wt% of ethanol) is around 84 °C, from this temperature onwards, the most volatile component evaporates more easily. Therefore, at feed temperatures far below that, a low enrichment of ethanol is obtained, since the energy provided by the condenser of the thermosyphon to the falling film tube will be demanded initially to heat the liquid film until the bubble point, and only after that distillation will occur. Low feed flow rates tend to improve the ethanol mass fraction in the distillate even at low feed temperatures. However, high ethanol mass fractions also can be obtained in the distillate when feed temperatures close to the bubble temperature are used, as can be seen in Figure 31 (a₁) and (a₂). This behavior is in line with the usual findings for separations with falling film distillers, where low feed flow rates are recommended (MOSCHOU *et al.*, 2013). With lower feed flow rates, a thinner liquid film thickness is obtained, and so there is a better heat transfer performance. However, very low feed flow rates make the flow pattern laminar, which reduces heat transfer and impairs separation, which can be seen in Figure 32 (a₁) and (a₂). Increasing the feed flow rate enhances the heat transfer performance of falling film distillation at first; however, when the feed flow rate reaches a certain value, it will hinder the improvement of heat transfer performance (LIU; MA; LI, 2011). In addition, it is important to note that at high feed flow rates, the velocity of the falling liquid film becomes very high, raising the number of waves on the surface of the falling film and also resulting in a shorter residence time on the heating surface of the distillation tube, which may hinder the distillation process (BATTISTI; MACHADO; MARANGONI, 2020).

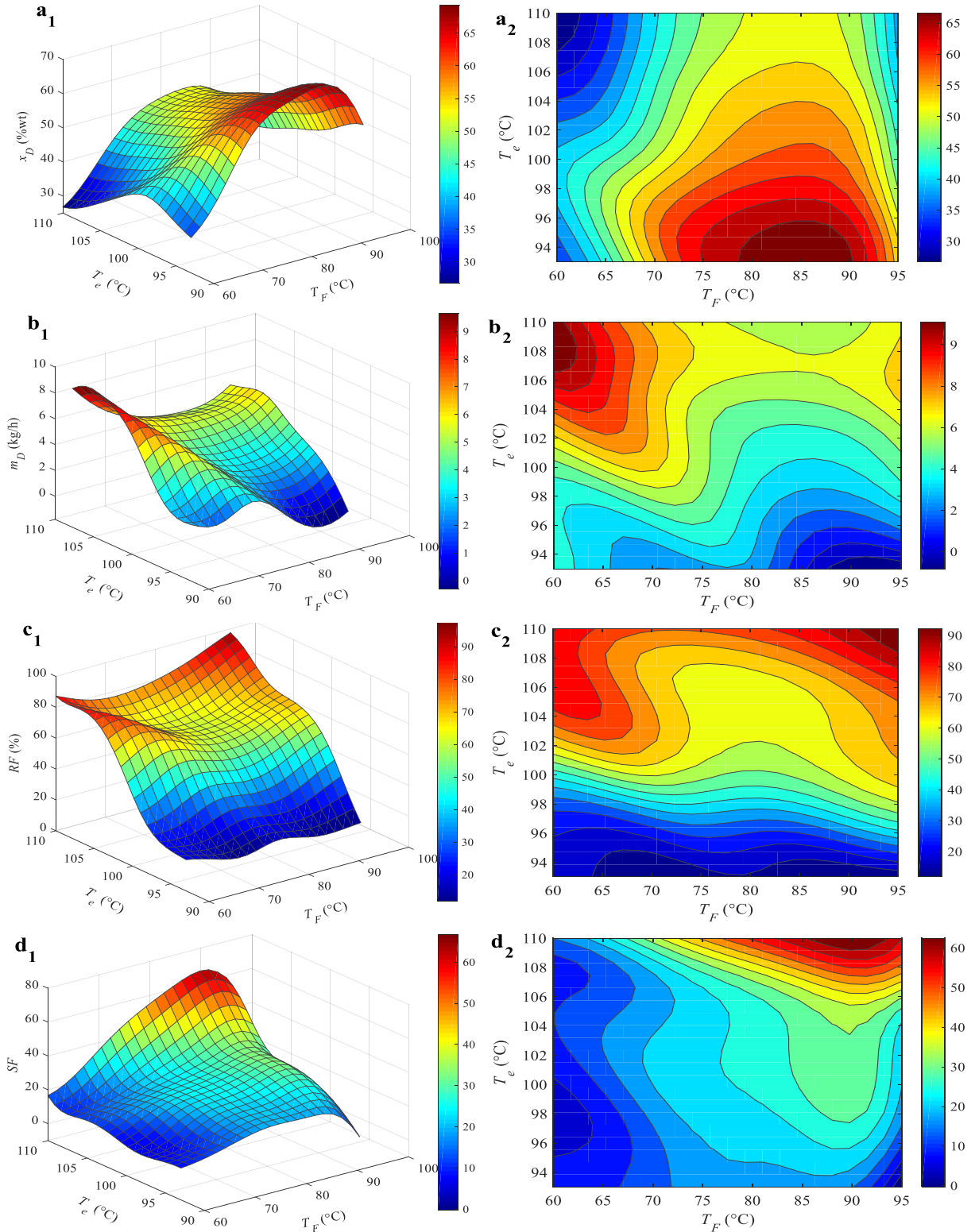
Regarding the distillate mass flow rate (\dot{m}_D), it is observed that there is a decisive influence of the evaporator temperature, i.e., the higher the evaporator temperature, the higher the distillate flow rate, as shown in Figure 30 (b₁) and (b₂). This result was already expected because when there is an increase in the evaporator temperature, there is an increase in heat flux towards the condenser of the thermosyphon for the distillation tube, which leads to an increase in the distillate flow rate. However, this increase in the distillate flow rate occurs associated with a decrease in the ethanol mass fraction in the distillate. This behavior is explained by the fact that water is also transferred to the vapor phase in higher temperatures, reducing the most volatile component concentration (MARANGONI *et al.*, 2019b). Therefore, it becomes clear that there is an important commitment relationship between productivity (expressed by the distillate flow rate) and quality or purity (expressed by the ethanol mass fraction in the distillate). The feed flow rate also has a significant impact on the distillate flow rate, and it is observed that there is a synergistic effect between the feed flow rate and the evaporator temperature on the distillate flow rate, as shown in Figure 32 (b₁) and (b₂), i.e., increasing both increases the distillate flow rate; however, ethanol mass fraction in this stream is reduced.

Due to this inverse commitment relationship between the distillate flow rate and the ethanol mass fraction, it was necessary to evaluate the performance of the Destubcal unit exploiting two other indicators: the recovery factor (RF) and the separation factor (SF). The recovery factor represents the ratio between the mass of ethanol in the distillate stream by the mass of ethanol fed into the unit, i.e., gives a quantitative indication of the recovered ethanol from the fed stream (VANE, 2008). It is possible to note that for a fixed $Q_F=23$ L/h, higher evaporator and feed temperatures favor the recovery factor, while the increase in feed flow rate tends to reduce the recovery factor. However, it is not possible to generalize to all cases due to the complex interactions between variables. The increase in the evaporator temperature leads to higher heat transfer rates in the liquid film and produces higher evaporation of ethanol, thus increasing the amount of ethanol recovered at the top of the column. Likewise, the increase in the feed temperature above the bubble point of the mixture favors the depletion of ethanol into the vapor stream that raises the distillation tube, and consequently also increases the recovery of ethanol at the top of the column. Meanwhile, when the feed flow rate is increased, the small contribution that this factor gives in increasing the distillate flow rate of vapor generated is not enough to overcome the amount of ethanol being fed into the column, which leads to a reduction in the recovery factor. As the recovery factor measure is a

global parameter of the amount of ethanol that is being recovered at the top, yet a high recovery factor does not mean that this condition has led to a stream with high purity, as there may be an amount of water that is not being taken into account. Thus, for satisfactory purification, it is desired that the distillation process has a high recovery factor with high purity. It is observed that at evaporator temperatures close to 110 °C (maximum limit studied), recovery factors greater than 95% were obtained, i.e., practically all ethanol present in the feed stream was recovered at the top, but with low purity, due to the presence of water.

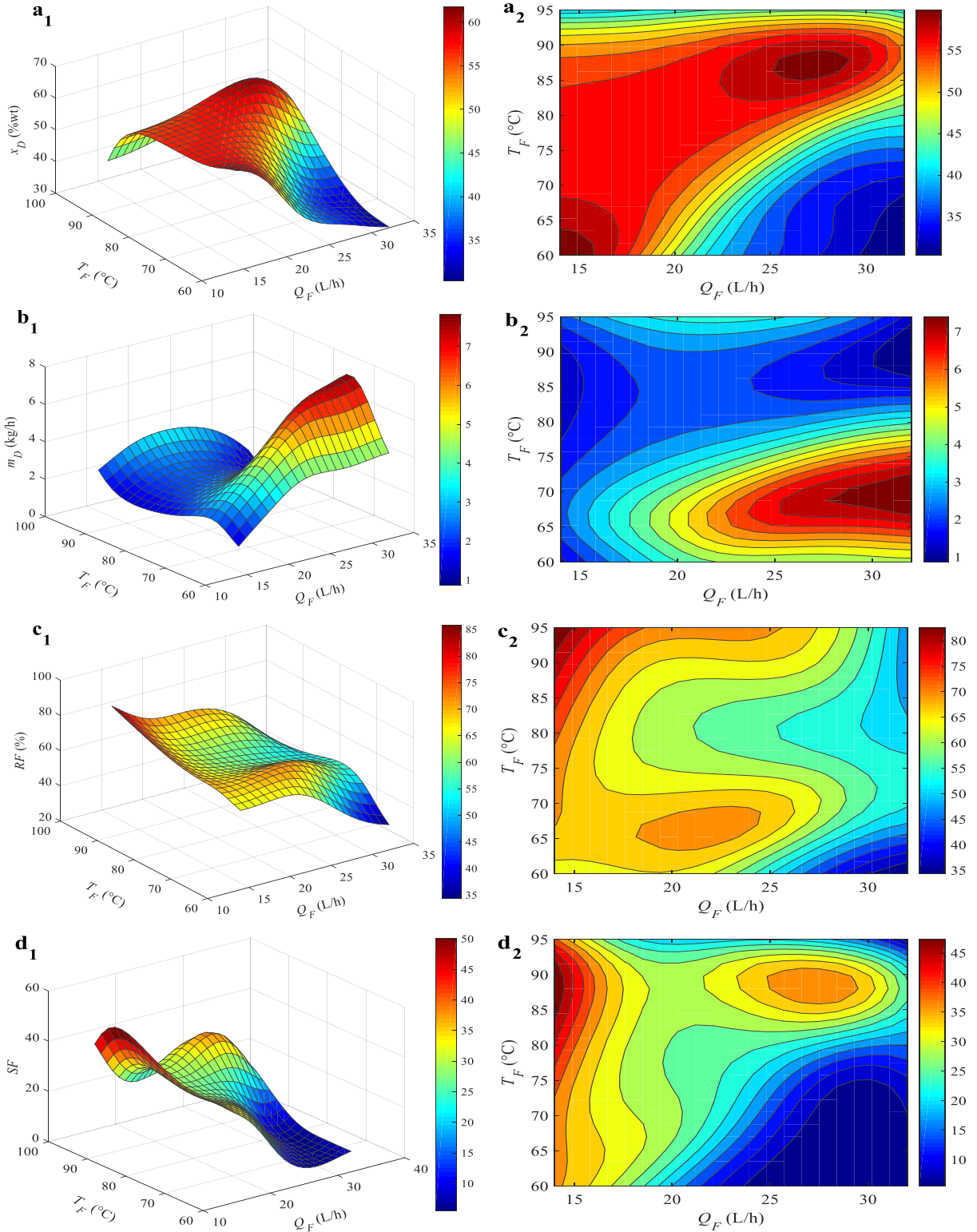
The analysis of the separation factor (SF), introduced by Skogestad (1997), helps to describe the degree of separation between two components in a column or a column section. Mathematically, this factor represents the ratio between the fractions of the light components to heavy components between the distillate and the bottom streams. Thus, this parameter represents the effectiveness of separation concerning purity, i.e., a high degree of separation factor indicates a high purity of the resulting components (NAG *et al.*, 2020). Analyzing the effect of the unit's operational variables on the separation factor, it is observed that there is an optimal feed temperature range, varying nearby 86 °C to 94 °C, which leads to an optimal separation factor condition. This can be clearly seen in Figure 30 (d₁) and (d₂), and Figure 31 (d₁) and (d₂), because in this temperature range the highest separation factor values are obtained. For the evaporator temperature and the feed flow rate there is a behavior in different directions: the separation factor is favored by increasing the evaporator temperature and by decreasing the feed flow rate. Thus, it is evident that there is a complex interaction between the three main operating variables chosen (T_e , T_F , and Q_F), and to extract the best performance of the Destubcal unit it should be necessary an optimization analysis to obtain the maximization of purity (ethanol mass fraction in the distillate) and productivity (distillate mass flow rate), leading to higher recovery and separation factors at the same time.

Figure 30 – Neural network generalization plots of predicted responses in 3D output surface showing the behavior of ethanol x_D (a₁), \dot{m}_D (b₁), RF (c₁), and SF (d₁); and 2D contour-line maps of ethanol x_D (a₂), \dot{m}_D (b₂), RF (c₂), and SF (d₂). All plots are in function of T_F and T_e varying for a fixed $Q_F=23$ L/h.



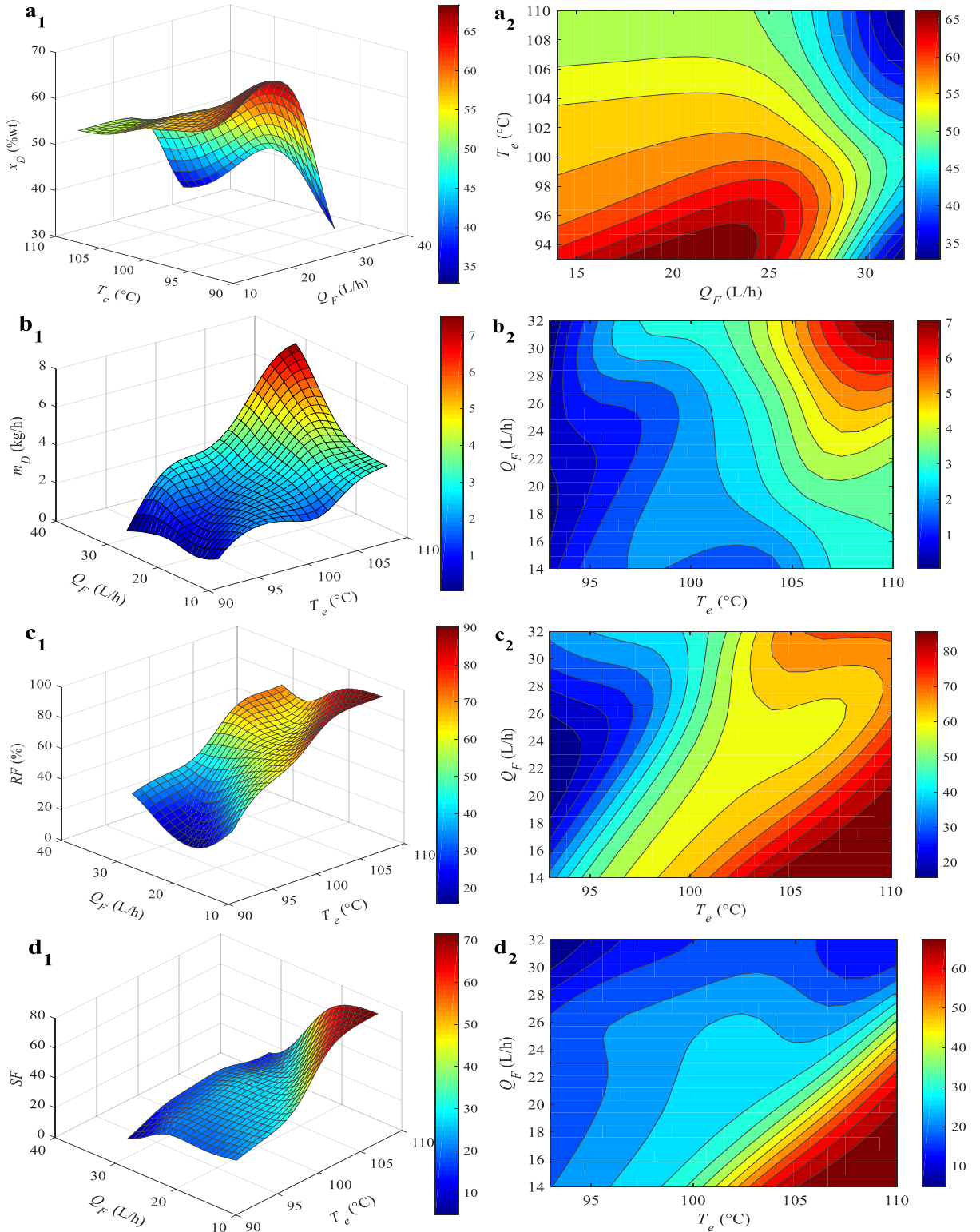
Source: Battisti *et al.* (2021a).

Figure 31 – Neural network generalization plots of predicted responses in 3D output surface showing the behavior of ethanol x_D (a₁), \dot{m}_D (b₁), RF (c₁), and SF (d₁); and 2D contour-line maps of ethanol x_D (a₂), \dot{m}_D (b₂), RF (c₂), and SF (d₂). All plots are in function of Q_F and T_F varying for a fixed $T_e = 101.5$ °C.



Source: Battisti *et al.* (2021a).

Figure 32 – Neural network generalization plots of predicted responses in 3D output surface showing the behavior of ethanol x_D (a₁), \dot{m}_D (b₁), RF (c₁), and SF (d₁); and 2D contour-line maps of ethanol x_D (a₂), \dot{m}_D (b₂), RF (c₂), and SF (d₂). All plots are in function of Q_F and T_e varying for a fixed $T_F = 83$ °C.



Source: Battisti *et al.* (2021a).

4.4.2 GA optimization

Obtaining the maximum benefit from a process, whether new or well established, implies in providing the required information to make a series of decision-making that will lead the professional to define the optimal operating conditions for the process (MANGILI; SANTOS; PRATA, 2019). In order to find the optimal values of the four response variables analyzed in the novel thermosyphon-assisted falling film distillation unit, a GA-based optimization was performed using the developed ML model previously described. The objective here was to reach the maximum values of ethanol mass fraction in the distillate, distillate mass flow rate, recovery factor, and separation factor, simultaneously. As GA always minimize the fitness function, the objective was converted to the inverse, as described in section 4.2.2. The computed optimal condition given by the ML model is summarized in Table 11. This condition corresponds to the following optimal values of the variables: $T_F = 90.6$ °C, $T_e = 109.6$ °C, and $Q_F = 26.3$ L/h. The optimized model parameters showed the performance maximization of the Destubcal unit, i.e., high purity combined with high productivity, should be achieved with feed temperature values above the mixture bubble temperature, and comparatively high evaporator temperature and feed flow rate combined.

Table 11 – Optimal conditions determined by the ML-GA method.

Optimal operating conditions	
Feed temperature, T_F (°C)	90.6
Evaporator temperature, T_e (°C)	109.6
Feed flow rate, Q_F (L/h)	26.3
Responses	
Mass fraction of ethanol in the distillate, x_{EtOH}^D (wt%)	50.6
Distillate mass flow rate, \dot{m}_D (kg/h)	4.91
Recovery factor, RF (%)	84.9
Separation factor, SF	57.4

Source: Battisti *et al.* (2021a).

In our recently published paper (BATTISTI *et al.*, 2020b), using the same falling film distillation apparatus, the optimal conditions obtained by response surface methodology (RSM) presented, for a feed flow rate of 27 L/h and evaporator temperature of 110.5 °C, an

ethanol mass fraction in the distillate of 48.8 wt%, but with a distillate flow rate of 1.35 L/h. In the case of maximizing the distillate flow rate, it reached a maximum value of 3.25 L/h, however with an associated purity of only 37.6 wt% of ethanol. It reinforces the previously reported commitment relationship between purity and productivity. In the present study, the optimal distillate mass flow rate reached 4.91 kg/h, i.e., 51.1% higher than in the RSM analysis. In addition, the ethanol mass fraction in the distillate was also 3.70% higher when compared to the RSM optimization study. Therefore, the ML-GA optimization methodology demonstrated to be able to extract a better performance in terms of purity and productivity from the Destubcal unit when compared to RSM, meeting literature findings in the same direction (DANTAS *et al.*, 2020; GIL *et al.*, 2018), which pointed out that ML models are more capable of data generalization than RSM models due to a higher accuracy of prediction.

4.5 SUMMARY AND CONCLUDING REMARKS

The ML model was proposed to predict four performance parameters, namely the ethanol mass fraction in the distillate, the distillate mass flow rate, the recovery factor, and the separation factor, considering the most important inputs variables influencing the falling film distillation process as the feed inlet temperature, the evaporator temperature, and feed flow rate. A feed-forward neural network based on LMA back-propagation algorithm with *logsig* transfer function at the hidden layer with 10 neurons, and a linear transfer function (*purelin*) at the output layer, was able to accurately predict the four output performance parameters with a good overall correlation coefficient of 0.980. According to the generalization plots, the operating variables influenced individually and synergistically the analyzed responses. It was quite clear that there is a commitment relationship with the purity of the top product, represented by the ethanol mass fraction in the distillate, and the productivity, represented by the distillate mass flow rate. Generally, high purity is achieved with lower distillate flow rates, and high productivity leads to low purity. Seeking to extract the maximum performance of the unit facing all responses simultaneously, GA-based optimization led to a 50.6 wt% of ethanol mass fraction in the distillate, 4.91 kg/h of distillate mass flow rate, with a recovery factor of 84.9%, and a separation factor of 57.4. Lastly, it can be concluded that ML modeling can be successfully applied to the novel thermosyphon-assisted falling film distillation process with good accuracy, and the GA optimization technique demonstrated the ability to extract high performance from the pilot-scale unit.

5 TECHNO-ECONOMIC AND ENERGETIC ASSESSMENT OF AN INNOVATIVE PILOT-SCALE THERMOSYPHON-ASSISTED FALLING FILM DISTILLATION UNIT FOR SANITIZER-GRADE ETHANOL RECOVERY

The content of this chapter is based on the following published article:

BATTISTI, Rodrigo; GALEAZZI, Andrea; PRIFTI, Kristiano; MANENTI Flavio; MACHADO, Ricardo Antonio Francisco; MARANGONI, Cintia. Techno-economic and energetic assessment of an innovative pilot-scale thermosyphon-assisted falling film distillation unit for sanitizer-grade ethanol recovery. **Applied Energy**, v. 297, p. 117185, 2021. DOI: 10.1016/j.apenergy.2021.117185.

5.1 INTRODUCTION

The emergence of the COVID-19 pandemic, caused by the novel coronavirus (SARS-CoV-2), has posed unprecedented challenges to populations worldwide (MANENTI *et al.*, 2020; ZHANG *et al.*, 2021). Brazil ranks among the most affected countries, where the virus outbreak has been very fast. One of the most effective and simple ways to prevent the spread and infection of this virus is handwashing with water and soap or using alcohol-based hand sanitizers (GOLIN; CHOI; GHAHARY, 2020; PASQUINI *et al.*, 2020). The high request for alcohol-based sanitizers and disinfectants by the population and healthcare services triggered by COVID-19 has caused a shortage in many cities of Brazil (ITIKI; ROY CHOWDHURY, 2020). World Health Organization (WHO) has guided local manufacturers regarding the preparation of alcohol-based formulations with ethanol or isopropanol (MAHMOOD *et al.*, 2020). Although health agencies around the world diverge on the minimum ethanol concentration, Brazilian Health Regulatory Agency (ANVISA) recommends the same content as the WHO, i.e., a concentration close to 70 vol% of ethanol effectively inactivates the SARS-CoV-2 virus, thus being safe and suitable for sanitation purposes (LESLIE; ZHOU; MACINGA, 2020).

Several initiatives have emerged to propose alternative methods of manufacturing ethanol-based sanitizers, including boosting biorefineries with biomass feedstocks (WEBER *et al.*, 2020), adapting breweries and distilleries facilities (THOMSON; BULLIED, 2020), and even fast deployment of ethanol-based disinfectants from fuel gas stations (ITIKI; ROY

CHOWDHURY, 2020). However, implementation is still timely difficult or faces complexities and safety issues. Currently, the main production process for ethanol is the fermentation of sugarcane and corn feedstocks (VOHRA *et al.*, 2014). A multicolumn distillation system is used in the conventional process for recovering ethanol from the fermentation broth (VANE, 2008). Nonconventional systems are being recently proposed as alternatives for ethanol recovery with energy savings and low investment costs, such as pervaporation (BELLO *et al.*, 2014), vacuum fermentation (NGUYEN *et al.*, 2011), adsorption (FUJITA *et al.*, 2011), gas stripping (PONCE *et al.*, 2016), solvent extraction (OFFEMAN *et al.*, 2005), and other alternative hybrid processes (VANE *et al.*, 2013). Despite that, the application of unconventional techniques for ethanol recovery has been realized in pilot scales just a few years ago, and the integration of these techniques in industrial large-scale is still limited (ZENTOU *et al.*, 2019).

Cost analysis of any new or alternative distillation system, especially renewable energy powered distillation, is highly recommended to overview the required initial investment, distillate production cost per liter and payback time of the system (REDDY; SHARON, 2017). In addition, a technical feasibility assessment is essential to quantify the overall performance towards consolidating the technology for a future industrial-scale application (KHAN; NORDBERG, 2019). Outcomes from a previous work indicated that the Destubcal unit is a promising technological option for separating and purifying ethanol over a wide range of feed flow rate, feed temperature, and evaporator temperature, reaching suitable ethanol purities (61.9–68.05 wt%) at different recovery levels (20.29–60.34%) (BATTISTI *et al.*, 2021a). Besides, meeting the increasing demand for ethanol-based sanitizers for medical and hygiene needs from the COVID-19 pandemic is urgent since the pandemic probably will continue for a long time and the need for alcohol-based sanitizing products tends to increase even more.

Hence, this chapter is dedicated to access the techno-economic viability of the pilot-scale thermosyphon-assisted falling film distillation unit for ethanol recovery in a suitable concentration for sanitization purposes (70 vol%), according to WHO and Brazilian health agency guidelines. Moreover, an energy efficiency evaluation of thermosyphon-assisted distillation device was carried, and an energetic and structural comparison analyses were performed between the Destubcal apparatus and a conventional column for the same ethanol-enriched recovering degree. Notably, this study fulfills a knowledge gap regarding the techno-economic and energetic assessment of the Destubcal technology that had not been elucidated.

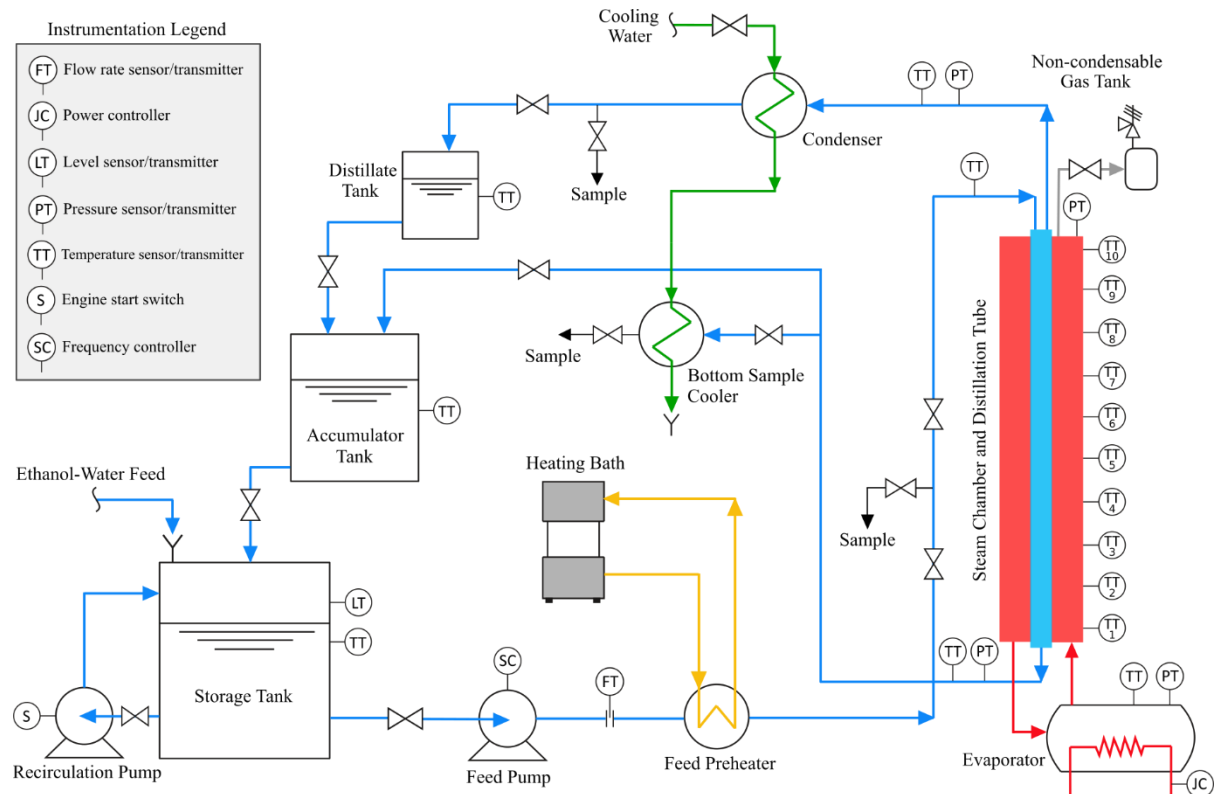
The previous works carried out in the pilot-scale Destubcal unit focused only on defining the best separation conditions. Therefore, the present study addresses substantial novelty towards consolidating the Destubcal technology as an energy-saving distillation process ready to be scaled-up and widespread. As it is a compact unit, it could be installed in small cooperatives or even by local producers, expanding the offer of sanitizer-grade ethanol producers, thus helping to face the serious public health scenario that has been plaguing the world.

5.2 EXPERIMENTAL SETUP AND METHODS

5.2.1 Pilot-scale plant description

The detailed process flowchart of the pilot-scale unit is shown in Figure 33, whose operation is described in the item 3.2.1. This flowchart presents all the process equipment with the exact quantity and the real location of the instrumentation used in the pilot-scale unit, which will be used for the subsequent techno-economic analysis.

Figure 33 – Detailed process flowchart of the pilot-scale Destubcal unit.



Source: Battisti et al. (2021b).

5.2.2 Thermosyphon-assisted distillation performance

Establishing the performance of the Destubcal technology in producing sanitizer-grade ethanol (minimum of 70 vol% in alcohol) constitutes the first part of this investigation. The mixture fed into the unit was composed of 10 wt% ethanol and 90 wt% water to simulate the fermentation broth output from bioethanol reactors (BALAT; BALAT; ÖZ, 2008). For determining which condition meets the fundamental requirement of enriching the distilled product to the desired ethanol purity of 70 vol% in alcohol (about 62.4 wt%), 64 experimental runs were conducted on the pilot-scale unit under different operating conditions, as shown in Table 12. The chosen operating ranges were based on the design operation limits of the equipment, and preliminary tests carried out with the ethanol-water mixture. A film breakage occurs below 14 L/h, causing dry spots on the column wall. Above 32 L/h, the distillate purity decreases considerably, possibly due to the decrease in the residence time of the liquid. For evaporator temperatures below 93 °C, no distillate product is formed, whereas, for evaporator temperatures above 110 °C, unfeasible ethanol recovery is observed. For feed temperatures below 60 °C, no top distillate product is formed. For feed temperatures above 95 °C, the vaporization of the feed flow starts to increase the pipeline pressure before entering the column, which is undesirable.

Table 12 – Experimental operating conditions adopted in the pilot-scale unit.

Feed temperature, T_F (°C)	Evaporator temperature, T_e (°C)	Feed flow rate, Q_F (L/h)
60	93	14
80	100	17
90	104	23
95	110	32

Source: Battisti *et al.* (2021b).

5.2.2.1 Recovery ratio

One of the performance parameters used to evaluate the separation efficiency of the thermosyphon-assisted distillation unit is the recovery ratio (RR), also called recovery factor, which is described in the item 4.3.1 of the previous chapter.

5.2.2.2 Specific thermal energy consumption

Another performance parameter evaluated to establish the best separation condition is the specific thermal energy consumption (*STEC*), which is defined as the power supplied to the pilot-scale plant through the electrical resistances in the evaporator (Q_{evap}) divided by the total distillate mass flow rate (\dot{m}_D) obtained at the top of the column, as shown in Eq. (44) (CHEN *et al.*, 2020).

$$STEC = \frac{Q_{evap}}{\dot{m}_D} \quad (44)$$

5.2.3 Energy efficiency

The energy efficiency of the thermosyphon-assisted falling film distillation tube can be obtained from the first law of thermodynamics, which is based on the conservation principle of energy in quantity, according to the energy balance given by Eq. (45) (RANJAN; KAUSHIK, 2013).

$$\sum E_{in} + \sum_{j=1}^n Q_j = \sum E_{out} + W_{net} \quad (45)$$

Where, E_{in} and E_{out} are the quantity of energy associated with mass entering and leaving the system, respectively. Q_j is the quantity of heat transferred to the system from a source, in this case, the electrical resistances in the evaporator. W_{net} is the net work output of the system, in this case, null, because there is no work in the system. Therefore, the energy efficiency (η_e) of the thermosyphon-assisted falling film distillation tube is defined as the energy ratio from the outlet to the inlet, according to Eq. (46).

$$\eta_e = \frac{E_{out}}{E_{in}} \quad (46)$$

5.3 TECHNO-ECONOMIC ASSESSMENT

5.3.1 Capital expenditure

Capital cost, also known as capital expenditure (CAPEX), can be defined as the fixed onetime expenses incurred through the purchase and construction of equipment used in the production of goods (SCHWANTES *et al.*, 2018). The capital cost includes direct and indirect capital costs. Direct capital cost considered in this study includes costs associated with equipment purchases, apparatus construction and installation, piping & instrumentation, insulation, and auxiliary facilities. The direct capital cost estimative was assessed based on the most up-to-date literature and information acquired from local vendors and manufacturers. Indirect capital costs might include insurance, construction overhead, owner's and contingency costs (HU; LI; YAN, 2012). In this analysis, the total indirect capital cost was estimated as 10% of total direct capital cost, as recommended by Macedonio *et al.* (2014) and Panagopoulos (2020). All the costs mentioned in this study reflect the local market price and were calculated in Brazilian reais (R\$), after being converted to American dollars (\$) at the ratio of R\$ 5.33 per \$ (average dollar exchange rate for the year 2020).

5.3.1.1 Major thermosyphon-assisted process equipment

Major pieces of process equipment are considered directly associated with the two-phase closed thermosyphon and the falling film distillation apparatus, such as the distillation tube coupled to the steam chamber (section usually called condenser of the thermosyphon), the evaporator, the feeding hollow cone system, the non-condensable gas reservoir, and the three process tanks. These major equipment were built in 304 stainless steel, so the cost estimative was made based on the total estimated weight of the devices and the average price of the stainless steel sheet (4.50 \$/kg) updated from Brazilian vendors in the year 2020.

5.3.1.2 Piping and auxiliary equipment

Auxiliary pieces of equipment include feed and recirculating pumps, heat exchangers, interconnecting piping, and vacuum pump. The cost of auxiliary equipment was assessed by the purchase price provided by vendors of local companies and Brazilian vendors

of international companies in 2020, according to the following specifications: feed pump (helical type, Netzsch/Nemo[®] model NM011BY02S12B), recirculation pump (centrifugal type, Schneider 1/3 hp), vacuum pump (water jet type, Fisatom 830), feed preheater (fusion-brazed plate heat exchanger, Alfa Laval with 30 plates, model AlfaNova 14), condenser (glass serpentine-type, 600 mm with two ground joints), bottom sample cooler (double tube heat exchanger, carbon steel 30 cm long). The thermostatic bath installed is the LAUDA high-temperature thermostat USH 400. This equipment was used because it was available in the laboratory, and for collecting experimental data, a fast and efficient temperature control was necessary. However, this equipment has been discontinued by the manufacturer. So, for this techno-economic analysis, the auxiliary equipment for heating the feed flow stream was considered a conventional heating bath with an external circulation system that reaches a temperature of 120 °C, whose configuration is satisfactory for this duty. The piping system was also built in 304 stainless steel, and the cost was estimated based on a total length of 16.5 m of seamless pipe with diameters calculated based on the recommended flow speed for each section. About 35% of the total installed piping is thermally insulated with glass wool covered by aluminium foil. Besides, the entire column and evaporator are also thermally insulated to prevent heat losses to the environment. The thermal insulation cost was based on the total occupied area and its purchase price of 2.70 \$/m² from local vendors.

5.3.1.3 Instrumentation and control system

The unit is instrumented with 12 manual ball valves, 7 Swagelok stainless steel valves, two pressure sensors (Warme WTP-4010), one level sensor (Warme WSC 404), 5 type K thermocouples (Consitec mineral head type), 10 points of temperature acquisition in the steam chamber, one flow sensor (Oval, super micro), one pressure transducer (Omega 43074), and one frequency inverter (Weg CFW-08). A power controller (Contemp P501) was used for the energy supply and control of electrical resistances. The unit's process and operation data are collected by a Campbell Scientific data acquisition system (model CR1000, combined with AM25T multiplexer), sent to a computer for further data processing. The ethanol composition analysis for quality control is done with a Gay-Lussac alcoholometer. All purchase costs of these measurement and control instruments were estimated with Brazilian suppliers at updated values for 2020.

5.3.1.4 Construction and installation

The engineering design, construction, and installation of the pilot-scale Destubcal unit were entirely conceived and carried out by our research team, composed of engineers, technicians, and specialists in distillation and heat pipes, in partnership with the Petrobras Brazilian oil company. Installation expenses were estimated by adding 10% of the purchase cost for conventional process equipment, auxiliary equipment, piping and instrumentation, while for equipment directly related to the core of the process, such as the thermosyphon coupled to the distillation tube, 50% was added. A higher installation cost was assumed for the thermosyphon-related equipment because it represents a relatively new technology that is not yet widespread and whose construction, and thus installation costs, could be higher than conventional distillation devices (VERGILI *et al.*, 2012).

5.3.1.5 Fermentation capital cost

Although the Destubcal plant was evaluated in this study operating experimentally with a 10 wt% ethanol-water feed mixture, the techno-economic evaluation performed here took into account the costs of fermentation steps to make the analysis more complete within the scope of ethanol production. Production of ethanol in a continuously stirred tank reactor (CSTR) is less time- and labor-intensive than a batch process (RICHTER; MARTIN; ANGENENT, 2013). Besides, the continuous supply of fresh medium would maintain the cell's activity for a longer period, improving process productivity (BOUALLAGUI *et al.*, 2013). The capital costs associated with process equipment, utilities, and raw materials for ethanol fermentation by a CSTR bioreactor can account for about 0.0199 \$/L/yr of a distillery plant capacity (MAIORELLA; BLANCH; WILKE, 1984) and were considered in this study according to the processing capacity of the pilot-scale plant.

5.3.1.6 Annualized capital cost

The sum of all capital costs results in the total capital cost (TAC). The annualized capital cost (CAPEX) is calculated using the net present value (NPV) (TAVAKKOLI *et al.*, 2017) method shown in Eq. (47), where i is the interest rate, which is assumed to be 5%

(KHAN; NORDBERG, 2019), and n is the expected plant life in years which is assumed to be 30 years (CHEN *et al.*, 2020).

$$\text{Annualized Capital Cost} \left(\frac{\$}{\text{yr}} \right) = \text{Total Capital Cost} \cdot \frac{i(1+i)^n}{(1+i)^n - 1} \quad (47)$$

5.3.2 Operating expenditure

The operating cost or expenditure (OPEX) represents the costs for electricity, cooling water, equipment replacement, service maintenance, labor, chemicals and cleaning, and others related to the plant's daily operation (SCHWANTES *et al.*, 2018). For OPEX estimation, plant availability factor (f) is assumed to be 95% (RAHIMI *et al.*, 2015), referring to the fraction of time per year the plant operates compared to the maximum possible operating time.

5.3.2.1 Electricity

The annual cost of electricity (C_{elec}) for the thermosyphon-assisted distillation unit was estimated according to Eq. (48). The total electricity requirement is equivalent to the sum of the major power consumption from the electrical resistances of the evaporator, the feed pump, the recirculation pump, the vacuum pump, and the thermostatic heating bath. The price of electricity was considered 0.095 \$/kWh, taken from the Brazilian Electricity Regulatory Agency (ANEEL) for the state of Santa Catarina (Brazil) in the year 2020.

$$C_{elec} \left(\frac{\$}{\text{yr}} \right) = \text{electr. requirement (kW)} \cdot 24 \left(\frac{\text{h}}{\text{day}} \right) \cdot \text{electr. cost} \left(\frac{\$}{\text{kWh}} \right) \cdot f \cdot 365 \left(\frac{\text{day}}{\text{yr}} \right) \quad (48)$$

5.3.2.2 Cooling water

The cooling water used to condense the ethanol-enriched vapor produced by the thermosyphon-assisted distillation column is from the domestic distribution network. Its cost was estimated as 2.28 \$/m³ provided by Catarinense Water and Sanitation Company (CASAN), located in the city of Florianópolis (Brazil), in the year 2020. The water is collected in a tap near the unit and directed to the column condenser with the aid of a plastic

hose. After passing through the condenser, the water is still at a temperature of around 35 – 40 °C, so the same water flow is used to cool the bottom samples passing through a double tube heat exchanger until reaching the drain.

5.3.2.3 Fermentation operating cost

The operating costs associated with the ethanol fermentation by a conventional CSTR bioreactor with sugarcane feedstock were considered to be 62.51 \$/m³ (MAIORELLA; BLANCH; WILKE, 1984). Thus, the fermentation operating cost (C_{fer}) can be estimated according to the following Eq. (49).

$$C_{fer} \left(\frac{\$}{yr} \right) = \text{Plant Capacity} \left(\frac{m^3}{day} \right) \cdot 365 \left(\frac{day}{yr} \right) \cdot f \cdot 62.51 \left(\frac{\$}{m^3} \right) \quad (49)$$

5.3.2.4 Labor

The unit is able to operate continuously, 24 hours per day, in three shifts. Labor costs were determined based on the recurring salary of a Chemical Production Operator according to the Brazilian Classification of Occupations (CBO) in 2020 (287.70 \$/month) for one worker per shift, as these small-scale plants are capable of operating almost unmanned (ARENA; DI GREGORIO; SANTONASTASI, 2010).

5.3.2.5 Other operating costs

Other relevant operating costs should include service and maintenance, cleaning and chemicals, and disposal costs. Service and maintenance cost was estimated at 2.5% of capital investment costs (AMAYA-VÍAS; LÓPEZ-RAMÍREZ, 2019). General cleaning and chemicals can cost up to 0.018 \$/m³ (NOOR; MARTIN; DAHL, 2020). Regarding disposal costs, the main effluent from ethanol distilleries, commonly named vinasse, is a liquid with an unpleasant odor containing water and a high concentration of organic substances and ions (NAKASHIMA; DE OLIVEIRA JUNIOR, 2020). Vinasse disposal represents an important potential impact due to the large amounts produced (0.011–0.014 m³ per m³ of ethanol) (GOLDEMBERG; COELHO; GUARDABASSI, 2008) and cannot be neglected in a

realistic techno-economic analysis. Thus, the disposal cost for vinasse treatment was taken as 0.028 \$/m³ (CRAVEIRO; SOARES; SCHMIDELL, 1986).

5.3.3 Financial analysis

The better economic return on the investment depends on the production cost of the distilled ethanol and its applicability. The cost of distilled sanitizer-grade ethanol per liter (*CPL*) can be calculated by dividing the total annualized cost of the process by the annual distillate production yielded by the thermosyphon-assisted falling film distiller expressed by Eq. (50) (KABEEL; HAMED; EL-AGOUZ, 2010).

$$CPL \left(\frac{\$}{L} \right) = \frac{\text{Total Annualized Cost}}{\text{Annual Distillate Production}} \quad (50)$$

The amount invested on the thermosyphon-assisted falling film distillation unit can be regained by selling the produced distilled sanitizer-grade ethanol directed to a number of applications ranging from direct use end consumers to hospitals and healthcare facilities. The time required for getting back the amount invested depends on the capital cost (*CC*) of the unit, the selling price (*SP*) of the product, the interest rate (*i*) at which the unit is financed, and the annual distillate (*M_{yearly}*) produced (REDDY; SHARON, 2017). Then, finance payback time (η_p) can be calculated by Eq. (51) (RANJAN; KAUSHIK, 2014).

$$\eta_p (yr) = \frac{\ln \left[\frac{M_{yearly} \cdot SP}{(M_{yearly} \cdot SP) - (CC \cdot i)} \right]}{\ln [1 + i]} \quad (51)$$

5.3.4 Comparative assessment with a conventional column

An energetic and structural analysis was performed via simulation through the Aspen Hysys[®] V8.8 software to compare the performance of the Destubcal column to a conventional distillation tray column for the same productivity. Experimental data of distillate flow rate and ethanol mass fraction in the distillate were acquired in the thermosyphon-assisted falling film distillation column for the run with the best *STEC* and *RR* performance, and these data were

used as inlet conditions in Hysys[®] to converge the simulation run of a conventional tray column with the same recovery degree. The optimum reflux ratio used for the conventional tray column was 1.2 times the minimum reflux ratio, and the spacing between trays of 0.35 m, as recommended by Kister (1992). The reboiler heat duty and the actual height of the conventional column were compared with the experimental data from the Destubcal plant.

5.4 RESULTS AND DISCUSSIONS

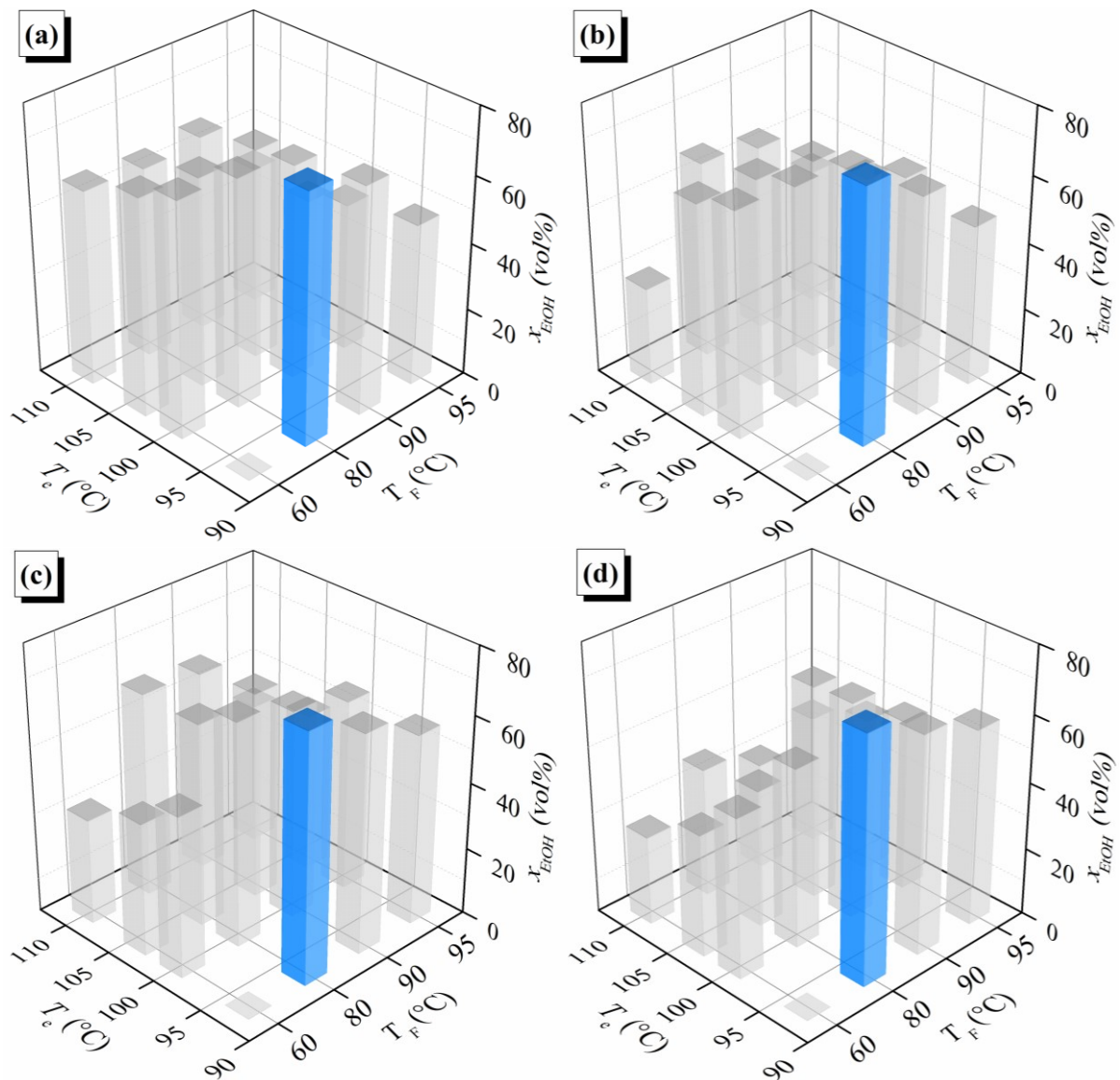
5.4.1 Thermosyphon-assisted distillation performance

Assuming that the ethanol-based liquid sanitizer must meet the requirements of the Brazilian Health Regulatory Agency, the process of ethanol distillation must result in a minimum concentration of 70 vol% in alcohol. In order to assess the ethanol production potential at this required concentration, different operating conditions were applied to the pilot-scale thermosyphon-assisted unit over a wide range of operability. Figure 34 shows the ethanol contents obtained for each operating condition applied to the Destubcal unit. Among the 64 experimental runs carried out at the pilot-scale unit, only four conditions reached the minimum required ethanol content of 70 vol% in alcohol, indicated by the blue bars in the 3D-graphs. It is remarkable to note that the required concentration was achieved for all the four feed flow rates studied (14 L/h, 17 L/h, 23 L/h, and 32 L/h), always at the same feed temperature (80 °C), and the same evaporator temperature (93 °C). These conditions meet the findings of previous studies, which demonstrated that higher purity at the top of the falling film column is achieved with feed temperatures closer to the bubble point of the mixture (in this case, around 83 °C) and with relatively low evaporator temperatures (BATTISTI *et al.*, 2020b, 2021a). The relatively low temperature required in the evaporator is a favorable condition from the sustainability point of view because the electrical resistances will consume less electricity to heat the thermal fluid, consequently helping to reduce the environmental impact of power generation.

At a feed temperature of 60 °C with the evaporator operating at 93 °C, no distillate was produced, given that the mixture was cooled far below the bubble point and did not generate enriched vapor during the residence time in the falling film column. As the evaporator temperature increases, more heat is transferred to the liquid film via the thermosyphon condenser, leading to a higher evaporation rate. However, more water is

dragged along in the distillate stream, which reduces the ethanol purity at the top of the column (CLAUMANN *et al.*, 2020). It is the reason for the highest ethanol purity was obtained with relatively low temperatures in the evaporator. This feature reveals an important advantage of the thermosyphon-assisted unit that should be highlighted: the heat distribution along the distillation tube improves the quality of the separation with less energy required – the lower the evaporator temperature, the lower the power applied to the electrical resistances. Therefore, as the ethanol purity in the distillate is favored with low evaporator temperatures, less electrical energy will be consumed, thus reducing the total energy cost.

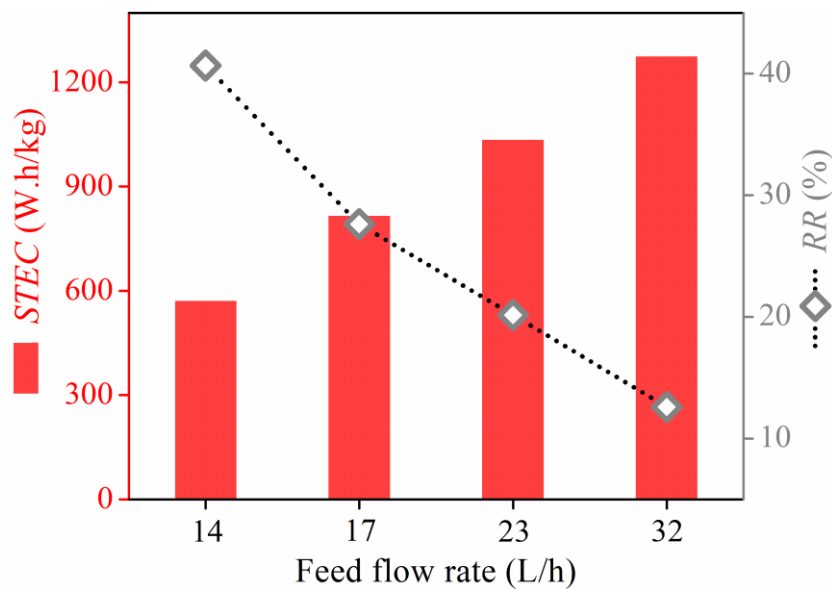
Figure 34 – Ethanol concentrations achieved in the distillate product under different operating conditions for the feed flow rates of 14 L/h (a), 17 L/h (b), 23 L/h (c), and 32 L/h (d).



Source: Battisti *et al.* (2021b).

To complement the unit's performance analysis, two other factors, the specific thermal energy consumption (*STEC*) and the recovery ratio (*RR*), were analyzed for the different operating conditions that reached the minimum required ethanol content (70 vol%) for sanitation purposes. Figure 35 shows the analysis of *STEC* and *RR* in relation to the feed flow rate applied in the pilot-scale unit. Higher feed flow rates resulted in higher *STEC*, as more energy is needed to be loaded in the evaporator to maintain the temperature of the thermosyphon coupled to the falling film column in the desired temperature. The *RR* factor denotes the amount of distilled ethanol that is recovered in relation to what was fed. It is observed that higher performance *RR* is also obtained at lower feed flow rates, mainly due to higher distillate purity produced (MOHAMED *et al.*, 2017). The higher the purity at the top, the more ethanol is recovered by the column, leading to increased *RR* performance. Therefore, the performance analysis reveals that pilot-scale unit operates under favorable conditions with the minimization of feed flow rate since it will minimize the specific thermal energy consumption, increasing the distillate ethanol recovery ratio at constant energy input. Thus, the operating conditions that were chosen to proceed with the techno-economic analysis were $Q_F = 14$ L/h, $T_e = 93$ °C, and $T_F = 80$ °C, as these conditions lead to the best performance of the pilot-scale unit in terms of separation efficiency and energy consumption.

Figure 35 – Energy and ethanol recovery performance under different operating conditions.

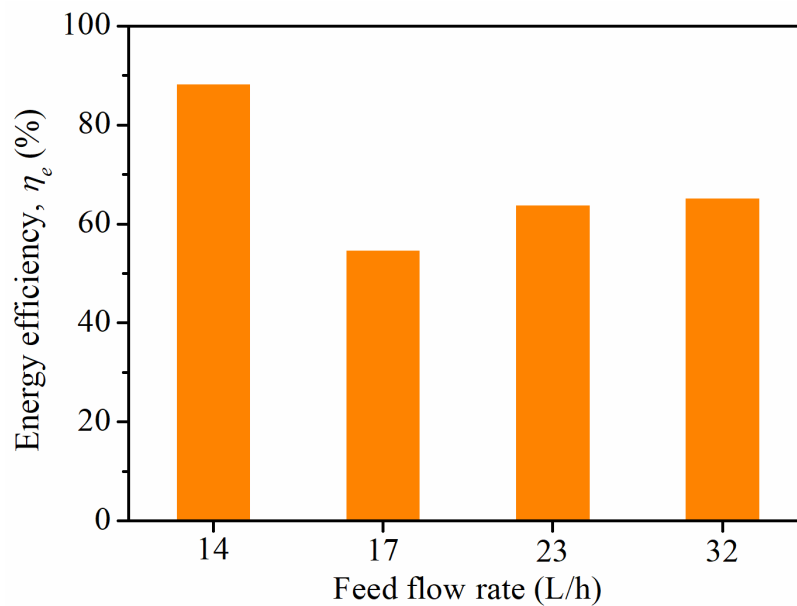


Source: Battisti *et al.* (2021b).

5.4.2 Energy efficiency

Improving the energy efficiency of distillation processes is a constant motivating factor since the thermodynamic efficiency of a conventional distillation column is very low, ranging around 5–20% (NAIR; BABU G; RAYKAR, 2017). Due to its constructive design, the conventional distillation column is an energy-inefficient device since the heat is supplied in the reboiler at a high-temperature level, and roughly the same amount of heat is rejected in the condenser at a low, often useless, temperature level (BRUINSMA *et al.*, 2012; ZIERHUT *et al.*, 2020). In this study, energy efficiency (Figure 36) was defined as the ratio of the outlet to the inlet, i.e., the energies associated with the leaving top and bottom streams and the energies entering the distillation tube (the energy associated with the feed stream and the energy supplied by the steam chamber of the thermosyphon).

Figure 36 – Energy efficiency over the different feed flow rates performed.



Source: Battisti *et al.* (2021b).

The energy efficiency of the thermosyphon-assisted distillation tube ranged from 88.5–54.9%, indicating that lower power in the evaporator results in higher energy efficiency. This behavior is associated with lower irreversibility; consequently, lower entropy resulted in this configuration (QUERINO; MACHADO; MARANGONI, 2019). The falling film distillation assisted by a two-phase closed thermosyphon proposal is a promising thermal alternative, as the energy efficiency found was higher than other unconventional systems as

membrane distillation (18–58%) (AL-OBAIDANI *et al.*, 2008), solar distillation (20–46%) (RANJAN; KAUSHIK, 2013), and molecular sieve adsorption (67–69%) (FRANKÓ; GALBE; WALLBERG, 2016). In addition, the energy efficiency analysis corroborates the previous findings, indicating that a feed flow rate of 14 L/h is the most favorable condition in terms of sanitizer-grade ethanol (70 vol%) recovery and energy efficiency. At 14 L/h, the minimum wetting rate (0.0468 kg/m·s) was reached, i.e., the minimum feed flow rate required to establish or maintain the surface of the distillation tube completely and evenly wet, avoiding film breakdown and dry spots (MORISON; WORTH; O'DEA, 2006). One way to enhance the energy efficiency in such film-type contactors is to maintain the film flow rate at the minimum wetting rate so that the solid transfer area is wetted by the thinnest possible uniform film (BRAUNER; MARON; HAREL, 1985). Therefore, 14 L/h is the minimum feed flow rate experimentally feasible which leads to the best energy efficiency condition.

5.4.3 Techno-economic assessment

The cost of the materials and components associated with the construction and assembly of the Destubcal pilot-scale unit was based on local market surveys and budget proposals from vendors of local companies or Brazilian representatives of international companies, summarized in Table 13. Stainless steel AISI 304 was the material chosen to fabricate the distillation and thermosyphon devices, storage tanks, and pipelines, as this material has a suitable life span of about 50 years (SOMMARIVA; HOGG; CALLISTER, 2001). Moreover, stainless steel AISI 304 is mostly inert to corrosion and undesirable chemical reactions (OLDFIELD; TODD, 1997), so an ethanol-enriched distilled product of high quality and free of impurities or contaminants can be expected. The pilot-scale unit construction in 304 stainless steel was executed after several stages of development in a borosilicate glass unit and simulation studies to assess and optimize the main design parameters. Even being an innovative technology, all associated processes and instrumentation equipment are easily accessible and widely used in consolidated chemical process units, making the Destubcal pilot-scale unit promising for replication in other locations worldwide.

Table 13 – Appraised cost of components associated with the construction of the Destubcal pilot-scale thermosyphon-assisted falling film distillation unit.

Item	List of components	Quantity (unit)	Cost (\$)
1	Stainless steel sheet metal	83.8 kg	377.26
2	Stainless steel pipeline	16.5 m	145.07
3	Centrifugal pump	1	73.26
4	Helical pump	1	748.03
5	Vacuum pump	1	932.62
6	Plate heat exchanger	1	112.57
7	Shell-tube heat exchanger	1	73.73
8	Glass condenser	1	26.21
9	Feed cone distributor	1	14.14
10	Heating bath	1	962.65
11	Electrical resistances	2	143.52
12	Ball valves	12	68.05
13	Swagelok valves	7	243.50
14	Plastic hose	10 m	10.17
15	Pressure sensors	3	168.86
16	Level sensor	1	14.99
17	Flow rate sensor	1	93.06
18	Type K thermocouples	15	213.70
19	Frequency inverter	1	183.86
20	Power controller	1	1010.49
21	Data acquisition system	1	1010.53
22	Glass wool insulation	2.4 m ²	6.51
Total (\$)			6,632.78

Source: Battisti *et al.* (2021b).

Currently, different distillation methods have been suggested and tested on pilot-scale facilities, such as internally heat-integrated distillation column (HIDiC) (BRUINSMA *et al.*, 2012), multi-effect distillation (PALENZUELA *et al.*, 2018), and membrane distillation (BINDELS *et al.*, 2020). However, the abovementioned methods still have limitations for large-scale applications such as complicated setup configurations, huge energy consumption, or low production efficiency. When analyzing the cost of equipment and components for

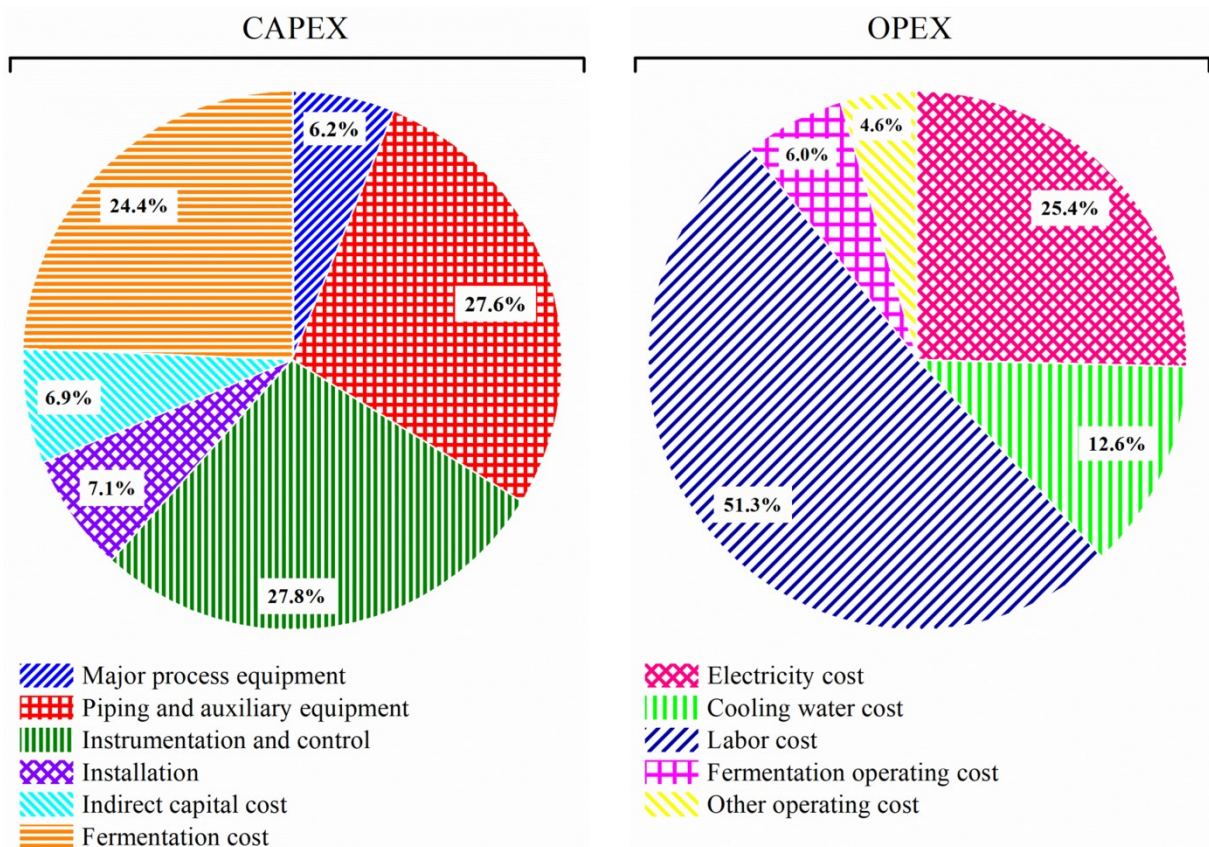
constructing the Destubcal plant normalized to its annual feeding capacity, the thermosyphon-assisted falling film distillation unit reveals a cost of 122.6 $\$/\text{m}^3/\text{yr}$. Compared to the other facilities mentioned above, this cost is higher than the cost of the multi-effect distillation pilot plant (68.9 $\$/\text{m}^3/\text{yr}$) (PALENZUELA *et al.*, 2018), lower than the cost of the pilot air-gap membrane distillation system (219.2 $\$/\text{m}^3/\text{yr}$) (BINDELS *et al.*, 2020), and considerably lower than the cost of the structured HIDiC pilot-scale plant facility with similar capacity (1778.2 $\$/\text{m}^3/\text{yr}$) (BRUINSMA *et al.*, 2012). Although HIDiC technology is promising in reducing energy consumption, its installation cost is still high because of its complex design. The Destubcal technology is favored by its simple design since it gathers two well-consolidated technologies (the falling film distillation and the supply of heat by a two-phase closed thermosyphon), which corroborates the relatively low cost of the Destubcal equipment.

To assess the cost impact of the elements in the total cost formulation, a comprehensive analysis of the percentage participation in the CAPEX and OPEX was carried out. Globally, the annualized capital cost portion was lower (24.2%) than the annualized operating cost portion (75.8%). Vasconcelos *et al.* (2020) recently reported that the capital cost for ethanol recovery through a conventional distillation system in a first-generation sugarcane biorefinery accounts for about 38% of the total production cost, showing that Destubcal technology requires proportionally less capital investment than a conventional distillery. Specifically, Figure 37 presents the percentage participation of the cost elements to the annual capital and operating costs. It is observed that instrumentation and control, and piping and auxiliary equipment are the two predominant cost elements (more than 55%) of the capital costs of the Destubcal unit, while major process equipment represent a small portion (6.2%) of the capital costs (CAPEX). Besides, as expected, the third-highest cost comprises the fermentation cost (24.4%) since it includes the cost of the feedstock, in this case, sugarcane. Feedstock costs represent one of the most significant components of ethanol's production cost, which could reach about 50% of the costs for some lignocellulosic raw materials (GNANSOUNOU; DAURIAT, 2010).

The Destubcal unit combines the falling film distillation technology, considered a simple constructive structure (BATTISTI; MACHADO; MARANGONI, 2020), with the heat supply through a two-phase closed thermosyphon, also considered a low-cost device to manufacture (BATTISTI *et al.*, 2020b; LATAOUI; JEMNI, 2017). It highlights the unit's low investment cost for major process equipment and contrasts with other unconventional technologies, such as HIDiC and membrane distillation. Tavakkoli *et al.* (2017) showed that

major equipment as membrane modules and storage tanks account for almost 45% of the capital cost of a direct contact membrane distillation plant. Schwantes *et al.* (2018) analyzed a configuration of air-gap membrane distillation and found that membrane modules exceed 66% of the CAPEX for a unit with a capacity of 10 m³/d. The authors also sought a design modification, proposing a configuration of vacuum air-gap membrane distillation, which reduced the percentage of the membrane module cost to 50% of CAPEX, which is still significantly higher than the Destubcal unit. Analyzing a hybrid multi-effect distillation/thermal vapor compression system, Panagopoulos (2020b) noted that primary equipment consisting of a series of four sequential effects are the predominant cost elements (38.8%) of the capital costs of the unit.

Figure 37 – Fractional contribution of various cost elements in the CAPEX and OPEX for sanitizer-grade ethanol recovery by the thermosyphon-assisted falling film distillation unit.



Source: Battisti *et al.* (2021b).

Concerning OPEX, the major cost-driver for the Destubcal pilot-scale plant is the labor cost, representing a 51.3% share. This relatively high percentage is explained by the fact

that the pilot-scale unit has a low capacity when compared to industrial plants. Specific labor costs are inherently dependent on plant capacity and decrease considerably with an increase in capacity (ERBA; APLIN, 1996). Schwantes *et al.* (2018) demonstrated that the labor cost of a plant with a feed capacity of 10 m³/d was 5.16 \$/m³, but when the capacity increases to 100 m³/d, the labor cost reduced to 1.72 \$/m³, and when a 1000 m³/d flow rate capacity was designed, the labor cost was reduced to 0.78 \$/m³. Lam *et al.* (2014) performed a techno-economic evaluation for a fermentative pilot-scale plant to produce succinic acid, also with three shifts of employees, obtaining a similar operating labor cost percentage of 48.5%. Electricity cost represents the second major share (25.4%) in the operating cost since electrical resistances are responsible for heating the thermal fluid stored in the evaporator, replacing the reboiler steam-heated of conventional columns. In the analyzed scenario, the electrical resistances of the evaporator consume 0.508 kW to maintain the evaporator temperature at 93 °C, as this is the ideal temperature to produce a distillate within the desired specification of 70 vol% in ethanol by the falling film column. Besides, the helical positive-displacement feed pump requires 0.2 kW, according to the manufacturer's catalog. The centrifugal recirculation pump (2.0 kW) is used to keep the mixture homogeneous in the storage tank, being sparingly used about 2 h per day. The vacuum pump removes non-condensable gases from inside the thermosyphon's condenser chamber and is used once a day for about 15 min. The third highest operating cost is the cooling water (12.6%) of the condenser. Fermentation operating cost and other minor operating costs share 6.0% and 4.6%, respectively.

The main contributors to the operating costs for conventional distillation processes are the reboiler heating and condenser cooling duties (ZHOU; CAI; YOU, 2018). For an extractive distillation sequence, for example, one of the most commonly used in ethanol distilleries, steam cost accounts for a major share of annual operating cost varying from 85–88% (ANIYA *et al.*, 2018), which is a fairly high share when compared to the electricity cost of the thermosyphon-assisted falling film distillation unit (25.4%). Muhammad and Rosentrater (2020) performed an economic comparison of bioethanol recovery with conventional and membrane distillation systems. Analyzing the operating costs of utilities normalized by the plant's feeding capacity, the authors pointed out that membrane distillation spends around 18.7 \$/m³_{feed}, while conventional distillation spends over 56.2 \$/m³_{feed}. Applying this same relation, it is found that the Destubcal unit spends on utilities costs around 31.6 \$/m³_{feed} to produce the sanitizer-grade ethanol, which is cheaper than the conventional

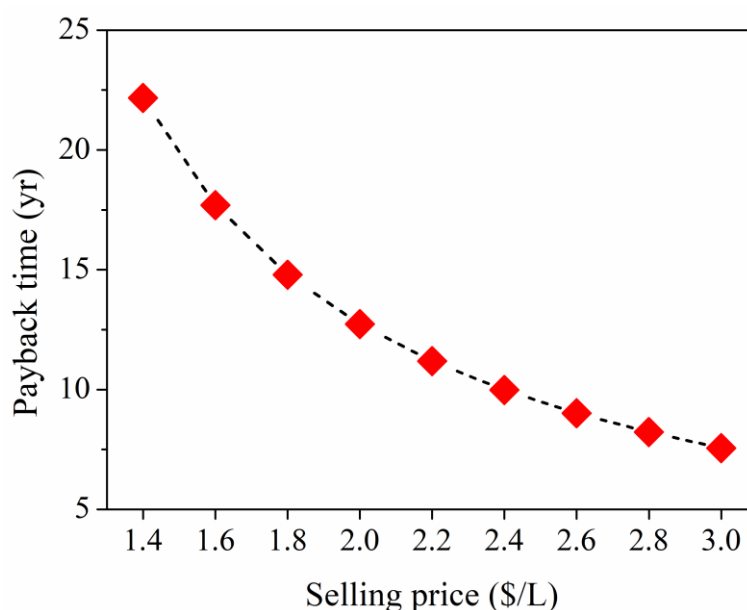
setting but more expensive than the membrane distillation setting. Although membrane distillation has been considered a more environmentally friendly and energy-saving process, the authors stated that membrane distillation still is not cost-effective for industrial bioethanol production due to its high capital investment cost. This compares favorably to the Destubcal unit. It demands a relatively low capital investment cost due to the simple and robust construction structure, besides saving operating costs compared to conventional columns due to the better energy distribution promoted by the thermosyphon coupled to the distillation tube.

From economic analysis, it is possible to predict the cost of the distilled sanitizer-grade ethanol per liter and the time required to get back the investment made in the Destubcal unit. The production cost per liter (*CPL*) by the pilot-scale thermosyphon-assisted falling film distillation unit, financed at a 5% interest rate and distilling ethanol with a 70 vol% minimum content, was 1.12 \$/L. Although the vast majority of techno-economic analyses for ethanol recovery in the literature are dealing with distillation plants to yield fuel ethanol in concentrations of about 92.5 wt% (hydrous) and 99.8 wt% (anhydrous), a comparison of the ethanol production cost per liter becomes reasonable to assess the feasibility of the proposed process. Based on the same raw material as sugarcane, the ethanol-producing cost equipped with a conventional distillation system varies around 0.98–1.18 \$/L for a first-generation (1G) biorefinery (MONCADA; EL-HALWAGI; CARDONA, 2013), and 0.42–0.52 \$/L for a first- and second-generation (1G2G) integrated biorefinery (VASCONCELOS *et al.*, 2020). Concerning lignocellulosic raw materials, the production cost varies significantly with the need for pretreatment of biomass, making the final product more expensive in some cases (STARFELT *et al.*, 2012). The production cost for the lignocellulosic raw materials ranges by 0.76–0.84 \$/kg for rice straw with conventional distillation system (TEWFIK; ABULNOUR; SOROUR, 2015); 0.64 \$/L for food waste with conventional distillation, and 1.65 \$/L with membrane distillation (MUHAMMAD; ROSENTRATER, 2020); 0.68 \$/L for coffee cut-stems, 0.64 \$/L for rice husk, and 0.58 \$/L for empty fruit bunches residues, using conventional distillation column settings (QUINTERO; MONCADA; CARDONA, 2013); 0.79–0.95 \$/L for sawdust and shavings, 0.42–0.52 \$/L for debarked fuel logs, 0.84–1.03 \$/L for fuel logs, 0.89–1.09 \$/L for early thinnings, 0.93–1.16 \$/L for tops and branches, and 1.32–1.71 \$/L for hog fuel, using conventional distillation and molecular sieve adsorption sequence (FRANKÓ; GALBE; WALLBERG, 2016). The ethanol production cost from the Destubcal unit is close to the values obtained in the literature. Although the sanitizer-grade

ethanol *CPL* is slightly above the values of ethanol from first-generation distilleries, partly explained by the presence of high-purity columns, it is remarkably more economically viable than ethanol from membrane distillation and some lignocellulosic feedstocks.

The sale of sanitizer-grade liquid ethanol is the cash inflow component. Depending on the selling price of the product, the interest rate at which the unit is financed, and the annual distillate produced, a longer or shorter payback time is achieved. The variation of payback time for the Destubcal unit under different minimum selling prices is illustrated in Figure 38. As expected, the payback time of the Destubcal unit decreases with the increase in the selling price. A market survey with the leading national brands of disinfectant liquid ethanol commercialized in the local market was performed and revealed that the selling price of the ethanol 70 vol% ranges from 1.13 \$/L to 3.39 \$/L. Working within this range, financed at an interest rate of 5%, which is an average of the last two years in Brazil, and with a production cost of 1.12 \$/L, the Destubcal unit showed a high payback time of 22.2 yr with a selling price of 1.4 \$/L. However, when the selling price increases to 3.0 \$/L, the payback time decreases to 7.5 yr, reducing 66.2%. Weber *et al.* (2020) performed a techno-economic analysis of a biorefinery to generate ethanol-based hand sanitizer from sweet potato waste and demonstrated that the selling price ranged from \$2.42 to \$3.72 per liter. When the selling price was taken as 2.42 \$/L, the conventional unit started to present positive economic results, with a payback time of 5.61 yr. With this same selling price, the Destubcal unit showed a payback time of 9.88 yr. However, when the selling price is taken as 3.72 \$/L, the payback time of the unit was 5.86 yr, which is reasonably acceptable for a pilot plant compared to a larger scale unit. Lam *et al.* (2014) also obtained a payback time of 7.2 yr for a fermentative pilot-scale plant, and pointed out that the project is still economically feasible even with a longer payback time.

Figure 38 – Payback time of the Destubcal unit for different selling prices of commercialized sanitizer-grade ethanol.

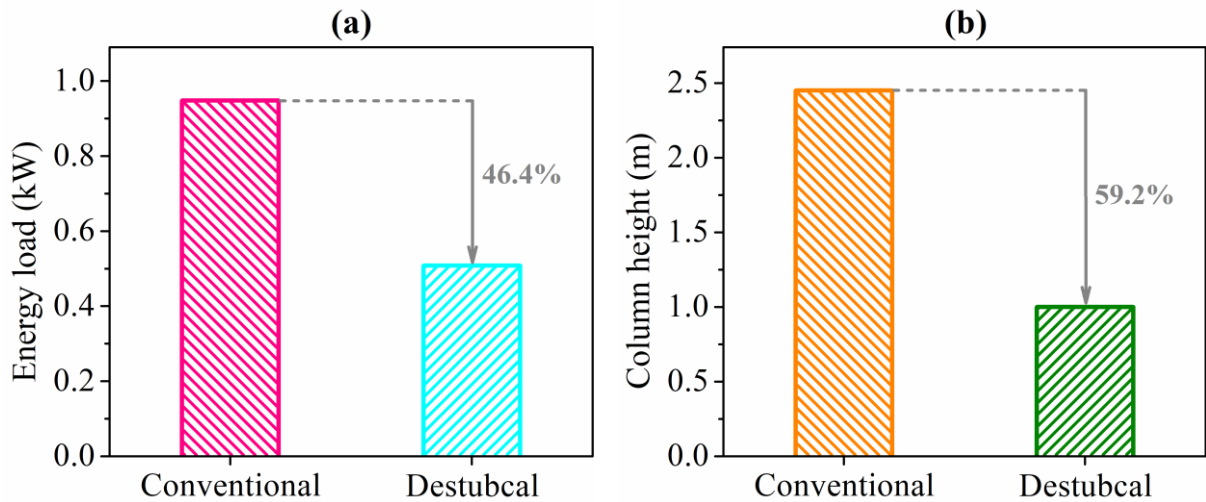


Source: Battisti *et al.* (2021b).

5.4.4 Comparative evaluation

Two key factors driving the intensification of distillation processes are reducing energy requirements and the space occupied by the column (TIAN *et al.*, 2018). The ethanol-water separation by conventional distillation in industrial distilleries consumes more than 50% of the total energy (ENWEREMADU; WAHEED; OJEDIRAN, 2009), and the optimal distillation sequences are usually equipped with columns of about 20 m in height (KISS; IGNAT, 2012). To analyze these two intensification factors, the Destubcal column was compared to a simulated conventional tray column for the same production rate and ethanol recovery, as shown in Figure 39. The energy loaded in the reboiler of the conventional tray column was 3.83 MJ/kg, whereas the Destubcal unit required only 2.06 MJ/kg, meaning an energetic saving of 46.4%. Regarding the column height, the conventional tower needed seven actual trays with a spacing of 0.35 m between trays, which resulted in a total height of 2.45 m, while the Destubcal unit is built with a distillation tube of 1.0 m of height, representing a reduction of 59.2% of occupied space. This space-saving in column height is interesting for small-scale processes installed in roofed environments, facilitating the operation and increasing the lifespan of control and instrumentation components.

Figure 39 – Comparison between Destubcal and conventional distillation units for energy load (a) and column height (b).



Source: Battisti *et al.* (2021b).

The energetic cost structure for the conventional column is dominated by the operational cost of the bottom reboiler steam (BATTISTI *et al.*, 2020c; BRUINSMA *et al.*, 2012). For this reason, reducing the energy consumption required to separate the components is so important for reducing costs in distillation processes. In the Destubcal unit, heat supply does not occur conventionally (role of the reboiler) but by a two-phase closed thermosyphon of steam chamber-type. Because of the constructive characteristics of the thermosyphon, energy is no longer supplied only at the bottom of the column but is evenly distributed over the entire length of the distillation tube. As a result, losses from thermal degradation are minimized, and heat is better harnessed, increasing the thermal efficiency of the Destubcal unit, which explains the specific energetic saving of about 1.78 MJ/kg (46.4%) of distilled product. This energy-saving is comparable to the findings by Kunnakorn *et al.* (2013), who performed an energetic comparison between azeotropic distillation (distillation followed by practical azeotropic distillation) and hybrid system (distillation followed by pervaporation system) for producing high-purity ethanol from a feed of 50:50 ethanol:water by weight. The authors demonstrated that the hybrid system with pervaporation using a zeolite membrane to separate water from the ethanol-water mixture requires 9.31 MJ/kg, while the azeotropic distillation requires 18.20 MJ/kg, resulting in savings of 48.8% of the total energy added to the reboiler.

5.5 SUMMARY AND CONCLUDING REMARKS

The techno-economic and energetic feasibility of a novel pilot-scale thermosyphon-assisted falling film distillation unit was assessed for recovering ethanol at 70 vol%, considered a suitable sanitizing degree according to recommendations established by WHO and the Brazilian health regulatory agency. Two performance indicators, recovery ratio (40.66%) and specific thermal energy consumption (571.12 W·h/kg), showed that the most appropriate operating conditions to purify ethanol in the desired content were the feed flow rate of 14 L/h, the feed temperature of 80 °C, and the evaporator temperature of 93 °C. The thermal behavior evaluation revealed that the thermosyphon-assisted distillation apparatus is an energy-efficient device (88.5%). Such parameters had not been evaluated yet in the pilot-scale unit but corroborated the previous studies carried out by the research group. The relatively low temperature required in the evaporator was a favorable condition from the economic point of view because the lower the temperature, the less electricity will be consumed to heat the thermal fluid, and consequently, the operating cost is reduced.

The cost impact of the components associated with the construction and installation of the Destubcal unit showed that instrumentation and control, and piping and auxiliary equipment are the predominant cost elements (more than 55%) of the capital cost, while major process equipment represent a small portion (6.2%), indicating a low capital investment cost when compared to other unconventional distillation devices. Regarding operating costs, labor (51.3%), and electricity and cooling water (38.0%) represent the major cost-share, corroborating that the Destubcal unit saves about 1.78 MJ per kg of distilled product (46.4%) from utility cost when compared to a conventional column due to the better energy distribution promoted by the thermosyphon coupled to the distillation tube. The final sanitizer-grade liquid ethanol had a production cost of 1.12 \$/L, close to the minimum selling prices found in the literature. Considering the local average selling price for ethanol 70 vol% (2.81 \$/L), a payback time of 8.19 yr is necessary to regain the investment, considered a reasonable value for a pilot-scale plant. Therefore, findings from this study indicate that the Destubcal pilot-scale thermosyphon-assisted falling film distillation unit is an energetic-saving and techno-economic feasible alternative to recover sanitizer-grade ethanol by 70 vol% in alcohol and may help to avoid shortages of this product caused by pandemics.

6 CONCLUSIONS

The integration of the falling film distillation with heat supply through a two-phase closed thermosyphon, which resulted in the Destubcal technology, represents notable improvements for the thermal separations field, since the combination of these two well-established technologies originated a novel distillation apparatus, more compact, safer, and less energy-intensive when compared to the conventional distillation column. As consequence of the raised challenges and perspectives, theoretical and experimental contributions were accomplished to fulfill the knowledge gaps found in the Destubcal technology, aiming to move forward towards the consolidation of this new distillation device as a heat-intensified process. The dissemination of this distillation apparatus for industrial applications mainly depends on the consolidation of this emerging technology in terms of knowledge of the thermal dynamics of the unit for control purposes, optimization of process and operating variables, and techno-economic evaluation of the plant, targets achieved by this work as remarkable contributions.

The easy-to-implement thermal network-based transient model developed was able to describe with good accuracy the dynamics of the innovative heat supply approach through a two-phase closed thermosyphon, and could be applied for the engineering design of future equipment with a higher capacity and different separation purposes. The neural network-based machine learning modeling was successfully applied showing good predictive capacity of the process and operating variables, and the optimization technique via genetic algorithm was able to extract a satisfactory performance of the pilot-scale unit. The techno-economic analysis showed that the Destubcal technology has the potential to be a feasible alternative for ethanol recovery in disinfectant grade of 70 vol% in alcohol, and can help to avoid shortages of this product caused by the pandemic of COVID-19. Finally, this work offers the possibility to further extensions in the comprehension of the dynamic behavior of the two-phase closed thermosyphon during the hardest transients such as the start-up, shutdown, and emergency shutdown. Advanced techniques for process control could be implemented, tested, and compared. Also, a techno-economic assessment of the pilot-scale unit processing second generation ethanol from some lignocellulosic material would be interesting to evaluate the cost-benefit compared to the first-generation ethanol made in this work, integrating the Destubcal technology to the sustainable future of green economy.

6.1 TECHNOLOGY PERSPECTIVES AND FUTURE DEVELOPMENTS

Destubcal technology emerges as a promising intensified distillation alternative for ethanol production with energy, size, and costs savings. Although this study has shown the feasibility of producing sanitizer-grade ethanol from sugarcane raw material (first-generation ethanol), a window of opportunity opens up for ethanol production from biomass waste (second-generation ethanol). Due to the low implementation cost and compact size, the Destubcal unit is feasible to be installed in small communities or farmers' cooperatives that can use agricultural waste as a raw material source for ethanol production, especially in developing countries with high availability of biomass. This sustainability aspect is of great relevance, given that it can boost the generation of jobs and skilled labor, improve the social condition of these locations, and avoid ethical conflict about ethanol production from edible raw materials. In addition, the compact and fully sealed structure of the Destubcal unit allows installation in roofed or outdoor locations with a long-life perspective. On the other hand, the design and construction of the Destubcal unit require technicians or engineers specialized in steam chamber-type heat pipes, which can be a point of difficulty, given that this technology is still not widespread in industrial environments. However, the operation of the Destubcal unit is less complex than other advanced distillation technologies, such as heat-integrated distillation column (HIDiC) or molecular distillation. Some structural modifications, such as assessing the separation with modified surfaces inside the distillation tube and the possibility of energetic integration of heat streams, are possible features that can be evaluated in order to further improve the technology. Finally, the Destubcal technology opens up development perspectives for other biofuels, such as biodiesel and bio-oil. As the Destubcal is a versatile distillation technology, it could be applied in the purification and recovery stages of other renewable biofuels.

REFERENCES

- ABDULLAH, Z.; AZIZ, N.; AHMAD, Z. Nonlinear Modelling Application in Distillation Column. **Chemical Product and Process Modeling**, v. 2, n. 3, 2007. Available in: <https://doi.org/10.2202/1934-2659.1082>
- ABIODUN, O. I.; JANTAN, A.; OMOLARA, A. E.; DADA, K. V.; MOHAMED, N. A.; ARSHAD, H. State-of-the-art in artificial neural network applications: A survey. **Heliyon**, v. 4, n. 11, p. e00938, 2018. Available in: <https://doi.org/10.1016/j.heliyon.2018.e00938>
- AGRAWAL, R. Synthesis of distillation column configurations for a multicomponent separation. **Industrial & Engineering Chemistry Research**, v. 35, n. 4, p. 1059–1071, 1996. Available in: <https://doi.org/10.1021/ie950323h>
- AGRAWAL, R. More operable fully thermally coupled distillation column configurations for multicomponent distillation. **Chemical Engineering Research and Design**, v. 77, n. 6, p. 543–553, 1999. Available in: <https://doi.org/10.1205/026387699526449>
- ÅKESJÖ, A.; GOURDON, M.; VAMLING, L.; INNINGS, F.; SASIC, S. Hydrodynamics of vertical falling films in a large-scale pilot unit – a combined experimental and numerical study. **International Journal of Multiphase Flow**, v. 95, p. 188–198, 2017. Available in: <https://doi.org/10.1016/j.ijmultiphaseflow.2017.06.003>
- ÅKESJÖ, A.; GOURDON, M.; VAMLING, L.; INNINGS, F.; SASIC, S. Experimental and numerical study of heat transfer in a large-scale vertical falling film pilot unit. **International Journal of Heat and Mass Transfer**, v. 125, p. 53–65, 2018. Available in: <https://doi.org/10.1016/j.ijheatmasstransfer.2018.04.052>
- AL-HOTMANI, O. M. A.; AL-OBAIDI, M. A.; FILIPPINI, G.; MANENTI, F.; PATEL, R.; MUJTABA, I. M. Optimisation of multi effect distillation based desalination system for minimum production cost for freshwater via repetitive simulation. **Computers & Chemical Engineering**, v. 135, p. 106710, 2020. Available in: <https://doi.org/10.1016/j.compchemeng.2019.106710>
- AL-OBAIDANI, S.; CURCIO, E.; MACEDONIO, F.; DI PROFIO, G.; AL-HINAI, H.; DRIOLI, E. Potential of membrane distillation in seawater desalination: Thermal efficiency, sensitivity study and cost estimation. **Journal of Membrane Science**, v. 323, n. 1, p. 85–98, 2008. Available in: <https://doi.org/10.1016/j.memsci.2008.06.006>
- ALAMMAR, A. A.; AL-DADAH, R. K.; MAHMOUD, S. M. Numerical investigation of effect of fill ratio and inclination angle on a thermosiphon heat pipe thermal performance. **Applied Thermal Engineering**, v. 108, p. 1055–1065, 2016. Available in: <https://doi.org/10.1016/j.applthermaleng.2016.07.163>
- ALBERT, C.; MARSCHALL, H.; BOTHE, D. Direct numerical simulation of interfacial mass transfer into falling films. **International Journal of Heat and Mass Transfer**, v. 69, p. 343–357, 2014. Available in: <https://doi.org/10.1016/j.ijheatmasstransfer.2013.10.025>

ALEKSEENKO, S. V.; ANTIPIN, V. A.; GUZANOV, V. V.; KHARLAMOV, S. M.; MARKOVICH, D. M. Three-dimensional solitary waves on falling liquid film at low Reynolds numbers. **Physics of Fluids**, v. 17, n. 12, p. 121704, 2005. Available in: <https://doi.org/10.1063/1.2158428>

ALHUSSEINI, A. A.; TUZLA, K.; CHEN, J. C. Falling film evaporation of single component liquids. **International Journal of Heat and Mass Transfer**, v. 41, n. 12, p. 1623–1632, 1998. Available in: [https://doi.org/10.1016/S0017-9310\(97\)00308-6](https://doi.org/10.1016/S0017-9310(97)00308-6)

ALVES, J. L. F.; SILVA FILHO, V. F. da; MACHADO, R. A. F.; MARANGONI, C. Ethanol enrichment from an aqueous stream using an innovative multi-tube falling film distillation column equipped with a biphasic thermosiphon. **Process Safety and Environmental Protection**, v. 139, p. 69–75, 2020. Available in: <https://doi.org/10.1016/j.psep.2020.03.039>

AMAYA-VÍAS, D.; LÓPEZ-RAMÍREZ, J. A. Techno-economic assessment of air and water gap membrane distillation for seawater desalination under different heat source scenarios. **Water (Switzerland)**, v. 11, n. 10, 2019. Available in: <https://doi.org/10.3390/w11102117>

ANEESH, V.; ANTONY, R.; PARAMASIVAN, G.; SELVARAJU, N. Distillation technology and need of simultaneous design and control: A review. **Chemical Engineering and Processing: Process Intensification**, v. 104, p. 219–242, 2016. Available in: <https://doi.org/10.1016/j.cep.2016.03.016>

ANIYA, V.; DE, D.; SINGH, A.; SATYAVATHI, B. Design and operation of extractive distillation systems using different class of entrainers for the production of fuel grade tert-butyl Alcohol: A techno-economic assessment. **Energy**, v. 144, p. 1013–1025, 2018. Available in: <https://doi.org/10.1016/j.energy.2017.12.099>

AOUNE, A.; RAMSHAW, C. Process intensification: heat and mass transfer characteristics of liquid films on rotating discs. **International Journal of Heat and Mass Transfer**, v. 42, n. 14, p. 2543–2556, 1999. Available in: [https://doi.org/10.1016/S0017-9310\(98\)00336-6](https://doi.org/10.1016/S0017-9310(98)00336-6)

ARAÚJO, A. B.; BRITO, R. P.; VASCONCELOS, L. S. Exergetic analysis of distillation processes—A case study. **Energy**, v. 32, n. 7, p. 1185–1193, 2007. Available in: <https://doi.org/10.1016/j.energy.2006.07.003>

ARENA, U.; DI GREGORIO, F.; SANTONASTASI, M. A techno-economic comparison between two design configurations for a small scale, biomass-to-energy gasification based system. **Chemical Engineering Journal**, v. 162, n. 2, p. 580–590, 2010. Available in: <https://doi.org/10.1016/j.cej.2010.05.067>

ARGYROPOULOS, C. D.; MARKATOS, N. C. Recent advances on the numerical modelling of turbulent flows. **Applied Mathematical Modelling**, v. 39, n. 2, p. 693–732, 2015. Available in: <https://doi.org/10.1016/j.apm.2014.07.001>

ARIAS, F. J. Film boiling in magnetic field in liquid metals with particular reference to fusion reactor project. **Journal of Fusion Energy**, v. 29, n. 2, p. 130–133, 2010. Available in: <https://doi.org/10.1007/s10894-009-9244-8>

ARMBRUSTER, R.; MITROVIC, J. Evaporative cooling of a falling water film on horizontal tubes. **Experimental Thermal and Fluid Science**, v. 18, n. 3, p. 183–194, 1998. Available in: [https://doi.org/10.1016/S0894-1777\(98\)10033-X](https://doi.org/10.1016/S0894-1777(98)10033-X)

ARPORNWICHANOP, A.; KOOMSUP, K.; ASSABUMRUNGRAT, S. Hybrid reactive distillation systems for n-butyl acetate production from dilute acetic acid. **Journal of Industrial and Engineering Chemistry**, v. 14, n. 6, p. 796–803, 2008. Available in: <https://doi.org/10.1016/j.jiec.2008.06.006>

AZIZ, K. H. H.; MAHYAR, A.; MIESSNER, H.; MUELLER, S.; KALASS, D.; MOELLER, D.; KHORSHID, I.; RASHID, M. A. M. Application of a planar falling film reactor for decomposition and mineralization of methylene blue in the aqueous media via ozonation, Fenton, photocatalysis and non-thermal plasma: A comparative study. **Process Safety and Environmental Protection**, v. 113, p. 319–329, 2018. Available in: <https://doi.org/10.1016/j.psep.2017.11.005>

BALAT, M.; BALAT, H.; ÖZ, C. Progress in bioethanol processing. **Progress in Energy and Combustion Science**, v. 34, n. 5, p. 551–573, 2008. Available in: <https://doi.org/10.1016/j.pecs.2007.11.001>

BALDEA, M. From process integration to process intensification. **Computers & Chemical Engineering**, v. 81, p. 104–114, 2015. Available in: <https://doi.org/10.1016/j.compchemeng.2015.03.011>

BANDINI, S.; GOSTOLI, C.; SARTI, G. C. Separation efficiency in vacuum membrane distillation. **Journal of Membrane Science**, v. 73, n. 2, p. 217–229, 1992. Available in: [https://doi.org/10.1016/0376-7388\(92\)80131-3](https://doi.org/10.1016/0376-7388(92)80131-3)

BANERJEE, S.; SCOTT, D. S.; RHODES, E. Mass transfer to falling wavy liquid films in turbulent flow. **Industrial & Engineering Chemistry Fundamentals**, v. 7, n. 1, p. 22–27, 1968. Available in: <https://doi.org/10.1021/i160025a004>

BARRDAHL, R. A. G. Mass transfer in falling films: Influence of finite-amplitude waves. **AIChE Journal**, v. 34, n. 3, p. 493–498, 1988. Available in: <https://doi.org/10.1002/aic.690340317>

BATISTELLA, C. B. **Tecnologia da destilação molecular: da modelagem matemática a obtenção de dados experimentais aplicada a produtos de química fina**. 1999. Thesis (Doctorate in Chemical Engineering) - Faculty of Chemical Engineering, State University of Campinas, Campinas, 1999. Available in: <http://www.repositorio.unicamp.br/handle/REPOSIP/266407>

BATISTELLA, C. B.; MACIEL, M. R. W. Modeling, simulation and analysis of molecular distillators: centrifugal and falling film. **Computers & Chemical Engineering**, v. 20, n. 96, p. 2–7, 1996. Available in: [https://doi.org/10.1016/0098-1354\(96\)00014-2](https://doi.org/10.1016/0098-1354(96)00014-2)

BATISTELLA, C. B.; MORAES, E. B.; FILHO, R. M.; MACIEL, M. R. W. Molecular distillation process for recovering biodiesel and carotenoids from palm oil. **Applied Biochemistry and Biotechnology**, v. 98, n. 1, p. 1149–1159, 2002. Available in:

<https://doi.org/10.1385/ABAB:98-100:1-9:1149>

BATTISTI, R.; CLAUMANN, C. A.; MANENTI, F.; MACHADO, R. A. F.; MARANGONI, C. Dynamic modeling with experimental validation and control of a two-phase closed thermosyphon as heat supplier of a novel pilot-scale falling film distillation unit. **Computers & Chemical Engineering**, v. 143, p. 107078, 2020 a. Available in: <https://doi.org/10.1016/j.compchemeng.2020.107078>

BATTISTI, R.; CLAUMANN, C. A.; MANENTI, F.; MACHADO, R. A. F.; MARANGONI, C. Machine learning modeling and genetic algorithm-based optimization of a novel pilot-scale thermosyphon-assisted falling film distillation unit. **Separation and Purification Technology**, v. 259, p. 118122, 2021 a. Available in: <https://doi.org/10.1016/j.seppur.2020.118122>

BATTISTI, R.; CLAUMANN, C. A.; MARANGONI, C.; MACHADO, R. A. F. Optimization of pressure-swing distillation by simulated annealing algorithm for ethanol anhydrous purification. **Brazilian Journal of Chemical Engineering**, v. 36, n. 1, p. 453–469, 2019. Available in: <https://doi.org/10.1590/0104-6632.20190361s20170379>

BATTISTI, R.; GALEAZZI, A.; PRIFTI, K.; MANENTI, F.; MACHADO, R. A. F.; MARANGONI, C. Techno-economic and energetic assessment of an innovative pilot-scale thermosyphon-assisted falling film distillation unit for sanitizer-grade ethanol recovery. **Applied Energy**, v. 297, p. 117185, 2021 b. Available in: <https://doi.org/10.1016/j.apenergy.2021.117185>

BATTISTI, R.; MACHADO, R. A. F.; MARANGONI, C. A background review on falling film distillation in wetted-wall columns: From fundamentals towards intensified technologies. **Chemical Engineering and Processing - Process Intensification**, v. 150, n. C, p. 107873, 2020. Available in: <https://doi.org/10.1016/j.cep.2020.107873>

BATTISTI, R.; MILANEZ, K. W.; MANTELLI, M. B. H.; DOS SANTOS, M. C.; MEDINA, L. C.; MARANGONI, C.; MACHADO, R. A. F. Energy conditions assessment of a two-phase annular thermosyphon used as heat supplier for a new pilot-scale falling film distillation unit. **Thermal Science and Engineering Progress**, p. 100648, 2020 b. Available in: <https://doi.org/10.1016/j.tsep.2020.100648>

BATTISTI, R.; URRUTH, N. S.; MACHADO, R. A. F.; MARANGONI, C. Optimization of Pressure-Swing Distillation for iC5-Methanol Azeotropic Mixture Purification. **Process Integration and Optimization for Sustainability**, 2020 c. Available in: <https://doi.org/10.1007/s41660-020-00115-w>

BELDEN, D. H.; BERWYN, I. **Distillation tower**. USA n. US2580646. Deposit: April 14, 1948. Concession: January 1, 1952.

BELLO, R. H.; LINZMEYER, P.; FRANCO, C. M. B.; SOUZA, O.; SELLIN, N.; MEDEIROS, S. H. W.; MARANGONI, C. Pervaporation of ethanol produced from banana waste. **Waste Management**, v. 34, n. 8, p. 1501–1509, 2014. Available in: <https://doi.org/10.1016/j.wasman.2014.04.013>

BHANDARKAR, M.; FERRON, J. R. Transport processes in thin liquid films during high-vacuum distillation. **Industrial & Engineering Chemistry Research**, v. 27, n. 6, p. 1016–1024, 1988. Available in: <https://doi.org/10.1021/ie00078a022>

BIENERT, W. B.; KROTIUK, W. J.; NIKITKIN, M. N. Thermal control with low power, miniature loop heat pipes. *In: International Conference On Environmental Systems*. SAE International, 1999. Available in: <https://doi.org/10.4271/1999-01-2008>

BILLS, D. D.; SLOAN, J. L. Removal of chlorinated insecticide residues from milk fat by molecular distillation. **Journal of Agricultural and Food Chemistry**, v. 15, n. 4, p. 676–678, 1967. Available in: <https://doi.org/10.1021/jf60152a032>

BINDELS, M.; CARVALHO, J.; GONZALEZ, C. B.; BRAND, N.; NELEMANS, B. Techno-economic assessment of seawater reverse osmosis (SWRO) brine treatment with air gap membrane distillation (AGMD). **Desalination**, v. 489, n. September, 2020. Available in: <https://doi.org/10.1016/j.desal.2020.114532>

BISHNOI, S.; ROCHELLE, G. T. Absorption of carbon dioxide in aqueous piperazine/methyldiethanolamine. **AIChE Journal**, v. 48, n. 12, p. 2788–2799, 2002. Available in: <https://doi.org/10.1002/aic.690481208>

BLAKE, T. R.; WILLOCKS, G. Virgin Islands water and power authority (VIWAPA) Horizontal Tube, Falling Film, Low Temperature 1.25 MGD Multi-Effect Distillation dual purpose plant. **Desalination**, v. 39, p. 311–322, 1981. Available in: [https://doi.org/10.1016/S0011-9164\(00\)86136-6](https://doi.org/10.1016/S0011-9164(00)86136-6)

BORGARELLO, A. V.; MEZZA, G. N.; PRAMPARO, M. C.; GAYOL, M. F. Thymol enrichment from oregano essential oil by molecular distillation. **Separation and Purification Technology**, v. 153, p. 60–66, 2015. Available in: <https://doi.org/10.1016/j.seppur.2015.08.035>

BOUALLAGUI, H.; TOUHAMI, Y.; HANAFI, N.; GHARIANI, A.; HAMDI, M. Performances comparison between three technologies for continuous ethanol production from molasses. **Biomass and Bioenergy**, v. 48, p. 25–32, 2013. Available in: <https://doi.org/10.1016/j.biombioe.2012.10.018>

BOUTEBILA, H. A theoretical model of a free flow solution over an inclined long flat plate solar still. **Desalination**, v. 249, n. 3, p. 1249–1258, 2009. Available in: <https://doi.org/10.1016/j.desal.2009.06.031>

BRADY, M. D. **A study of thermal effects involved in the performance of a wetted-wall column**. 1969. Thesis (PhD in Chemical Engineering) - Department of Chemical Engineering, Oregon State University, Corvallis, 1969.

BRAUER, H. **Strömung und wärmeübergang bei rieselfilmen**. Düsseldorf: VDI-Forschungshof, 1956.

BRAUNER, N.; MARON, D. M.; HAREL, Z. Wettability, rewettability and breakdown of thin films of aqueous salt solutions. **Desalination**, v. 52, n. 3, p. 295–307, 1985. Available in:

[https://doi.org/10.1016/0011-9164\(85\)80039-4](https://doi.org/10.1016/0011-9164(85)80039-4)

BRAVO, J. L.; FAIR J. R. Generalized correlation for mass transfer in packed distillation columns. **Industrial & Engineering Chemistry Process Design and Development**, v. 21, n. 1, p. 162–170, 1982. Available in: <https://doi.org/10.1021/i200016a028>

BRUINSMA, O. S. L.; KRIKKEN, T.; COT, J.; SARIĆ, M.; TROMP, S. A.; OLUJIĆ, Ž.; STANKIEWICZ, A. I. The structured heat integrated distillation column. **Chemical Engineering Research and Design**, v. 90, n. 4, p. 458–470, 2012. Available in: <https://doi.org/10.1016/j.cherd.2011.08.023>

CABRERA-RUIZ, J.; JIMÉNEZ-GUTIÉRREZ, A.; SEGOVIA-HERNÁNDEZ, J. G. Assessment of the implementation of heat-integrated distillation columns for the separation of ternary mixtures. **Industrial and Engineering Chemistry Research**, v. 50, n. 4, p. 2176–2181, 2011. Available in: <https://doi.org/10.1021/ie101939e>

CAO, Y.; FAGHRI, A. Transient two-dimensional compressible analysis for high-temperature heat pipes with pulsed heat input. **Numerical Heat Transfer, Part A: Applications: An International Journal of Computation and Methodology**, v. 18, n. 4, p. 483–502, 1991. Available in: <https://doi.org/10.1080/10407789008944804>

CATALDO, F.; THOME, J. R. Experimental evaluation of the thermal performances of a thermosyphon cooling system rejecting heat by natural and forced convection. **Applied Thermal Engineering**, v. 127, p. 1404–1415, 2017. Available in: <https://doi.org/10.1016/j.applthermaleng.2017.08.166>

CHANG, Y.-W.; CHENG, C.-H.; WANG, J.-C.; CHEN, S.-L. Heat pipe for cooling of electronic equipment. **Energy Conversion and Management**, v. 49, n. 11, p. 3398–3404, 2008. Available in: <https://doi.org/https://doi.org/10.1016/j.enconman.2008.05.002>

CHAROGIANNIS, A.; ZADRAZIL, I.; MARKIDES, C. N. Thermographic particle velocimetry (TPV) for simultaneous interfacial temperature and velocity measurements. **International Journal of Heat and Mass Transfer**, v. 97, n. June, p. 589–595, 2016. Available in: <https://doi.org/10.1016/j.ijheatmasstransfer.2016.02.050>

CHATLYNNE, C. J. **A Study of the Effects of Heat Transfer on the Performance of a Wetted-wall Column: a Refinement of the Design Correlation of Chilton-Colburn**. 1972. Thesis (PhD in Chemical Engineering) - Department of Chemical Engineering, Oregon State University, Corvallis, 1972.

CHEN, Q.; MUHAMMAD, B.; AKHTAR, F. H.; YBYRAIYMKUL, D.; MUHAMMAD, W. S.; LI, Y.; NG, K. C. Thermo-economic analysis and optimization of a vacuum multi-effect membrane distillation system. **Desalination**, v. 483, n. January, p. 114413, 2020. Available in: <https://doi.org/10.1016/j.desal.2020.114413>

CHEN, X.; WANG, N. A DNA based genetic algorithm for parameter estimation in the hydrogenation reaction. **Chemical Engineering Journal**, v. 150, n. 2, p. 527–535, 2009. Available in: <https://doi.org/10.1016/j.cej.2009.03.016>

CHIEN, K. L.; HRONES, J. A.; RESWICH, I. B. On the Automatic Control of Generalized Passive Systems. **Transactions of ASME**, v. 74, p. 175–185, 1972. Available in: <https://ci.nii.ac.jp/naid/10003093715/>

CHILTON, T. H.; COLBURN, A. P. Mass Transfer (Absorption) Coefficients Prediction from Data on Heat Transfer and Fluid Friction. **Industrial & Engineering Chemistry**, v. 26, n. 11, p. 1183–1187, 1934. Available in: <https://doi.org/10.1021/ie50299a012>

CHILTON, T. H.; COLBURN, A. P. Distillation and Absorption in Packed Columns A Convenient Design and Correlation Method. **Industrial & Engineering Chemistry**, v. 27, n. 3, p. 255–260, 1935. Available in: <https://doi.org/10.1021/ie50303a004>

CHURCHILL, S. W.; BERNSTEIN, M. A Correlating Equation for Forced Convection From Gases and Liquids to a Circular Cylinder in Crossflow. **Journal of Heat Transfer**, v. 99, n. 2, p. 300–306, 1977. Available in: <https://doi.org/10.1115/1.3450685>

CLAUMANN, C. A.; BATTISTI, R.; PERUZZO, T.; BOLZAN, A.; MARANGONI, C.; MACHADO, R. A. F. Nonequilibrium stage based modelling of a falling film distillation unit. **Theoretical Foundations of Chemical Engineering**, v. 54, p. 1156–1172, 2020. Available in: <https://doi.org/10.1134/S0040579520060147>

CLAUMANN, C. A.; CANCELIER, A.; DA SILVA, A.; ZIBETTI, A. W.; LOPES, T. J.; MACHADO, R. A. F. Fitting semi-empirical drying models using a tool based on wavelet neural networks: Modeling a maize drying process. **Journal of Food Process Engineering**, v. 41, n. 1, p. e12633, 2018. Available in: <https://doi.org/10.1111/jfpe.12633>

COHEN, G. H.; COON, G. A. Theoretical Consideration of Retarded Control. **Trans. ASME**, v. 75, p. 827–834, 1953. Available in: <https://ci.nii.ac.jp/naid/10030928086/>

CONG, H.; LI, X.; LI, H.; MURPHY, J. P.; GAO, X. Performance analysis and structural optimization of multi-tube type heat integrated distillation column (HIDiC). **Separation and Purification Technology**, v. 188, n. 29, p. 303–315, 2017. Available in: <https://doi.org/10.1016/j.seppur.2017.07.047>

CRAUSE, J. C.; NIEUWOUDT, I. Mass transfer in a short wetted-wall column. 1. Pure components. **Industrial and Engineering Chemistry Research**, v. 38, n. 12, p. 4928–4932, 1999. Available in: <https://doi.org/10.1021/ie990029f>

CRAVEIRO, A. M.; SOARES, H. M.; SCHMIDELL, W. Technical Aspects and Cost Estimations for Anaerobic Systems Treating Vinasse and Brewery/Soft Drink Wastewaters. **Water Science and Technology**, v. 18, n. 12, p. 123–134, 1986. Available in: <https://doi.org/10.2166/wst.1986.0168>

DA SILVA, A. K.; MANTELLI, M. B. H. Thermal applicability of two-phase thermosyphons in cooking chambers—experimental and theoretical analysis. **Applied Thermal Engineering**, v. 24, n. 5, p. 717–733, 2004. Available in: <https://doi.org/10.1016/j.applthermaleng.2003.09.013>

DANCKWERTS, P. V.; SAWISTOWSKI, H.; SMITH, W. The effects of heat-transfer and

interfacial tension in distillation. *In: Proceedings of the International Symposium on Distillation*, 1960, Brighton, England, p. 7–12.

DANTAS, T. N. C.; CABRAL, T. J. O.; NETO, A. A. D.; MOURA, M. C. P. A. Enrichment of patchoulol extracted from patchouli (*Pogostemon cablin*) oil by molecular distillation using response surface and artificial neural network models. **Journal of Industrial and Engineering Chemistry**, v. 81, p. 219–227, 2020. Available in: <https://doi.org/10.1016/j.jiec.2019.09.011>

DAVIES, J. T. Mass-Transfer and Interfacial Phenomena. *In: DREW, T. B.; HOOPES, J. W.; VERMEULEN, T. B. T.-A. in C. E. (org.). Advances in Chemical Engineering*. New York: Academic Press, 1964. v. 4, p. 1–50. *E-book*. Available in: [https://doi.org/10.1016/S0065-2377\(08\)60238-0](https://doi.org/10.1016/S0065-2377(08)60238-0)

DAVIS, E. J.; HUNG, S. C.; DUNN, C. S. Simultaneous heat and mass transfer with liquid film vacuum distillation. **Chemical Engineering Science**, v. 28, n. 8, p. 1519–1533, 1973. Available in: [https://doi.org/10.1016/0009-2509\(73\)80095-8](https://doi.org/10.1016/0009-2509(73)80095-8)

DAVIS, J. F.; TUNG, H.-H.; MAH, R. S. H. Fractionation with condensation and evaporation in wetted-wall columns. **AIChE Journal**, v. 30, n. 2, p. 328–338, 1984. Available in: <https://doi.org/10.1002/aic.690300223>

DE KOEIJER, G.; KJELSTRUP, S. Application of irreversible thermodynamics to distillation. **International Journal of Thermodynamics**, v. 7, n. 3, p. 107–114, 2004. Available in: <https://dergipark.org.tr/tr/download/article-file/65646>

DEFRAEYE, T.; BLOCKEN, B.; CARMELIET, J. Analysis of convective heat and mass transfer coefficients for convective drying of a porous flat plate by conjugate modelling. **International Journal of Heat and Mass Transfer**, v. 55, n. 1, p. 112–124, 2012. Available in: <https://doi.org/10.1016/j.ijheatmasstransfer.2011.08.047>

DEJANOVIĆ, I.; MATIJAŠEVIĆ, L.; HALVORSEN, I. J.; SKOGESTAD, S.; JANSEN, H.; KAIBEL, B.; OLUJIĆ, Ž. Designing four-product dividing wall columns for separation of a multicomponent aromatics mixture. **Chemical Engineering Research and Design**, v. 89, n. 8, p. 1155–1167, 2011. Available in: <https://doi.org/10.1016/j.cherd.2011.01.016>

DETERMAN, M. D.; GARIMELLA, S. Ammonia–water desorption heat and mass transfer in microchannel devices. **International Journal of Refrigeration**, v. 34, n. 5, p. 1197–1208, 2011. Available in: <https://doi.org/10.1016/j.ijrefrig.2011.02.004>

DIEDRICH, G. E.; LOTZ, C. W. **Distillation apparatus having corrugated heat transfer surfaces**. USA n. US3291704. Deposit: June 28, 1963. Concession: December 13, 1966.

DIETZE, G. F.; AL-SIBAI, F.; KNEER, R. Experimental study of flow separation in laminar falling liquid films. **Journal of Fluid Mechanics**, v. 637, p. 73–104, 2009. Available in: <https://doi.org/10.1017/S0022112009008155>

DIETZE, G. F.; KNEER, R. Flow separation in falling liquid films. **Frontiers in Heat and Mass Transfer**, v. 2, n. January, p. 1–14, 2011. Available in:

<https://doi.org/10.5098/hmt.v2.3.3001>

DOBRAN, F. Steady-state characteristics and stability thresholds of a closed two-phase thermosyphon. **International Journal of Heat and Mass Transfer**, v. 28, n. 5, p. 949–957, 1985. Available in: [https://doi.org/10.1016/0017-9310\(85\)90276-5](https://doi.org/10.1016/0017-9310(85)90276-5)

DODGE, B. F. Review of Distillation Processes for the Recovery of Fresh Water from Saline Waters. **Advances In Chemistry Series**, v. 38, p. 1–26, 1963. Available in: <https://doi.org/10.1021/ba-1963-0038.ch001>

DONG, L.; QUAN, X.; CHENG, P. An experimental investigation of enhanced pool boiling heat transfer from surfaces with micro/nano-structures. **International Journal of Heat and Mass Transfer**, v. 71, p. 189–196, 2014. Available in: <https://doi.org/10.1016/j.ijheatmasstransfer.2013.11.068>

DRIBIKA, M.; SANDALL, C. Simultaneous heat and mass transfer for multicomponent distillation in a wetted-wall column. **Chemical Engineering Science**, v. 34, p. 733–739, 1979. Available in: [https://doi.org/10.1016/0009-2509\(79\)85121-0](https://doi.org/10.1016/0009-2509(79)85121-0)

DZIAK, J.; KUBALA, M. Heat and mass transfer during thin-film evaporation of two-component liquid solutions. *In*: 2010, **20th European Symposium on Computer Aided Process Engineering – ESCAPE20**. Naples, Italy: Elsevier B. V., 2010. p. 2–7.

EGGER, L. S.; FIEG, G. Process control for energy efficient operation of reactive dividing wall columns. **Chemical Engineering Research and Design**, v. 144, p. 397–404, 2019. Available in: <https://doi.org/10.1016/j.cherd.2019.02.026>

EGOSHI, N.; KAWAKAMI, H.; ASANO, K. Mass Transfer in Ternary Distillation of Nitrogen-Argon-Oxygen System in Wetted-Wall Column. **Journal Of Chemical Engineering Of Japan**, v. 32, n. 4, p. 409–416, 1999. Available in: <https://doi.org/10.1252/jcej.32.409>

EGOSHI, N.; KUSUNO, T.; KAWAKAMI, H. Mass transfer in binary distillation of nitrogen-oxygen and argon-oxygen systems in a wetted-wall column. **Journal Of Chemical Engineering Of Japan**, v. 30, n. 1, p. 7–12, 1997. Available in: <https://doi.org/10.1252/jcej.30.7>

ELSHEIKH, A. H.; SHARSHIR, S. W.; ELAZIZ], M. [Abd; KABEEL, A. E.; GUILAN, W.; HAIYOU, Z. Modeling of solar energy systems using artificial neural network: A comprehensive review. **Solar Energy**, v. 180, p. 622–639, 2019. Available in: <https://doi.org/10.1016/j.solener.2019.01.037>

ENGELL, S. Feedback control for optimal process operation. **Journal of Process Control**, v. 17, n. 3, p. 203–219, 2007. Available in: <https://doi.org/10.1016/j.jprocont.2006.10.011>

ENWEREMADU, C.; WAHEED, A.; OJEDIRAN, J. Parametric study of an ethanol-water distillation column with direct vapour recompression heat pump. **Energy for Sustainable Development**, v. 13, n. 2, p. 96–105, 2009. Available in: <https://doi.org/10.1016/j.esd.2009.05.001>

ERBA, E. M.; APLIN, R. D. Factors Affecting Labor Productivity and Cost per Gallon in Fluid Milk Plants. **Journal of Dairy Science**, v. 79, n. 7, p. 1304–1312, 1996. Available in: [https://doi.org/10.3168/jds.S0022-0302\(96\)76485-8](https://doi.org/10.3168/jds.S0022-0302(96)76485-8)

FAGHRI, A.; ZHANG, Y. **Transport Phenomena in Multiphase Systems**. Boston: Academic Press, 2006. *E-book*. Available in: <https://doi.org/10.1016/B978-0-12-370610-2.50018-0>

FANG, J.; CHENG, X.; LI, Z.; LI, H.; LI, C. A review of internally heat integrated distillation column. **Chinese Journal of Chemical Engineering**, 2018. Available in: <https://doi.org/https://doi.org/10.1016/j.cjche.2018.08.021>

FARSI, H.; JOLY, J.-L.; MISCEVIC, M.; PLATEL, V.; MAZET, N. An experimental and theoretical investigation of the transient behavior of a two-phase closed thermosyphon. **Applied Thermal Engineering**, v. 23, n. 15, p. 1895–1912, 2003. Available in: [https://doi.org/10.1016/S1359-4311\(03\)00147-9](https://doi.org/10.1016/S1359-4311(03)00147-9)

FERNANDEZ-SEARA, J.; PARDINAS, A. A. Refrigerant falling film evaporation review: Description, fluid dynamics and heat transfer. **Applied Thermal Engineering**, v. 64, n. 1–2, p. 155–171, 2014. Available in: <https://doi.org/10.1016/j.applthermaleng.2013.11.023>

FERNÁNDEZ, M. C.; PANTANO, M. N.; SERRANO, E.; SCAGLIA, G. Multivariable Tracking Control of a Bioethanol Process under Uncertainties. **Mathematical Problems in Engineering**, p. 1–16, 2020. Available in: <https://doi.org/10.1155/2020/8263690>

FERRANDI, C.; IORIZZO, F.; MAMELI, M.; ZINNA, S.; MARENGO, M. Lumped parameter model of sintered heat pipe: Transient numerical analysis and validation. **Applied Thermal Engineering**, v. 50, n. 1, p. 1280–1290, 2012. Available in: <https://doi.org/10.1016/j.applthermaleng.2012.07.022>

FERRIS, S. W.; LAMSON, E. R.; SMITH, D. M. **Falling film distillation apparatus**. USA n. US2514944. Deposit: March 23, 1946. Concession: July 11, 1950.

FORD, J. D.; MISSEN, R. W. On the conditions for stability of falling films subject to surface tension disturbances; the condensation of binary vapors. **The Canadian Journal of Chemical Engineering**, v. 46, n. 5, p. 309–312, 1968. Available in: <https://doi.org/10.1002/cjce.5450460505>

FRANCO, A.; FILIPPESCHI, S. Closed loop two-phase thermosyphon of small dimensions: a review of the experimental results. **Microgravity Science and Technology**, v. 24, n. 3, p. 165–179, 2012. Available in: <https://doi.org/10.1007/s12217-011-9281-6>

FRANKÓ, B.; GALBE, M.; WALLBERG, O. Bioethanol production from forestry residues: A comparative techno-economic analysis. **Applied Energy**, v. 184, n. 2016, p. 727–736, 2016. Available in: <https://doi.org/10.1016/j.apenergy.2016.11.011>

FREGOLENTE, P. B. L.; PINTO, G. M. F.; WOLF-MACIEL, M. R.; FILHO, R. M. Monoglyceride and diglyceride production through lipase-catalyzed glycerolysis and molecular distillation. **Applied Biochemistry and Biotechnology**, v. 160, n. 7, p. 1879–1887,

2010. Available in: <https://doi.org/10.1007/s12010-009-8822-6>

FUJITA, H.; QIAN, Q.; FUJII, T.; MOCHIZUKI, K.; SAKODA, A. Isolation of ethanol from its aqueous solution by liquid phase adsorption and gas phase desorption using molecular sieving carbon. **Adsorption**, v. 17, n. 5, p. 869–879, 2011. Available in: <https://doi.org/10.1007/s10450-011-9354-2>

FULFORD, G. D. The flow of liquids in thin films. *In*: DREW, T. B.; HOOPES, J. W.; VERMEULEN, T.; COKELET, G. R. (org.). **Advances in Chemical Engineering**. New York: Academic Press, 1964. v. 5p. 151–236. *E-book*. Available in: [https://doi.org/10.1016/S0065-2377\(08\)60008-3](https://doi.org/10.1016/S0065-2377(08)60008-3)

FULLARTON, D.; SCHLÜNDER, E. U. Diffusion distillation - a new separation process for azeotropic mixtures Part I: Selectivity and transfer efficiency. **Chemical Engineering and Processing**, v. 20, n. 5, p. 265–270, 1986. Available in: [https://doi.org/10.1016/0255-2701\(86\)80019-8](https://doi.org/10.1016/0255-2701(86)80019-8)

GABBAY, S. S. **The performance of pulsed-pressure wetted-wall distillation columns**. Thesis (Doctorate in Chemical Engineering) - School of Aeronautical, Automotive, Chemical and Materials Engineering, Loughborough University, Leicestershire, 1970. Available in: <https://repository.lboro.ac.uk/account/articles/9238424>

GAIKAR, V. G.; MAHAPATRA, A.; SHARMA, M. M. Separation of close boiling point mixtures (p-cresol/m-cresol, guaiacol/alkylphenols, 3-picoline/4-picoline, substituted anilines) through dissociation extractive crystallization. **Industrial & Engineering Chemistry Research**, v. 28, n. 2, p. 199–204, 1989. Available in: <https://doi.org/10.1021/ie00086a012>

GE, L.; LI, H.; SHAN, J. Reliability and loading-following studies of a heat pipe cooled, AMTEC conversion space reactor power system. **Annals of Nuclear Energy**, v. 130, p. 82–92, 2019. Available in: <https://doi.org/10.1016/j.anucene.2019.02.029>

GHEZZAR, M. R.; OGNIER, S.; CAVADIAS, S.; ABDELMALEK, F.; ADDOU, A. DBDplate-TiO₂ treatment of Yellow Tartrazine azo dye solution in falling film. **Separation and Purification Technology**, v. 104, p. 250–255, 2013. Available in: <https://doi.org/10.1016/j.seppur.2012.11.026>

GIL, J. D.; RUIZ-AGUIRRE, A.; ROCA, L.; ZARAGOZA, G.; BERENGUEL, M. Prediction models to analyse the performance of a commercial-scale membrane distillation unit for desalting brines from RO plants. **Desalination**, v. 445, p. 15–28, 2018. Available in: <https://doi.org/10.1016/j.desal.2018.07.022>

GILBERT, W. W. **Characteristics of a wetted-wall column the effect of reflux ratio and composition on the height of a transfer unit**. Dissertation (Master of Science in Chemical Engineering) - School of Chemical and Biomolecular Engineering, Georgia School of Technology, 1947. Available in: <http://hdl.handle.net/1853/10910>

GILLILAND, E. R.; SHERWOOD, T. K. Diffusion of vapors into air streams. **Industrial & Engineering Chemistry**, v. 26, n. 5, p. 516–523, 1934. Available in: <https://doi.org/10.1021/ie50293a010>

GNANSOUNOU, E.; DAURIAT, A. Techno-economic analysis of lignocellulosic ethanol: A review. **Bioresource Technology**, v. 101, p. 4980–4991, 2010. Available in: <https://doi.org/10.1016/j.biortech.2010.02.009>

GOEDECKE, R. **Fluidverfahrenstechnik: Grundlagen, Methodik, Technik, Praxis**. Wiley, 2006. *E-book*. Available in: <https://books.google.com.br/books?id=TVIAOTkhUFQC>

GOLDEMBERG, J.; COELHO, S. T.; GUARDABASSI, P. The sustainability of ethanol production from sugarcane. **Energy Policy**, v. 36, n. 6, p. 2086–2097, 2008. Available in: <https://doi.org/10.1016/j.enpol.2008.02.028>

GOLIN, A. P.; CHOI, D.; GHAHARY, A. Hand sanitizers: A review of ingredients, mechanisms of action, modes of delivery, and efficacy against coronaviruses. **American Journal of Infection Control**, v. 48, n. 9, p. 1062–1067, 2020. Available in: <https://doi.org/10.1016/j.ajic.2020.06.182>

GONÇALVES, C. S.; QUADRI, M. B.; MACHADO, R. A. F.; TRAMONTIN, D. P.; MIOTTO, F. Simulação de películas líquidas descendentes pela parede interna de um tubo vertical. *In*: 2014, **Anais do Congresso Brasileiro de Engenharia Química**. Florianópolis, p. 1–8. Available in: <https://doi.org/10.5151/chemeng-cobeq2014-1712-17936-159659>

GRAND, F. le; ODIO, C. E. **Distillation column**. United States n. US4657638A. Deposit: July 29, 1985. Concession: April 14, 1987.

GROSS, U. Reflux condensation heat transfer inside a closed thermosyphon. **International Journal of Heat and Mass Transfer**, v. 35, n. 2, p. 279–294, 1992. Available in: [https://doi.org/10.1016/0017-9310\(92\)90267-V](https://doi.org/10.1016/0017-9310(92)90267-V)

GUO, Z.; WANG, S.; GU, Y.; XU, G.; LI, X.; LUO, Z. Separation characteristics of biomass pyrolysis oil in molecular distillation. **Separation and Purification Technology**, v. 76, n. 1, p. 52–57, 2010. Available in: <https://doi.org/10.1016/j.seppur.2010.09.019>

HIDL, J.; REJL, F. J.; VALENZ, L.; KORDAČ, M.; MOUCHA, T.; LABÍK, L.; SCHULTES, M. Absorption in wetted-wall column with phase properties close to distillation conditions. **Chemical Engineering Science**, v. 144, p. 126–134, 2016. Available in: <https://doi.org/10.1016/j.ces.2015.12.027>

HALICI, F.; TAYMAZ, İ.; GÜNDÜZ, M. The effect of the number of tube rows on heat, mass and momentum transfer in flat-plate finned tube heat exchangers. **Energy**, v. 26, n. 11, p. 963–972, 2001. Available in: [https://doi.org/10.1016/S0360-5442\(01\)00048-2](https://doi.org/10.1016/S0360-5442(01)00048-2)

HAMBLETON, W. T.; HUTCHINS, N.; MARUSIC, I. Simultaneous orthogonal-plane particle image velocimetry measurements in a turbulent boundary layer. **Journal of Fluid Mechanics**, v. 560, p. 53–64, 2006. Available in: <https://doi.org/10.1017/S0022112006000292>

HAMMER, J. B.; SOMERS, E. V. **Falling film distillation unit apparatus**. USA n. US3211633. Deposit: May 28, 1962. Concession: October 12, 1965.

HARLEY, C.; FAGHRI, A. Complete transient two-dimensional analysis of two-phase closed thermosyphons including the falling condensate film. **Journal of Heat Transfer**, v. 116, n. 3, p. 418–426, 1994. Available in: <https://doi.org/10.1115/1.2911414>

HASELDEN, G. G. An approach to minimum power consumption in low temperature gas separation. **Trans. Inst. Chem. Eng.**, v. 36, p. 123–132, 1958. Available in: https://jglobal.jst.go.jp/en/detail?JGLOBAL_ID=201602010052796345

HAUSEN, H. The Definition of the Degree of Exchange on Rectifying Plates for Binary and Ternary Mixtures. **Chem. Ingr. Tech.**, v. 25, n. 595, p. 595–597, 1953. Available in: <https://doi.org/10.1002/cite.330251014>

HAUSNER, J. K. **Rotary film distillation and gas refrigerant condensing apparatus**. US n. US3226306. Deposit: Oct. 2, 1961. Concession: Dec. 28, 1965.

HE, J.; MIAO, J.; BAI, L.; LIN, G.; ZHANG, H.; WEN, D. Effect of non-condensable gas on the startup of a loop heat pipe. **Applied Thermal Engineering**, v. 111, p. 1507–1516, 2017. Available in: <https://doi.org/10.1016/j.applthermaleng.2016.07.154>

HE, T.; MEI, C.; LONGTIN, J. P. Thermosyphon-assisted cooling system for refrigeration applications. **International Journal of Refrigeration**, v. 74, p. 165–176, 2017. Available in: <https://doi.org/10.1016/j.ijrefrig.2016.10.012>

HENLEY, E. J.; SEADER, J. D. **Equilibrium-stage separation operations in chemical engineering**. New York: Wiley, 1981.

HICKMAN, K. C. D. High-vacuum Short-path Distillation-A Review. **Chemical Reviews**, v. 34, n. 1, p. 51–106, 1944. Available in: <https://doi.org/10.1021/cr60107a002>

HILPERT, R. Heat Transfer from Cylinders. **Forsch. Geb. Ingenieurwes**, v. 4, p. 215–24, 1933. Available in: <https://doi.org/10.1007/BF02719754>

HO, C. K.; UDELL, K. K. An experimental investigation of air venting of volatile liquid hydrocarbon mixtures from homogeneous and heterogeneous porous media. **Journal of Contaminant Hydrology**, v. 11, n. 3, p. 291–316, 1992. Available in: [https://doi.org/10.1016/0169-7722\(92\)90021-6](https://doi.org/10.1016/0169-7722(92)90021-6)

HOLLAND, C. D. **Fundamentals and modeling of separation processes: absorption, distillation, evaporation and extraction**. Englewood Cliffs, NJ: Prentice-Hall, 1975.

HOLLAND, C. D.; MCMAHON, K. S. Comparison of vaporization efficiencies with Murphree-type efficiencies in distillation—I. **Chemical Engineering Science**, v. 25, n. 3, p. 431–436, 1970. Available in: [https://doi.org/10.1016/0009-2509\(70\)80041-0](https://doi.org/10.1016/0009-2509(70)80041-0)

HONORAT, A.; SANDALL, O. C. Simultaneous heat and mass transfer in a packed binary distillation column. **Chemical Engineering Science**, v. 33, n. 6, p. 635–640, 1978. Available in: [https://doi.org/10.1016/0009-2509\(78\)80039-6](https://doi.org/10.1016/0009-2509(78)80039-6)

HSU, Y. Y.; WESTWATER, J. W. Film boiling from vertical tubes. **AIChE Journal**, v. 4, n.

1, p. 58–62, 1958. Available in: <https://doi.org/10.1002/aic.690040112>

HU, Y.; LI, H.; YAN, J. Techno-economic evaluation of the evaporative gas turbine cycle with different CO₂ capture options. **Applied Energy**, v. 89, n. 1, p. 303–314, 2012. Available in: <https://doi.org/10.1016/j.apenergy.2011.07.034>

HUANG, K.; HU, Y.; DENG, X. Experimental study on heat and mass transfer of falling liquid films in converging-diverging tubes with water. **International Journal of Heat and Mass Transfer**, v. 126, p. 721–729, 2018. Available in: <https://doi.org/10.1016/j.ijheatmasstransfer.2018.05.134>

HUANG, K.; SHAN, L.; ZHU, Q.; QIAN, J. Design and control of an ideal heat-integrated distillation column (ideal HiDiC) system separating a close-boiling ternary mixture. **Energy**, v. 32, n. 11, p. 2148–2156, 2007. Available in: <https://doi.org/10.1016/j.energy.2007.04.007>

HUMINIC, G.; HUMINIC, A.; MORJAN, I.; DUMITRACHE, F. Experimental study of the thermal performance of thermosyphon heat pipe using iron oxide nanoparticles. **International Journal of Heat and Mass Transfer**, v. 54, n. 1, p. 656–661, 2011. Available in: <https://doi.org/10.1016/j.ijheatmasstransfer.2010.09.005>

HUTCHISON, H. P.; LUSIS, M. A. Distillation efficiencies of binary and ternary mixtures in a wetted-wall column. **Transactions of The Institution of Chemical Engineers**, v. 46, n. 5, p. T158–T166, 1968.

IBRAHIM, G. A.; NABHAN, M. B. W.; ANABTAWI, M. Z. An investigation into a falling film type cooling tower. **International Journal of Refrigeration**, v. 18, n. 8, p. 557–564, 1995. Available in: [https://doi.org/10.1016/0140-7007\(96\)81783-X](https://doi.org/10.1016/0140-7007(96)81783-X)

IMURA, H.; KUSUDA, H.; OGATA, J. I.; MIYAZAKI, T.; SAKAMOTO, N. Heat transfer in two-phase closed-type thermosyphons. **Japan Society of Mechanical Engineers, Transactions, Series B**, v. 45, p. 712–722, 1979. Available in: <https://doi.org/10.1299/kikaib.45.712>

ITIKI, R.; ROY CHOWDHURY, P. Fast deployment of COVID-19 disinfectant from common ethanol of gas stations in Brazil. **Health Policy and Technology**, v. 9, n. 3, p. 384–390, 2020. Available in: <https://doi.org/10.1016/j.hlpt.2020.07.002>

ITO, A.; ASANO, K. Simultaneous heat and mass transfer in binary distillation. **Kagaku Kogaku Ronbunshu**, v. 6, n. 4, p. 352–358, 1980. Available in: <https://doi.org/10.1252/kakoronbunshu.6.352>

ITO, A.; ASANO, K. Thermal effects in non-adiabatic binary distillation: Effects of partial condensation of mixed vapors on the rates of heat and mass transfer and prediction of H.T.U. **Chemical Engineering Science**, v. 37, n. 7, p. 1007–1014, 1982. Available in: [https://doi.org/10.1016/0009-2509\(82\)80131-0](https://doi.org/10.1016/0009-2509(82)80131-0)

IWAKABE, K.; NAKAIWA, M.; HUANG, K.; NAKANISHI, T.; RØSJORDE, A.; OHMORI, T.; ENDO, A.; YAMAMOTO, T. Energy saving in multicomponent separation using an internally heat-integrated distillation column (HiDiC). **Applied Thermal**

Engineering, v. 26, n. 13, p. 1362–1368, 2006. Available in:
<https://doi.org/10.1016/j.applthermaleng.2005.05.026>

IWAKABE, K.; NAKAIWA, M.; NAKANISHI, T.; HUANG, K.; ZHU, Y.; SJORDE, A. Analysis of the energy savings by HiDiC for the multicomponent separation. *In*: 2004, **Asian Pacific Confederation of Chemical Engineering Congress**. Kitakyushu, Japan, 2004. p. 241. Available in: <https://doi.org/10.11491/apcche.2004.0.241.0>

JACKSON, L.; CEAGLSKE, N. Distillation, Vaporization, and Gas Absorption in a Wetted-Wall Column. **Industrial and Engineering Chemistry**, v. 42, n. 6, p. 1188–1198, 1950. Available in: <https://doi.org/10.1021/ie50486a032>

JACKSON, M. L. Liquid films in viscous flow. **Aiche Journal**, v. 1, n. 2, p. 231–240, 1955. Available in: <https://doi.org/10.1002/aic.690010217>

JAFARI, D.; FILIPPESCHI, S.; FRANCO, A.; DI MARCO, P. Unsteady experimental and numerical analysis of a two-phase closed thermosyphon at different filling ratios. **Experimental Thermal and Fluid Science**, v. 81, p. 164–174, 2017. Available in: <https://doi.org/10.1016/j.expthermflusci.2016.10.022>

JAFARI, D.; FRANCO, A.; FILIPPESCHI, S.; MARCO, P. Di. Two-phase closed thermosyphons: A review of studies and solar applications. **Renewable and Sustainable Energy Reviews**, v. 53, p. 575–593, 2016. Available in: <https://doi.org/10.1016/j.rser.2015.09.002>

JANA, A. K. Heat integrated distillation operation. **Applied Energy**, v. 87, n. 5, p. 1477–1494, 2010. Available in: <https://doi.org/10.1016/j.apenergy.2009.10.014>

JANA, A. K. Advances in heat pump assisted distillation column: A review. **Energy Conversion and Management**, v. 77, p. 287–297, 2014. Available in: <https://doi.org/10.1016/j.enconman.2013.09.055>

JANA, A. K. An energy efficient middle vessel batch distillation: Techno-economic feasibility, dynamics and control. **Applied Thermal Engineering**, v. 123, n. August, p. 411–421, 2017. Available in: <https://doi.org/10.1016/j.applthermaleng.2017.05.106>

JANG, J. H.; FAGHRI, A.; CHANG, W. S. Analysis of the one-dimensional transient compressible vapor flow in heat pipes. **International Journal of Heat and Mass Transfer**, v. 34, n. 8, p. 2029–2037, 1991. Available in: [https://doi.org/10.1016/0017-9310\(91\)90214-Y](https://doi.org/10.1016/0017-9310(91)90214-Y)

JANGA REDDY, M.; NAGESH KUMAR, D. Evolutionary algorithms, swarm intelligence methods, and their applications in water resources engineering: a state-of-the-art review. **H2Open Journal**, v. 3, n. 1, p. 135–188, 2020. Available in: <https://doi.org/10.2166/h2oj.2020.128>

JAWAD, J.; HAWARI, A. H.; ZAIDI, S. Modeling of forward osmosis process using artificial neural networks (ANN) to predict the permeate flux. **Desalination**, v. 484, p. 114427, 2020. Available in: <https://doi.org/10.1016/j.desal.2020.114427>

JEONG, Y. H.; CHANG, W. J.; CHANG, S. H. Wettability of heated surfaces under pool boiling using surfactant solutions and nano-fluids. **International Journal of Heat and Mass Transfer**, v. 51, n. 11, p. 3025–3031, 2008. Available in: <https://doi.org/10.1016/j.ijheatmasstransfer.2007.09.023>

JOHANSSON, M.; VAMLING, L.; OLAUSSON, L. Heat transfer in evaporating black liquor falling film. **International Journal of Heat and Mass Transfer**, v. 52, n. 11–12, p. 2759–2768, 2009. Available in: <https://doi.org/10.1016/j.ijheatmasstransfer.2008.09.040>

JOHNSTONE, H. F.; PIGFORD, R. L. Distillation in a Wetted-wall Column. **Trans. Am. Inst. Chem. Engrs.**, v. 38, n. 38, p. 25–51, 1942.

JOUHARA, H.; ROBINSON, A. J. Experimental investigation of small diameter two-phase closed thermosyphons charged with water, FC-84, FC-77 and FC-3283. **Applied Thermal Engineering**, v. 30, p. 201–211, 2010. Available in: <https://doi.org/10.1016/j.applthermaleng.2009.08.007>

JOUNG, W.; LEE, J. Effect of sink temperature on the stability of the pressure-controlled loop heat pipe. **Journal of Heat Transfer**, v. 141, n. 9, 2019. Available in: <https://doi.org/10.1115/1.4043956>

KABEEL, A. E.; HAMED, A. M.; EL-AGOUZ, S. A. Cost analysis of different solar still configurations. **Energy**, v. 35, n. 7, p. 2901–2908, 2010. Available in: <https://doi.org/10.1016/j.energy.2010.03.021>

KALATHINGAL, M. S. H.; BASAK, S.; MITRA, J. Artificial neural network modeling and genetic algorithm optimization of process parameters in fluidized bed drying of green tea leaves. **Journal of Food Process Engineering**, v. 43, n. 1, p. e13128, 2020. Available in: <https://doi.org/10.1111/jfpe.13128>

KALLIADASIS, S.; RUYER-QUIL, C.; SCHEID, B.; VELARDE, M. G. **Falling Liquid Films**. Applied Ma ed. London, UK: Springer, 2012. Available in: <https://doi.org/10.1007/978-1-84882-367-9>

KANE, A.; MONNIER, H.; TONDEUR, D.; FALK, L. Capability of a falling film microstructured contactor for the separation of binary mixtures. **Chemical Engineering Journal**, v. 167, n. 2–3, p. 455–467, 2011. Available in: <https://doi.org/10.1016/j.cej.2010.09.090>

KANNAN, M.; NATARAJAN, E. Thermal performance of a two-phase closed thermosyphon for waste heat recovery system. **Journal of Applied Sciences**, v. 10, n. 5, p. 413–418, 2010. Available in: <https://doi.org/10.3923/jas.2010.413.418>

KAPITZA, P. L.; KAPITZA, S. P. Wave flow of thin layers of a viscous fluid. In: HAAR, D. T. E. R. (org.). **Collected Papers of P.L. Kapitza**. Oxford: Pergamon, 1965. p. 662–709. *E-book*. Available in: <https://doi.org/10.1016/B978-0-08-010973-2.50013-6>

KARIMI, G.; KAWAJI, M. An experimental study of freely falling films in a vertical tube. **Chemical Engineering Science**, v. 53, n. 20, p. 3501–3512, 1998. Available in:

[https://doi.org/10.1016/S0009-2509\(98\)00159-6](https://doi.org/10.1016/S0009-2509(98)00159-6)

KATAOKA, K.; NODA, H.; MUKAIDA, T.; NISHIMURA, G.; YAMAJI, H. Boost to bioethanol distillation by internal heat-integrated distillation column (HIDiC). **Advanced Chemical Engineering Research**, v. 3, p. 48–57, 2014.

KATARIYA, A. M.; KAMATH, R. S.; MOUDGALYA, K. M.; MAHAJANI, S. M. Non-equilibrium stage modeling and non-linear dynamic effects in the synthesis of TAME by reactive distillation. **Computers & Chemical Engineering**, v. 32, p. 2243–2255, 2008. Available in: <https://doi.org/10.1016/j.compchemeng.2007.11.009>

KAWALA, Z.; DAKINIEWICZ, P. Influence of evaporation space geometry on rate of distillation in high-vacuum evaporator. **Separation Science and Technology**, v. 37, n. 8, p. 1877–1895, 2002. Available in: <https://doi.org/10.1081/SS-120003049>

KAYIHAN, F.; SANDALL, O. C.; MELLICHAMP, D. A. Simultaneous heat and mass transfer in binary distillation—I: Theory. **Chemical Engineering Science**, v. 30, n. 11, p. 1333–1339, 1975. Available in: [https://doi.org/10.1016/0009-2509\(75\)85062-7](https://doi.org/10.1016/0009-2509(75)85062-7)

KAYIHAN, F.; SANDALL, O. C.; MELLICHAMP, D. A. Simultaneous heat and mass transfer in binary distillation—II: Experimental. **Chemical Engineering Science**, v. 32, n. 7, p. 747–754, 1977. Available in: [https://doi.org/10.1016/0009-2509\(77\)80124-3](https://doi.org/10.1016/0009-2509(77)80124-3)

KEIL, F. J. Process intensification. **Reviews in Chemical Engineering**, v. 34, n. 2, p. 135. Available in: <https://doi.org/10.1515/revce-2017-0085>

KHAN, E. U.; NORDBERG, Å. Thermal integration of membrane distillation in an anaerobic digestion biogas plant – A techno-economic assessment. **Applied Energy**, v. 239, n. September, p. 1163–1174, 2019. Available in: <https://doi.org/10.1016/j.apenergy.2019.02.023>

KHAYET, M.; COJOCARU, C. Artificial neural network modeling and optimization of desalination by air gap membrane distillation. **Separation and Purification Technology**, v. 86, p. 171–182, 2012. Available in: <https://doi.org/10.1016/j.seppur.2011.11.001>

KHAYET, M.; COJOCARU, C. Artificial neural network model for desalination by sweeping gas membrane distillation. **Desalination**, v. 308, p. 102–110, 2013. Available in: <https://doi.org/10.1016/j.desal.2012.06.023>

KHAYET, M.; COJOCARU, C.; ESSALHI, M. Artificial neural network modeling and response surface methodology of desalination by reverse osmosis. **Journal of Membrane Science**, v. 368, n. 1, p. 202–214, 2011. Available in: <https://doi.org/10.1016/j.memsci.2010.11.030>

KIENLE, A.; GROEBEL, M.; GILLES, E. D. Multiple steady states in binary distillation—Theoretical and experimental results. **Chemical Engineering Science**, v. 50, n. 17, p. 2691–2703, 1995. Available in: [https://doi.org/10.1016/0009-2509\(95\)00113-J](https://doi.org/10.1016/0009-2509(95)00113-J)

KIM, Y. H. Design and control of energy-efficient distillation columns. **Korean Journal of Chemical Engineering**, v. 33, n. 9, p. 2513–2521, 2016. Available in:

<https://doi.org/10.1007/s11814-016-0124-4>

KIMMEL, E. J. **Characteristics of a falling film distillation column**. Master thesis (Master of Chemical Engineering) - Department of Chemical Engineering, University of Louisville, Louisville, 1947. Available in: <https://doi.org/10.18297/etd/2000>

KING, C. J. **Separation processes**. 2nd ed. New York: McGraw-Hil, 1980.

KISS, A. A. Distillation technology – still young and full of breakthrough opportunities. **Journal of Chemical Technology & Biotechnology**, v. 89, n. July, p. 479–498, 2013. Available in: <https://doi.org/10.1002/jctb.4262>

KISS, A. A.; IGNAT, R. M. Innovative single step bioethanol dehydration in an extractive dividing-wall column. **Separation and Purification Technology**, v. 98, p. 290–297, 2012. Available in: <https://doi.org/10.1016/j.seppur.2012.06.029>

KISS, A. A.; LANDAETA, S. J. F.; FERREIRA, C. A. I. Towards energy efficient distillation technologies - Making the right choice. **Energy**, v. 47, n. 1, p. 531–542, 2012. Available in: <https://doi.org/10.1016/j.energy.2012.09.038>

KISS, A. A.; OLUJIC, Ž. A review on process intensification in internally heat-integrated distillation columns. **Chemical Engineering and Processing: Process Intensification**, v. 86, p. 125–144, 2014. Available in: <https://doi.org/10.1016/j.cep.2014.10.017>

KISTER, H. Z. **Distillation Design**. New York: McGraw-Hill Education, 1992.

KLETT, R. J. **Entrance effect and film thickness in a vertically falling film**. Thesis (Doctorate in Chemical Engineering) - School of Chemical Engineering, Georgia Institute of Technology, Atlanta, 1965.

KLYKOV, M. V; ALUSHKINA, T. V. Modeling of liquid distribution in multipass rising film evaporators. **Chemical and Petroleum Engineering**, v. 53, n. 9, p. 13–16, 2018. Available in: <https://doi.org/10.1007/s10556-018-0384-4>

KOOIJMAN, H. A.; TAYLOR, R. Modelling mass transfer in multicomponent distillation. **The Chemical Engineering Journal and the Biochemical Engineering Journal**, v. 57, n. 2, p. 177–188, 1995. Available in: [https://doi.org/10.1016/0923-0467\(94\)02952-0](https://doi.org/10.1016/0923-0467(94)02952-0)

KOSUGE, H.; ASANO, K. Mass and heat transfer in ternary distillation of methanol-ethanol-water systems by a wetted-wall column. **Journal of Chemical Engineering of Japan**, v. 15, n. 4, p. 268–273, 1982. Available in: <https://doi.org/10.1252/jcej.15.268>

KOSUGE, H.; ASANO, K. Effect of column length and vapor condensation on heat and mass transfer in ternary distillation by a wetted-wall column. **Kagaku Kogaku Ronbunshu**, v. 10, n. 1, p. 1–6, 1984 a. Available in: <https://doi.org/10.1252/kakoronbunshu.10.1>

KOSUGE, H.; ASANO, K. Simulation of separation performance of ternary distillation by wetted-wall columns. **Journal of Chemical Engineering of Japan**, v. 17, n. 4, p. 400–405, 1984 b. Available in: <https://doi.org/10.1252/jcej.17.400>

KOSUGE, H.; JOHKOH, T.; ASANO, K. Experimental Studies of Diffusion Fluxes of Ternary Distillation of the Acetone-Methanol-Ethanol Systems By a Wetted-Wall Column. **Chemical Engineering Communications**, v. 34, n. 1–6, p. 111–122, 1985. Available in: <https://doi.org/10.1080/00986448508911191>

KOTSIANTIS, S. B.; ZAHARAKIS, I. D.; PINTELAS, P. E. Machine learning: a review of classification and combining techniques. **Artificial Intelligence Review**, v. 26, n. 3, p. 159–190, 2006. Available in: <https://doi.org/10.1007/s10462-007-9052-3>

KRISHNA, R. A film model analysis of non-equimolar distillation of multicomponent mixtures. **Chemical Engineering Science**, v. 32, n. 10, p. 1197–1203, 1977. Available in: [https://doi.org/10.1016/0009-2509\(77\)80052-3](https://doi.org/10.1016/0009-2509(77)80052-3)

KRISHNA, R.; STANDART, G. L. A multicomponent film model incorporating a general matrix method of solution to the Maxwell-Stefan equations. **AIChE Journal**, v. 22, n. 2, p. 383–389, 1976. Available in: <https://doi.org/10.1002/aic.690220222>

KRISHNA, R.; STANDART, G. L. Mass and energy transfer in multicomponent systems. **Chemical Engineering Communications**, v. 3, n. 4–5, p. 201–275, 1979. Available in: <https://doi.org/10.1080/00986447908935865>

KRISHNAMURTHY, R.; TAYLOR, R. A nonequilibrium stage model of multicomponent separation processes. Part I: Model description and method of solution. **AIChE Journal**, v. 31, n. 3, p. 449–456, 1985 a. Available in: <https://doi.org/10.1002/aic.690310312>

KRISHNAMURTHY, R.; TAYLOR, R. A nonequilibrium stage model of multicomponent separation processes. Part II: Comparison with experiment. **AIChE Journal**, v. 31, n. 3, p. 456–465, 1985 b. Available in: <https://doi.org/10.1002/aic.690310313>

KRISHNAMURTHY, R.; TAYLOR, R. A nonequilibrium stage model of multicomponent separation processes. Part III: The influence of unequal design problems component-efficiencies in process. **AIChE Journal**, v. 31, n. 12, p. 1973–1985, 1985 c. Available in: <https://doi.org/10.1002/aic.690311207>

KRUPICZKA, R.; ROTKEGEL, A. An experimental study of diffusional cross-effects in multicomponent mass transfer. **Chemical Engineering Science**, v. 52, n. 6, p. 1007–1017, 1997. Available in: [https://doi.org/10.1016/S0009-2509\(97\)86093-9](https://doi.org/10.1016/S0009-2509(97)86093-9)

KUMAR, A.; MAZUMDER, S. Assessment of the dilute approximation for the prediction of combined heat and mass transfer rates in multi-component systems. **Heat and Mass Transfer**, v. 43, n. 12, p. 1329–1337, 2007. Available in: <https://doi.org/10.1007/s00231-006-0223-6>

KUNDU, P. K.; ELKAMEL, A.; VARGAS, F. M.; FAROOQ, M. U. Genetic algorithm for multi-parameter estimation in sorption and phase equilibria problems. **Chemical Engineering Communications**, v. 205, n. 3, p. 338–349, 2018. Available in: <https://doi.org/10.1080/00986445.2017.1390455>

KUNNAKORN, D.; RIRKSOMBOON, T.; SIEMANOND, K.; AUNGKAVATTANA, P.;

KUANCHERTCHOO, N.; CHUNTANALERG, P.; HEMRA, K.; KULPRATHIPANJA, S.; JAMES, R. B.; WONGKASEMJIT, S. Techno-economic comparison of energy usage between azeotropic distillation and hybrid system for water-ethanol separation. **Renewable Energy**, v. 51, p. 310–316, 2013. Available in: <https://doi.org/10.1016/j.renene.2012.09.055>

LAM, K. F.; LEUNG, C. C. J.; LEI, H. M.; LIN, C. S. K. Economic feasibility of a pilot-scale fermentative succinic acid production from bakery wastes. **Food and Bioproducts Processing**, v. 92, n. 3, p. 282–290, 2014. Available in: <https://doi.org/10.1016/j.fbp.2013.09.001>

LAM, K. F.; SORENSEN, E.; GAVRIILIDIS, A. Review on gas – liquid separations in microchannel devices. **Chemical Engineering Research and Design**, v. 1, n. May, p. 1941–1953, 2013. Available in: <https://doi.org/10.1016/j.cherd.2013.07.031>

LATAOUI, Z.; JEMNI, A. Experimental investigation of a stainless steel two-phase closed thermosyphon. **Applied Thermal Engineering**, v. 121, p. 721–727, 2017. Available in: <https://doi.org/10.1016/j.applthermaleng.2017.04.135>

LEI, Z.; LI, C.; CHEN, B. Extractive distillation: A review. **Separation & Purification Reviews**, v. 32, n. 2, p. 121–213, 2003. Available in: <https://doi.org/10.1081/SPM-120026627>

LESLIE, R. A.; ZHOU, S. S.; MACINGA, D. R. Inactivation of SARS-CoV-2 by commercially available alcohol-based hand sanitizers. **American Journal of Infection Control**, v. 49, n. 3, p. 401–402, 2020. Available in: <https://doi.org/10.1016/j.ajic.2020.08.020>

LEWIS, W. K. The efficiency and design of rectifying columns for binary mixtures. **Industrial & Engineering Chemistry**, v. 14, n. 6, p. 492–496, 1922. Available in: <https://doi.org/10.1021/ie50150a010>

LI, H.; WU, Y.; LI, X.; GAO, X. State-of-the-art of advanced distillation technologies in China. **Chemical Engineering and Technology**, v. 39, n. 5, p. 815–833, 2016 a. Available in: <https://doi.org/10.1002/ceat.201500656>

LI, H.; YI, F.; LI, X.; PAVLENKO, A. N.; GAO, X. Numerical simulation for falling film flow characteristics of refrigerant on the smooth and structured surfaces. **Journal of Engineering Thermophysics**, v. 27, n. 1, p. 1–19, 2018. Available in: <https://doi.org/10.1134/S1810232818010010>

LI, W.; WEI, S.; JIAO, W.; QI, G.; LIU, Y. Modelling of adsorption in rotating packed bed using artificial neural networks (ANN). **Chemical Engineering Research and Design**, v. 114, p. 89–95, 2016 b. Available in: <https://doi.org/10.1016/j.cherd.2016.08.013>

LI, Y.; XU, S. L. DSMC simulation of vapor flow in molecular distillation. **Vacuum**, v. 110, p. 40–46, 2014. Available in: <https://doi.org/10.1016/j.vacuum.2014.08.001>

LIANG, S.; CAO, Y.; LIU, X.; LI, X.; ZHAO, Y.; WANG, Y.; WANG, Y. Insight into pressure-swing distillation from azeotropic phenomenon to dynamic control. **Chemical Engineering Research and Design**, v. 117, p. 318–335, 2017. Available in:

<https://doi.org/10.1016/j.cherd.2016.10.040>

LIANG, Z. (Henry) *et al.* Recent progress and new developments in post-combustion carbon-capture technology with amine based solvents. **International Journal of Greenhouse Gas Control**, v. 40, p. 26–54, 2015. Available in: <https://doi.org/10.1016/j.ijggc.2015.06.017>

LICHTENSTEIN, J.; BUCALO, B. J. **Falling film convective distillation unit with direct contact condensation**. US n. US3214351. Deposit: Feb. 26, 1962. Concession: Oct. 26, 1965.

LINDSAY, A. L.; BROMLEY, L. A. Thermal conductivity of gas mixtures. **Industrial & Engineering Chemistry**, v. 42, n. 8, p. 1508–1511, 1950. Available in: <https://doi.org/10.1021/ie50488a017>

LINDSEY, E. E.; KIEFER, J. M.; HUFFINES, C. L. Distillation in a multitube wetted-wall column. **Industrial & Engineering Chemistry**, v. 44, n. 1, p. 225–231, 1952. Available in: <https://doi.org/10.1021/ie50505a061>

LINEK, V.; MOUCHA, T.; PROKOPOVÁ, E.; REJL, J. F. Simultaneous determination of vapour- and liquid-side volumetric mass transfer coefficients in distillation column. **Chemical Engineering Research and Design**, v. 83, n. 8 A, p. 979–986, 2005. Available in: <https://doi.org/10.1205/cherd.03311>

LINEK, V.; MOUCHA, T.; REJL, F. J. Hydraulic and mass transfer characteristics of packings for absorption and distillation columns. Rauschert-metall-sattel-rings. **Chemical Engineering Research and Design**, v. 79, n. 7, p. 725–732, 2001. Available in: <https://doi.org/10.1205/026387601753192046>

LINEK, V.; SINKULE, J.; BREKKE, K. A critical-evaluation of the use of absorption mass-transfer data for the design of packed distillation-columns. **Chemical Engineering Research & Design**, v. 73, n. 4, p. 398–405, 1995. Available in: <https://www.cheric.org/research/tech/periodicals/view.php?seq=51621>

LIU, F.; WANG, D.; WANG, Q.; GA, J. The optimum design of falling-film evaporator and numerical simulation of distributor. **Procedia Engineering**, v. 205, p. 3867–3872, 2017. Available in: <https://doi.org/10.1016/j.proeng.2017.10.061>

LIU, H.; MA, H. G.; LI, C. S. Experimental Investigation of Falling Film Evaporation on Horizontal Tubes at Low-Pressure. **Advanced Materials Research**. v. 236-238, p. 1572-1575, 2011. Available in: <https://doi.org/10.4028/www.scientific.net/AMR.236-238.1572>

LIU, P.; HO, J. Y.; WONG, T. N.; TOH, K. C. Laminar film condensation inside and outside vertical diverging/converging small channels: A theoretical study. **International Journal of Heat and Mass Transfer**, v. 149, p. 119193, 2020. Available in: <https://doi.org/10.1016/j.ijheatmasstransfer.2019.119193>

LIU, X.; QIAN, J. Modeling, control, and optimization of ideal internal thermally coupled distillation columns. **Chemical Engineering & Technology**, v. 23, n. 3, p. 235–241, 2000. Available in: [https://doi.org/10.1002/\(SICI\)1521-4125\(200003\)23:3<235::AID-CEAT235>3.0.CO;2-K](https://doi.org/10.1002/(SICI)1521-4125(200003)23:3<235::AID-CEAT235>3.0.CO;2-K)

LIU, Z.-Y.; JOBSON, M. The effect of operating pressure on distillation column throughput. **Computers & Chemical Engineering**, v. 23, p. S831–S834, 1999. Available in: [https://doi.org/10.1016/S0098-1354\(99\)80204-X](https://doi.org/10.1016/S0098-1354(99)80204-X)

LU, Y.; STEHMANN, F.; YUAN, S.; SCHOLL, S. Falling film on a vertical flat plate – Influence of liquid distribution and fluid properties on wetting behavior. **Applied Thermal Engineering**, v. 123, p. 1386–1395, 2017. Available in: <https://doi.org/10.1016/j.applthermaleng.2017.05.110>

LUEPRASITSAKUL, V.; HASEBE, S.; HASHIMOTO, I.; TAKAMATSU, T. Study of energy efficiency of a wetted-wall distillation column with internal heat integration. **Journal of Chemical Engineering of Japan**, v. 23, n. 5, p. 580–587, 1990. Available in: <https://doi.org/10.1252/jcej.23.580>

LUKACH, Y. Y.; RADCHENKO, L. B.; TANANAYIKO, Y. M. Determination of the average thickness of a film of water during gravitation of flow along the exterior surface of vertical polymeric pipes. **International Chemical Engineering**, v. 12, p. 517–519, 1972.

LUTIŠAN, J.; CVENGROŠ, J. Mean free path of molecules on molecular distillation. **The Chemical Engineering Journal and the Biochemical Engineering Journal**, v. 56, n. 2, p. 39–50, 1995. Available in: [https://doi.org/10.1016/0923-0467\(94\)02857-7](https://doi.org/10.1016/0923-0467(94)02857-7)

LUYBEN, W. L. Distillation column pressure selection. **Separation and Purification Technology**, v. 168, p. 62–67, 2016. Available in: <https://doi.org/10.1016/j.seppur.2016.05.015>

MACEDONIO, F.; ALI, A.; POERIO, T.; EL-SAYED, E.; DRIOLI, E.; ABDEL-JAWAD, M. Direct contact membrane distillation for treatment of oilfield produced water. **Separation and Purification Technology**, v. 126, p. 69–81, 2014. Available in: <https://doi.org/10.1016/j.seppur.2014.02.004>

MACIVER, A.; HINGE, S.; ANDERSEN, B. J.; NIELSEN, J. B. New trend in desalination for Japanese nuclear power plants, based on multiple effect distillation, with vertical titanium plate falling film heat transfer configuration. **Desalination**, v. 182, n. 1, p. 221–228, 2005. Available in: <https://doi.org/10.1016/j.desal.2005.04.014>

MADAENI, S. S.; HASANKIADEH, N. T.; KURDIAN, A. R.; RAHIMPOUR, A. Modeling and optimization of membrane fabrication using artificial neural network and genetic algorithm. **Separation and Purification Technology**, v. 76, n. 1, p. 33–43, 2010. Available in: <https://doi.org/10.1016/j.seppur.2010.09.017>

MAHMOOD, A.; EQAN, M.; PERVEZ, S.; ALGHAMDI, H. A.; TABINDA, A. B.; YASAR, A.; BRINDHADEVI, K.; PUGAZHENDHI, A. COVID-19 and frequent use of hand sanitizers; human health and environmental hazards by exposure pathways. **Science of the Total Environment**, v. 742, p. 140561, 2020. Available in: <https://doi.org/10.1016/j.scitotenv.2020.140561>

MAIORELLA, B. L.; BLANCH, H. W.; WILKE, C. R. Economic evaluation of alternative ethanol fermentation processes. **Biotechnology and Bioengineering**, v. 26, n. 9, p. 1003–

1025, 1984. Available in: <https://doi.org/10.1002/bit.260260902>

MANENTI, F.; GALEAZZI, A.; BISOTTI, F.; PRIFTI, K.; DELL'ANGELO, A.; DI PRETORO, A.; ARIATTI, C. Analogies between SARS-CoV-2 infection dynamics and batch chemical reactor behavior. **Chemical Engineering Science**, v. 227, p. 115918, 2020. Available in: <https://doi.org/10.1016/j.ces.2020.115918>

MANGILI, P. V.; SANTOS, L. S.; PRATA, D. M. A systematic methodology for comparing the sustainability of process systems based on weighted performance indicators. **Computers & Chemical Engineering**, v. 130, p. 106558, 2019. Available in: <https://doi.org/10.1016/j.compchemeng.2019.106558>

MANOUCHEHRI, R.; BANISTER, C. J.; COLLINS, M. R. Impact of small tilt angles on the performance of falling film drain water heat recovery systems. **Energy and Buildings**, v. 102, p. 181–186, 2015. Available in: <https://doi.org/10.1016/j.enbuild.2015.05.024>

MANOVA, S.; ASIRVATHAM, L. G.; NIMMAGADDA, R.; BOSE, J. R.; WONGWISES, S. Cooling of high heat flux electronic devices using ultra-thin multiport minichannel thermosyphon. **Applied Thermal Engineering**, v. 169, p. 114669, 2020. Available in: <https://doi.org/10.1016/j.applthermaleng.2019.114669>

MANTELLI, M. B. H. Thermosyphon technology for industrial applications. *In*: VASILIEV, L. L.; KAKAC, S. (org.). **Heat Pipes and Solid Sorption Transformations - Fundamentals and Practical Applications**. 1st Edition. Boca Raton: CRC Press, 2013. p. 54. Available in: <https://doi.org/doi.org/10.1201/b14864>

MANTELLI, M. B. H.; ÂNGELO, W. B.; BORGES, T. Performance of naphthalene thermosyphons with non-condensable gases – Theoretical study and comparison with data. **International Journal of Heat and Mass Transfer**, v. 53, n. 17, p. 3414–3428, 2010. Available in: <https://doi.org/10.1016/j.ijheatmasstransfer.2010.03.041>

MARANGONI, C. *et al.* Falling film distillation column with heat transfer by means of a vapor chamber. Part II: operation with a temperature profile. **Chemical Engineering Communications**, v. 206, n. 8, p. 1006–1014, 2019 a. Available in: <https://doi.org/10.1080/00986445.2018.1542255>

MARANGONI, C.; MENEGUELO, A. P.; TELEKEN, J. G.; WERLED, L. O.; MILANEZ, K. W.; MANTELLI, M. B. H.; QUADRI, M. B.; BOLZAN, A.; SANTOS, M. C. dos; MEDINA, L. C.; MACHADO, R. A. F. Falling film distillation column with heat transfer by means of a vapor chamber – part I: isothermal operation. **Chemical Engineering Communications**, v. 206, n. 8, p. 994–1005, 2019 b. Available in: <https://doi.org/10.1080/00986445.2018.1542250>

MARANGONI, C.; MENEGUELO, P. A.; TELEKEN, G. J.; PARISOTTO, I. G. B.; WERLE, L. O.; MACHADO, R. A. F.; DOS SANTOS, M. C.; GOMES, A. O.; MEDINA, L. C. New configuration of a distillation process with reduced dimensions. **Chemical Engineering Transactions**, v. 24, n. 2000, p. 799–804, 2011. Available in: <https://doi.org/10.3303/CET1124134>

MARTIN, J. J. Wetted-Wall Tube-Plate Column. **Industrial & Engineering Chemistry**, v. 44, n. 4, p. 920–924, 1952. Available in: <https://doi.org/10.1021/ie50508a057>

MARTINS, P. F.; BATISTELLA, C. B.; MACIEL-FILHO, R.; WOLF-MACIEL, M. R. Comparison of two different strategies for tocopherols enrichment using a molecular distillation process. **Industrial & Engineering Chemistry Research**, v. 45, n. 2, p. 753–758, 2006. Available in: <https://doi.org/10.1021/ie050614i>

MATALLAH, H.; NEWTON, W.; JAMES, D.; CAMERON, I.; SIENZ, J.; ROMOCKI, S.; LAVERY, N. P. The development of a sub-atmospheric two-phase thermosyphon natural gas preheater using a lumped capacitance model and comparison with experimental results. **Applied Thermal Engineering**, v. 104, p. 767–778, 2016. Available in: <https://doi.org/10.1016/j.applthermaleng.2016.05.078>

MATSUDA, A.; HONDA, K.; OKADA, K.; MUNAKATA, T. Distillation performance of wetted-wall column under reduced pressure. **Kagaku Kogaku Ronbunshu**, v. 6, n. 5, p. 489–494, 1980. Available in: <https://doi.org/10.1252/kakoronbunshu.6.489>

MAZIERO, E. V.; SALLES, R. B.; TOVAR, L. P.; TANABE, E. H.; BERTUOL, D. A. Fractionation of polyethylene wax by pilot-scale molecular distillation: new insights on process development. **Chemical Engineering Research and Design**, v. 152, p. 201–215, 2019. Available in: <https://doi.org/10.1016/j.cherd.2019.09.041>

MAZUR, J. E. Mathematical Models and the Experimental Analysis of Behavior. **Journal of the Experimental Analysis of Behavior**, v. 85, n. 2, p. 275–291, 2006. Available in: <https://doi.org/10.1901/jeab.2006.65-05>

MEDINA, L. C.; SANTOS, M. C.; MACHADO, R. A. F.; MANTELLI, M.; MARANGONI, C.; MENEGUELO, A. P.; MILANEZ, K. W. **Equipamento e processo de destilação com controle de energia pela demanda**. Brasil n. BR10201402976. Concession: 2014.

MELLO, G. N.; BATTISTI, R.; URRUTH, N. S.; MACHADO, R. A. F.; MARANGONI, C. New distributed-action control strategy with simultaneous heating and cooling in trays of a pilot-scale diabatic distillation column. **Chemical Engineering Research and Design**, 2020. Available in: <https://doi.org/10.1016/j.cherd.2020.05.001>

MELNICK, C.; HODES, M.; ZISKIND, G.; CLEARY, M.; MANNO, V. P. Thermoelectric module-variable conductance heat pipe assemblies for reduced power temperature control. **IEEE Transactions on Components, Packaging and Manufacturing Technology**, v. 2, n. 3, p. 474–482, 2012. Available in: <https://doi.org/10.1109/TCPMT.2011.2178413>

MILANEZ, F.; MANTELLI, M. B. H. Heat transfer limit due to pressure drop of a two-phase loop thermosyphon. **Heat Pipe Science and Technology, An International Journal**, v. 1, n. 10, p. 237–250, 2010. Available in: <https://doi.org/10.1615/HeatPipeScieTech.2011003082>

MOHAMED, E. S.; BOUTIKOS, P.; MATHIOULAKIS, E.; BELESSIOTIS, V. Experimental evaluation of the performance and energy efficiency of a Vacuum Multi-Effect Membrane Distillation system. **Desalination**, v. 408, p. 70–80, 2017. Available in: <https://doi.org/10.1016/j.desal.2016.12.020>

MOLZ, M.; MANTELLI, M. B. H.; MILANEZ, F. Transient Modeling of a Closed Two-Phase Thermosyphon for Heat Exchanger Applications. *In: 13th International Heat Pipe Conference (13th IHPC)*. Shanghai, China, 2004. p. 21–25.

MONCADA, J.; EL-HALWAGI, M. M.; CARDONA, C. A. Techno-economic analysis for a sugarcane biorefinery: Colombian case. **Bioresource Technology**, v. 135, p. 533–543, 2013. Available in: <https://doi.org/10.1016/j.biortech.2012.08.137>

MONNIER, H.; KANE, A.; FALK, L. Intensification of heat transfer during evaporation of a falling liquid film in vertical microchannels — Experimental investigations. **Chemical Engineering Science**, v. 75, p. 152–166, 2012. Available in: <https://doi.org/10.1016/j.ces.2012.03.008>

MORISON, K. R.; BROOME, S. R. Upward vapour flows in falling film evaporators and implications for distributor design. **Chemical Engineering Science**, v. 114, p. 1–8, 2014. Available in: <https://doi.org/10.1016/j.ces.2014.04.015>

MORISON, K. R.; WORTH, Q. A. G.; O'DEA, N. P. Minimum wetting and distribution rates in falling film evaporators. **Food and Bioprocess Processing**, v. 3, n. 4, p. 302–310, 2006. Available in: <https://doi.org/10.1205/fbp06031>

MOSCHOU, P.; CROON, M. H. J. M.; DER SCHAAF, J. van; SCHOUTEN, J. C. Liquid flow rate effects during partial evaporation in a falling film micro contactor. **Chemical Engineering and Processing: Process Intensification**, v. 69, p. 95–103, 2013. Available in: <https://doi.org/10.1016/j.cep.2013.03.007>

MUELLER, W. A. **Fractional distillation column with inclined wall sections**. United States n. US3249516. Deposited: May 15, 1962. Concession: May 3, 1966.

MUHAMMAD, N. I. S.; ROSENTRATER, K. A. Economic assessment of bioethanol recovery using membrane distillation for food waste fermentation. **Bioengineering**, v. 7, n. 1, p. 1–10, 2020. Available in: <https://doi.org/10.3390/bioengineering7010015>

MUJTABA, I. M. Optimization of batch extractive distillation processes for separating close boiling and azeotropic mixtures. **Chemical Engineering Research and Design**, v. 77, n. 7, p. 588–596, 1999. Available in: <https://doi.org/10.1205/026387699526629>

MUNAKATA, T.; MATSUDA, A. Operating range of falling film column in vacuum distillation. **Journal of Chemical Engineering of Japan**, v. 6, n. 1, p. 58–63, 1973. Available in: <https://doi.org/10.1252/jcej.6.58>

MUNAKATA, T.; MATSUDA, A.; WATANABE, K. Experimental study of operating limits of falling film column in vacuum distillation. **Journal of Chemical Engineering of Japan**, v. 7, n. 4, p. 316–319, 1974. Available in: <https://doi.org/10.1252/jcej.7.316>

MURPHREE, E. V. Rectifying Column Calculations. **Industrial & Engineering Chemistry**, v. 17, n. 7, p. 747–750, 1925. Available in: <https://doi.org/10.1021/ie50187a044>

MUSTAFA, M. F.; SAMAD, N. A. F. A.; IBRAHIM, K. A.; HAMID, M. K. A. Methodology

development for designing energy efficient distillation column systems. **Energy Procedia**, v. 61, p. 2550–2553, 2014. Available in: <https://doi.org/10.1016/j.egypro.2014.12.043>

NAG, S.; ANANTHAKRISHNA, G.; MAITI, P. K.; YASHONATH, S. Separating hydrocarbon mixtures by driving the components in opposite directions: high degree of separation factor and energy efficiency. **Physical Review Letters**, v. 124, n. 25, p. 255901, 2020. Available in: <https://doi.org/10.1103/PhysRevLett.124.255901>

NAIR, R. R.; G, U. B. B.; RAYKAR, A. Performance investigation of vapour recompressed batch distillation for separating ternary wide boiling constituents. **Resource-Efficient Technologies**, v. 3, n. 4, p. 452–458, 2017. Available in: <https://doi.org/10.1016/j.refit.2017.04.007>

NAKAIWA, M.; HUANG, K.; ENDO, A.; OHMORI, T.; AKIYA, T.; TAKAMATSU, T. Internally Heat-Integrated Distillation Columns: A Review. **Chemical Engineering Research and Design**, v. 81, n. January, p. 162–177, 2003. Available in: <https://doi.org/10.1205/026387603321158320>

NAKAIWA, M.; HUANG, K.; OWA, M.; AKIYA, T.; NAKANE, T.; SATO, M.; TAKAMATSU, T. Energy savings in heat-integrated distillation columns. **Energy**, v. 22, n. 6, p. 621–625, 1997. Available in: [https://doi.org/https://doi.org/10.1016/S0360-5442\(96\)00157-0](https://doi.org/https://doi.org/10.1016/S0360-5442(96)00157-0)

NAKANISHI, T.; ADACHI, N.; NISHIDA, N.; IWAKABE, K.; HORIUCHI, K.; NAKAIWA, M. Basic Design of a Double-Pipe Unit Type Internally Heat Integrated Distillation Column (HIDiC). *In*: 2008, **Annual AIChE Meeting**. Philadelphia, PA. p. 16–21.

NAKASHIMA, R. N.; DE OLIVEIRA JUNIOR, S. Comparative exergy assessment of vinasse disposal alternatives: Concentration, anaerobic digestion and fertirrigation. **Renewable Energy**, v. 147, p. 1969–1978, 2020. Available in: <https://doi.org/10.1016/j.renene.2019.09.124>

NANDAGOPAL, M. S. G.; ABRAHAM, E.; SELVARAJU, N. Advanced neural network prediction and system identification of liquid-liquid flow patterns in circular microchannels with varying angle of confluence. **Chemical Engineering Journal**, v. 309, p. 850–865, 2017. Available in: <https://doi.org/10.1016/j.cej.2016.10.106>

NARVÁEZ-ROMO, B.; CHHAY, M.; ZAVALA-AGUILAR, E. W.; SIMÕES-MOREIRA, J. R. A critical review of heat and mass transfer correlations for LiBr-H₂O and NH₃-H₂O absorption refrigeration machines using falling liquid film technology. **Applied Thermal Engineering**, v. 123, n. August, p. 1079–1095, 2017. Available in: <https://doi.org/10.1016/j.applthermaleng.2017.05.092>

NEVES, F. J. M.; SILVA, D. C. M.; OLIVEIRA, N. M. C. A robust strategy for optimizing complex distillation columns. **Computers & Chemical Engineering**, v. 29, n. 6, p. 1457–1471, 2005. Available in: <https://doi.org/10.1016/j.compchemeng.2005.02.002>

NGAN, D. Y.-K.; SANBORN, R. A.; STEIN, L. E.; RAUL JASSO GARCIA, S.; GRIESHOP, V. J. **Wetted wall vapor/liquid separator**. USA n. US6376732. Deposited:

Mar. 8, 2000. Concession: Apr. 23, 2002.

NGUYEN, V. D.; AURESENIA, J.; KOSUGE, H.; TAN, R. R.; BRONDIAL, Y. Vacuum fermentation integrated with separation process for ethanol production. **Biochemical Engineering Journal**, v. 55, n. 3, p. 208–214, 2011. Available in: <https://doi.org/10.1016/j.bej.2011.05.001>

NIELSEN, C. H. E.; KIIL, S.; THOMSEN, H. W.; DAM-JOHANSEN, K. Mass transfer in wetted-wall columns: Correlations at high Reynolds numbers. **Chemical Engineering Science**, v. 53, n. 3, p. 495–503, 1998. Available in: [https://doi.org/10.1016/S0009-2509\(97\)00320-5](https://doi.org/10.1016/S0009-2509(97)00320-5)

NODA, H.; TAKAMATSU, T.; ASO, K.; NAKANISHI, T.; YOSHIDA, K.; NAKAIWA, M.; MUKAIDA, T.; KURATANI, N. Development on a coaxial heat integrated distillation column (HIDiC). **Korean Journal of Chemical Engineering**, v. 17, n. 5, p. 593–596, 2000. Available in: <https://doi.org/10.1007/BF02707172>

NOIE, S. H. Heat transfer characteristics of a two-phase closed thermosyphon. **Applied Thermal Engineering**, v. 25, n. 4, p. 495–506, 2005. Available in: <https://doi.org/10.1016/j.applthermaleng.2004.06.019>

NOOR, I.; MARTIN, A.; DAHL, O. Techno-economic system analysis of membrane distillation process for treatment of chemical mechanical planarization wastewater in nano-electronics industries. **Separation and Purification Technology**, v. 248, n. January, p. 117013, 2020. Available in: <https://doi.org/10.1016/j.seppur.2020.117013>

NORILER, D.; MEIER, H. F.; BARROS, A. A. C.; MACIEL, M. R. W. Thermal fluid dynamics analysis of gas – liquid flow on a distillation sieve tray. **Chemical Engineering Journal**, v. 136, n. 2–3, p. 133–143, 2008. Available in: <https://doi.org/10.1016/j.cej.2007.03.023>

NOSOKO, T.; MIYARA, A.; NAGATA, T. Characteristics of falling film flow on completely wetted horizontal tubes and the associated gas absorption. **International Journal of Heat and Mass Transfer**, v. 45, n. 13, p. 2729–2738, 2002. Available in: [https://doi.org/10.1016/S0017-9310\(01\)00357-X](https://doi.org/10.1016/S0017-9310(01)00357-X)

NULL, H. R. Heat pumps in distillation. **Chemical Engineering Progress**, v. 72, n. 7, p. 58–64, 1976. Available in: <https://www.osti.gov/biblio/7239419>

OCHOA-ESTOPIER, L. M.; JOBSON, M.; SMITH, R. The use of reduced models for design and optimisation of heat-integrated crude oil distillation systems. **Energy**, v. 75, p. 5–13, 2014. Available in: <https://doi.org/10.1016/j.energy.2014.06.043>

OFFEMAN, R. D.; STEPHENSON, S. K.; ROBERTSON, G. H.; ORTS, W. J. Solvent extraction of ethanol from aqueous solutions. I. Screening methodology for solvents. **Industrial and Engineering Chemistry Research**, v. 44, n. 17, p. 6789–6796, 2005. Available in: <https://doi.org/10.1021/ie0500319>

OLBRICHT, M.; LUKE, A. Falling film evaporation of aqueous lithium bromide solution at

low pressure. **Heat and Mass Transfer**, v. 54, n. 8, p. 2507–2520, 2018. Available in: <https://doi.org/10.1007/s00231-018-2409-0>

OLDFIELD, J. W.; TODD, B. Environmental aspects of corrosion in MSF and RO desalination plants. **Desalination**, v. 108, n. 1–3, p. 27–36, 1997. Available in: [https://doi.org/10.1016/S0011-9164\(97\)00005-2](https://doi.org/10.1016/S0011-9164(97)00005-2)

OLUJIĆ, Ž. Chapter 1 - Types of Distillation Column Internals. In: GÓRAK, A.; OLUJIĆ, Ž. (org.). **Distillation**. Boston: Academic Press, 2014. p. 1–34. *E-book*. Available in: <https://doi.org/10.1016/B978-0-12-386878-7.00001-2>

OLUJIC, Z.; JODECKE, M.; SHILKIN, A.; SCHUCH, G.; KAIBEL, B. Equipment improvement trends in distillation. **Chemical Engineering and Processing: Process Intensification**, v. 48, n. 6, p. 1089–1104, 2009. Available in: <https://doi.org/10.1016/j.cep.2009.03.004>

OLUMAYEGUN, O.; WANG, M. Dynamic modelling and control of supercritical CO₂ power cycle using waste heat from industrial processes. **Fuel**, v. 249, p. 89–102, 2019. Available in: <https://doi.org/10.1016/j.fuel.2019.03.078>

OVEJERO, G.; GRIEKEN, R. Van; RODRIGUEZ, L.; VALVERDE, J. L. The use of gas absorption correlations for mass transfer coefficients in distillation processes. **International Journal of Heat and Mass Transfer**, v. 35, n. 11, p. 2963–2968, 1992. Available in: [https://doi.org/10.1016/0017-9310\(92\)90316-K](https://doi.org/10.1016/0017-9310(92)90316-K)

PALENZUELA, P.; MIRALLES-CUEVAS, S.; CABRERA-REINA, A.; CORNEJO-PONCE, L. Techno-economic assessment of a multi-effect distillation plant installed for the production of irrigation water in Arica (Chile). **Science of the Total Environment**, v. 643, p. 423–434, 2018. Available in: <https://doi.org/10.1016/j.scitotenv.2018.06.183>

PANAGOPOULOS, A. Process simulation and techno-economic assessment of a zero liquid discharge/multi-effect desalination/thermal vapor compression (ZLD/MED/TVC) system. **International Journal of Energy Research**, v. 44, n. 1, p. 473–495, 2020 a. Available in: <https://doi.org/10.1002/er.4948>

PANAGOPOULOS, A. Techno-economic evaluation of a solar multi-effect distillation/thermal vapor compression hybrid system for brine treatment and salt recovery. **Chemical Engineering and Processing - Process Intensification**, v. 152, n. December 2019, p. 107934, 2020 b. Available in: <https://doi.org/10.1016/j.cep.2020.107934>

PARISOTTO, I. G. B. **Destilação por Película para Misturas Binárias**. 2013. Dissertation (Master in Chemical Engineering) - Department of Chemical Engineering, Federal University of Santa Catarina, Florianópolis, 2013.

PARK, H.; KIM, Y.; JO, S.; CHOI, J.; YANG, S.; HEE, M.; KOOK, D. Heat and mass transfer of binary distillation in a vertical wetted-wall column. **Chemical Engineering Research and Design**, v. 128, p. 49–58, 2017. Available in: <https://doi.org/10.1016/j.cherd.2017.09.032>

PARK, Y. J.; KANG, H. K.; KIM, C. J. Heat transfer characteristics of a two-phase closed thermosyphon to the fill charge ratio. **International Journal of Heat and Mass Transfer**, v. 45, n. 23, p. 4655–4661, 2002. Available in: [https://doi.org/10.1016/S0017-9310\(02\)00169-2](https://doi.org/10.1016/S0017-9310(02)00169-2)

PARK, Y. J.; KIM, C. J.; HONG, S. E. A study of the heat transfer characteristics of an FC-72(C6F14) two-phase closed thermosyphon with helical grooves on the inner surface. **Heat Transfer Engineering**, v. 25, n. 8, p. 60–68, 2004. Available in: <https://doi.org/10.1080/01457630490520293>

PASQUINI, C.; HESPANHOL, M. C.; CRUZ, K. A. M. L.; PEREIRA, A. F. Monitoring the quality of ethanol-based hand sanitizers by low-cost near-infrared spectroscopy. **Microchemical Journal**, v. 159, n. July, 2020. Available in: <https://doi.org/10.1016/j.microc.2020.105421>

PEHLIVAN, H.; ÖZDEMİR, M. Experimental and theoretical investigations of falling film evaporation. **Heat and Mass Transfer**, v. 48, n. 6, p. 1071–1079, 2012. Available in: <https://doi.org/10.1007/s00231-011-0962-x>

PERUZZO, T. **Avaliação da desidratação de trietilenoglicol através do processo de destilação por filme descendente**. 2013. Dissertation (Master in Chemical Engineering) - Department of Chemical Engineering, Federal University of Santa Catarina, Florianópolis, 2013.

PETREK, J. P.; CANTRELL, C. M. **Multiple effect thin film distillation system and process**. USA n. US4402793. Deposited: Feb. 19, 1980. Concession: Sep. 6, 1983.

PICCINNO, F.; HISCHIER, R.; SEEGER, S.; SOM, C. From laboratory to industrial scale: a scale-up framework for chemical processes in life cycle assessment studies. **Journal of Cleaner Production**, v. 135, p. 1085–1097, 2016. Available in: <https://doi.org/10.1016/j.jclepro.2016.06.164>

PIRES, A. P. B. **Recuperação de monoetilenoglicol em coluna de destilação de película descendente**. 2016. Dissertation (Master in Chemical Engineering) - Department of Chemical Engineering, Federal University of Santa Catarina, Florianópolis, 2016.

PIRES, A. P. B.; DA SILVA FILHO, V. F.; ALVES, J. L. F.; MARANGONI, C.; BOLZAN, A.; MACHADO, R. A. F. Application of a new pilot-scale distillation system for monoethylene glycol recovery using an energy saving falling film distillation column. **Chemical Engineering Research and Design**, v. 153, n. 263–275, 2020. Available in: <https://doi.org/10.1016/j.cherd.2019.10.033>

PONCE-ORTEGA, J. M.; AL-THUBAITI, M. M.; EL-HALWAGI, M. M. Process intensification: New understanding and systematic approach. **Chemical Engineering and Processing: Process Intensification**, v. 53, p. 63–75, 2012. Available in: <https://doi.org/10.1016/j.cep.2011.12.010>

PONCE, G. H. S. F.; MOREIRA NETO, J.; DE JESUS, S. S.; MIRANDA, J. C. de C.; MACIEL FILHO, R.; DE ANDRADE, R. R.; WOLF MACIEL, M. R. Sugarcane molasses fermentation with in situ gas stripping using low and moderate sugar concentrations for

ethanol production: Experimental data and modeling. **Biochemical Engineering Journal**, v. 110, p. 152–161, 2016. Available in: <https://doi.org/10.1016/j.bej.2016.02.007>

PORRU, M.; BARATTI, R.; ALVAREZ, J. Energy saving through control in an industrial multicomponent distillation column. **IFAC-PapersOnLine**, v. 48, n. 8, p. 1138–1143, 2015. Available in: <https://doi.org/10.1016/j.ifacol.2015.09.121>

PORTALSKI, S. Eddy formation in film flow down a vertical plate. **Industrial & Engineering Chemistry Fundamentals**, v. 3, n. 1, p. 49–53, 1964. Available in: <https://doi.org/10.1021/i160009a009>

PORTALSKI, S.; CLEGG, A. J. Interfacial area increase in rippled film flow on wetted wall columns. **Chemical Engineering Science**, v. 26, n. 6, p. 773–784, 1971. Available in: [https://doi.org/10.1016/0009-2509\(71\)83039-7](https://doi.org/10.1016/0009-2509(71)83039-7)

PORTHA, J.-F.; FALK, L.; COMMENGE, J.-M. Local and global process intensification. **Chemical Engineering and Processing: Process Intensification**, v. 84, p. 1–13, 2014. Available in: <https://doi.org/10.1016/j.cep.2014.05.002>

POSSAMAI, F. C.; SETTER, I.; VASILIEV, L. L. Miniature heat pipes as compressor cooling devices. **Applied Thermal Engineering**, v. 29, n. 14, p. 3218–3223, 2009. Available in: <https://doi.org/10.1016/j.applthermaleng.2009.04.030>

PROVERBIO, E.; BONACCORSI, L. M. Erosion-corrosion of a stainless steel distillation column in food industry. **Engineering Failure Analysis**, v. 9, n. 6, p. 613–620, 2002. Available in: [https://doi.org/10.1016/S1350-6307\(02\)00027-4](https://doi.org/10.1016/S1350-6307(02)00027-4)

QIU, Q.; ZHANG, X.; QUAN, S.; ZHU, X.; SHEN, S. 3D numerical study of the liquid film distribution on the surface of a horizontal-tube falling-film evaporator. **International Journal of Heat and Mass Transfer**, v. 124, p. 943–952, 2018. Available in: <https://doi.org/10.1016/j.ijheatmasstransfer.2018.04.020>

QUERINO, M. V.; MACHADO, R. A. F.; MARANGONI, C. Energy and exergetic evaluation of the multicomponent separation of petrochemical naphtha in falling film distillation columns. **Brazilian Journal of Chemical Engineering**, v. 36, n. 3, p. 1357–1365, 2019. Available in: <https://doi.org/10.1590/0104-6632.20190363s20180379>

QUERINO, M. V.; MARANGONI, C.; MACHADO, R. A. F. Indirect series of falling film distillation column to process synthetic naphtha. **Chemical Engineering Transactions**, v. 69, p. 679–684, 2018. Available in: <https://doi.org/10.3303/CET1869114>

QUINTERO, J. A.; MONCADA, J.; CARDONA, C. A. Techno-economic analysis of bioethanol production from lignocellulosic residues in Colombia: A process simulation approach. **Bioresource Technology**, v. 139, p. 300–307, 2013. Available in: <https://doi.org/10.1016/j.biortech.2013.04.048>

RAHIMI, B.; MAY, J.; CHRIST, A.; REGENAUER-LIEB, K.; CHUA, H. T. Thermo-economic analysis of two novel low grade sensible heat driven desalination processes. **Desalination**, v. 365, p. 316–328, 2015. Available in:

<https://doi.org/10.1016/j.desal.2015.03.008>

RAICHLE, L.; BILLET, R. Vacuum rectification in high efficiency equipment. **Industrial & Engineering Chemistry**, v. 57, n. 4, p. 52–60, 1965. Available in: <https://doi.org/10.1021/ie50664a009>

RANDALL, D. G. **Fractional distillation apparatus**. United States n. US2608387. Deposited: Aug. 15, 1949. Concession: Aug. 26, 1952.

RANJAN, K. R.; KAUSHIK, S. C. Energy, exergy and thermo-economic analysis of solar distillation systems: A review. **Renewable and Sustainable Energy Reviews**, v. 27, p. 709–723, 2013. Available in: <https://doi.org/10.1016/j.rser.2013.07.025>

RANJAN, K. R.; KAUSHIK, S. C. Economic feasibility evaluation of solar distillation systems based on the equivalent cost of environmental degradation and high-grade energy savings. **International Journal of Low-Carbon Technologies**, v. 11, n. 1, p. 8–15, 2014. Available in: <https://doi.org/10.1093/ijlct/ctt048>

RASSAMAKIN, B.; KHAIRNASOV, S.; ZARIPOV, V.; RASSAMAKIN, A.; ALFOROVA, O. Aluminum heat pipes applied in solar collectors. **Solar Energy**, v. 94, n. August, p. 145–154, 2013. Available in: <https://doi.org/10.1016/j.solener.2013.04.031>

REAY, D.; MCGLLEN, R.; KEW, P. **Heat Pipes: Theory, Design and Applications**. Sixth ed. Amsterdam: Elsevier Science, 2013. Available in: <https://doi.org/10.1016/C2011-0-08979-2>

REAY, D.; RAMSHAW, C.; HARVEY, A. **Process intensification: engineering for efficiency, sustainability and flexibility**. 2nd ed. Waltham, MA: Butterworth-Heinemann, 2013. Available in: <https://doi.org/10.1016/C2012-0-00253-0>

REDDY, K. S.; SHARON, H. Energy-environment-economic investigations on evacuated active multiple stage series flow solar distillation unit for potable water production. **Energy Conversion and Management**, v. 151, n. September, p. 259–285, 2017. Available in: <https://doi.org/10.1016/j.enconman.2017.08.064>

REJL, F. J.; HAIDL, J.; VALENZ, L.; MOUCHA, T.; SCHULTES, M. Analogy of absorption and distillation processes. Wetted-wall column study. **Chemical Engineering Science**, v. 153, p. 146–154, 2016. Available in: <https://doi.org/10.1016/j.ces.2016.07.021>

REJL, J. F.; VALENZ, L.; LINEK, V. “Profile Method” for the measurement of $k_L a$ and $k_V a$ in distillation columns measured along the column. **Industrial & Engineering Chemistry Research**, v. 49, n. 9, p. 4383–4398, 2010. Available in: <https://doi.org/10.1021/ie901690m>

RIBATSKI, G.; JACOBI, A. M. Falling-film evaporation on horizontal tubes—a critical review. **International Journal of Refrigeration**, v. 28, n. 5, p. 635–653, 2005. Available in: <https://doi.org/10.1016/j.ijrefrig.2004.12.002>

RICHTER, H.; MARTIN, M. E.; ANGENENT, L. T. A two-stage continuous fermentation system for conversion of syngas into ethanol. **Energies**, v. 6, n. 8, p. 3987–4000, 2013.

Available in: <https://doi.org/10.3390/en6083987>

RIVERA-ORTEGA, P.; PICÓN-NÚÑEZ, M.; TORRES-REYES, E.; GALLEGOS-MUÑOZ, A. Thermal integration of heat pumping systems in distillation columns. **Applied Thermal Engineering**, v. 19, n. 8, p. 819–829, 1999. Available in: [https://doi.org/10.1016/S1359-4311\(98\)00088-X](https://doi.org/10.1016/S1359-4311(98)00088-X)

RODRÍGUEZ, M.; LI, P. Z.; DÍAZ, I. A control strategy for extractive and reactive dividing wall columns. **Chemical Engineering and Processing: Process Intensification**, v. 113, p. 14–19, 2017. Available in: <https://doi.org/10.1016/j.cep.2016.10.004>

RONG, B.-G.; KRASLAWSKI, A.; NYSTRÖM, L. Design and synthesis of multicomponent thermally coupled distillation flowsheets. **Computers & Chemical Engineering**, v. 25, n. 4, p. 807–820, 2001. Available in: [https://doi.org/10.1016/S0098-1354\(01\)00673-1](https://doi.org/10.1016/S0098-1354(01)00673-1)

RUAN, J.; LIU, J.; XU, X.; CHEN, J.; LI, G. Experimental study of an R290 split-type air conditioner using a falling film condenser. **Applied Thermal Engineering**, v. 140, p. 325–333, 2018. Available in: <https://doi.org/10.1016/j.applthermaleng.2018.05.022>

RUSSO, V.; MILICIA, A.; SERIO, M. Di; TESSER, R. Falling film reactor modelling for sulfonation reactions. **Chemical Engineering Journal**, v. 377, p. 120464, 2019. Available in: <https://doi.org/10.1016/j.cej.2018.11.162>

SAHA, A. K.; BANDYOPADHYAY, S. S.; BISWAS, A. K. Kinetics of absorption of CO₂ into aqueous solutions of 2-amino-2-methyl-1-propanol. **Chemical Engineering Science**, v. 50, n. 22, p. 3587–3598, 1995. Available in: [https://doi.org/10.1016/0009-2509\(95\)00187-A](https://doi.org/10.1016/0009-2509(95)00187-A)

SAIFUTDINOV, A. F.; BEKETOV, O. E.; LADUSHKIN, V. S.; NESTEROV, G. A. Distillation breakthrough reduces tower height. **Hydrocarbon Processing**, p. 26, 2002 a.

SAIFUTDINOV, A. F.; BEKETOV, O. E.; LADUSHKIN, V. S.; NESTEROV, G. A. Distillation technology for the 21st century. **Hydrocarbon Asia**, v. 12, n. 8, p. 40–43, 2002 b.

SAIFUTDINOV, A. F.; BEKETOV, O. Y.; LADOSHKIN, V. S.; NESTEROV, G. A.; TLOUSTY, A. S.; IVANOV, G. I. **Compact rectifying unit for separation of mixed fluids and rectifying process for separation of such mixed fluids**. Publication number WO/2003/078014. Concession: 2009.

SAIFUTDINOV, A. F.; TLUSTY, A. .; BEKETOV, O. E.; LADUSHKIN, V. S. **Separation method of multi components mixtures B01D314-328**. RU, Russia n. (11) 2132214 (13)C1. Concession: 1999.

SALVAGNINI, W. M.; TAQUEDA, M. E. S. A falling-film evaporator with film promoters. **Industrial & Engineering Chemistry Research**, v. 43, n. 21, p. 6832–6835, 2004. Available in: <https://doi.org/10.1021/ie0307636>

SANGWAN, K. S.; SAXENA, S.; KANT, G. Optimization of Machining Parameters to Minimize Surface Roughness using Integrated ANN-GA Approach. **Procedia CIRP**, v. 29, p. 305–310, 2015. Available in: <https://doi.org/10.1016/j.procir.2015.02.002>

SAUCIUC, I.; AKBARZADEH, A.; JOHNSON, P. Characteristics of two-phase closed thermosiphons for medium temperature heat recovery applications. **Heat Recovery Systems and CHP**, v. 15, n. 7, p. 631–640, 1995. Available in: [https://doi.org/10.1016/0890-4332\(95\)90043-8](https://doi.org/10.1016/0890-4332(95)90043-8)

SAUCIUC, I.; AKBARZADEH, A.; JOHNSON, P. Temperature control using variable conductance closed two-phase heat pipe. **International Communications in Heat and Mass Transfer**, v. 23, n. 3, p. 427–433, 1996. Available in: [https://doi.org/10.1016/0735-1933\(96\)00028-0](https://doi.org/10.1016/0735-1933(96)00028-0)

SCHNABEL, G.; SCHLUENDER, E. U. Wärmeübergang von senkrechten Wänden an nichtsiedende und siedende Rieselfilme. “Heat Transfer from Vertical Walls to Falling Liquid Films with or Without Evaporation.” **Verfahrenstechnik**, v. 14, n. 2, p. 79–83, 1980.

SCHOENBECK, L. C. **Distillation process and apparatus**. USA n. US3558438. Deposited: Oct. 30, 1968. Concession: Jan. 26, 1971.

SCHOENMAKERS, H.; SPIEGEL, L. Chapter 10 - Laboratory distillation and scale-up. *In*: GÓRAK, A.; OLUJIĆ, Ž. (org.). **Distillation**. Boston: Academic Press, 2014. p. 319–339. *E-book*. Available in: <https://doi.org/10.1016/B978-0-12-386878-7.00010-3>

SCHWANTES, R.; CHAVAN, K.; WINTER, D.; FELSMANN, C.; PFAFFEROTT, J. Techno-economic comparison of membrane distillation and MVC in a zero liquid discharge application. **Desalination**, v. 428, p. 50–68, 2018. Available in: <https://doi.org/10.1016/j.desal.2017.11.026>

SELKER, M. L.; BURK, R. E.; LANKELMA, H. P. An efficient low-holdup laboratory column. **Industrial & Engineering Chemistry Analytical Edition**, v. 12, n. 6, p. 352–355, 1940. Available in: <https://doi.org/10.1021/ac50146a020>

SEMA, T.; NAAMI, A.; LIANG, Z.; SHI, H.; RAYER, A. V.; SUMON, K. Z.; WATTANAPHAN, P.; HENNI, A.; IDEM, R.; SAIWAN, C.; TONTIWACHWUTHIKUL, P. Part 5b: Solvent chemistry: reaction kinetics of CO₂ absorption into reactive amine solutions. **Carbon Management**, v. 3, n. 2, p. 201–220, 2012. Available in: <https://doi.org/10.4155/cmt.12.13>

SHAHSAVAND, A.; CHENAR, M. P. Neural networks modeling of hollow fiber membrane processes. **Journal of Membrane Science**, v. 297, n. 1, p. 59–73, 2007. Available in: <https://doi.org/10.1016/j.memsci.2007.03.011>

SHAHZAD, M. W.; MYAT, A.; CHUN, W. G.; NG, K. C. Bubble-assisted film evaporation correlation for saline water at sub-atmospheric pressures in horizontal-tube evaporator. **Applied Thermal Engineering**, v. 50, n. 1, p. 670–676, 2013. Available in: <https://doi.org/10.1016/j.applthermaleng.2012.07.003>

SHEN, C.; WANG, L.; LI, Q. Optimization of injection molding process parameters using combination of artificial neural network and genetic algorithm method. **Journal of Materials Processing Technology**, v. 183, n. 2, p. 412–418, 2007. Available in: <https://doi.org/10.1016/j.jmatprotec.2006.10.036>

SHILKIN, A.; KENIG, E. Y.; OLUJIC, Z. Hydrodynamic-analogy-based model for efficiency of structured packing columns. **AIChE Journal**, v. 52, n. 9, p. 3055–3066, 2006. Available in: <https://doi.org/10.1002/aic.10937>

SILVA FILHO, V. F. da; ALVES, J. L. F.; REUS, G. F.; MACHADO, R. A. F.; MARANGONI, C.; BOLZAN, A. Experimental evaluation of the separation of aromatic compounds using falling film distillation on a pilot scale. **Chemical Engineering and Processing - Process Intensification**, v. 130, n. August, p. 296–308, 2018. Available in: <https://doi.org/10.1016/j.cep.2018.06.026>

SINGH, N.; PRASAD, R. Fuel grade ethanol by diffusion distillation: An experimental study. **Journal of Chemical Technology and Biotechnology**, v. 86, n. 5, p. 724–730, 2011. Available in: <https://doi.org/10.1002/jctb.2579>

SKIBOROWSKI, M.; WESSEL, J.; MARQUARDT, W. Efficient Optimization-Based Design of Membrane-Assisted Distillation Processes. **Industrial & Engineering Chemistry Research**, v. 53, n. 40, p. 15698–15717, 2014. Available in: <https://doi.org/10.1021/ie502482b>

SKOGESTAD, S. Dynamics and Control of Distillation Columns: A Tutorial Introduction. **Chemical Engineering Research and Design**, v. 75, n. 6, p. 539–562, 1997. Available in: <https://doi.org/10.1205/026387697524092>

SMITH, R.; JOBSON, M. Distillation. In: WILSON, I. D. (org.). **Encyclopedia of Separation Science**. Oxford: Academic Press, 2000. p. 84–103. Available in: <https://doi.org/10.1016/B0-12-226770-2/00041-7>

SOMMARIVA, C.; HOGG, H.; CALLISTER, K. Forty-year design life: The next target material selection and operating conditions in thermal desalinations plants. **Desalination**, v. 136, n. 1–3, p. 169–176, 2001. Available in: [https://doi.org/10.1016/S0011-9164\(01\)00179-5](https://doi.org/10.1016/S0011-9164(01)00179-5)

SØRENSEN, E.; LAM, K. F.; SUDHOFF, D. Chapter 9 - Special Distillation Applications. In: GÓRAK, A.; SCHOENMAKERS, H. (org.). **Distillation**. Boston: Academic Press, 2014. p. 367–401. *E-book*. Available in: <https://doi.org/10.1016/B978-0-12-386876-3.00009-0>

SRIKHIRIN, P.; APHORN RATANA, S.; CHUNGPAIBULPATANA, S. A review of absorption refrigeration technologies. **Renewable and Sustainable Energy Reviews**, v. 5, n. 4, p. 343–372, 2001. Available in: [https://doi.org/10.1016/S1364-0321\(01\)00003-X](https://doi.org/10.1016/S1364-0321(01)00003-X)

STARFELT, F.; DAIANOVA, L.; YAN, J.; THORIN, E.; DOTZAUER, E. The impact of lignocellulosic ethanol yields in polygeneration with district heating - A case study. **Applied Energy**, v. 92, p. 791–799, 2012. Available in: <https://doi.org/10.1016/j.apenergy.2011.08.031>

STERN, S. V. **The effect of pressures below one atmosphere on the performance of a wetted wall distillation column**. 1962. Thesis (Doctorate in Chemical Engineering) - School of Chemical Engineering, Georgia Institute of Technology, Atlanta, 1962. Available in: <http://hdl.handle.net/1853/10083>

STEVANOVIC, V. D.; STOSIC, Z. V.; STOLL, U. Three-dimensional numerical simulation of non-condensables accumulation induced by steam condensation in a non-vented pipeline. **International Journal of Heat and Mass Transfer**, v. 49, n. 15, p. 2420–2436, 2006. Available in: <https://doi.org/10.1016/j.ijheatmasstransfer.2006.01.029>

STIRBA, C.; HURT, D. M. Turbulence in falling liquid films. **AIChE Journal**, v. 1, n. 2, p. 178–184, 1955. Available in: <https://doi.org/10.1002/aic.690010209>

STOUT, T. R. **Structure for multiple-effect distillation**. USA n. US5423952. Deposited: Jul. 22, 1992. Concession: Jun. 13, 1995.

STOUT, T. R. **Structure for multiple-effect distillation using tubes or plates**. US7476298. Deposited: Feb. 27, 2003. Concession: Jan. 13, 2009.

SUGIYAMA, T.; KATO, Y.; ENOKIDA, Y.; YAMAMOTO, I. Simultaneous solution of concentration profiles in vapor-liquid phases of wetted-wall distillation column for H₂O-H₂O isotope separation. **Journal of Nuclear Science and Technology**, v. 35, n. 1, p. 60–65, 1998. Available in: <https://doi.org/10.1080/18811248.1998.9733820>

SUN, B.; ZHU, M.; LIU, B. T.; LIU, C. J.; YUAN, X. G. Investigation of falling liquid film Flow on novel structured packing. **Industrial & Engineering Chemistry Research**, v. 52, n. 13, p. 4950–4956, 2013. Available in: <https://doi.org/10.1021/ie302272s>

SUROWIEC, A. J.; FURNAS, C. C. Distillation in a Wetted-wall Tower. **Trans. Am. Inst. Chem. Engrs.**, v. 38, p. 55–89, 1942.

TAILBY, S. R.; PORTALSKI, S. The hydrodynamics of liquid films flowing on a vertical surface. **Transactions of the Institution of Chemical Engineers**, v. 38, p. 324–334, 1960.

TAVAKKOLI, S.; LOKARE, O. R.; VIDIC, R. D.; KHANNA, V. A techno-economic assessment of membrane distillation for treatment of Marcellus shale produced water. **Desalination**, v. 416, n. April, p. 24–34, 2017. Available in: <https://doi.org/10.1016/j.desal.2017.04.014>

TAYLOR, R.; KRISHNA, R.; KOOIJMAN, H. Real-World Modeling of Distillation. **Reactions and Separations**, n. July, p. 28–39, 2003.

TEHLAH, N.; KAEWPRADIT, P.; MUJTABA, I. M. Artificial neural network based modeling and optimization of refined palm oil process. **Neurocomputing**, v. 216, p. 489–501, 2016. Available in: <https://doi.org/10.1016/j.neucom.2016.07.050>

TELEKEN, J. G. **Modelagem matemática e análise fluidodinâmica do processo de destilação por filme líquido descendente**. 2013. Thesis (Doctorate in Chemical Engineering) - Department of Chemical Engineering, Federal University of Santa Catarina, Florianópolis, 2013.

TELEKEN, J. G.; WERLE, L. O.; PARISOTTO, I. G. B.; MARANGONI, C.; MENEGUELO, A. P.; BOLZAN, A.; MACHADO, R. A. F. Computational fluid dynamics simulation of the feed distribution system of a falling film distillation device. **Computer**

Aided Chemical Engineering, v. 31, p. 845–849, 2012. Available in:
<https://doi.org/10.1016/B978-0-444-59507-2.50161-X>

TEWFIK, S. R.; ABULNOUR, A. G. M. G.; SOROUR, M. H. Techno-economic and environmental aspects of the production of medium scale ligno-cellulosic ethanol under Egyptian conditions. **Egyptian Journal of Petroleum**, v. 24, n. 4, p. 375–381, 2015. Available in: <https://doi.org/10.1016/j.ejpe.2015.10.002>

THOME, J. R. Falling film evaporation: state-of-the-art review of recent work. **Journal of Enhanced Heat Transfer**, v. 6, n. 2, p. 263–277, 1999. Available in: <https://doi.org/10.1615/JEnhHeatTransf.v6.i2-4.140>

THOMSON, E. L.; BULLIED, A. R. Production of ethanol-based hand sanitizer in breweries during the COVID-19 crisis. **Technical Quarterly**, v. 57, n. 1, p. 47–52, 2020. Available in: <https://doi.org/10.1094/tq-57-1-0417-01>

TIAN, Y.; DEMIREL, S. E.; HASAN, M. M. F.; PISTIKOPOULOS, E. N. An overview of process systems engineering approaches for process intensification: State of the art. **Chemical Engineering and Processing - Process Intensification**, v. 133, p. 160–210, 2018. Available in: <https://doi.org/10.1016/j.cep.2018.07.014>

TONG, L. S.; TANG, Y. S. **Boiling Heat Transfer And Two-Phase Flow**. Second ed. Boca Raton: Taylor & Francis, 1997. Available in: <https://doi.org/10.1201/9781315138510>

TOOR, H. L. Diffusion in three-component gas mixtures. **AIChE Journal**, v. 3, n. 2, p. 198–207, 1957. Available in: <https://doi.org/10.1002/aic.690030214>

TORRES, A.; MISHKINIS, D.; KULAKOV, A.; ROMERA, F.; GREGORI, C. Thermal control of loop heat pipe with pressure regulating valve. **Heat Pipe Science and Technology, An International Journal**, n. September, 2012. Available in: <https://doi.org/10.1615/heatpipescietch.2012004205>

TORSNER, E. Solving corrosion problems in biofuels industry. **Corrosion Engineering, Science and Technology**, v. 45, n. 1, p. 42–48, 2010. Available in: <https://doi.org/10.1179/147842209X12579401586726>

TOVAR, L. P.; MACIEL, M. R. W.; PINTO, G. M. F.; FILHO, R. M.; GOMES, D. R. Factorial design applied to concentrate bioactive component of *Cymbopogon citratus* essential oil using short path distillation. **Chemical Engineering Research and Design**, v. 88, n. 2, p. 239–244, 2010. Available in: <https://doi.org/10.1016/j.cherd.2009.07.018>

TOVAR, L. P.; PINTO, G. M. F.; WOLF-MACIEL, M. R.; BATISTELLA, C. B.; MACIEL-FILHO, R. Short-path-distillation process of lemongrass essential oil: Physicochemical characterization and assessment quality of the distillate and the residue products. **Industrial and Engineering Chemistry Research**, v. 50, n. 13, p. 8185–8194, 2011. Available in: <https://doi.org/10.1021/ie101503n>

VAN ES, J. P.; HEERTJES, P. M. On the condensation of a vapour of a binary mixture in a vertical tube. **Chemical Engineering Science**, v. 5, n. 5, p. 217–225, 1956. Available in:

[https://doi.org/10.1016/0009-2509\(56\)80033-X](https://doi.org/10.1016/0009-2509(56)80033-X)

VANE, L. M. Separation technologies for the recovery and dehydration of alcohols from fermentation broths. **Biofuels, Bioproducts and Biorefining**, v. 2, n. 6, p. 553–588, 2008. Available in: <https://doi.org/10.1002/bbb.108>

VANE, L. M.; ALVAREZ, F. R.; ROSENBLUM, L.; GOVINDASWAMY, S. Efficient ethanol recovery from yeast fermentation broth with integrated distillation-membrane process. **Industrial and Engineering Chemistry Research**, v. 52, n. 3, p. 1033–1041, 2013. Available in: <https://doi.org/10.1021/ie2024917>

VASCONCELOS, M. H.; MENDES, F. M.; RAMOS, L.; DIAS, M. O. S.; BONOMI, A.; JESUS, C. D. F.; WATANABE, M. D. B.; JUNQUEIRA, T. L.; MILAGRES, A. M. F.; FERRAZ, A.; SANTOS, J. C. dos. Techno-economic assessment of bioenergy and biofuel production in integrated sugarcane biorefinery: Identification of technological bottlenecks and economic feasibility of dilute acid pretreatment. **Energy**, v. 199, p. 117422, 2020. Available in: <https://doi.org/10.1016/j.energy.2020.117422>

VERGILI, I.; KAYA, Y.; SEN, U.; GÖNDER, Z. B.; AYDINER, C. Techno-economic analysis of textile dye bath wastewater treatment by integrated membrane processes under the zero liquid discharge approach. **Resources, Conservation and Recycling**, v. 58, p. 25–35, 2012. Available in: <https://doi.org/10.1016/j.resconrec.2011.10.005>

VINCENT, C. C. J.; KOK, J. B. W. Investigation of the overall transient performance of the industrial two-phase closed loop thermosyphon. **International Journal of Heat and Mass Transfer**, v. 35, n. 6, p. 1419–1426, 1992. Available in: [https://doi.org/10.1016/0017-9310\(92\)90033-O](https://doi.org/10.1016/0017-9310(92)90033-O)

VOHRA, M.; MANWAR, J.; MANMODE, R.; PADGILWAR, S.; PATIL, S. Bioethanol production: Feedstock and current technologies. **Journal of Environmental Chemical Engineering**, v. 2, n. 1, p. 573–584, 2014. Available in: <https://doi.org/10.1016/j.jece.2013.10.013>

WALSH, T. J. High temperature distillation. **Industrial & Engineering Chemistry**, v. 39, n. 1, p. 17–18, 1947. Available in: <https://doi.org/10.1021/ie50445a012>

WANG, H.; CUI, C.; LYU, H.; SUN, J. Design and economic evaluation of energy-saving industrial distillation processes for separating close-boiling cyclohexanone-cyclohexanol mixture. **Separation and Purification Technology**, v. 211, p. 279–289, 2019. Available in: <https://doi.org/10.1016/j.seppur.2018.09.025>

WANG, L.; AN, S.; LI, Q.; YU, S.; WU, S. Phase change behavior and kinetics of CO₂ absorption into DMBA/DEEA solution in a wetted-wall column. **Chemical Engineering Journal**, v. 314, n. April, p. 681–687, 2017. Available in: <https://doi.org/10.1016/j.cej.2016.12.033>

WANG, Q.; MA, X.; LAN, Z.; CHEN, J.; BAI, T. Heat transfer characteristics of falling film process on coated division tubes: Effect of the surface configurations. **Industrial and Engineering Chemistry Research**, v. 49, n. 14, p. 6622–6629, 2010. Available in:

<https://doi.org/10.1021/ie9018676>

WASDEN, F. K.; DUKLER, A. E. A numerical study of mass transfer in free falling wavy films. **AIChE Journal**, v. 36, n. 9, p. 1379–1390, 1990. Available in: <https://doi.org/10.1002/aic.690360911>

WATANABE, K.; MUNAKATA, T. Distillation performance of wetted-wall column with improved wetting characteristics in the range of low reflux rate under reduced pressure. **Journal of Chemical Engineering of Japan**, v. 9, n. 2, p. 107–112, 1976. Available in: <https://doi.org/10.1252/jcej.9.107>

WEBER, C. T.; RANZAN, L.; LIESEGANG, L. L. M.; TRIERWEILER, L. F.; TRIERWEILER, J. O. A circular economy model for ethanol and alcohol-based hand sanitizer from sweet potato waste in the context of COVID-19. **Brazilian Journal of Operations & Production Management**, v. 17, n. 3, p. 1–12, 2020. Available in: <https://doi.org/10.14488/bjopm.2020.028>

WEI, Z.; ZHANG, B.; WU, S.; CHEN, Q.; TSATSARONIS, G. Energy-use analysis and evaluation of distillation systems through avoidable exergy destruction and investment costs. **Energy**, v. 42, n. 1, p. 424–433, 2012. Available in: <https://doi.org/10.1016/j.energy.2012.03.026>

WEN, T.; LU, L.; HE, W.; MIN, Y. Fundamentals and applications of CFD technology on analyzing falling film heat and mass exchangers: A comprehensive review. **Applied Energy**, v. 261, n. January, p. 114473, 2020. Available in: <https://doi.org/10.1016/j.apenergy.2019.114473>

WESTHAVER, J. W. Theory of open-tube distillation columns. **Industrial & Engineering Chemistry**, v. 34, n. 1, p. 126–130, 1942. Available in: <https://doi.org/10.1021/ie50385a026>

WHITESELL, J. M. **Wetted wall tube packing for distillation columns**. 1947. Thesis (Master of Science in Chemical Engineering) - Department of Chemical Engineering, University of Southern California, Los Angeles, 1947.

WILAMOWSKI, B. M.; YU, H. Improved Computation for Levenberg–Marquardt Training. **IEEE Transactions on Neural Networks**, v. 21, n. 6, p. 930–937, 2010. Available in: <https://doi.org/10.1109/TNN.2010.2045657>

WILKE, C. R.; CHANG, P. Correlation of diffusion coefficients in dilute solutions. **AIChE Journal**, v. 1, n. 2, p. 264–270, 1955. Available in: <https://doi.org/10.1002/aic.690010222>

WILLINGHAM, C. B.; SEDLAK, V. A.; ROSSINI, F. D.; WESTHAVER, J. W. Rotary Concentric-Tube Distilling Column. **Industrial & Engineering Chemistry**, v. 39, n. 6, p. 706–712, 1947. Available in: <https://doi.org/10.1021/ie50450a004>

WILSON, G. M. Vapor-liquid equilibrium. A new expression for the excess free energy of mixing. **Journal of the American Chemical Society**, v. 86, n. 2, p. 127–130, 1964. Available in: <https://doi.org/10.1021/ja01056a002>

WUEST, T.; WEIMER, D.; IRGENS, C.; THOBEN, K.-D. Machine learning in manufacturing: advantages, challenges, and applications. **Production & Manufacturing Research**, v. 4, n. 1, p. 23–45, 2016. Available in: <https://doi.org/10.1080/21693277.2016.1192517>

XU, L.; CHEN, D.; YAN, B.; YUAN, X. Experimental investigation on heat exchange and separation performance of an annular structured internal heat-integrated distillation column. **Chinese Journal of Chemical Engineering**, v. 22, n. 10, p. 1087–1091, 2014. Available in: <https://doi.org/10.1016/j.cjche.2013.05.002>

YAMAMURA, M.; MATSUNAGA, S.; MAWATARI, Y.; KAGE, H. Drying behavior of thin liquid films in a condenser dryer with a solvent-trapping screen. **Chemical Engineering and Processing: Process Intensification**, v. 48, n. 3, p. 1427–1431, 2009. Available in: <https://doi.org/10.1016/j.cep.2009.07.010>

YANG, C.; PENG, X.; ZHAO, Y.; WANG, X.; FU, J.; LIU, K.; LI, Y.; LI, P. Prediction model to analyze the performance of VMD desalination process. **Computers & Chemical Engineering**, v. 132, p. 106619, 2020. Available in: <https://doi.org/10.1016/j.compchemeng.2019.106619>

YEONG, K. K.; GAVRIILIDIS, A.; ZAPF, R.; HESSEL, V. Experimental studies of nitrobenzene hydrogenation in a microstructured falling film reactor. **Chemical Engineering Science**, v. 59, n. 16, p. 3491–3494, 2004. Available in: <https://doi.org/10.1016/j.ces.2004.04.022>

YI, J.; WANG, Q.; ZHAO, D.; WEN, J. T. BP neural network prediction-based variable-period sampling approach for networked control systems. **Applied Mathematics and Computation**, v. 185, n. 2, p. 976–988, 2007. Available in: <https://doi.org/10.1016/j.amc.2006.07.020>

YILDIRIM, Ö.; KISS, A. A.; KENIG, E. Y. Dividing wall columns in chemical process industry: A review on current activities. **Separation and Purification Technology**, v. 80, p. 403–417, 2011. Available in: <https://doi.org/10.1016/j.seppur.2011.05.009>

YINGJIAN, L.; XINKUI, Y.; QI, Q.; JIEZHI, L. The study on the evaporation cooling efficiency and effectiveness of cooling tower of film type. **Energy Conversion and Management**, v. 52, n. 1, p. 53–59, 2011. Available in: <https://doi.org/10.1016/j.enconman.2010.06.036>

YOSHIMURA, P. N.; NOSOKO, T.; NAGATA, T. Enhancement of mass transfer into a falling laminar liquid film by two-dimensional surface waves—Some experimental observations and modeling. **Chemical Engineering Science**, v. 51, n. 8, p. 1231–1240, 1996. Available in: [https://doi.org/10.1016/0009-2509\(95\)00387-8](https://doi.org/10.1016/0009-2509(95)00387-8)

ZADRAZIL, I.; MATAR, O. K.; MARKIDES, C. N. An experimental characterization of downwards gas – liquid annular flow by laser-induced fluorescence: Flow regimes and film statistics. **International Journal of Multiphase Flow**, v. 60, n. April, p. 87–102, 2014. Available in: <https://doi.org/10.1016/j.ijmultiphaseflow.2013.11.008>

ZAKHAROV, M. K.; MARTYNOVA, M. M.; PRUSACHENKOVA, M. I. Comparison of heat consumption in the separation of binary mixtures using distillation and rectification. **Theoretical Foundations of Chemical Engineering**, v. 52, n. 4, p. 730–734, 2018. Available in: <https://doi.org/10.1134/S0040579518040322>

ZANFIR, M.; GAVRIILIDIS, A.; WILLE, C.; HESSEL, V. Carbon Dioxide Absorption in a Falling Film Microstructured Reactor: Experiments and Modeling. **Industrial & Engineering Chemistry Research**, v. 44, n. 6, p. 1742–1751, 2005. Available in: <https://doi.org/10.1021/ie049726k>

ZENTOU, H.; ABIDIN, Z. Z.; YUNUS, R.; BIAK, D. R. A.; KORELSKIY, D. Overview of alternative ethanol removal techniques for enhancing bioethanol recovery from fermentation broth. **Processes**, v. 7, n. 7, p. 1–16, 2019. Available in: <https://doi.org/10.3390/pr7070458>

ZHANG, H. *et al.* 1.6 Million transactions replicate distributed PV market slowdown by COVID-19 lockdown. **Applied Energy**, v. 283, p. 116341, 2021. Available in: <https://doi.org/10.1016/j.apenergy.2020.116341>

ZHANG, H.; CHEN, G.; YUE, J.; YUAN, Q. Hydrodynamics and mass transfer of gas–liquid flow in a falling film microreactor. **AIChE Journal**, v. 55, n. 5, p. 1110–1120, 2009. Available in: <https://doi.org/10.1002/aic.11743>

ZHANG, J.; MORRIS, A. J. A Sequential Learning Approach for Single Hidden Layer Neural Networks. **Neural Networks**, v. 11, n. 1, p. 65–80, 1998. Available in: [https://doi.org/10.1016/S0893-6080\(97\)00111-1](https://doi.org/10.1016/S0893-6080(97)00111-1)

ZHANG, X.; XU, C.; ZHOU, M. Modeling of falling film molecular distillator. **Separation Science and Technology**, v. 40, n. 6, p. 1371–1386, 2005. Available in: <https://doi.org/10.1081/SS-200053027>

ZHENG, Y.; CHEN, G.; ZHAO, X.; SUN, W.; MA, X. Falling liquid film periodical fluctuation over a superhydrophilic horizontal tube at low spray density. **International Journal of Heat and Mass Transfer**, v. 147, p. 118938, 2020. Available in: <https://doi.org/10.1016/j.ijheatmasstransfer.2019.118938>

ZHONG, W.; HE, T.; LONGTIN, J. Pulsed laminar falling films in vertical tubes: Maintaining a continuous liquid film with reduced film thickness. **Experimental Thermal and Fluid Science**, v. 113, p. 110011, 2020. Available in: <https://doi.org/10.1016/j.expthermflusci.2019.110011>

ZHOU, H.; CAI, Y.; YOU, F. Systems Design, Modeling, and Thermoeconomic Analysis of Azeotropic Distillation Processes for Organic Waste Treatment and Recovery in Nylon Plants. **Industrial & Engineering Chemistry Research**, v. 57, p. 9994–10010, 2018. Available in: <https://doi.org/10.1021/acs.iecr.8b00275>

ZHOU, X.; COLLINS, R. E. Condensation in a gas-loaded thermosyphon. **International Journal of Heat and Mass Transfer**, v. 38, n. 9, p. 1605–1617, 1995. Available in: [https://doi.org/10.1016/0017-9310\(94\)00287-6](https://doi.org/10.1016/0017-9310(94)00287-6)

ZHOU, Y.; YU, J.; GAO, M. An experimental study of falling film evaporation in vertical channels with perforated fins of a plate-fin heat exchanger. **Chemical Engineering and Processing - Process Intensification**, v. 145, p. 107672, 2019. Available in: <https://doi.org/10.1016/j.cep.2019.107672>

ZHOU, Z.; PENG, J.; ZHANG, Y.; ZHUGE, W. Instabilities of viscoelastic liquid film coating tube in the presence of surfactant. **Journal of Non-Newtonian Fluid Mechanics**, v. 204, n. February, p. 94–103, 2014. Available in: <https://doi.org/10.1016/j.jnnfm.2013.12.007>

ZHU, K.; LI, X.; LI, H.; YANG, Z.; WANG, Y. Experimental investigation on the effect of heat sink temperature on operational characteristics of a new-type loop heat pipe. **Energy Procedia**, v. 158, p. 2423–2429, 2019. Available in: <https://doi.org/10.1016/j.egypro.2019.01.298>

ZIAPOUR, B. M.; SHAKER, H. Heat transfer characteristics of a two-phase closed thermosyphon using different working fluids. **Heat and Mass Transfer**, v. 46, n. 3, p. 307–314, 2010. Available in: <https://doi.org/10.1007/s00231-009-0570-1>

ZIEGLER, J. G.; NICHOLS, N. B. Optimum settings for automatic controllers. **Trans. ASME**, v. 64, n. 11, p. 759–765, 1942.

ZIERHUT, E. J.; BATTISTI, R.; MACHADO, R. A. F.; MARANGONI, C. Distributed control strategy with Smith's predictor in a pilot-scale diabatic distillation unit. **Chemical Engineering & Technology**, 2020. Available in: <https://doi.org/10.1002/ceat.202000102>

ZUIDERWEG, F. J.; HARMENS, A. The influence of surface phenomena on the performance of distillation columns. **Chemical Engineering Science**, v. 9, n. 2, p. 89–103, 1958. Available in: [https://doi.org/10.1016/0009-2509\(58\)80001-9](https://doi.org/10.1016/0009-2509(58)80001-9)

ZUÑIGA LIÑAN, L.; LIMA, N. M. N.; MANENTI, F.; WOLF MACIEL, M. R.; FILHO, R. M.; MEDINA, L. C. Experimental campaign, modeling, and sensitivity analysis for the molecular distillation of petroleum residues 673.15K+. **Chemical Engineering Research and Design**, v. 90, n. 2, p. 243–258, 2012. Available in: <https://doi.org/10.1016/j.cherd.2011.07.001>

ZUO, J.; FAGHRI, A. A network thermodynamic analysis of the heat pipe. **International Journal of Heat and Mass Transfer**, v. 41, n. 11, p. 1473–1484, 1998. Available in: [https://doi.org/10.1016/S0017-9310\(97\)00220-2](https://doi.org/10.1016/S0017-9310(97)00220-2)

APPENDIX A – Constructive design data of the apparatus

The design data of the equipment and construction materials involved in the thermal network-based mathematical model proposed for the two-phase closed thermosyphon coupled to the pilot-scale falling film distillation unit are shown in the following Worksheet 1.

Worksheet 1 – Constructive design data of the equipment involved.

Parameter	Dimension/unit
Electrical resistances	
Inner diameter	12.7 mm
Outer diameter	18.7 mm
Wall thickness	3.0 mm
Length	0.4 m
Total power	9,600 W
Material type	Stainless steel 304
Distillation tube	
Inner diameter	26.0 mm
Outer diameter	32.0 mm
Wall thickness	3.0 mm
Length	1.0 m
Material type	Stainless steel 304
Evaporator	
Length	0.4 m
Inner diameter	101.6 mm
Outer diameter	107.6 mm
Wall thickness	3.0 mm
Filling ratio	75%
Liquid volume	0.0061 m ³
Material type	Stainless steel 304
Thermal insulation	
Insulation thickness	25.4 mm
Material type	Glass wool

Source: Battisti et al. (2020).

APPENDIX B – Thermophysical properties of materials

The thermophysical properties of the materials (fluids and solids) involved in the thermal network-based model equations were compiled and are presented in the following worksheets, for each material, separately. The properties of water (liquid and vapor phase) were taken from Faghri and Zhang (2006), who specified the polynomial expression (Eq. B1) for the thermodynamic and transport properties of pure water, valid for temperatures in the range of 20 °C to 200 °C.

$$\ln(\text{Prop.}) = \alpha_0 + \alpha_1 T + \alpha_2 T^2 + \alpha_3 T^3 + \alpha_4 T^4 + \alpha_5 T^5 \quad (\text{B1})$$

Where α_0 to α_5 are the coefficients of the adjusted polynomial equation specified for each property, as shown in the Worksheet 2.

Worksheet 2 – Coefficients of the polynomial equation for water properties.

Prop. (unit)^a	α_0	$\alpha_1 \times 10^3$	$\alpha_2 \times 10^5$	$\alpha_3 \times 10^7$	$\alpha_4 \times 10^9$	$\alpha_5 \times 10^{12}$
p_v (10 ⁵ Pa)	5.0945	72.280	-28.625	9.2341	-2.0295	2.1645
$h_{\ell v}$ (kJ/kg)	7.8201	-0.5891	-0.9135	0.8474	-0.3963	0.5915
ρ_{ℓ} (kg/m ³)	6.9094	0.0201	-0.5987	0.2592	-0.0932	0.1210
ρ_v (kg/m ³)	-5.3225	68.366	-27.243	8.4522	-1.6558	1.5514
μ_{ℓ} (10 ⁻⁷ Ns/m ²)	9.7620	-31.154	20.029	-9.5815	2.7772	-3.5075
μ_v (10 ⁻⁷ Ns/m ²)	4.3995	3.8789	2.1181	-3.4406	1.6730	-2.8030
k_{ℓ} (W/mK)	-0.5653	3.1743	-1.4392	-0.1322	0.2553	-0.6445
k_v (W/mK)	-4.0406	3.2288	0.5338	-0.6714	0.4097	-0.6958
$c_{p,\ell}$ (kJ/kgK)	1.4338	-0.2264	0.4282	-0.2741	0.1470	-0.2259
$c_{p,v}$ (kJ/kgK)	0.6208	0.31420	0.1611	0.4016	0.0348	-0.2071

^a The error (%) varies for each property, all within the range of $0.01 \leq E \leq 0.07$.

Source: Battisti et al. (2020).

The thermophysical properties of ethanol (liquid and vapor) were also taken from Faghri and Zhang (2006), and also follow the polynomial expression represented by Eq. (B1). The values obtained through the polynomial equation for the thermodynamic and transport properties of ethanol are valid for temperatures in the range of 0 °C to 240 °C, except for k_v which is valid between 0 °C to 220 °C; $c_{p,\ell}$ valid between 0 °C to 140 °C, and $c_{p,v}$ valid

between 0 °C to 120 °C. Worksheet 3 shows the coefficients of the polynomial equation of thermophysical properties for ethanol (liquid and vapor).

Worksheet 3 – Coefficients of the polynomial equation for ethanol properties.

Prop. (unit)^a	α_0	$\alpha_1 \times 10^3$	$\alpha_2 \times 10^5$	$\alpha_3 \times 10^7$	$\alpha_4 \times 10^9$	$\alpha_5 \times 10^{12}$
p_v (10 ⁵ Pa)	-4.4114	87.650	-63.182	39.958	-14.340	20.359
$h_{\ell v}$ (kJ/kg)	1048.6	-1092.1	1065.1	-2069.3	1123.1	-2492.8
ρ_{ℓ} (10 ³ kg/m ³)	-0.1079	-7.7201	15.906	-16.139	7.1873	-12.075
ρ_v (kg/m ³)	-3.3681	52.492	5.1630	-19.542	8.6893	-11.451
μ_{ℓ} (10 ⁻³ Ns/m ²)	0.5894	-22.540	10.283	-8.8574	4.7884	-9.7493
μ_v (10 ⁻⁵ Ns/m ²)	-0.2576	4.5249	-3.1212	3.9144	-2.3733	5.1450
k_{ℓ} (W/mK)	-1.6976	-1.2505	0.0753	0.52361	-0.3499	0.64599
k_v (W/mK)	-4.4346	3.3797	21.001	-34.778	20.462	-40.325
$c_{p,\ell}$ (kJ/kgK)	0.81763	2.6793	1.3888	-0.00044	-0.4442	1.5104
$c_{p,v}$ (kJ/kgK)	0.2925	1.2271	8.0938	-18.513	16.850	-53.880

^a The error (%) varies for each property, all within the range of $0.10 \leq E \leq 4.95$.

Source: Battisti et al. (2020).

The properties of the 304 stainless steel were obtained from the regression of literature data presented by Faghri and Zhang (2006). The polynomial equation for the thermophysical properties is shown in Eq. (B2), valid for interpolation up to 1500 °C.

$$Prop. = \alpha_0 + \alpha_1 T + \alpha_2 T^2 + \alpha_3 T^3 \quad (B2)$$

Where the coefficients α_0 to α_3 of the polynomial equation were adjusted by proper regression, and are specified for each thermophysical property in question, as shown in Worksheet 4.

Worksheet 4 – Coefficients of the polynomial equation for 304 stainless steel properties.

Prop. (unit)^a	α_0	$\alpha_1 \times 10^1$	$\alpha_2 \times 10^5$	$\alpha_3 \times 10^7$	$\alpha_3 \times 10^{12}$
ρ (kg/m ³)	8057.6	-3.363	-10.00	1.000	--
k (W/mK)	8.1914	0.2538	-0.8333	--	--
c_p (kJ/kgK)	0.1023	0.0021	-0.3473	0.02601	-0.6870

^a Properties valid for temperatures up to 1500 °C.

Source: Battisti et al. (2020).

APPENDIX C – Material balance data of the falling film distillation

The experiments carried out to collect the mass balance data on the thermosyphon-assisted pilot-scale falling film distillation unit are shown in Worksheet 5. The mixture fed in the column was ethanol-water in a concentration kept constant within the range of 10.50 ± 0.7 wt% (ethanol), which simulates the output stream of industrial bioreactors. The process streams analyzed were the distilled vapor output from the top of the column, and the liquid output at the bottom of the column. The analysis of ethanol mass fraction was performed with the aid of a calibrated alcoholometer.

Worksheet 5 – Experimental mass balance data from the falling film distillation unit.

Input variables			Process outputs			
T_{feed} (°C)	T_e (°C)	Q_{feed} (L/h)	x_{EtOH}^D (wt%)	\dot{m}_D (kg/h)	x_{EtOH}^B (wt%)	\dot{m}_B (kg/h)
80	93	14	66.83 ± 1.10	0.87 ± 0.02	6.64 ± 0.01	12.88 ± 0.02
80	93	17	68.34 ± 1.84	0.59 ± 0.20	9.52 ± 0.72	16.04 ± 0.22
80	93	23	66.72 ± 1.10	0.66 ± 0.08	9.36 ± 0.18	20.90 ± 0.08
80	93	32	65.90 ± 0.93	0.58 ± 0.04	9.15 ± 0.05	30.32 ± 0.04
80	100	14	60.17 ± 0.52	1.94 ± 0.93	2.31 ± 0.16	11.82 ± 0.05
80	100	17	57.67 ± 0.52	1.96 ± 0.50	5.44 ± 0.11	14.66 ± 0.05
80	100	23	58.91 ± 1.04	2.22 ± 0.04	5.87 ± 0.22	20.29 ± 0.04
80	100	32	45.57 ± 1.03	3.54 ± 0.03	5.64 ± 0.82	27.37 ± 0.03
80	104	14	54.65 ± 0.46	2.46 ± 0.02	1.51 ± 0.01	11.30 ± 0.02
80	104	17	54.09 ± 0.10	2.50 ± 0.05	3.95 ± 0.18	14.12 ± 0.05
80	104	23	52.69 ± 1.40	3.24 ± 0.03	3.83 ± 0.17	18.42 ± 0.03
80	104	32	34.10 ± 0.27	5.76 ± 0.69	4.74 ± 0.87	25.15 ± 0.69
80	110	14	49.18 ± 0.83	3.27 ± 0.12	1.16 ± 0.03	11.78 ± 0.73
80	110	17	50.63 ± 0.48	3.28 ± 0.03	2.06 ± 0.22	13.36 ± 0.03
80	110	23	53.19 ± 0.19	3.80 ± 0.17	2.14 ± 0.51	17.86 ± 0.17
80	110	32	31.96 ± 3.23	7.16 ± 0.85	3.65 ± 0.04	23.74 ± 0.85

Source: Battisti et al. (2020).

APPENDIX D – Experimental dataset for the ML modeling

The experimental dataset used for the construction of the ML model proposed for the pilot-scale thermosyphon-assisted falling film distillation unit are shown in the Worksheet 6.

Worksheet 6 – Experimental dataset for the ML modeling.

Run		Input variables			Responses			
Trial	Type	T_F (°C)	T_e (°C)	Q_F (L/h)	x_{EtOH}^D (wt%)	\dot{m}_D (kg/h)	RF (%)	SF
1	Training	60	96	17	66.39	0.71	24.48	21.51
2	Training	60	96	23	37.20	1.71	24.66	5.97
3	Training	60	100	14	61.91	1.57	60.34	32.68
4	Training	60	100	23	40.59	3.03	47.64	9.54
5	Training	60	104	14	56.85	2.25	79.55	49.86
6	Training	60	104	23	33.04	5.76	73.79	12.26
7	Training	60	110	14	50.36	2.93	91.70	90.97
8	Training	60	110	23	26.02	10.08	84.21	11.68
9	Training	80	93	17	68.34	0.59	20.81	20.51
10	Training	80	93	23	66.72	0.66	18.28	19.42
11	Training	80	100	23	58.91	2.22	52.31	22.98
12	Training	80	104	14	54.65	2.46	88.72	78.55
13	Training	80	104	17	54.09	2.50	70.80	28.62
14	Training	80	104	32	34.10	5.76	62.22	10.40
15	Training	80	110	17	50.63	3.27	85.75	48.82
16	Training	80	110	23	53.19	3.80	84.14	52.08
17	Training	90	93	14	59.97	0.86	36.39	19.59
18	Training	90	93	17	56.87	0.71	21.07	12.46
19	Training	90	93	23	57.58	1.39	32.81	16.08
20	Training	90	93	32	57.15	1.64	26.61	13.71
21	Training	90	100	14	55.97	1.95	76.73	43.46
22	Training	90	100	17	54.25	2.21	62.11	22.20
23	Training	90	100	23	54.10	2.60	57.57	21.42
24	Training	90	100	32	56.33	3.16	51.41	19.84
25	Training	90	104	14	55.01	2.20	84.95	63.88
26	Training	90	104	17	51.69	2.98	79.92	36.63
27	Training	90	104	23	53.80	3.22	70.90	30.37
28	Training	90	104	32	55.67	4.15	66.71	27.69
29	Training	90	110	14	50.95	2.81	91.89	87.77
30	Training	90	110	17	47.78	3.75	91.32	68.29
31	Training	90	110	23	51.80	4.52	90.80	80.50
32	Training	95	93	23	49.19	2.54	53.09	16.09
33	Training	95	93	32	50.52	2.80	45.02	15.37

34	Training	95	100	17	44.92	2.74	68.27	18.43
35	Training	95	100	32	43.31	3.57	49.26	12.15
36	Training	95	104	14	33.30	3.91	93.11	48.50
37	Training	95	104	23	40.01	4.54	77.19	21.01
38	Training	95	110	14	34.67	3.93	88.59	28.02
39	Training	95	110	17	33.82	4.90	91.83	38.84
40	Training	95	110	23	38.03	5.77	93.25	62.10
41	Training	95	110	32	31.83	7.82	75.70	13.63
42	Validation	60	96	32	29.22	2.02	16.15	3.75
43	Validation	60	100	17	58.95	1.89	58.02	27.16
44	Validation	60	104	17	55.15	2.63	75.22	38.37
45	Validation	80	93	14	66.83	0.87	40.51	28.31
46	Validation	80	93	32	65.90	0.58	12.03	19.18
47	Validation	80	100	17	57.67	1.96	58.62	23.67
48	Validation	80	100	32	45.57	3.54	51.07	14.00
49	Validation	80	104	23	52.69	3.24	70.76	27.93
50	Validation	90	110	32	26.17	12.16	91.92	23.16
51	Validation	95	93	14	40.90	2.24	65.37	15.22
52	Test	60	96	14	68.05	0.48	20.29	22.04
53	Test	60	100	32	40.17	3.14	34.60	7.69
54	Test	60	104	32	30.70	6.73	56.58	6.87
55	Test	60	110	17	23.93	6.91	85.82	12.46
56	Test	60	110	32	21.64	14.34	85.05	9.10
57	Test	80	100	14	60.17	1.94	81.06	63.98
58	Test	80	110	14	49.18	3.27	92.17	82.44
59	Test	80	110	32	31.96	7.16	72.56	12.41
60	Test	95	93	17	40.52	2.11	47.49	9.48
61	Test	95	100	14	37.17	2.82	74.80	17.13
62	Test	95	100	23	46.42	3.27	64.55	18.57
63	Test	95	104	17	39.41	3.46	75.58	18.23
64	Test	95	104	32	38.65	4.94	60.79	12.45

Source: Battisti *et al.* (2020a).